



TECHNISCHE
UNIVERSITÄT
WIEN

DISSERTATION

Molybdenum and Tungsten PNP Pincer Complexes

ausgeführt zum Zwecke der Erlangung des akademischen Grades einer
Doktorin der technischen Wissenschaften unter der Leitung von

a.o. Univ.Prof. Dr. Karl Kirchner

Institut 163

für Angewandte Synthesechemie

eingereicht an der Technischen Universität Wien

Fakultät für Technische Chemie

von

Sara Raquel Mota Merelo de Aguiar

1327297

Gießaufgasse 1 Top 14

1050 Wien

Wien, am

Sara Aguiar

Acknowledgements

First of all, I would like to express my deepest gratitude to my supervisor Prof. Karl Kirchner, for all the help, patience, dedication and knowledge that will follow throughout my entire life, thank you so much.

I thank the Technical University of Vienna for allowing me the realization of this study and for the financial support of FWF.

An enormous gratitude to Prof. Helmuth Hoffmann for the kindness of accepting me in his laboratory and for all clarifications about IR spectroscopy.

My most appreciations to Ernst Pittenauer, Prof. Luis F. Veiros, Dr. Berthold Stöger and Dr. Michael Puchberger for all NMR, ESI MS and X-ray measurements and spend time that helped me complete this work.

I would also like to thank the members of my PhD committee for generously given their time and expertise to improve my work.

I am also very grateful to all persons, lab colleagues and friends which I met during this period of my life. All the memories and shared experiences that I will treasure forever.

To all my friends, that gave me support and motivation to continue and achieve this new and important step in my life.

Huge thanks to my family for all their support and affection, especially to my mother for their absolute love and friendship throughout my life.

Finally, to the one being special in my heart, my beloved dog Loba who loves me unconditionally and makes my life brighter.

My most sincere thanks

If your dreams don't scare you they aren't big enough

Abstract

Transition metal complexes containing pincer ligands exhibit a remarkable versatility due to the balance between thermal stability and reactivity which can be controlled by appropriate ligand modifications and/or variation of the metal center. In such systems, modifications of the ligand architecture will strongly influence the steric and electronic properties of transition metal complexes. Pincer ligands that contain pyridine (Y = N) or benzene (Y = C) backbones with phosphines or phosphites as donor groups (PYP) are the most widely studied class. Therefore, the main objective of this thesis was to explore the chemistry of molybdenum and tungsten PNP pincer complexes.

A general overview of the chemistry of pincer ligands is discussed in Chapter 1 including all the possible modifications in the ligand frame, all types of metalation of the pincer ligands with both precious and non-precious transition metals and their applications in catalysis.

In Chapter 2, the history behind the design and synthesis of PYP pincer ligands is described. The advantages of these type ligands are reviewed to show the reasoning behind the development of a new series of 2,6-diaminopyridine-based PNP pincer ligands with different phosphine moieties.

The synthesis of a series of tricarbonyl molybdenum and tungsten complexes $[M(\text{PNP})(\text{CO})_3]$ (M = Mo, W) are discussed in Chapter 3. These complexes were afforded by a simple and practical solvothermal method. Moreover, this research allowed a direct comparison of steric and electronic properties of Mo and W metal PNP pincer complexes.

In Chapter 4, the reaction of $[M(\text{PNP})(\text{CO})_3]$ (M = Mo, W) with HBF_4 in CH_2Cl_2 is described which led to the protonation at the metal center and formation of hydrido carbonyl complexes of the type $[M(\text{PNP})(\text{CO})_3\text{H}]^+$. These Mo(II) and W(II) complexes exhibit fluxional behavior in solution. Protonation is full reversible and upon addition of a base such as trimethylamine the $[M(\text{PNP})(\text{CO})_3]$ complexes are reformed. Attempts to utilize the hydrido Mo complexes as catalysts for hydrogenations were unsuccessful. On the other hand, these complexes were catalytically active for the isomerization of terminal alkenes.

In order to better understand how the properties of the ligands affect the reactivity of the metal complexes, a comparative study of a series of halocarbonyl Mo(II) and W(II) complexes featuring PNP pincer ligands was carried out which is described in Chapter 5. These complexes were obtained by treatment of $[M(\text{PNP})(\text{CO})_3]$ with stoichiometric amounts of I_2 and Br_2 , respectively.

In the case of the PNP with NH linkers the general cationic seven-coordinate complexes of the type $[M(\text{PNP})(\text{CO})_3\text{X}]^+$ were obtained, while with NMe and NPh spacers neutral seven-coordinate complexes of the type $[M(\text{PNP})(\text{CO})_2\text{X}_2]$ were afforded. DFT calculations suggest that all complexes are under thermodynamic control. The only exception is the molybdenum in conjunction with the $\text{PNP}^{\text{Me-}i\text{Pr}}$ ligand, where the coordinatively unsaturated complex $[\text{Mo}(\text{PNP}^{\text{Me-}i\text{Pr}})(\text{CO})\text{X}_2]$ is formed. The introduction of different amino linkers in the pincer framework with concomitant modification of the phosphine moieties changed the steric and electronic properties of the PNP ligand significantly and led to different types of halocarbonyl complexes. Reactivity studies clearly show that complexes of type $[M(\text{PNP})(\text{CO})_3\text{X}]^+$ are also intermediates of the other two Mo and W halocarbonyl complexes, $[M(\text{PNP})(\text{CO})_2\text{X}_2]$ (M = Mo and W) and $[\text{Mo}(\text{PNP})(\text{CO})\text{X}_2]$.

In Chapter 6, the synthesis of cationic coordinately unsaturated mono oxo Mo (IV) complexes of the type $[\text{Mo}(\text{PNP}^{\text{Me-}i\text{Pr}})(\text{O})\text{X}]^+$ was achieved through an interplay between water and molecular oxygen from the $[\text{Mo}(\text{PNP}^{\text{Me-}i\text{Pr}})(\text{CO})\text{X}]^+$. This intermediate is prepared *in situ* by reacting $[\text{Mo}(\text{PNP}^{\text{Me-}i\text{Pr}})(\text{CO})\text{X}_2]$ with 1 equiv of a silver salt. ESI MS measurements with labeled water (H_2^{18}O) and molecular oxygen ($^{18}\text{O}_2$) reveal that the oxygen of the $\text{Mo}\equiv\text{O}$ unit originates from water and DFT calculations support this experimental finding.

In Chapter 7, the synthesis and characterization of a series of Mo(III) complexes of the type $[\text{Mo}(\text{PNP})\text{Br}_3]$ is described. However, no further reactions were carried out with these compounds.

In Chapter 8, similar to the analogous PNP systems, a preliminary study of PCP pincer ligands to obtain hydridocarbonyl Mo(II) and W(II) complexes of the type $[M(\text{PCP}^{\text{Me-}i\text{Pr}})(\text{CO})_3\text{H}]$ was carried out. In the case of Cr and Mo agostic complexes $[M(\kappa^3\text{P},\text{CH},\text{P}-\text{P}(\text{CH})\text{P}^{\text{Me-}i\text{Pr}})(\text{CO})_3]$ were formed and no C-H bond cleavage took place, while with W the expected W(II) hydride complex was formed.

Zusammenfassung

Übergangsmetallkomplexe, die Pincer Liganden enthalten, zeigen aufgrund ihrer thermischen Stabilität und Reaktivität eine bemerkenswerte Vielseitigkeit. Das kann durch entsprechende Ligandenmodifikationen (Modifikationen der sterischen und elektronischen Eigenschaften) oder Variation des Metallzentrums gesteuert werden. Pincer Liganden, die Phosphine oder Phosphite als Donorgruppen (PYP) enthalten, sind die am häufigsten in der Literatur gefundene Substanzklasse. Das Hauptziel dieser Arbeit war es, Molybdän- und Wolfram PNP- und auch PCP Pincer Komplexe zu synthetisieren und deren Chemie zu untersuchen.

In diesem Zusammenhang wird in Kapitel 1 ein allgemeiner Überblick über die Chemie der Pincer Liganden gegeben, der alle möglichen Modifikationen dieses Ligandentyps beleuchtet. Dabei werden sowohl edle, wie auch unedle Metallkomplexe mit Pincer Liganden beschrieben.

In Kapitel 2 wird die Geschichte hinter dem Design und der Synthese von PYP-Pincer Liganden beschrieben. Die Vorteile dieses Ligandentyps werden überprüft, um die Argumentation hinter der Entwicklung einer neuen Reihe von 1,6-Diaminopyridin-basierten PNP-Pinzettenliganden mit verschiedenen Phosphinresten zu zeigen.

Die Synthese einer Reihe von Tricarbonylmolybdän- und Wolframkomplexen, die die PNP-Liganden betreffen wird in Kapitel 3 diskutiert. Die Komplexe, $[M(\text{PNP})(\text{CO})_3]$ ($M = \text{Mo}, \text{W}$) wurden durch eine einfache und praktische solvotherme Methode dargestellt. Darüber hinaus ermöglicht diese Untersuchung einen direkten Vergleich von sterischen und elektronischen Eigenschaften von Mo und W-Metall-PNP-Pincer Komplexen.

In Kapitel 4 führte die Reaktion von $[M(\text{PNP})(\text{CO})_3]$ ($M = \text{Mo}, \text{W}$) mit HBF_4 in CH_2Cl_2 zur Protonierung am Metallzentrum unter Bildung von Hydrido Carbonylkomplexe des Typs $[M(\text{PNP})(\text{CO})_3\text{H}]^+$. Diese Mo(II) und W(II) Komplexe zeigten ein dynamisches Verhalten in Lösung und können bei Zugabe einer Base, wie Trimethylamin, wieder leicht reversibel deprotoniert werden. Versuche die Hydrido Molybdänkomplexe als Katalysatoren für Hydrierungen einzusetzen waren nicht erfolgreich. Auf der anderen Seite waren diese Komplexe aktive Katalysatoren für die Isomerisierung von terminalen Alkenen.

Um besser zu verstehen, wie sich die Eigenschaften der Liganden auf die Reaktivität und Stabilität der Metallkomplexe auswirken, wurde in Kapitel 5 eine Vergleichsstudie einer Reihe von Halogencarbonyl Mo(II) und W(II) PNP Pincer Komplexen durchgeführt. Die Halogencarbonyl Komplexe wurden durch Umsatz von $[M(\text{PNP})(\text{CO})_3]$ mit stöchiometrischen Mengen von I_2 bzw. Br_2 dargestellt. Im Falle der

PNP Komplexe mit NH-Linkern wurden kationische siebenfach koordinierte Komplexe vom Typ $[M(\text{PNP})(\text{CO})_3\text{X}]^+$ erhalten. Mit Systemen mit NMe und NPh-Linker wurden neutrale siebenfach koordinierte Komplexe vom Typ $[M(\text{PNP})(\text{CO})_2\text{X}_2]$ gebildet. DFT-Berechnungen weisen darauf hin, dass alle Komplexe unter thermodynamischer Kontrolle stehen. Die einzige Ausnahme sind Molybdänkomplexe in Verbindung mit dem $\text{PNP}^{\text{Me-}i\text{Pr}}$ -Liganden, bei dem der koordinativ ungesättigte Komplex $[\text{Mo}(\text{PNP}^{\text{Me-}i\text{Pr}})(\text{CO})\text{X}_2]$ gebildet wird. Die Einführung verschiedener Linker mit gleichzeitiger Modifikation der Phosphinreste veränderte die sterischen und elektronischen Eigenschaften des PNP-Liganden signifikant und führte zu verschiedenen Arten von Halogenacetylkomplexen. Reaktivitätsstudien zeigen deutlich, dass Komplexe vom Typ $[M(\text{PNP})(\text{CO})_3\text{X}]^+$ auch Zwischenprodukte der beiden anderen Mo und W Halogenacetylkomplexe $[M(\text{PNP})(\text{CO})_2\text{X}_2]$ ($M = \text{Mo}$ und W) und $[\text{Mo}(\text{PNP})(\text{CO})\text{X}_2]$ sind.

In Kapitel 6 wurde die Synthese von kationischen, koordinativ ungesättigten mono oxo Mo(IV) Komplexen des Typs $[\text{Mo}(\text{PNP}^{\text{Me-}i\text{Pr}})(\text{O})\text{X}]^+$ synthetisiert. Diese Verbindung wurde durch ein Zusammenspiel von Wasser und molekularem Sauerstoff mit $[\text{Mo}(\text{PNP}^{\text{Me-}i\text{Pr}})(\text{CO})\text{X}]^+$ erhalten. Dieser Komplex wurde *in situ* durch Umsetzung von $[\text{Mo}(\text{PNP}^{\text{Me-}i\text{Pr}})(\text{CO})\text{X}_2]$ mit Silbersalzen hergestellt. ESI-MS-Messungen mit markiertem Wasser (H_2^{18}O) und molekularem Sauerstoff ($^{18}\text{O}_2$) zeigen, dass der Sauerstoff der $\text{Mo}\equiv\text{O}$ -Einheit aus Wasser stammt. Dies wird auch durch DFT-Berechnungen untermauert.

Eine Reihe von neuen Tribromo Mo(III) PNP Komplexen vom Typ $[\text{Mo}(\text{PNP})\text{Br}_3]$ wurden in Kapitel 7 beschrieben. Es wurden jedoch keine weiteren Reaktionen erfolgreich durchgeführt.

In Kapitel 8 wurde dann eine Untersuchung von PCP-Pincer Liganden zur Darstellung von Hydridocarbonyl-Mo(II) und W(II) Komplexen vom Typ $[M(\text{PCP}^{\text{Me-}i\text{Pr}})(\text{CO})_3\text{H}]$ durchgeführt. Im Falle von Cr und Mo wurden jedoch die agostischen Komplexe $[M(\kappa^3\text{P},\text{CH},\text{P}-\text{P}(\text{CH})\text{P}^{\text{Me-}i\text{Pr}})(\text{CO})_3]$ gebildet und es erfolgte keine CH Bindungsspaltung. Bei Wolfram hingegen wurde der erwartete Hydridocarbonyl-W(II) Komplex erhalten.

Index

Acknowledgements.....	i
Abstract.....	ii
Zusammenfassung.....	iv
Chapter 1 – Introduction.....	1
1.1. Fragments of the pincer framework.....	2
1.2. Binding modes and metalation of pincer ligands.....	4
1.3. Transition metals for pincer complexes.....	7
1.4. Example for applications.....	8
1.5. Aim of the thesis.....	12
1.6. References.....	13
Chapter 2 – Phosphine Based Pincer Ligands.....	15
2.1. Pyridine backbone.....	17
2.2. Amine spacers.....	18
2.3. Synthesis of PNP ligands.....	19
2.4. Results and discussion.....	21
2.5. Conclusions.....	23
2.6. Experimental part.....	24
2.6.1. Synthesis.....	24
2.7. References.....	26
Chapter 3 – Tricarbonyl Molybdenum and Tungsten PNP Pincer Complexes..	28
3.1. Carbonyl ligand.....	29
3.2. Carbonyl pincer complexes.....	31
3.3. Synthesis of Mo and W PNP carbonyl complexes.....	34
3.4. Results and discussion.....	35
3.4.1. Pyridine versus triazine backbones.....	40
3.4.2. Steric effect of linkers.....	41
3.5. Conclusions.....	43
3.6. Experimental part.....	43
3.6.1. Syntheses.....	43
3.6.2. X-ray structure determinations.....	53
3.7. References.....	53
Chapter 4 – Hydrides Hydrido Carbonyl Molybdenum and Tungsten PNP Pincer Complexes.....	56
4.1. Metal-hydrogen bond.....	57
4.2. Mo and W hydrides.....	57

4.3. Mo and W pincer hydrides.....	60
4.4. Results and discussion.....	62
4.4.1. Catalytic applications.....	65
4.5. Conclusions.....	67
4.6. Experimental part.....	67
4.6.1. Synthesis.....	67
4.6.2. General procedure for the catalytic applications.....	74
4.7. References.....	74
Chapter 5 – Halocarbonyl Molybdenum and Tungsten PNP pincer complexes	76
5.1. Molybdenum and tungsten.....	77
5.2. Mo and W PNP pincer halocarbonyl.....	78
5.3. Results and discussion.....	79
5.3.1. Reactivity.....	91
5.3.2. Fluorine complexes.....	99
5.4. Conclusions.....	102
5.5. Experimental part.....	102
5.5.1. Syntheses.....	103
5.5.2. Computational details.....	120
5.6. References.....	121
5.7. Annex.....	124
Chapter 6 – Mono Oxo Molybdenum (IV) PNP Pincer Complexes.....	128
6.1. Metal-oxo.....	129
6.2. Molybdenum oxo complexes.....	130
6.3. Results and discussion.....	131
6.3.1. Mono oxo molybdenum complexes.....	136
6.4. Conclusions.....	145
6.5. Experimental part.....	146
6.5.1. Synthesis.....	146
6.6. References.....	150
Chapter 7 – Molybdenum (III) PNP Pincer Complexes.....	152
7.1. Molybdenum and tungsten pincer halides.....	153
7.2. Results and discussion.....	155
7.3. Conclusions.....	158
7.4. Experimental part.....	159
7.4.1. Synthesis.....	159
7.5. References.....	161
Chapter 8 – PCP vs PNP Pincer Complexes.....	162

8.1. Pincer complexes with agnostic interaction.....	164
8.2. Results and Discussion.....	165
8.2.1. Mechanist study.....	173
8.2.2. Reactivity.....	176
8.3. Conclusions.....	177
8.4. Experimental part.....	178
8.4.1. Syntheses.....	178
8.5. References.....	181
8.6. Annex.....	184
Chapter 9 – Curriculum Vitae.....	187

Chapter 1

Introduction

The synthesis of well-defined catalysts is a very important topic in organometallic and organic chemistry, especially with respect to the development and improving of chemical processes that are efficient, selective, high yielding and environmentally friendly. A starting point for the discovery of new and improved catalysts is the creation of appropriate ligand systems, which are able to stabilize a reactive metal center in a unique coordination environment while simultaneously conferring desirable reactivity properties.

Therefore, from a wide range of polydentate ligand systems available in literature, the one attracting considerable attention in the last decades are so called pincer ligands. This tridentate ligand system, named after their particular coordination mode to the metal center, exhibit an aromatic or aliphatic backbone bound to two-electron donor fragments by a variety of spacer groups. The major advantages of pincer ligands lie in the formation of metal complexes that are incredibly robust and have unusual thermal stability. These are the key factors for a variety of applications such as medicinal chemistry, chemical sensing and catalysis, especially the ones requiring high temperatures and pressures. Nevertheless, the modular nature of this tridentate ligand design offers an attractive way of manipulating the steric and electronic features of the subsequent metal complexes.^{1,2}

For metal complexes created from pincer ligands, nomenclature shown in Figure 1.1. is used, where the three atoms directly attached to the metal center are indicated by EYE'. The pioneer and most widely studied complexes of this type are the phosphine-based PCP pincer complexes reported by Shaw in the 1970s.³ Since then, significant effort has been devoted to the synthesis of systems where strategic alterations have been introduced to the pincer framework.^{1,2}

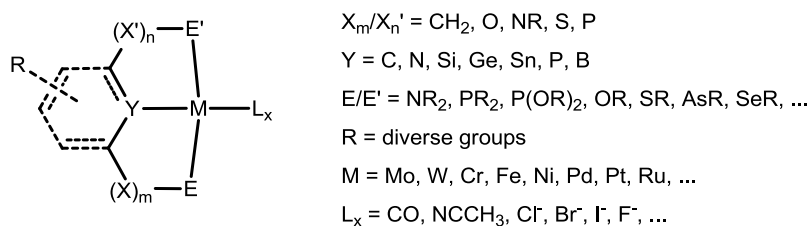


Figure 1.1. Schematic structure of pincer complexes

1.1. Fragments of the pincer framework

The advantage of pincer ligands is their huge variability of possible modifications to the central moiety, the donor fragments and changes of

electronic/steric effects, which can be accomplished in numerous ways, some examples are depicted in Figure 1.2.. The first change is the ligand backbone, which is most commonly an aromatic ring. However, possible modifications are in the ring itself (benzene, pyridine, acridine, pyrrole, etc.) (**A₁**), in the ring size (five, six, or seven membered), in the nature of the ring (aromatic or aliphatic), or even conversion of the ring in an acyclic pincer (**A₂**). Nonetheless, the properties can be change in the presence of diverse substituents either in the aromatic or in the aliphatic central group, in many cases, providing unsymmetrical backbones (**A₃**).^{1,2}

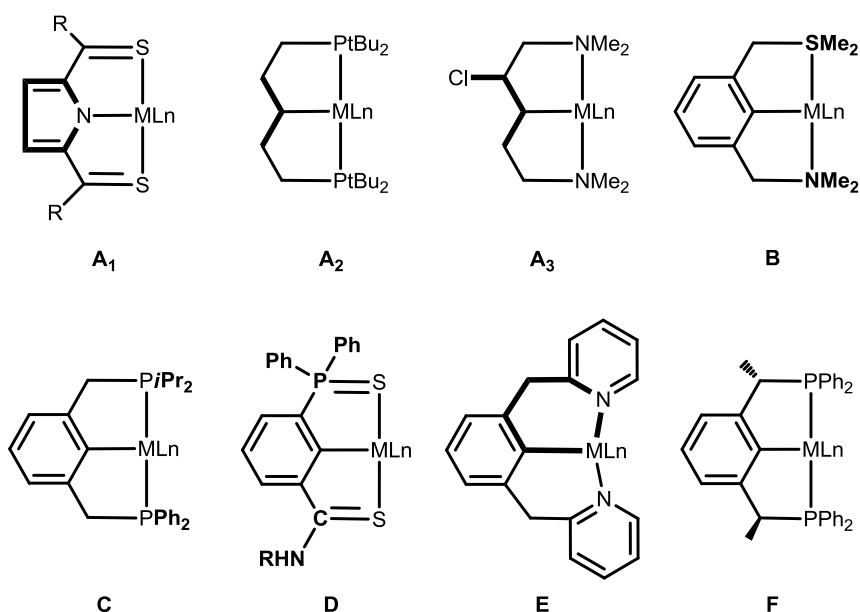


Figure 1.2. Examples of different pincer complexes

The central donor (Y) has largely been restricted to the elements C and N, however in recent years the study of pincer ligands featuring other types of central donor elements, such as B, Si, Ge, Sn and P, can be found in the literature. Depending on the formal charge on the central atom, two main categories are distinguished, the anionic and the neutral ones.

Regarding the donor groups (E/E'), typically amines (NR₂), phosphines (PR₂), phosphites (P(OR)₂), ethers (OR), thioethers (SR), and even N-heterocyclic carbenes (NHCs), arsines (AsR₂), and selenoethers (SeR) are used. In general these fragments are identical, however systems with two different donor groups (**B**), or with identical donating atoms but with different substituents (**C**), structuring an unsymmetrical pincer, were already reported.

The substituents E/E' are connected to the ligand backbone by different spacers (X/X') that contain elements like C, N, P, O and S empowering the possibility of methylene groups, amines and so fourths. These linkers can be identical but there are some examples in literature where these are unequal (**D**). The extension of the spacer groups forming pincer complexes featuring differently membered fused metallacycles (**E**) is another possible modification. Additionally to all of these transformations a further possibility is the implementation of chiral ligand (**F**), which is a field of growing interest.^{1,2}

1.2. Binding modes and metalation of pincer ligands

All of the possible modifications in the framework of the ligand provide a huge range of pincer ligands that routinely coordinates in a terdentate way to the metal center. In some cases the pincer complexes present other binding modes such as κ^1 -Y monodentate (**A**) (Figure 1.3.) or κ^2 -E,Y bidentate (**B**). The dominant tridentate coordination mode is usually the meridional (**C**), nonetheless facial coordination (**D**) occasionally has been observed. Another rare bonding mode that has been reported is the center atom binding to two metals (**E**).^{1,2}

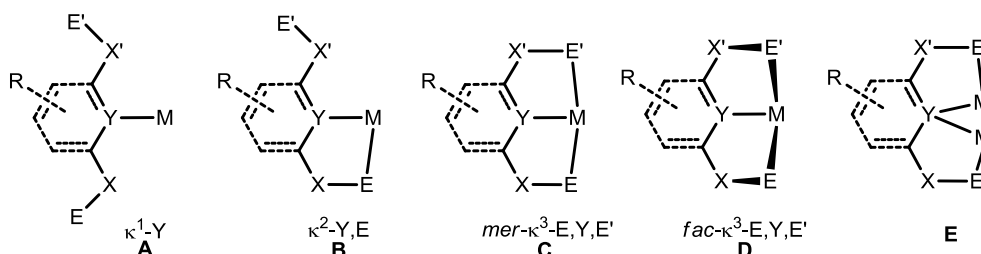
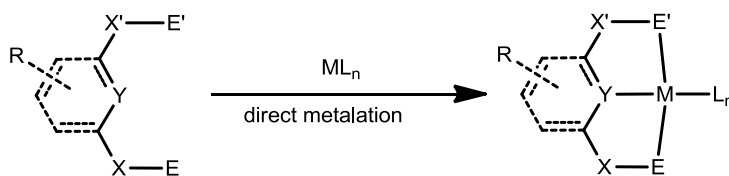


Figure 1.3. Coordination modes found for EYE' pincer complexes

Considering the attention that pincer metal complexes are attracting, the strategies for metalation of these ligands have played a significant role in the synthesis of such compounds. Diverse methods for the metalation of the pincer ligands have been developed and it was discovered that the appropriate route of synthesis strongly depends on the transition metal (M) and the nature of the E and E' donor atoms of the ligand.^{1,2}

Presumably, the simplest and most efficient way to synthesize pincer complexes is implementing the direct metalation (Scheme 1.1.), however it is restricted to the synthesis of those complexes incorporating heteroatoms in the three

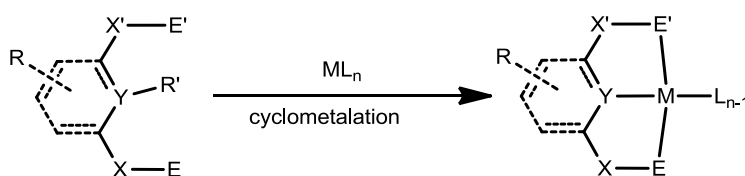
coordination sites, where the cleavage of a bond is not necessary. The steric effect around the donor centers of the pincer ligand has great impact on the probability of bonding to the metal center.



Scheme 1.1. Direct metalation of pincer ligands

In this method, the use of a suitable metal precursor with labile coligands is sufficient, due to the chelating coordination mode of the pincer ligands, the metal precursor coligands are easily displaced and the coordination usually takes place in short reaction time under mild conditions. The best candidates for this type of method are the pyridine based pincer ligands, e.g. PNP, PNN, PNS, NNN.

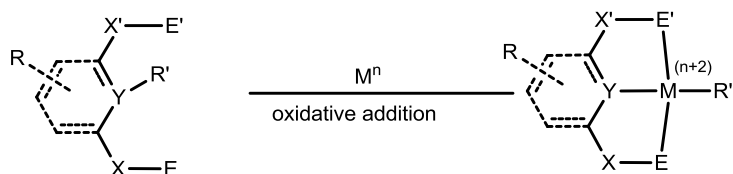
When the pincer ligands require the cleavage of a bond, one particularly attractive method is the direct cyclometalation (Scheme 1.2.) since it does not need prefunctionalization of the pincer ligands to form the new M-C bond.



Scheme 1.2. Cyclometalation of pincer ligands

Cyclometalation refers to the transition metal-mediated activation of a C-R bond to form a metallacycle comprising a new metal-carbon σ -bond. Some types of pincer ligands, such as PCP with a wide variety of phosphanes, were successfully used in this type of metalation.

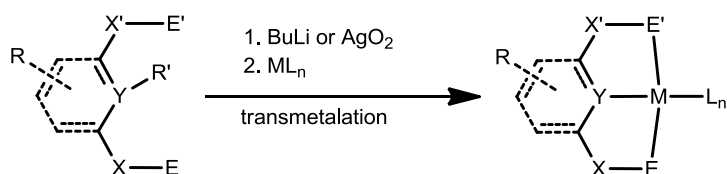
Another method to synthesize pincer complexes is oxidative addition (Scheme 1.3.), necessary for some ligands, such as NCN, since they are more resistant to direct cyclometalation.



Scheme 1.3. Oxidative addition of pincer ligands

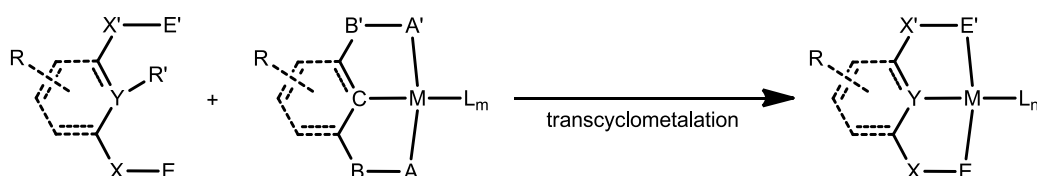
The metal precursor in a low oxidation state adds to the carbon-halogen bond of the pincer ligand via oxidative addition. This prevents the formation of acid-labile or thermally unstable substituents and has the advantage of reaction under milder conditions.

Transmetalation (Scheme 1.4.) is a reaction that involves the transfer of ligands from one metal to another. During transmetalation the metal–carbon bond is activated, leading to the formation of new metal–carbon bonds. Silver or lithium pincer complexes easily undergo exchange reaction with metal precursors, due to formation of very stable precipitating salts.



Scheme 1.4. Transmetalation addition of pincer ligands

Additionally, the exchange of a cyclometallated ligand at the metal center with another one without the formation of significant amounts of purely inorganic compounds is designated a transcyclometalation (Scheme 1.5.).



Scheme 1.5. Transcyclometalation addition of pincer ligands

In this method, the relatively weakly coordinated ligand is substituted by an incoming stronger bonding ligand, such as the substitution of NCN with PCP, where the hard amine ligands are replaced by the phosphine ligands.

1.3. Transition metals for pincer complexes

Over the years, the chemistry of pincer complexes were mainly focus on the platinum group metals (Ru, Os, Rh, Ir, Pd, Pt), some examples are display in Figure 1.4.. The formation and the properties of a large variety of these pincers complexes have provided direct access to a fundamental understanding of a variety of reactions in organometallic chemistry and to a range of new applications of these complexes.⁴⁻⁹

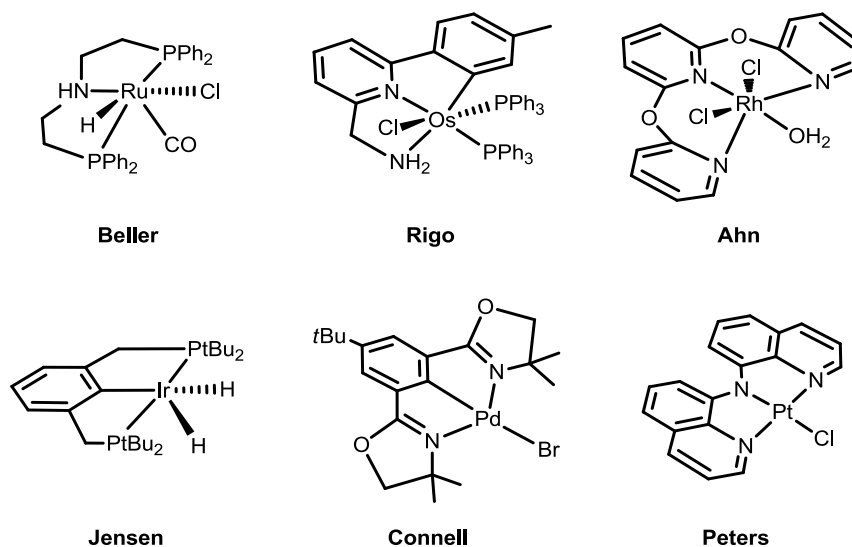


Figure 1.4. Examples of precious metals pincer complexes

Pincer complexes with precious metals possess a long and successful history in homogeneous catalysis, however the limited availability of precious metals, their high price and their toxicity diminish their attractiveness in the long run. Therefore, more economical and environmentally friendly alternatives have to be found which are in the line with green chemistry strategies. A few examples of this type of compounds are depicted in Figure 1.5..¹⁰⁻¹⁵

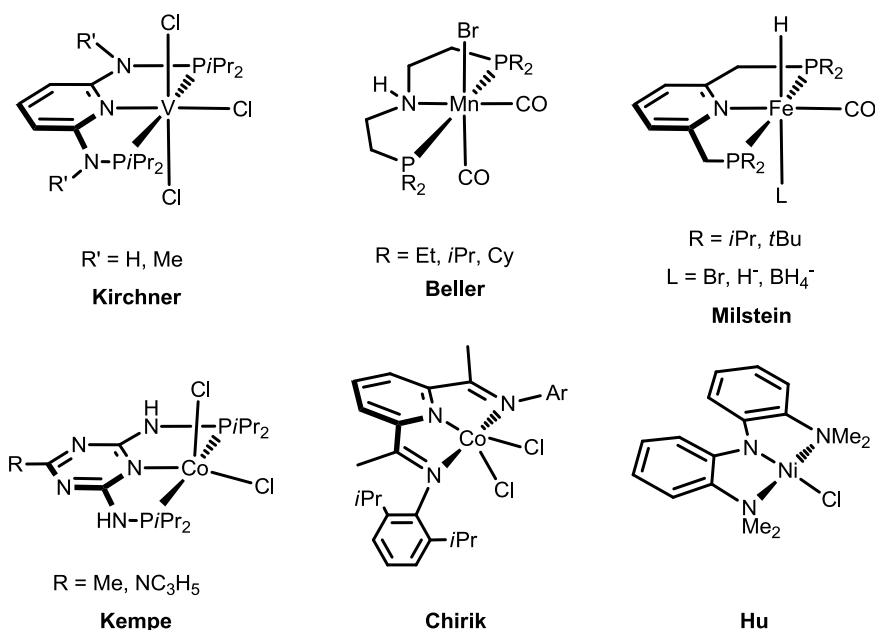
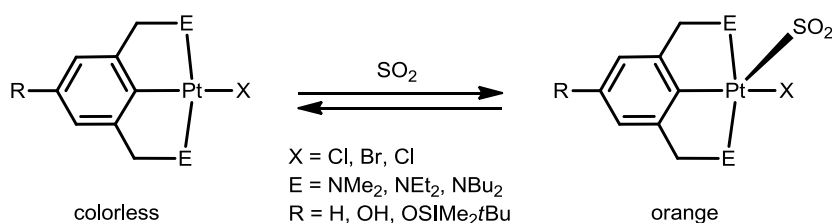


Figure 1.5. Examples of non-precious metal pincer complexes

1.4. Examples for applications

In terms of chemical sensing, an example are complexes with organoplatinum NCN pincer ligands (Albrecht and van Koten, 1999) that turned out to be excellent candidates for SO_2 detection (Scheme 1.6.). These complexes bind SO_2 reversibly in the solid state and in solution accompanied by color change upon coordination of SO_2 .¹⁶



Scheme 1.6. Example of a pincer complex applied as gas sensor (SO_2 detection)

An example for a medical application are the new fluorescent Re tricarbonyl bioconjugates (Figure 1.6.) synthesized by Doyle, Zubieta, and co-workers that targeted the cubilin receptor through the vitamin B12 uptake pathway. This study demonstrated great potential of cubilin as a new target for the delivery of B12 based conjugates for cancer diagnostics and treatment.¹⁷

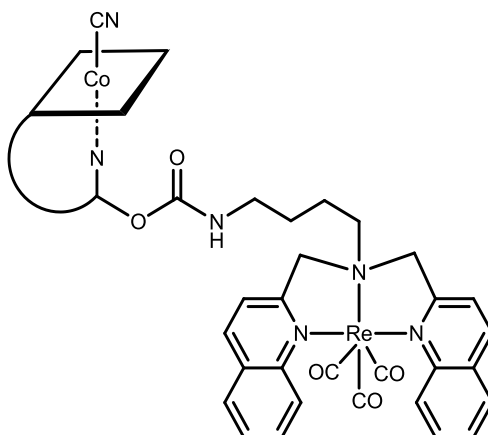
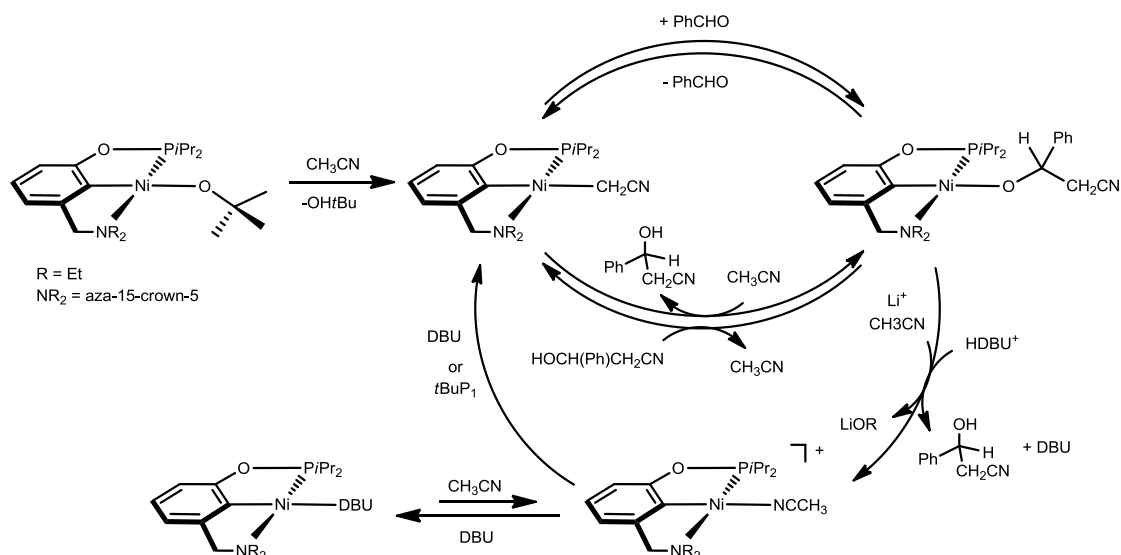


Figure 1.6. Example of a pincer complex applied in medical applications

Among all possible applications, the major focus is in homogeneous catalysis, since these species exhibit a well-defined stoichiometry, which allows conscious catalyst design and fine-tuning of the reactivity and selectivity of the catalyst. Not to mention the unusual thermal stability of the metal complexes provided by the special tridentate ligands. Some recent examples of catalytically active pincer complexes and the reactions they catalyze are noteworthy.

Neutral and cationic nickel catalysts supported by diethylamine- or aza-crown ether-containing aminophosphinite (NCOP) pincer ligands catalyze the insertion of benzaldehyde into a C-H bond of acetonitrile (Scheme 1.7.).

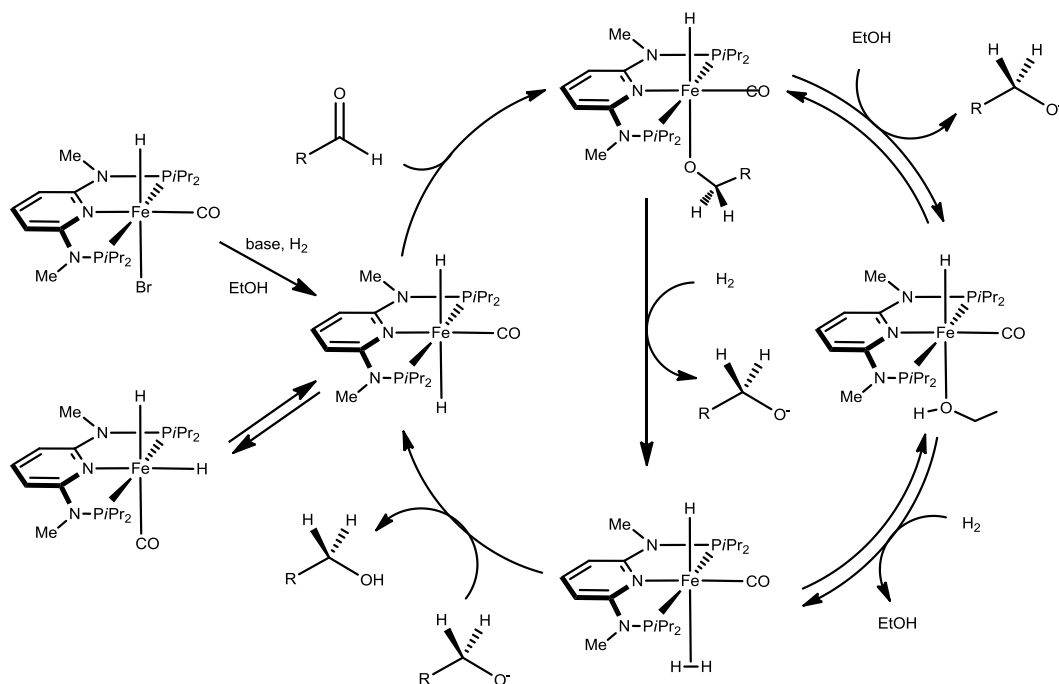
The neutral tert-butoxide precatalysts are active without any added base and give good yields of product after 24 h, while the cationic precatalysts require a base cocatalyst and operate more slowly. The deactivated cationic species is inactive under standard base-free conditions. However catalysis can be reinitiated by the addition of catalytic amounts of base.¹⁸



Scheme 1.7. Proposed mechanism for the Ni-catalyzed benzaldehyde insertion into a C-H bond

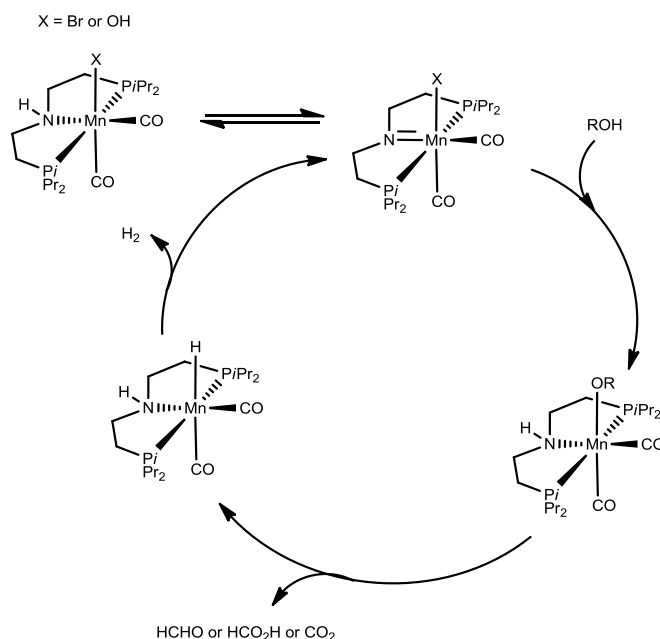
In 2016, an inexpensive and robust homogeneous precatalyst and catalyst using earth-abundant iron, $[\text{Fe}(\text{PNP}^{\text{Me}}\text{-}i\text{Pr})(\text{CO})(\text{H})(\text{Br})]$ and $[\text{Fe}(\text{PNP}^{\text{Me}}\text{-}i\text{Pr})(\text{H})_2(\text{CO})]$, based on the 2,6-diaminopyridine scaffold where the $PiPr_2$ moieties of the PNP ligand connect to the pyridine ring via NMe spacers, was developed and applied to the hydrogenation of several aldehydes to alcohols in the presence of DBU as base (Scheme 1.8.).

These systems were found to be among the most efficient catalysts for this process reported to date and constitute rare examples of a catalytic process which allows selective reduction of aldehydes in the presence of ketones and other reducible functionalities. In some cases, TONs and TOFs of up to 80000 and 20000 h^{-1} , respectively, were reached.¹⁹



Scheme 1.8. Proposed simplified catalytic cycle for the chemoselective hydrogenation of aldehydes with dihydrogen to give alcohols on the bases of experimental findings

In the same year, it was demonstrated for the first time that pincer complexes based on nontoxic and easily available manganese successfully promote the selective dehydrogenation of aqueous methanol (Scheme 1.9.). Under optimized reaction conditions, an impressive TON of more than 20000 was attained and the catalyst was still active after one month. These promising results show that such molecularly defined nonnoble metal catalysts can be extremely stable and robust, which is also of importance for future applications.²⁰



Scheme 1.9. Proposed catalytic cycle for the Mn-catalyzed aqueous-phase reforming of methanol

1.5. Aim of the research

The central focus of the work presented in this thesis involves the study of coordination and reactivity of molybdenum and tungsten PNP pincer complexes based on a 2,6-diaminopyridine scaffold with modifications on the amino group and different phosphine moieties. The unique reactivity displayed by pincer complexes, coupled with their great thermal stability, makes the synthesis of novel pincer ligands and complexes a highly relevant and important field of research. The modular nature of pincer ligands gives rise to a large number of opportunities for innovation. Therefore, the first keystone of this project deals with the synthesis of new PNP pincer ligands using different substituents on the phosphorus donor and on the spacer groups.

Molybdenum and tungsten compounds are found to be stable in a wide variety of oxidation states (M^0 - M^{VI}) and because of the possibility to switch easily between these oxidation states they are commonly used for catalytic applications. Surprisingly, the chemistry of pincer complexes with Mo and W is still hardly explored. Consequently, an important part of this thesis involves the synthesis of Mo and W complexes in different oxidation states with diverse PNP pincer ligands. To assess the impact of the modifications on the pincer ligands comparative studies of the Mo and W complexes and mechanistic studies will be investigate.

Several important reactions that can be efficiently catalyzed by Mo, such as olefin metathesis, olefin epoxidation and fixation and activation of dinitrogen. Therefore, reactions will be carried out with molybdenum compounds, to evaluate their effects on the catalytic activity. Finally, parallel to this study is the preliminary research of PNP versus PCP pincer complexes of molybdenum and tungsten.

1.6. References

- [1] For reviews on pincer complexes, see: a) Gossage, R. A.; van de Kuil, L. A.; van Koten, G.; *Acc. Chem. Res.*, **1998**, *31*, 423-431; b) Albrecht, M.; Van Koten, G.; *Angew. Chem., Int. Ed.*, **2001**, *40*, 3750-3781; c) Van der Boom, M. E.; Milstein, D.; *Chem. Rev.*, **2003**, *103*, 1759-1792; d) Singleton, J. T.; *Tetrahedron*, **2003**, *59*, 1837-1857; e) Morales-Morales, D.; *Rev. Soc. Quím. Méx.*, **2004**, *48*, 338-346; f) Liang, L. C.; *Coord. Chem. Rev.*, **2006**, *250*, 1152-1177; g) Nishiyama, H.; *Chem. Soc. Rev.*, **2007**, *36*, 1133-1141; h) Morales-Morales, D.; Jensen, C. M.; *The Chemistry of Pincer Compounds*, **2007**, Elsevier, Amsterdam; i) Benito-Garagorri, D.; Kirchner, K.; *Acc. Chem. Res.*, **2008**, *41*, 201-213; j) Vlugt, J. I.; Reek, J. N. H.; *Angew. Chem. Int. Ed.*, **2009**, *48*, 8832-8846; k) Bhattacharya, P.; Guan, H.; *Comment. Inorg. Chem.*, **2011**, *32*, 88-112; l) Choi, J.; MacArthur, A. H. R.; Brookhart, M.; Goldman, A. S.; *Chem. Rev.*, **2011**, *111*, 1761-1779; m) Selander, N.; Szabo, K. J. *J. Chem. Rev.*, **2011**, *111*, 2048-2076; n) Schneider, S.; Meiners, J.; Askevold, B.; *Eur. J. Inorg. Chem.*, **2012**, 412-429; o) Wang, Z.; Liu, N.; *Eur. J. Inorg. Chem.*, **2012**, 901-911; p) Van Koten, G.; Milstein, D.; *Top. Organomet. Chem., in Organometallic Pincer Chemistry, ed.*, **2013**, Springer, Berlin; q) Szabo, K. J.; Wendt, O. F.; *Pincer and Pincer-Type Complexes: Applications in Organic Synthesis and Catalysis*, **2014**, Wiley-VCH, Germany; r) Deng, Q.; Melen, R. L.; Gade, L. H.; *Acc. Chem. Res.*, **2014**, *47*, 3162-3173.
- [2] For recent reviews on pincer complexes a) Asay, M.; Morales-Morales D.; *Dalton Trans.*, **2015**, *44*, 17432-17447; b) Li, H.; Zheng, B.; Huang, K.; *Coordination Chemistry Reviews*, **2015**, *293-294*, 116-138; c) Younus, H. A.; Su, W.; Ahmad, N.; Chen, S.; Verpoort, F.; *Adv. Synth. Catal.*, **2015**, *357*, 283-330; d) Murugesan, S.; Kirchner, K.; *Dalton Trans.*, **2016**, *45*, 416-439; e) Koten, G. V.; Gossage, R. A.; *Top. Organomet. Chem., in The Privileged Pincer-Metal Platform: Coordination Chemistry & Applications, ed.*, **2016**, Springer, Berlin; f) Renaud, J.; Gaillard, S.; *Synthesis*, **2016**, *48*, 3659-3683.
- [3] Moulton, C. J.; Shaw, B. L.; *J. Chem. Soc., Dalton. Trans.*, **1976**, 1020-1024.
- [4] Monney, A.; Barsch, E.; Sponholz, P.; Junge, H.; Ludwig R.; Beller, M.; *Chem. Commun.*, **2014**, *50*, 707-709.
- [5] Baratta, W.; Ballico, M.; Chelucci, G.; Siega, K.; Rigo, P.; *Angew. Chem. Int. Ed.*, **2008**, *47*, 4362-4365.
- [6] Raja, M. U.; Ramesh, R.; Ahn, K. H.; *Tetrahedron Letters*, **2009**, *50*, 7014-7017.
- [7] Jensen, C. M.; *Chem. Commun.*, **1999**, 2443-2449.

- [8] Bugarin, A.; Connell, B. T.; *Chem. Commun.*, **2011**, 47, 7218-7220.
- [9] Harkins, S. B.; Peters, J. C.; *Organometallics*, **2002**, 21, 1753-1755.
- [10] Mastalir, M.; Glatz, M.; Stöger, B.; Weil, M.; Pittenauer, E.; Allmaier, G.; Kirchner, K.; *Inorganica Chimica Acta*, **2017**, 455, 707-714.
- [11] Elangovan, S.; Garbe, M.; Jiao, H.; Spannenberg, A.; Junge, K.; Beller, M.; *Angew. Chem. Int. Ed.*, **2016**, 55, 15364 –15368.
- [12] Zell, T.; Milstein, D.; *Acc.Chem.Res.*, **2015**, 48, 1979-1994.
- [13] Rösler, S.; Obenauf, J.; Kempe, R.; *J. Am. Chem. Soc.*, **2015**, 137, 7998-8001.
- [14] Bowman, A. C.; Milsman, C.; Atienza, C. C. H.; Lobkovsky, E.; Wieghardt, K.; Chirik, P. J.; *J. AM. CHEM. SOC.*, **2010**, 132, 1676-1684.
- [15] Franco, T. D.; Epenoy, A.; Hu, X.; *Org. Lett.*, **2015**, 17, 4910-4913.
- [16] Korotcenkov, G; *Handbook of Gas Sensor Materials: Properties, Advantages and Shortcomings for Applications, Volume 2 New Trends and Technologies*, **2014**, Springer.
- [17] Viola-Villegas, N.; Rabideau, A. E.; Bartholoma, M.; Zubieta, J.; Doyle, R. P.; *J. Med. Chem.*, **2009**, 52, 5253-5261.
- [18] Smith, J. B.; Miller, A. J. M.; *Organometallics*, **2015**, 34, 4669-4677.
- [19] Gorgas, N.; Stöger, B.; Veiros, L. F.; Kirchner, K.; *ACS Catal.*, **2016**, 6, 2664-2672.
- [20] Andérez-Fernández, M.; Vogt, L. K.; Fischer, S.; Zhou, W.; Jiao, H.; Garbe, M.; Elangovan, S.; Junge, K.; Junge, H.; Ludwig, R.; Beller, M.; *Angew. Chem. Int. Ed.*, **2017**, 56, 559-562.

Chapter 2

Phosphine Based Pincer

Ligands

Among the legion of pincer complexes reported in the literature, the ones which demonstrated the highest applicability contain at least one phosphorus atom directly attached to the metal center. The benefit of incorporating this group donor is due to its soft electronic nature and its σ -donor/ π -acceptor character.¹ The PYP metal complexes are famous for their performance in homogenous catalysis and small molecule activation. Reactions such as Kumada² (**A**) (Figure 2.1.), Heck (**B**),³ Suzuki–Miyaura (**C**),⁴ Sonogashira (**D**),⁵ and Negishi (**E**) cross-coupling⁶ as well as hydroaminations (**F**),⁷ hydrogenations (**G**)⁸ and conversion of alcohols to esters, amides or peptides (**H**)⁹ are examples of their potential.

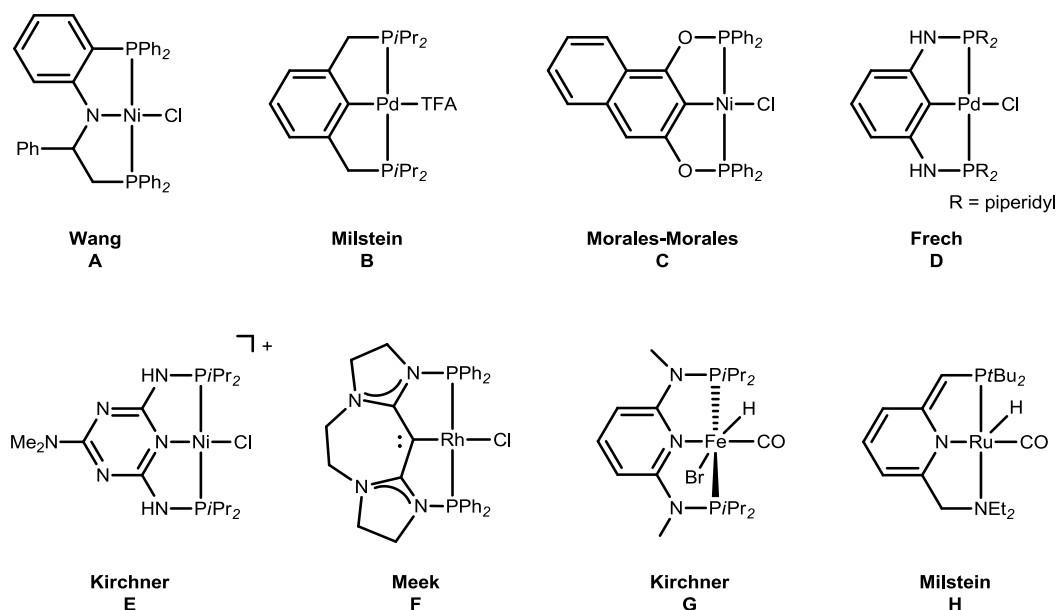


Figure 2.1. Examples of PYP pincer ligands applied in different catalytic reactions

In contrast to the N or O donor sites that only act as σ -donor, the σ -donor and π -acceptor properties of the phosphines donate electron density from their lone pair to an empty d-orbital of the metal center and simultaneously interact with filled d-orbitals of the metal center via their empty σ^* orbitals (Figure 2.2.).¹⁰

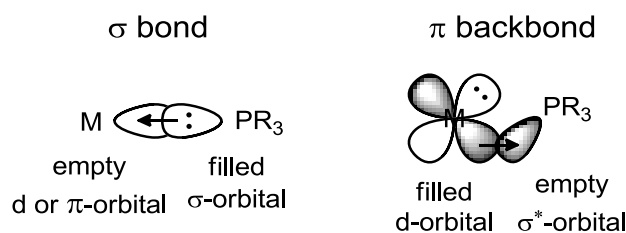


Figure 2.2. Coordination between metal and phosphines

The atomic radii of the phosphorus atom is another aspect to take in consideration since it promotes steric constrains, the metal-phosphorus bond is longer than for example the nitrogen bond.

The donor/acceptor properties of the phosphines fluctuate with their electronic assets, i.e., electron withdrawing substituents at the phosphine decrease its σ donation and strengthen the π -backbonding by reducing the energy of the σ^* orbital. Therefore, strong σ donors, such as triphenylphosphine increase the electronic density on the metal center, in opposite weak donors withdraw the electronic density (Figure 2.3.).¹¹

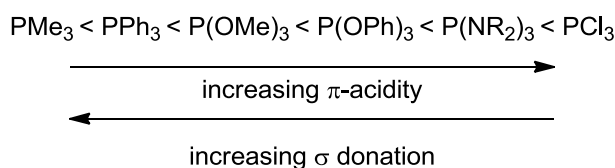


Figure 2.3. Classification of different phosphines

Additionally, the incorporation of phosphine arms in the pincer ligands' framework provides a convenient tool for monitoring the reactions by $^{31}\text{P}\{^1\text{H}\}$ NMR spectroscopy. This technique is very useful because the phosphorus δ -shifts depend on the nature, electronegativity, steric properties, π -bonding effects and bond angles of the substituents at the phosphorus atom. For example, the presence of aryl or primary amino as well as sterically demanding substituents increase the shielding effect.¹²

2.1. Pyridine backbone

Innumerable transformations can be performed with the pincer framework, previously described in Chapter 1, with respect to the phosphine based pincer ligands the central donor atom can change from B, C, Si, Ge, Sn, N, P to O and are inserted in an aromatic or aliphatic backbone, some examples are illustrated in Figure 2.4..¹³

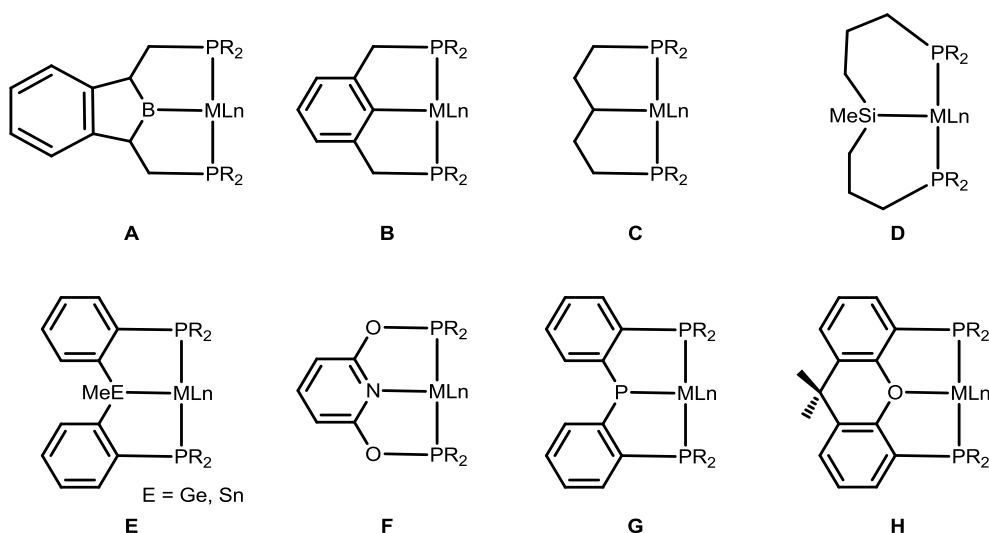


Figure 2.4. Examples of PYP pincer ligands

The selection of the central atom is an important task since it offers strong variation of the donor properties. In the early 1980s, Fryzuk *et al.*¹⁴ was the first to explore the chemistry of pincers incorporating a central amido donor and boosted the PNP pincer ligands. Over the years the central amido donor have gain an increase attention, unfortunately until recent years this type of ligands are still less common compared with PCP pincers.¹

The amido ligand is a stronger π -donor and has a weaker *trans*-influence. Therefore, PNP ligands provide an environment that incorporates comparatively soft phosphine donors and a hard amido donor. In the literature it is possible to find anionic or neutral PNP pincer ligands that incorporate core structures such as diarylamide, disilylamide, dialkylamide, triazine, pyridine, pyrrole and acridine.^{1,15}

From all the possibilities that a central amido donor implement, pyridine is the most alluring, since it is easy to modify and is capable of acting as either a π or σ ligand. The strength of the pyridine varies from metal to metal and depends on the steric interactions in the inner coordination sphere.

2.2. Amine spacers

Focusing on the PNP pincer ligands that exhibit a central pyridine functionality and peripheral phosphine donor groups, a few types of spacer groups can be found in literature. Several synthetic routes have been explored for the straightforward synthesis of PNP ligands with CH_2 spacers by different groups, such as Sacco,¹⁶ Taube¹⁷ and Milstein¹⁸ (Figure 2.5.). In the last years, Balakrishna¹⁹ achieved a derivation of this

spacer group by implementing a carbonyl linker. Furthermore, Ozama²⁰ was the first to synthesized a PNP ligand containing a linker with a P=C bond. In addition to CR spacers, other linkers have also been explored, like the pyridine analogue of Brookhart's²¹ POCOP ligands recently synthesized by the same group. The introduction of heteroatoms into the skeleton of the PNP ligand has accomplished by Haupt and co-workers²² and continues to be explored by the Kirchner's²³ group.

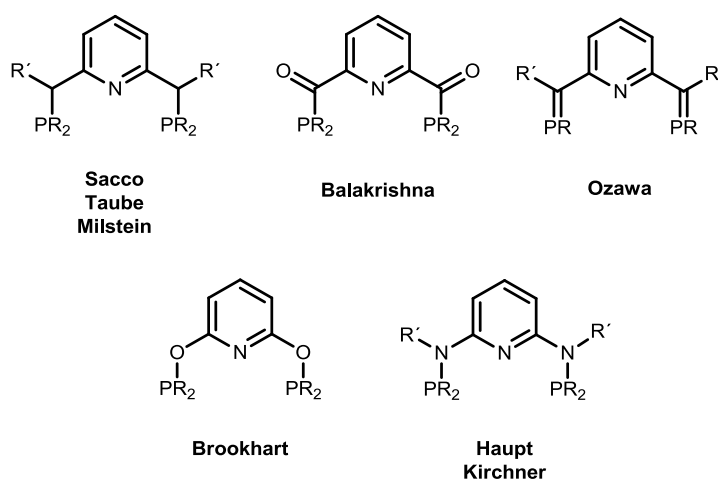


Figure 2.5. Examples of PNP pincer ligands with pyridine backbones

Since spacers have a profound impact on the steric of the ligands and consequently on the reactivity of transition metal PNP complexes, amine linkers seem to be most promising due to the lack of a general methodology for PNP pincer ligands as well as the difficulty of introducing chirality into the pincer structure.

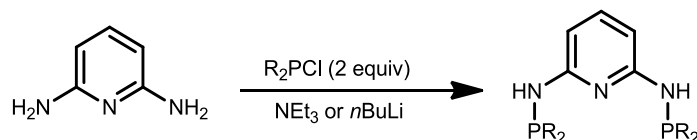
Aminophosphines are very thermally stable, but for their safe handling a dry and inert atmosphere is required. Due to the higher electronegativity of nitrogen, they are sensitive to oxidation by air and moisture. This even the case with stabilization by the aromatic ring.²⁴

2.3. Synthesis of PNP* ligands

The first phosphine based pincer ligand featuring a pyridine backbone and amine spacer was the N,N'-bis(diphenylphosphino)-N,N'-2,6-diaminopyridine (PNP-Ph) reported by Haupt and co-workers.²² The synthetic pathway to achieve this type of PNP

* The generic terminology “PNP” will be applied to pincer ligands based on a 2,6-diaminopyridine scaffold with different phosphine moieties

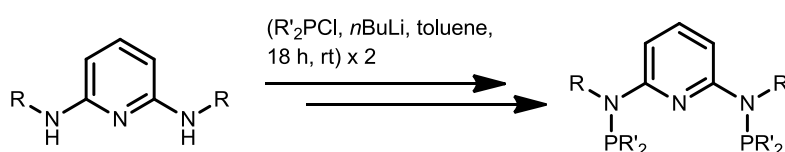
ligands is through a simple nucleophilic substitution on the phosphorus. Over the years, a series of PNP ligands were developed by Kirchner's working group from a wide range of chlorophosphines starting with a 2,6-diaminopyridine scaffold (Scheme 2.1.).²³



Scheme 2.1. Synthesis of PNP ligands

This reaction is accomplished in aprotic solvents (toluene, THF) under inert conditions at room temperature in the presence of an excess of base and leads to the desired product in yields >90 %. The P-N bond is established by deprotonation by a base followed by a condensation reaction releasing HCl. The incorporation of N-alkyl or N-Aryl spacers in the pincer framework represents a challenge, especially since the 2,6-diaminopyridines are commercially not available.

The first synthetic approach, carried out in 2006, presents an acylation followed by a reduction with LiAlH_4 of the 2,6-diaminopyridine to create different N,N'-disubstituted 2,6-diamino pyridines. Surprisingly, the next step occurs differently from the methodology applied for the PNP ligands with a 2,6-diaminopyridine scaffold, since double deprotonation doesn't occur simultaneously. Several phosphorus-containing species were formed including tetraphenyldiphosphine and tetraphenyldiphosphine monoxide. To achieve the desirable PNP pincer ligand it is necessary to employ a two-step procedure with intermediate workup (Scheme 2.2.).²³

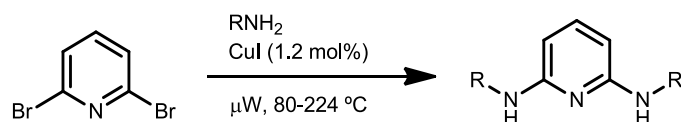


Scheme 2.2. Synthesis of PNP ligands with different amine spacers

Unfortunately this procedure is not appropriate to prepare N,N-dimethylpyridine-2,6-diamine. Thus, in 2013 a new method has been developed via a three-step procedure involving borane protection of the phosphine, a deprotonation/alkylation step, and deprotection of the phosphine starting at the PNP-*i*Pr.²⁵

However, a simple, general method for the selective formation of N,N'-disubstituted 2,6-diamino pyridines is still of great importance for the design of new PNP

ligands. In 2015 a different approach was developed using microwave assisted copper-catalyzed amination (Scheme 2.3).²⁶



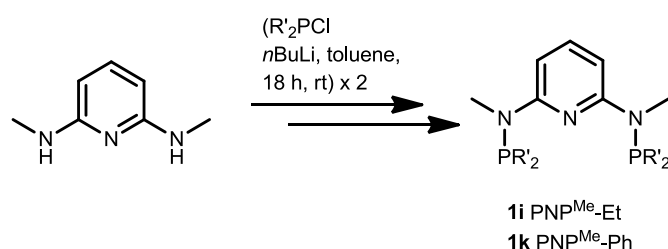
Scheme 2.3. Synthesis of N,N'-di-substituted 2,6-diamino pyridines

This process provides a selective substitution of one or two halogens by aryl or alkylamines with little reaction time to afford the different 2,6-diaminopyridines in a good to excellent yield. The synthesis of the bis-phosphorylated 2,6-diaminopyridines was carried out by the same reaction shown in Scheme 2.2..

2.4. Results and discussion

In the last years, a series of PNP pincer ligands with a NH bridge has been developed. The expansion of the pincer series by substitution of the amine spacer groups (N-alkyl and N-aryl) and the phosphine moieties is the major focus. This modification promotes a significant change in the steric and electronic properties of the PNP ligand and consequently influences the stability and reactivity of the pincer metal complexes.

In this thesis, the new PNP ligands PNP^{Me}-Et and PNP^{Me}-Ph²⁷ were synthesized analogously to a previously reported methodology (Scheme 2.4.). The precursor for this synthesis was afforded by the method depicted in Scheme 2.3..²⁶



Scheme 2.4. The PNP ligands synthesized in this research

The reaction display in Scheme 2.4. is performed in toluene under inert conditions at 80 °C and in the presence of an excess of base. This two-step procedure can be carried out also as a one-pot reaction. Alternatively, upon workup with NaHCO₃

and extraction after the first step, the purity and yield of the ligand increases. The ligands were isolated as yellow oil containing small amounts of impurities of unreacted starting materials that upon purification were obtained as white oil and white solid, respectively.

The PNP pincer ligands investigated in this research is shown in Figure 2.6.. All feature a pyridine backbone with diverse amine spacers (NR, R = H, Me, Ph) and different phosphines as donor groups.^{22,23,25,27-30}

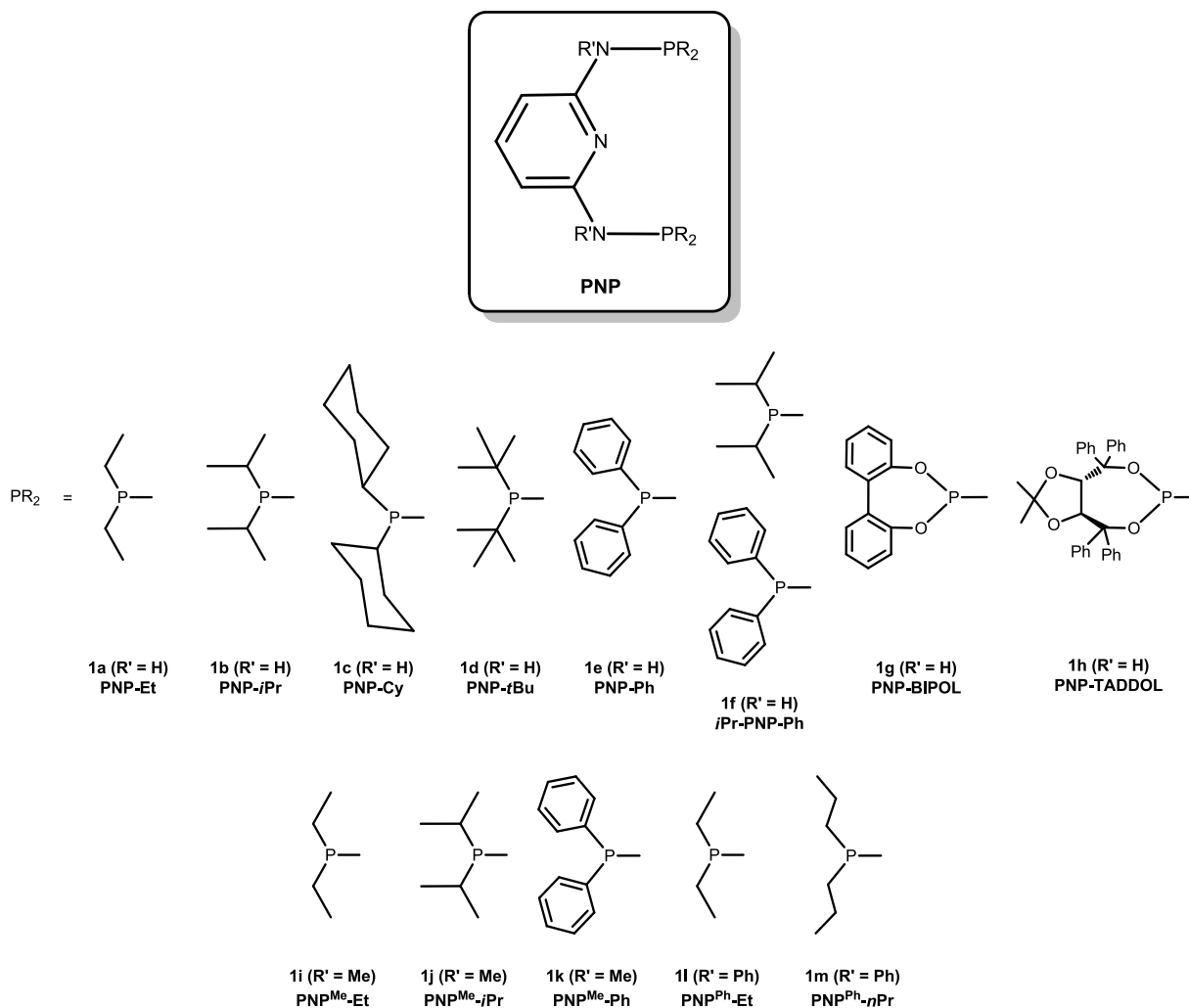


Figure 2.6. The PNP ligands investigated in this research

Characterization of all PNP pincer ligands was accomplished by ¹H, ¹³C{¹H} and ³¹P{¹H} NMR spectroscopy and elemental analysis. In the ³¹P{¹H} NMR spectra one singlet at varying δ -values is observed, depicted in Tables 2.1. and 2.2.. The only exception is the *i*Pr-PNP-Ph ligand that exhibits two singlets as the substituents in the phosphines are not equivalent.

Table 2.1. $^{31}\text{P}\{^1\text{H}\}$ NMR shifts of PNP-R ligands

PNP	Et	<i>i</i> Pr	Cy	<i>t</i> Bu	Ph	<i>i</i> Pr-Ph	BIPOL	TADDOL
$^{31}\text{P}\{^1\text{H}\} / \delta$ (ppm)	33.3	47.8	41.3	58.8	26.0	48.0/25.7	146.0	134.0

Table 2.2. $^{31}\text{P}\{^1\text{H}\}$ NMR shifts of PNP^R-R ligands

PNP	^{Me} -Et	^{Me} - <i>i</i> Pr	^{Me} -Ph	^{Ph} -Et	^{Ph} - <i>n</i> Pr
$^{31}\text{P}\{^1\text{H}\} / \delta$ (ppm)	51.3	69.3	49.6	57.0	49.6

The phosphorus δ -values depend on several factors. It is possible to roughly order phosphines according to their σ -donor π -acceptor properties.¹² This classification was described and published by Tolman³¹ in 1977 where he introduced the Tolman's cone angle to describe the space occupied by a coordinated phosphine. The substituent steric effect seems to play an important role in the influence of the δP values. Compounds with very similar environment around the phosphorus centre exhibit a very similar δP value.

A rough ordering the pincer ligands PNP-Ph < PNP-Et < PNP-Cy < PNP-*i*Pr < PNP^{Me}-Ph \approx PNP^{Ph}-*n*Pr < PNP^{Me}-Et < PNP^{Ph}-Et < PNP-*t*Bu < PNP^{Me}-*i*Pr < PNP-TADDOL < PNP-BIPOL. The donating/withdrawing properties also affect the basicity of the phosphine. Being a moderately strong Lewis base, depending on the substituents, the $\text{p}K_{\text{a}}$ -values vary between 2.7 to 11.4. An ordering of the π -accepting and σ -donating capabilities of phosphines can be accomplished by synthesizing a series of complexes in which the only difference is the nature of the phosphine ligand.

2.5. Conclusions

In sum, it was shown that new achiral and chiral PNP ligands are easily prepared from commercially available and inexpensive 2,6-diaminopyridine, which can be varied in modular fashion by choosing the appropriate chlorophosphine R_2PCl . In addition, to incorporate N-alkyl or N-aryl spacers into the ligands' framework is necessary to perform the amination via a microwave protocol. The different 2,6-diaminopyridines are valuable precursors for the synthesis of bis-phosphorylated 2,6-diaminopyridines which are used as PNP pincer ligands in transition metal complexes.

2.6. Experimental part

All manipulations were performed under inert atmosphere of argon by using Schlenk techniques. The solvents were purified according to standard procedures.³² Commercially available substrates were purchased via Sigma-Aldrich and used without further purification. The deuterated solvents were purchased from Aldrich and dried over 4 Å molecular sieves. ¹H, ¹³C{¹H}, and ³¹P{¹H} NMR spectra were recorded on Bruker AVANCE-250, AVANCE-400 DPX and AVANCE-600 spectrometers. ¹H and ¹³C{¹H} NMR spectra were referenced internally to residual solvent resonances and are reported relative to tetramethylsilane ($\delta = 0$ ppm). ³¹P{¹H} NMR spectra were referenced externally to H₃PO₄ (85%) ($\delta = 0$ ppm).[†] The ligand precursor 2,6-N,N'-dimethyldiaminopyridine and the ligands N,N'-Bis(diethylphosphino)-2,6-diaminopyridine (PNP-Et) (**1a**), N,N'-bis(di-*iso*-propylphosphino)-2,6-diaminopyridine (PNP-*i*Pr) (**1b**), N,N'-bis(dicyclohexylphosphino)-N,N'-dimethyl-2,6-diaminopyridine (PNP-Cy) (**1c**), N,N'-bis(di-*tert*-butylphosphino)-2,6-diaminopyridine (PNP-*t*Bu) (**1d**), N,N'-bis(diphenylphosphino)-2,6-diaminopyridine (PNP-Ph) (**1e**), N,N'-bis(*iso*-propylphosphino, phenylphosphino)-2,6-diaminopyridine (*i*Pr-PNP-Ph) (**1f**), N,N'-bis(dibenzo[d,f][1,3,2]dioxaphosphine)-2,6-diaminopyridine (PNP-BIPOL) (**1g**), N,N'-bis((3aR,8aR)-2,2-dimethyl-4,4,8,8-tetraphenyltetrahydro-[1,3]dioxolo[4,5-e][1,2,3]-dioxaphosphenin-6-yl)pyridine-2,6-diaminopyridine (PNP-TADDOL) (**1h**), N,N'-bis(di-*iso*-propylphosphino)-N,N'-dimethyl-2,6-diaminopyridine (PNP^{Me}-*i*Pr) (**1j**), N,N'-Bis(ethylphosphino)-N,N'-diphenyl-2,6-diaminopyridine (PNP^{Ph}-Et) (**1l**) and N,N'-Bis(*n*-propylphosphino)-N,N'-diphenyl-2,6-diaminopyridine (PNP^{Ph}-*n*Pr) (**1m**), were prepared according to literature and available in the working group.^{22,23,25-30}

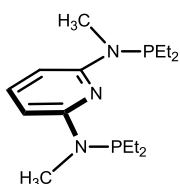
2.6.1. Synthesis

A solution of 2,6-N,N'-dimethyldiaminopyridine (36.45 mmol) in toluene (125 mL) was cooled down to -20 °C and *n*-BuLi (2.5 M solution in hexane, 38.28 mmol) was added. The mixture was stirred at room temperature for 2 h. After this period, the mixture was cooled down to -60 °C and then PR₂Cl (R = Et, Ph; 36.45 mmol) was added. The mixture was stirred for 2 h at room temperature and then refluxed overnight at 80 °C. The mixture was allowed to cool down to room temperature and 8 mL of a saturated solution of NaHCO₃ was added. The two phases were separated and anhydrous Na₂SO₄ was added to the organic phase. The mixture was filtered and the

[†] The same experimental conditions in the following chapters.

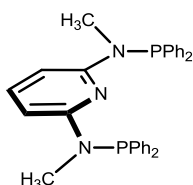
solvent was evaporated under reduced pressure leading to a yellow oil. The oil was dissolved in 125 mL of toluene and cooled down to -20 °C and then *n*-BuLi (2.5 M solution in hexane, 38.28 mmol) was added. The mixture was stirred at room temperature for 2 h. After this period, the mixture was cooled down to -60 °C and then again PR₂Cl (R = Et, Ph; 36.45 mmol) was added. The mixture was stirred for 2 h at room temperature and then refluxed overnight at 80 °C. After this period a saturated solution of NaHCO₃ was added to the mixture at room temperature. The two phases were separated and anhydrous Na₂SO₄ was added to the organic phase. The mixture was filtered and the solvent was removed under reduced pressure yielding a yellow oil for PNP^{Me}-Et and a yellow oil together with a white precipitate for PNP^{Me}-Ph. The crude product of PNP^{Me}-Et was purified with CH₃CN at low temperature to give a white oil and PNP^{Me}-Ph was purified by washing with hot CH₃CN yielding white powder.

N,N'-bis(diethylphosphino)-N,N'-methyl-2,6-diaminopyridine (PNP^{Me}-Et) (1i)



The product was obtained as a white oil in 61.6% yield. Anal. Calcd. for C₁₅H₂₉N₃P₂ (313.36). C, 57.49; H, 9.33; N, 13.41. Found: C, 56.71; H, 9.57; N, 13.59. ¹H NMR (δ, CDCl₃, 20 °C): 7.26 (t, J = 8.0 Hz, 1H, py⁴), 5.76 (d, J = 7.8 Hz, 2H, py^{3,5}), 3.02 (d, J = 2.4 Hz, 6H, NCH₃), 1.92-1.72 (m, 4H, CH₂), 1.60-1.40 (m, 4H, CH₂), 1.12-0.94 (m, 12H, CH₃). ¹³C{¹H} NMR (δ, CDCl₃, 20 °C): 160.5 (d, J = 23.2 Hz, py^{2,6}), 137.3 (py⁴), 99.3 (d, J = 23.5 Hz, py^{3,5}), 30.0 (t, J = 5.0 Hz, NCCH₃), 21.1 (d, J = 13.3 Hz, CH₂), 9.3 (d, J = 16.1 Hz, CH₃). ³¹P{¹H} NMR (δ, CDCl₃, 20 °C): 51.3.

N,N'-bis(diphenylphosphino)-N,N'-methyl-2,6-diaminopyridine (PNP^{Me}-Ph) (1k)



The product was obtained as a white solid in 54.2% yield. Anal. Calcd. for C₃₁H₂₉N₃P₂ (505.54): C, 73.65; H, 5.78; N, 8.31%. Found: C, 73.79; H, 5.50; N, 8.23%. ¹H NMR (δ, CDCl₃, 20 °C): 7.38-7.44 (m, 21H, Ph, py⁴), 6.87 (d, J = 7.4 Hz, 2H, py^{3,5}), 2.89 (s, 6H, NCH₃). ¹³C{¹H} NMR (δ, CDCl₃, 20 °C): 159.6 (vd, J = 27.4 Hz, py^{2,6}), 138.4 (vt, J = 3.0 Hz, py⁴), 137.5 (vd, J = 16.0 Hz, Ph¹), 132.2 (vd, J = 20.8 Hz, Ph^{2,6}), 129.2 (Ph⁴), 128.5

(vd, $J = 5.9$ Hz, $\text{Ph}^{3,5}$), 99.9 (vd, $J = 21.2$ Hz, $\text{py}^{3,5}$), 34.1 (vd, $J = 8.6$ Hz, NCH_3). $^{31}\text{P}\{^1\text{H}\}$ NMR (δ , CDCl_3 , 20°C): 49.6. ESI-MS (m/z , CH_3OH , HCOOH) positive ion: 506.19 [$\text{M} + \text{H}$] $^+$.

2.7. References

- [1] a) Peruzzini, M.; Gonsalvi, L.; *Phosphorus Compounds: Advanced Tools in Catalysis and Material Sciences*, **2011**, Springer; b) Morales-Morales, D.; Jensen, C.; *The chemistry of pincer compounds*, **2007**, Elsevier, Oxford.
- [2] Sun, K.; Wang, L.; Wang, Z.; *Organometallics*, **2008**, *27*, 5649-5656.
- [3] Ohff, M.; Ohff, A.; van der Boom, M. E.; Milstein, D.; *J. Am. Chem. Soc.*, **1997**, *119*, 11687-11688.
- [4] Estudiante-Negrete, F.; Hernández-Ortega, S.; Morales-Morales, D. *Inorganica Chimica Acta*, **2012**, *387*, 58-63.
- [5] Bolligera, J. L.; Frech, C. M.; *Adv. Synth. Catal.*, **2009**, *351*, 891-902.
- [6] Mastalir, M.; Kirchner, K.; *Monatsh Chem*, **2017**, *148*, 105-109.
- [7] Goldfogel, M. J.; Roberts, C. C.; Meek, S. J.; *J. Am. Chem. Soc.*, **2014**, *136*, 6227-6230.
- [8] Gorgas, N.; Stöger, B.; Veiros, L. F.; Kirchner K.; *ACS Catal.*, **2016**, *6*, 2664-2672.
- [9] Szabó, K. J.; Wendt, O. F.; *Pincer and Pincer-Type Complexes*, **2014**, Wiley-VCH, Germany.
- [10] a) Yamanaka, M.; Mikami, K.; *Organometallics*, **2005**, *24*, 4579-4587; b) Astruc, D.; *Organometallic Chemistry and Catalysis*, **2007**, Springer-Verlag Berlin Heidelberg.
- [11] a) Streitwieser, A.; McKeown, A. E.; Hasanayn, F.; Davis, N. R.; *Org. Lett.*, **2005**, *7*, 1259-1262; b) Henderson, W. A.; Streuli, C. A.; *Journal of the American Chemical Society*, **1960**, *82*, 5791-5797.
- [12] Gopalakrishnan, J.; Rao, M. N. S.; *Bull. Chem. Soc. Ethiop.*, **2006**, *20*, 207-218.
- [13] a) Hill, A. F.; Lee, S. B.; Park, J.; Shang, R.; Willis, A. C.; *Organometallics*, **2010**, *29*, 5661-5669; b) Ogawa, H.; Yamashita, M.; *Dalton Trans.*, **2013**, *42*, 625-629; c) Bushnell, G. W.; Casado, M. A.; Stobart, S. R.; *Organometallics*, **2001**, *20*, 601-603; d) Kameo, H.; Ishii, S.; Nakazawa, H.; *Dalton Trans.*, **2012**, *41*, 11386-11392; e) Takaya, J.; Nakamura, S.; Iwasawa, N.; *Chem. Lett.*, **2012**, *41*, 967-969; f) Liang, L.; *Coord. Chem. Rev.*, **2006**, *250*, 1152-1177; g) Mazzeo, M.; Strianese, M.; Kühn, O.; Peters, J. C.; *Dalton Trans.*, **2011**, *40*, 9026-9033; h) Derrah, E. J.; Martin, C.; Mallet-Ladeira, S.; Miqueu, K.; Bouhadir, G.; Bourissou, D.; *Organometallics*, **2013**, *32*, 1121-1128; i) Haibach, M. C.; Wang, D. Y.; Emge, T. J.; Krogh-Jespersen, K.; Goldman, A. S.; *Chem. Sci.*, **2013**, *4*, 3683-3692.
- [14] Fryzuk, M. D.; Leznoff, D. B.; Thompson, R. C.; Rettig, S. J.; *J. Am. Chem. Soc.*, **1998**, *120*, 10126-10135.
- [15] a) Kinauer, M.; Scheibel, M. G.; Abbenseth, J.; Heinemann, F. W.; Stollberg, P.; Würtele, C.; Schneider, S.; *Dalton Trans.*, **2014**, *43*, 4506; b) Rösler, S.; Obenauf, J.; Kempe, R.; J.

- Am. Chem. Soc.*, **2015**, *137*, 7998–8001; c) Hillebrand, S.; Bartkowska, B.; Bruckmann, J.; Kriiger, C.; Haenel, M. W.; *Tetrahedron Letters*, **1998**, *39*, 813-816; d) Grüger, N.; Wadeohl, H.; Gade, L. H.; *Dalton Trans.*, **2012**, *41*, 14028-14030; e) Srimani, D.; Diskin-Posner, Y.; Ben-David, Y.; Milstein, D.; *Angew. Chem. Int. Ed.*, **2013**, *52*, 14131-14134.
- [16] Giannoccaro, P.; Vasapollo, G.; Nobile, C. F.; Sacco, A.; *Inorganica Chimica Acta*, **1982**, *61*, 69-75.
- [17] a) Hahn, C.; Sielerb, J.; Taube, R.; *Chem. Ber.*, **1997**, *130*, 939-945; b) Hahn, C.; Spiegler, M.; Herdtweck, E.; Taube, R.; *Eur. J. Inorg. Chem.*, **1999**, 435-440.
- [18] a) Hermann, D.; Gandelman, M.; Rozenberg, H.; Shimon, L. J. W.; Milstein, D.; *Organometallics*, **2002**, *21*, 812-818; b) Zhang, J.; Gandelman, M.; Herrman, D.; Leitus, G.; Shimon, L. J. W.; Ben-David, Y.; Milstein, D.; *Inorganica Chimica Acta*, **2006**, *359*, 1955-1960.
- [19] Kumar, P.; Kashid, V. S.; Reddi, Y.; Mague, J. T.; Sunoj R. B.; Balakrishna, M. S.; *Dalton Trans.*, **2015**, *44*, 4167–4179.
- [20] Nakajima, Y.; Nakao, Y.; Sakaki, S.; Tamada, Y.; Ono, T.; Ozawa, F.; *J. AM. CHEM. SOC.*, **2010**, *132*, 9934–9936.
- [21] Bernskoetter, W. H.; Hanson, S. K.; Buzak, S. K.; Davis, Z.; White, P. S.; Swartz, R.; Goldberg, K. I.; Brookhart, M.; *J. AM. CHEM. SOC.*, **2009**, *131*, 8603-8613.
- [22] a) Schirmer, W.; Flörke, U.; Haupt, H.-J. *Z. Anorg. Allg. Chem.* **1987**, *545*, 83; b) Schirmer, W.; Flörke, U.; Haupt, H.-J. *Z. Anorg. Allg. Chem.* **1989**, *574*, 239.
- [23] a) Benito-Garagorri, D.; Becker, E.; Wiedermann, J.; Lackner, W.; Pollak, M.; Mereiter, K.; Kisala, J.; Kirchner, K.; *Organometallics*, **2006**, *25*, 1900-1913; b) Benito-Garagorri, D.; Kirchner, K.; *Accounts of Chemical Research*, **2008**, *41*, 201-213.
- [24] Gopalakrishnan, J.; *Appl. Organometal. Chem.*, **2009**, *23*, 291-318.
- [25] Öztopcu, Ö.; Holz hacker, C.; Puchberger, M.; Weil, M.; Mereiter, K.; Veiros, L. F.; Kirchner, K.; *Organometallics*, **2013**, *32*, 3042-3052.
- [26] Mastalir, M.; Rosenberg, E. E.; Kirchner, K.; *Tetrahedron*, **2015**, *71*, 8104-8110.
- [27] de Aguiar, S. R. M. M.; Stöger, B.; Pittenauer, E.; Puchberger, M.; Allmaier, G.; Veiros, L. F.; Kirchner, K.; *Journal of Organometallic Chemistry*, **2014**, *760*, 74-83.
- [28] Glatz, M.; Bichler, B.; Mastalir, M.; Stöger, B.; Weil, M.; Mereiter, K.; Pittenauer, E.; Allmaier, G.; Veiros, L. F.; Kirchner, K.; *Dalton Trans.*, **2015**, *44*, 281-294.
- [29] Glatz, M.; Holz hacker, C.; Bichler, B.; Mastalir, M.; Stöger, B.; Mereiter, K.; Weil, M.; Veiros, L. F.; Mös ch-Zanetti, N. C.; Kirchner, K.; *Eur. J. Inorg. Chem.*, **2015**, *2015*, 5053-5065.
- [30] Holz hacker, C.; *Design of novel achiral and chiral iron(II) pincer complexes*, Dissertation, Vienna University of Technology, **2015**.
- [31] Tolman, C. A.; *Chem. Rev.*, **1977**, *77*, 313-348.
- [32] Perrin, D. D.; Armarego, W. L. F.; *Purification of Laboratory Chemicals*, third ed., **1988**, Pergamon, New York.

Chapter 3
Tricarbonyl
Molybdenum and
Tungsten Complexes

Chapter 3 – Tricarbonyl Molybdenum and Tungsten Complexes

Metal carbonyl complexes possess a very unique focus of interest in the inorganic and organometallic chemistry becoming over the years one of the most important families of compounds. For every transition metal there is at least one known type of carbonyl derivative, as well as evidence supporting the existence of the carbonyls of some lanthanides and actinides, although often in combination with other ligands.¹⁻³

Many carbonyl compounds are conventional starting materials for the synthesis of low-valent metal complexes and clusters. The ability of the carbonyl ligand to provide electron density to the π orbitals to form π backbonds is responsible for the stability of metals in low oxidation states. A large number of other ligands may substitute carbonyl ligands, however the presence of the remaining CO groups provides, among others, stability against oxidation or thermal decomposition, properties that are important for further applications.¹⁻⁴

Through the years, carbonyl compounds were involved in the preparation of high purity metals as in the Mond process for the extraction of nickel from its ores, in the synthesis of organic compounds and plays an essential role in many catalytic processes. Detailed mechanistic studies on metal carbonyls have become increasingly important in understanding the factors influencing ligand substitution processes, especially as they apply to catalytic activity.²

3.1. Carbonyl ligand

Carbon monoxide, CO, has unique properties as a ligand due the remarkable donating and accepting capabilities. In many cases, CO acts like a good spectator ligand, strongly bound and inert, but can also act as a reacting partner. Ligands isoelectronic to CO are also wellknown in metal compounds among them relatively stable molecules or ions such as N_2 , NO^+ , and CN^- , as well as less stable species such as vinylidene. Nonetheless, the number of complexes with neutral isoelectronic diatomic molecules terminally ligated to transition metals is somewhat limited, mainly restricted to complexes with ligands of the type CE (E = S, Se, Te, NR, CH_2) and N_2 . However, none of these other ligands seems to be as versatile as CO.¹⁻⁵

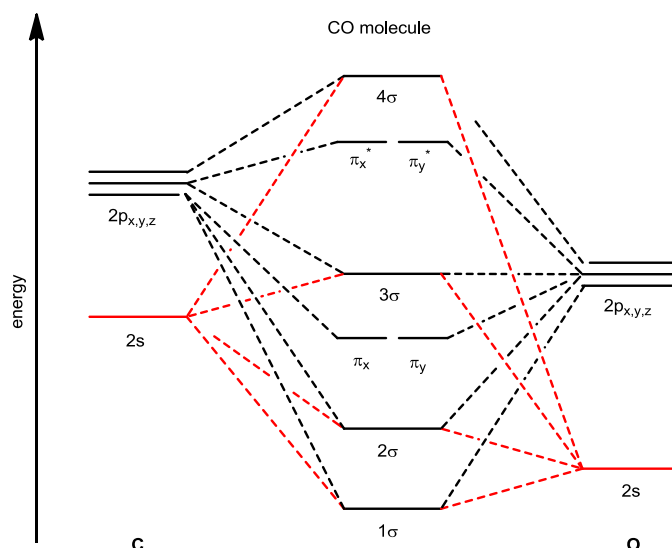


Figure 3.1. MO diagram of Carbon monoxide

The HOMO in CO is the 3σ orbital which contains a nonbonding lone pair of electrons situated on the carbon atom, recognized in the molecular orbital diagram (Figure 3.1.). The larger lobe of this orbital projects out of the molecule, in line with the C-O bond. The LUMO contains the pair of doubly degenerate antibonding π orbitals. This combination of frontier orbitals allows the carbonyl ligand not only to donate electrons via a σ -bond, but also to accept electrons via π -back donation from the metal. The CO group donates its electrons from the 3σ HOMO, into a vacant d -orbital of σ symmetry on the metal, forming a weak σ bond. This is accompanied by π -back donation by the metal, from a filled d -orbital, into the vacant $2\pi^*$ molecular orbitals on the ligand. The effect of π -back donation weakens the carbon-oxygen bond, since electron density is being forced into the n^* antibonding orbitals of this bond (Figure 3.2.). There is a fundamental similarity between the nature of carbonyl-metal bonding and that of alkenes, acetylenes, phosphines and dihydrogen.^{3,6}

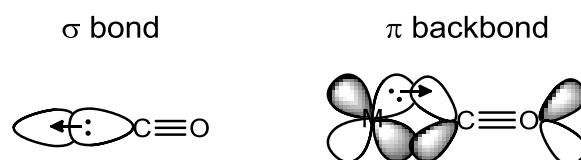


Figure 3.2. Coordinated bond between metal and carbonyl

The two components of this bonding are synergistic, the more sigma donation by the carbonyl (or other sigma-donors on the metal center) the stronger the π -backbonding interaction. Notice that although this involves the occupation of a π^*

orbital on the CO, it is still a bonding interaction as far as the metal center is concerned. The presence of strongly electron-donating groups on a metal center, such as alkyl phosphines, tends to increase the electron density available for back donation, enhancing its effect and weakening the C-O bonds.

The variations in carbon-oxygen bond strength are reflected in the frequency of their ν_{CO} bands observed in the IR spectra. These are indicative for the bond strength that correlates to the relative electron density on the metal, and hence its ability to back donate electrons. In such a manner, two consequences are expected from the weakening of the carbon-oxygen bonds (stronger back donation) that would be a lengthening of the C-O bond and a decrease in the carbonyl stretching frequency. Consequently, ν_{CO} can serve as a reliable qualitative indicator of the level of electron density on a particular metal center when compared with other metal carbonyl complexes, where the variations of the frequency are from 2125 to 1850 cm^{-1} for terminal CO (free CO $\sim 2143 \text{ cm}^{-1}$). Also with each charge added to the metal center, the CO stretching frequency decreases by approximately 100 cm^{-1} .^{3,6}

The presence of the other ligands coordinated to the metal influence the CO stretching frequency, as better the sigma-donating capability (or worse the pi-acceptor ability) of the other ligands on the metal, the lower the CO stretching frequency.

Many transition metal carbonyl complexes contain more than one CO ligand so the symmetry plays an important role in the determination of the number of IR CO stretching bands. Generally, group theory is used to predict which vibrational modes will be IR active or inactive. In practice, the number of anticipated CO stretching bands and their relative intensities can be modeled for a range of substituted carbonyl complexes.^{3,6}

3.2. Carbonyl pincer complexes

The chemistry of pincer complexes with carbon monoxide is fundamental to better understand the chemical nature of these compounds and allows further modification of the donor properties of pincer ligands. This better understanding of the electronics of different substituents in the pincer backbone provided by the presence of CO, allows envisioning the potential employment of these compounds in industrially relevant catalytic processes.^{5,7}

Some carbonyl pincer complexes have been identified as kinetic resting pools in different catalytic processes and transformations mediated by pincer complexes. Thus, it is expected that the development pincer compounds have witnessed in the past few

Chapter 3 – Tricarbonyl Molybdenum and Tungsten Complexes

years will continue, with carbon monoxide as common partner, for the study, understanding, and discovery of novel pincer species.^{5,7}

This class of compounds normally embodies every pincer complex that possesses at least one CO ligand, independently of the other type of ligands bond to the metal. In this Chapter only pincer complexes with carbonyl ligands are discussed. Carbonyl pincer complexes can be obtained from the reaction of pincer ligands with metal carbonyls as starting materials (**A**, **B**, Figure 3.3.),^{8,9} from the direct reaction of pincer species with carbon monoxide (**C**, **D**),^{10,11} as well as from decarbonylative processes of organic substrates (**E**, **F**).^{7a,7e}

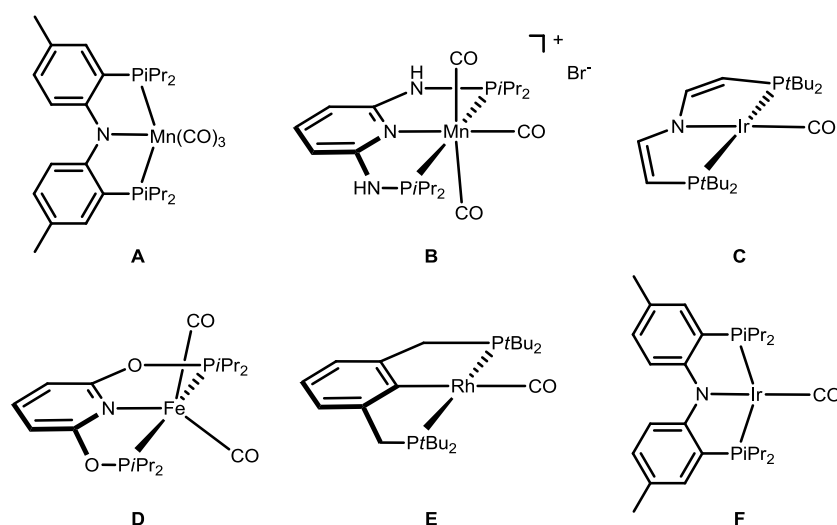


Figure 3.3. Mono, di and tri-carbonyl complexes with several PNP pincer ligands

Only a few examples of the molybdenum and tungsten PNP pincer carbonyl complexes have been described, however group VI carbonyl complexes without pincer ligands have been of great relevance. They can play different roles like acting as catalysts, biological assays, or as therapeutic measures depending on the substituents.¹²⁻¹⁷

The first molybdenum and tungsten carbonyl pincer complexes of the type $[M(\text{PNP-Ph})(\text{CO})_3]$ ($M = \text{Mo}, \text{W}$; $\text{PNP-Ph} = \text{N,N'}$ -bis(diphenylphosphino)- N,N' -2,6-diaminopyridine) were reported by Haupt and co-workers (Figure 3.4.).¹⁸

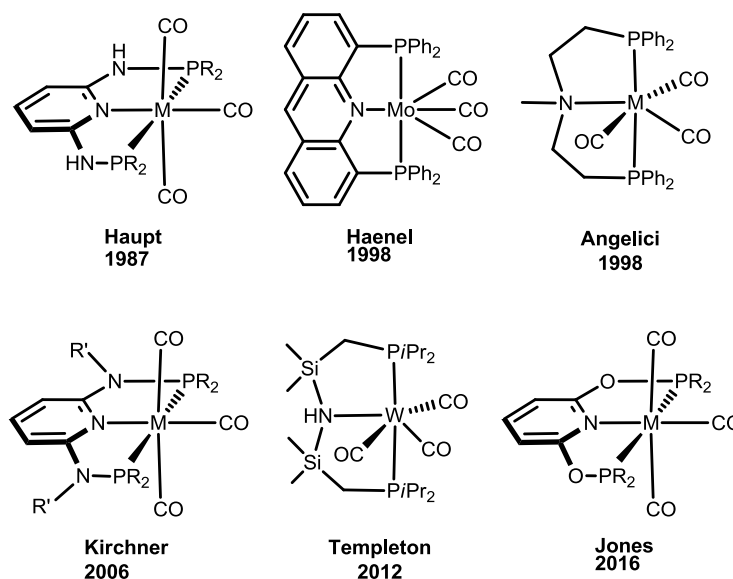


Figure 3.4. Tricarbonyl complexes with several PNP pincer ligands (M = Mo or W)

In 1998 Haenel *et al*¹⁹ published a patent including the preparation of novel transition metal (Pd, Ni, Pt, Rh, Mo) compounds featuring a 4,5-diphosphinoacridine ligand. In all cases the coordination to the transition metals is accomplished through both phosphorus atoms and the acridine nitrogen. In the particular case of molybdenum, the tricarbonyl complex is formed.

In the same year coordination to both tungsten and molybdenum has been observed with a neutral six electron donor PNP ligand $\text{H}_3\text{CN}(\text{CH}_2\text{CH}_2\text{PPh}_2)_2$ to provide the respective tricarbonyl pincer complexes.²⁰ The ligand backbone is flexible enough to adopt either a facial or a meridional coordination mode. However, the methyl group on the amino nitrogen limits the flexibility.

A series of PNP molybdenum and tungsten tricarbonyl complexes were developed by Kirchner and coworkers. The pincer ligands based on a 2,6-diaminopyridine scaffold with some modifications on the amino group and with different phosphine moieties.²¹

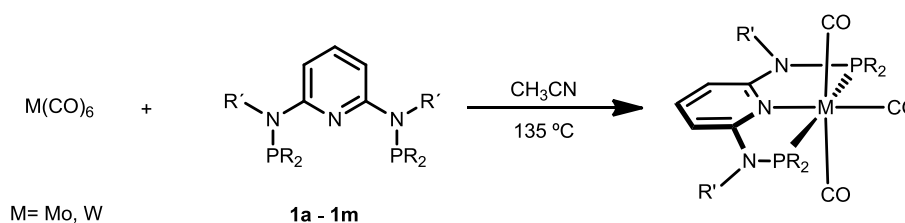
Templeton and co-workers synthesized tungsten tricarbonyl pincer complexes featuring a PNP pincer-type ligand $\text{HN}(\text{SiMe}_2\text{CH}_2\text{PPh}_2)_2$, both facial and meridional isomers, in a similar way of the Angelici group.²²

In 2016 the Jones's group investigated the chemistry of molybdenum and tungsten complexes featuring PONOP pincer ligand based on a 2,6-dihydroxypyridine scaffold with different phosphine moieties.²³

3.3. Synthesis of Mo and W PNP carbonyl complexes

In general, the synthesis of the Mo and W PNP pincer tricarbonyl complexes is accomplished by a simple reaction of the ligand with $[M(CO)_6]$ ($M = Mo, W$) under refluxing conditions. The first pincer complex of the type $[M(PNP)(CO)_3]$ ($M = Mo, W$; PNP = N,N'-bis(diphenylphosphino)-N,N'-2,6-diaminopyridine (PNP-Ph)) was reported by Haupt and co-workers.¹⁸

Over the years, Kirchner and coworkers used the same synthetic pathway developing a series of PNP tricarbonyl complexes. Reacting the intermediate compound $[M(CO)_3(CH_3CN)_3]$ ($M = Mo, W$), prepared *in situ* by refluxing a solution of $[M(CO)_6]$ ($M = Mo, W$) in CH_3CN with the PNP ligands (Scheme 3.1).^{21,24}



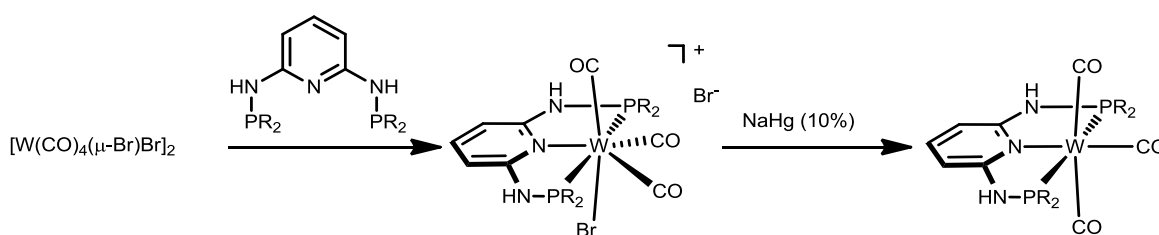
Scheme 3.1. Synthesis of $[MPNP(CO)_3]$ ($M = Mo, W$) complexes

However, in general the traditional thermal synthesis of these complexes is not very effective, since it requires high temperatures, extensive reaction times (days) and affords low yields, especially in the case of tungsten. This may explain the lack of examples from the Mo and W carbonyl complexes described in literature. Accordingly, an alternative simple and efficient route to synthesize these types of complexes is desirable. Diverse strategies have been used to improve the reaction conditions such as the employment of catalysts like sodium borohydride and sodium hydroxide or performing the reactions at high temperatures or at high pressures (e.g. under microwave conditions).^{15,16,25}

An alternative method was developed to obtain tricarbonyl complexes, special for the tungsten $[W(PNP)(CO)_3]$, via the intermediacy of the known dinuclear complex $[W(CO)_4(\mu-Br)Br]_2$, prepared *in situ* from $W(CO)_6$ and stoichiometric amounts of Br_2 in CH_2Cl_2 at $-70\text{ }^\circ\text{C}$. Treatment of a solution of $[W(CO)_4(\mu-Br)Br]_2$ in CH_2Cl_2 at room temperature with the PNP ligands produce the seven coordinated tungsten(II) complexes $[W(PNP)(CO)_3Br]Br$. Which subsequently were reduced with an excess of 10% sodium amalgam in THF to yield the desired $W(0)$ complexes $[W(PNP)(CO)_3]$ in

Chapter 3 – Tricarbonyl Molybdenum and Tungsten Complexes

70–80% isolated yields (Scheme 3.2.).²⁴ This methodology also yields the analogous Mo(0) complexes thus being an alternative method to that described previously.

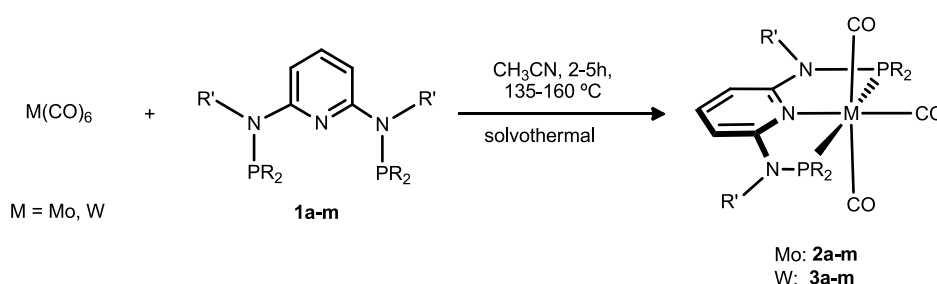


Scheme 3.2. Two-step synthesis of W(0) complexes via the $[\text{W}(\text{PNP})(\text{CO})_3\text{Br}]\text{Br}$ intermediate

3.4. Results and discussion

In this Chapter the synthesis and reactivity of new tricarbonyl molybdenum and tungsten complexes containing PNP pincer ligands with different amine linkers and phosphine substitutes, $\text{NR}'\text{PR}_2$, was expounded. In the beginning, the molybdenum tricarbonyl complex $[\text{Mo}(\text{PNP}^{\text{Me}}\text{-Ph})(\text{CO})_3]$ ²⁶ was synthesized by the method described above (Scheme 3.1.). Nevertheless in order to further develop the chemistry of Mo and W pincer systems, is essential to establish a new synthetic protocol that improves reaction times and yields and reduces steps, especially for the tungsten.

In 2016 the improved synthesis of several Mo and W carbonyl pincer complexes from the corresponding hexacarbonyl complexes using a solvothermal process (Scheme 3.3.) was developed.²⁷



Scheme 3.3. Synthesis of $[\text{MPNP}(\text{CO})_3]$ ($\text{M} = \text{Mo, W}$) complexes under solvothermal conditions in CH_3CN

A suspension of hexacarbonyl complexes $\text{M}(\text{CO})_6$ ($\text{M} = \text{Mo, W}$) and PNP ligands **1a-m** in CH_3CN were placed in a sealed microwave glass tube and stirred for 2–5 h at 135–160 °C. This methodology allows the generation of higher pressures and

Chapter 3 – Tricarbonyl Molybdenum and Tungsten Complexes

superheating of the solvent, resulting in significantly decreased reaction times and highly increased product yields and purity.

The acetonitrile binds sufficiently strong to give isolable adducts but is labile enough for facile substitution. The synthesis conditions support the use of thermally more sensitive ligands because of reduced reaction times and guarantees the exclusion of moisture. Moreover, the formation of crystals in almost every reaction was observed, for example Figure 3.5..

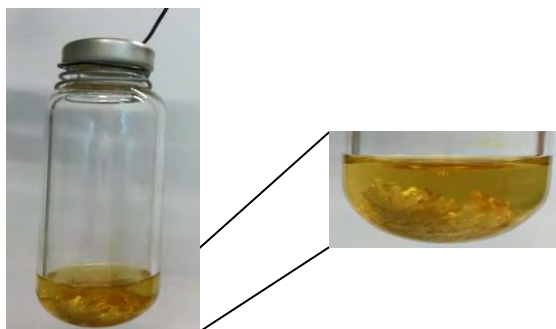


Figure 3.5. Sealed microwave glass tube with the $[\text{Mo}(\text{PNP-Et})(\text{CO})_3]$ complex

All complexes in this Chapter are yellow solids obtained in 79-99% isolated yields. They are thermally and air stable in solid state but slowly decompose in solution. Characterization was accomplished by combination of ^1H , $^{13}\text{C}\{^1\text{H}\}$, and $^{31}\text{P}\{^1\text{H}\}$ NMR spectroscopy, IR spectroscopy, and elemental analysis.

Characteristic features comprise, in the $^{13}\text{C}\{^1\text{H}\}$ NMR spectrum, two low-field triplet resonances (1:2 ratio) in the range of 234–206 ppm for the molybdenum complexes (Table 3.1.) and of 225–196 ppm for the tungsten complexes (Table 3.2.) assignable to the carbonyl carbon atoms trans and cis to the pyridine nitrogen, respectively. The $^{31}\text{P}\{^1\text{H}\}$ NMR spectra exhibit singlet resonances in the range of 205 - 104 ppm, except for $[\text{Mo}(i\text{Pr-PNP-Ph})(\text{CO})_3]$ (**2f**) that gives two singlets due to the unequal phosphines (132.1 and 104.7 ppm). In the case of the tungsten complexes (Table 3.2.), the $^{31}\text{P}\{^1\text{H}\}$ NMR spectra exhibit singlet resonances with $^1J_{\text{WP}}$ coupling constants of 319-495 Hz. The tungsten–phosphorus coupling was observed as a doublet satellite due to ^{183}W , 14% abundance with $I = 1/2$, superimposed over the dominant singlet.

The π -accepting/ σ -donating capabilities of phosphines can be studied through the δP values, since the nature of the phosphine ligand is the only difference in the series of tricarbonyl complexes, allowing the order $\text{PNP-Ph} < \text{PNP-Et} < \text{PNP-Cy} \approx \text{PNP}^{\text{Ph-}i\text{Pr}} < \text{PNP}^{\text{Ph-Et}} < \text{PNP}^{\text{Me-Ph}} < \text{PNP}^{\text{Me-Et}} < \text{PNP-}i\text{Pr} < \text{PNP-}t\text{Bu} < \text{PNP}^{\text{Me-}i\text{Pr}} <$

Chapter 3 – Tricarbonyl Molybdenum and Tungsten Complexes

PNP-TADDOL < PNP-BIPOL (Table 3.1. and 3.2.). Concerning the free ligands, the order of the δP values varies slightly for some of them PNP-*i*Pr < PNP^{Me}-Ph \approx PNP^{Ph}-*n*Pr < PNP^{Me}-Et < PNP^{Ph}-Et (Chapter 2).

Table 3.1. Selected $^{13}\text{C}\{^1\text{H}\}$ and $^{31}\text{P}\{^1\text{H}\}$ NMR and IR data of pincer tricarbonyl Mo complexes

Complexes	$^{13}\text{C}\{^1\text{H}\} / \delta$		$^{31}\text{P}\{^1\text{H}\} / \delta$	IR / cm^{-1}		
	CO	CO		ν_{CO}	ν_{CO}	ν_{CO}
[Mo(PNP-Et)(CO) ₃] (2a)	230.3	213.8	111.3	1929	1840	1780
[Mo(PNP- <i>i</i> Pr)(CO) ₃] (2b*)	231.4	216.9	132.7	1936	1809	1790
[Mo(PNP-Cy)(CO) ₃] (2c)	231.1	216.4	122.6	1941	1828	1790
[Mo(PNP- <i>t</i> Bu)(CO) ₃] (2d*)	233.1	224.0	148.8	1922	1808	1771
[Mo(PNP-Ph)(CO) ₃] (2e*)	228.4	211.2	104.0	1964	1858	1765
[Mo(<i>i</i> Pr-PNP-Ph)(CO) ₃] (2f)	229.4	213.8	132.1/104.7	1956	1844	1757
[Mo(PNP-BIPOL)(CO) ₃] (2g)	224.7	208.4	204.8	1985	1876	-
[Mo(PNP-TADDOL)(CO) ₃] (2h)	221.6	206.7	172.7	1980	1946	1867
[Mo(PNP ^{Me} -Et)(CO) ₃] (2i)	230.6	214.9	132.3	1942	1822	1806
[Mo(PNP ^{Me} - <i>i</i> Pr)(CO) ₃] (2j*)	230.8	217.9	159.0	1936	1810	1795
[Mo(PNP ^{Me} -Ph)(CO) ₃] (2k)	227.8	211.9	131.0	1956	1911	1850
[Mo(PNP ^{Ph} -Et)(CO) ₃] (2l)	229.9	214.3	129.5	1949	1815	-
[Mo(PNP ^{Ph} - <i>n</i> Pr)(CO) ₃] (2m)	229.6	213.8	122.6	1951	1857	1821

*Previous prepared in the literature^{18,21,24}

Both the carbonyl resonances (δCO) and the phosphorus resonances (δP) exhibit a significant upfield shift comparing Mo and W (Table 3.1 and 3.2.). Upon coordination with to the metal, the proton of the NH linker becomes more acidic. This is evident from the downfield shift of the corresponding signal in the ^1H NMR for both Mo and W complexes.

In all complexes, the PNP pincer ligand adopts the typical *mer* coordination mode with no evidence for any *fac* isomers. The IR spectra show, in most cases, the typical three strong to medium absorption bands of a *mer* CO arrangement assignable to one weaker symmetric and two strong asymmetric ones. The ν_{CO} frequencies, in particular the symmetric CO stretch which presents the highest stretching frequency, is indicative for the increasing electron donor strengths of the PNP ligands and follow the order PNP-BIPOL < PNP-TADDOL < PNP-Ph < *i*Pr-PNP-Ph \approx PNP^{Me}-Ph < PNP^{Ph}-*n*Pr < PNP^{Ph}-Et < PNP^{Me}-Et < PNP-Cy < PNP-*i*Pr \approx PNP^{Me}-*i*Pr < PNP-Et < PNP-*t*Bu (Tables 3.1. and 3.2.). Due to the higher electron density at the tungsten, there is a slight shift for lowest ν_{CO} frequencies of the three carbonyls ligands.

Table 3.2. Selected $^{13}\text{C}\{^1\text{H}\}$ and $^{31}\text{P}\{^1\text{H}\}$ NMR and IR data of the pincer tricarbonyl W complexes

Complexes	$^{13}\text{C}\{^1\text{H}\} / \delta$		$^{31}\text{P}\{^1\text{H}\} / \delta$	IR / cm^{-1}		
	CO	CO		ν_{CO}	ν_{CO}	ν_{CO}
[W(PNP-Et)(CO) ₃] (3a)	222.0	208.2	94.0	1921	1834	1768
[W(PNP- <i>i</i> Pr)(CO) ₃] (3b *)	221.1	210.6	116.5	1929	1805	1784
[W(PNP-Cy)(CO) ₃] (3c)	222.3	211.3	109.5	1933	1807	1773
[W(PNP- <i>t</i> Bu)(CO) ₃] (3d *)	224.7	219.4	135.2	1914	1799	1759
[W(PNP-Ph)(CO) ₃] (3e *)	206.0	196.6	88.2	1955	1847	1759
[W(PNP-BIPOL)(CO) ₃] (3g)	215.5	201.4	188.2	1979	1858	-
[W(PNP ^{Me} -Et)(CO) ₃] (3i)	222.4	208.9	115.8	1934	1795	-
[W(PNP ^{Me} - <i>i</i> Pr)(CO) ₃] (3j)	222.5	211.6	144.0	1928	1890	1797
[W(PNP ^{Me} -Ph)(CO) ₃] (3k)	221.1	207.4	114.7	1954	1839	1801
[W(PNP ^{Ph} -Et)(CO) ₃] (3l)	221.7	208.4	112.7	1934	1804	-

*Previous prepared in the literature²⁴

In addition to spectroscopic characterization, the solid-state structures of **2h**, **2k** and **3l** were determined by single-crystal X-ray diffraction. Structural views are depicted in Figures 3.6.-3.8. with selected bond distances given in the captions. The coordination geometry around the molybdenum center of **2h** and **2k** corresponds to a distorted octahedron with a P-Mo-P and trans-C_{CO}-Mo-C_{CO} bond angle of 155.61(5)^o and 175.8(2)^o (Mo(PNP-TADDOL)(CO)₃) and of 155.48(1)^o and 166.15(5)^o (Mo(PNP^{Me}-Ph)(CO)₃), respectively.

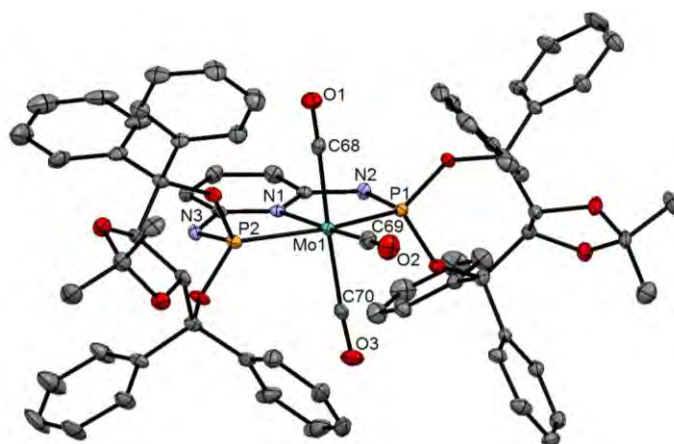


Figure 3.6. Structural view of [Mo(PNP-TADDOL)(CO)₃] \cdot CH₂Cl₂ (**2h** \cdot CH₂Cl₂) showing 50% thermal ellipsoids (hydrogen atoms and solvent omitted for clarity). Selected bond lengths (Å) and bond angles (°): Mo1-C68 2.029(6), Mo1-C69 1.967(6), Mo1-C70 2.037(6), Mo1-P1 2.329(1), Mo1-P2 2.361(1), Mo-N1 2.242(4), P1-Mo1-P2 155.61(5), N1-Mo1-C69 175.3(2), C68-Mo1-C70 175.8(2)

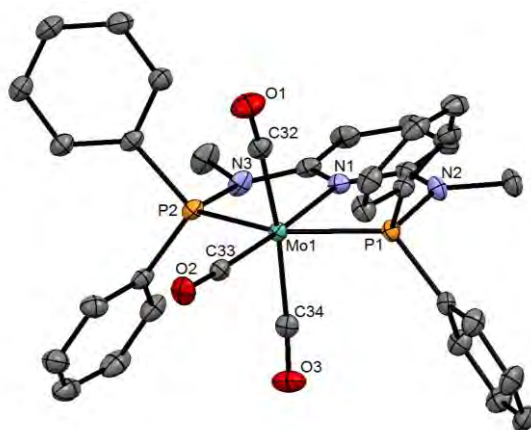


Figure 3.7. Structural view of $[\text{Mo}(\text{PNP}^{\text{Me}}\text{-Ph})(\text{CO})_3] \cdot \text{CH}_2\text{Cl}_2$ (**2k**· CH_2Cl_2) showing 50% thermal ellipsoids (hydrogen atoms and solvent omitted for clarity). Selected bond lengths (Å) and bond angles ($^\circ$): Mo1-C32 2.020(1), Mo1-C33 1.957(1), Mo1-C34 2.030(1), Mo1-P1 2.3816(4), Mo1-P2 2.3890(4), Mo-N1 2.246(1), P1-Mo1-P2 155.48(1), N1-Mo1-C33 176.22(5), C32-Mo1-C34 166.15(5)

For comparison, in the $[\text{Mo}(\text{PNP})(\text{CO})_3]$ complexes **2b**, **2d**, **2e**, **2j** the P1–Mo–P2 angles are also hardly affected by the size of the substituents of the phosphorus atoms, being $155.0(2)^\circ$, $155.62(1)^\circ$, $155.3(1)^\circ$, and $151.73(1)^\circ$, respectively. The carbonyl-Mo-carbonyl angles of the CO ligands trans to one another deviate significantly from 180° and typically vary strongly with the bulkiness of the PR_2 moiety ($\text{PNP-TADDOL} < \text{PNP-Ph} < \text{PNP}^{\text{Me}}\text{-Ph} > \text{PNP-}i\text{Pr} < \text{PNP}^{\text{Me}}\text{-}i\text{Pr} < \text{PNP-}t\text{Bu}$). Reflecting a decrease from $175.8(2)^\circ$ in $[\text{Mo}(\text{PNP-TADDOL})(\text{CO})_3]$ (**2h**) to $171.1(8)^\circ$ in $[\text{Mo}(\text{PNP-Ph})(\text{CO})_3]$ ¹⁸ to $166.15(5)^\circ$ in $[\text{Mo}(\text{PNP}^{\text{Me}}\text{-Ph})(\text{CO})_3]$ (**2k**) to $166.03(5)^\circ$ in $[\text{Mo}(\text{PNP-}i\text{Pr})(\text{CO})_3]$ ²¹ to $162.93(7)^\circ$ in $[\text{Mo}(\text{PNP}^{\text{Me}}\text{-}i\text{Pr})(\text{CO})_3]$ ²⁴, and finally to $156.53(4)^\circ$ in $[\text{Mo}(\text{PNP-}t\text{Bu})(\text{CO})_3]$ ²¹.

The coordination geometry around the tungsten center, as in the case of analogous molybdenum complexes, corresponds to a distorted octahedron. The complex $[\text{W}(\text{PNP}^{\text{Ph}}\text{-Et})(\text{CO})_3]$ (Figure 3.8.) presents P–W–P and trans- $\text{C}_{\text{CO}}\text{-W-C}_{\text{CO}}$ bond angles $156.11(3)^\circ$ and $164.6(1)^\circ$ (**3i**). For comparison, in the $[\text{W}(\text{PNP})(\text{CO})_3]$ complexes **3b** and **3d** the P1–W–P2 angles are $154.43(4)^\circ$ and $151.42(2)^\circ$, respectively.

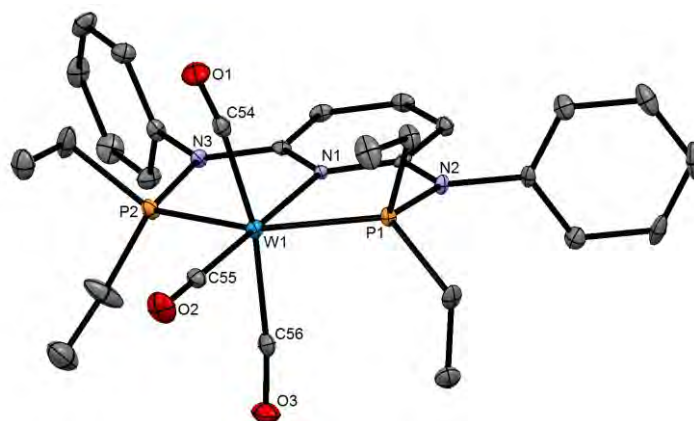


Figure 3.8. Structural view of $[W(\text{PNP}^{\text{Ph}}\text{-Et})(\text{CO})_3]\cdot\text{CH}_3\text{CN}$ (**3I** $\cdot\text{CH}_3\text{CN}$) showing 50% thermal ellipsoids (hydrogen atoms and solvent omitted for clarity). Selected bond lengths (Å) and bond angles ($^\circ$): W1-C54 2.04(3), W1-C55 1.966(3), W1-C56 2.015(3), W1-P1 2.405(1), W1-P2 2.385(1), W1-N1 2.262(2), P1-W1-P2 156.11(3), N1-W1-C55 179.8(1), C54-W1-C56 164.6(1)

Similar to the analogous $[\text{Mo}(\text{PNP})(\text{CO})_3]$ complexes the P1-M-P2 angles are slightly affected by the size of the substituents of the phosphorus atoms. The carbonyl-W-carbonyl angles vary with the bulkiness of the PR_2 moiety and decrease from $165.7(2)^\circ$ in $[\text{W}(\text{PNP-}i\text{Pr})(\text{CO})_3]^{24}$ to $164.6(1)^\circ$ in $[\text{W}(\text{PNP}^{\text{Ph}}\text{-Et})(\text{CO})_3]$ (**2k**) and finally to $156.53(4)^\circ$ in $[\text{W}(\text{PNP-}t\text{Bu})(\text{CO})_3]^{24}$. Accordingly, the bulkiness of the PNP ligands follows roughly the order (PNP- *i*Pr < $\text{PNP}^{\text{Ph}}\text{-Et}$ < PNP-*t*Bu).

3.4.1. Pyridine versus triazine backbones

The alterations on the atoms in the backbone influence the central atom that consequently suggests strong variation of the donor properties. With this in mind, the substitution of pyridine with triazine, that under normal conditions is an electron poor unimportant and weak coordinative ligand, was performed (Figure 3.9.). The increasing number of nitrogen atoms in the aromatic ring makes the π electron density in the ring decreases, making the backbone of the pincer ligands more electron-deficient.²⁸

Over the years new pincer molybdenum tricarbonyl complexes, based on a 2,6-diamino-1,3,5-triazine scaffold with some modification on the para position, were developed by Kirchner and coworkers through the same methodology (Figure 3.9.).^{21,29}

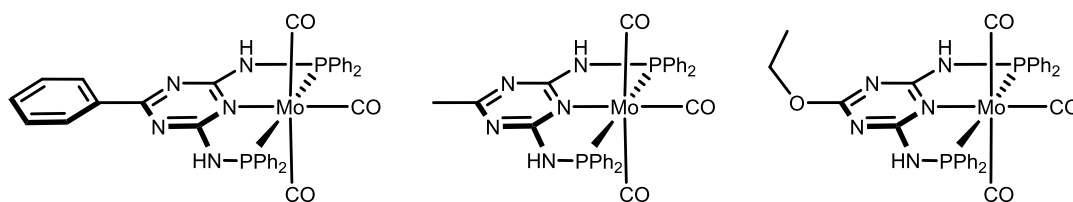


Figure 3.9. Pincer triazine-based tricarbonyl Mo complexes

In this work, only one example is presented, the pincer ligand with 2,6-diamino-4-methyl-1,3,5-triazine scaffold (Triaz^{Me}-*i*Pr) that was coordinated to Mo and W following the same procedure developed for pyridine-based systems (**2n**, **3n**).

Both the carbonyl resonances (δ_{CO}) and the phosphorus resonances (δ_P) exhibit an upfield shift on going from pyridine to a triazine backbone for both Mo and W tricarbonyl complexes (Table 3.3.). The $^{31}P\{^1H\}$ NMR of the W complex spectra exhibit singlet resonances with $^1J_{WP}$ coupling constant of 318 Hz lower than the others tricarbonyl tungsten complexes (Table 3.2.). The $[Mo(Triaz^{Me}-Ph)(CO)_3]$ complex, already described in literature, behaves in an identical way when compared with its analogous complex $[Mo(PNP-Ph)(CO)_3]$.

Table 3.3. Selected $^{13}C\{^1H\}$ NMR and $^{31}P\{^1H\}$ NMR and IR data of the triazine-based tricarbonyl Mo and W PNP pincer complexes

Complexes	$^{13}C\{^1H\} / \delta$		$^{31}P\{^1H\} / \delta$	IR / cm^{-1}	
	CO	CO		ν_{CO}	ν_{CO}
$[Mo(Triaz^{(Me)}-iPr)(CO)_3]$ (2n)	228.9	215.4	131.0	1946	1822
$[W(Triaz^{(Me)}-iPr)(CO)_3]$ (3n)	220.6	209.2	113.2	1943	1818

One more time, the mer coordination mode is preferred, with no evidence for any fac isomers. The IR spectra show, two strong to medium absorption bands in the range of 1946–1818 cm^{-1} assignable to one weaker symmetric and the merged two strong asymmetric ν_{CO} stretching modes. When compared with the $[M(PNP-*i*Pr)(CO)_3]$ (M = Mo, W), the ν_{CO} frequencies shift for an highest numbers, which means less backdonation that implies that the backbone of the pincer ligand decreases the electron density at the metal center, like it was expected.

3.4.2. Steric effect of linkers

Since spacers have a profound impact on the steric demand of the ligands and consequently on the reactivity of transition metal PNP complexes, in addition to the

Chapter 3 – Tricarbonyl Molybdenum and Tungsten Complexes

previous investigation, the research of molybdenum and tungsten complexes featuring different bridges in the PNP ligands possess a necessary obligation. Aside from the previous series of Mo and W tricarbonyl PNP pincer complexes with diverse amine spacers (NR, R = H, Me, Ph), recently a series of molybdenum and tungsten PONOP pincer complexes were synthesized by Jones's²³ working group (Figure 3.10.).

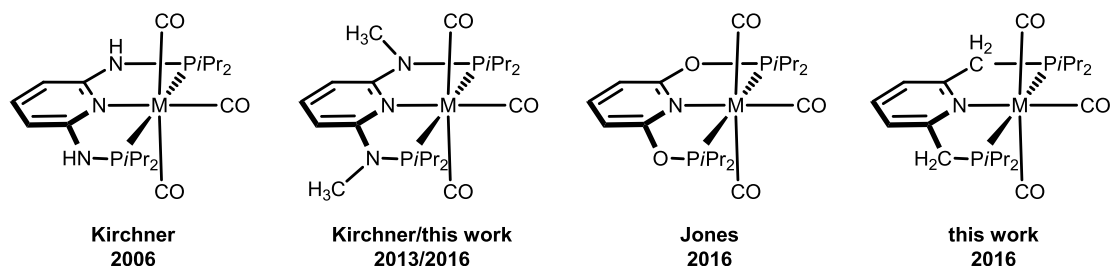


Figure 3.10. Mo and W PNP pincer tricarbonyl complexes with different linkers

The famous PNP ligand with a CH₂ linker is well known for forming complexes with a variety of transition metals (e.g., Fe, Ru, Rh, Ir, Pd, Pt)³⁰, except for Mo and W. Compounds **2p** and **3p** were synthesized by a solvothermal reaction. The ¹³C{¹H} NMR spectra of these complexes present also two low-field triplet resonances (1:2 ratio) in the range of 236–215 ppm (Table 3.4.). In comparison to the complexes M(PNP-*i*Pr)(CO)₃ (**2b**, **3b**), M(PNP^{Me}-*i*Pr)(CO)₃ (**2j**, **3j**) and M(PONOP-*i*Pr)(CO)₃ (**2o**, **3o**), the carbonyl resonances (δCO) exhibit an downfield shift for all the complexes with CH₂ linker and always an upfield shift for the O linker (Table 3.1., 3.2., 3.4.). The carbonyl resonances (δCO) also exhibit a significant upfield shift on going from Mo to W.

Table 3.4. Selected ¹³C{¹H} NMR and ³¹P{¹H} NMR and IR data of the pincer tricarbonyl Mo and W complexes with “O” and “CH₂” linkers

Complexes	¹³ C{ ¹ H} / δ		³¹ P{ ¹ H} / δ	IR / cm ⁻¹		
	CO	CO		ν _{CO}	ν _{CO}	ν _{CO}
Mo(PONOP- <i>i</i> Pr)(CO) ₃ (2o *)	226.6	216.5	228.9	1957	1861	1833
Mo(PNP(CH ₂)- <i>i</i> Pr)(CO) ₃ (2p)	235.9	219.8	81.2	1928	1816	1793
W(PONOP- <i>i</i> Pr)(CO) ₃ (3o *)	217.9	210.2	209.8	1950	1839	1820
W(PNP(CH ₂)- <i>i</i> Pr)(CO) ₃ (3p)	227.8	215.1	67.5	1920	1808	1787

*Previous prepared in the literature²³

Similar to the carbonyl resonances (δCO) the phosphorus resonances (δP) exhibit a significant upfield shift on going from the O, NCH₃, NH to the CH₂ linker,

ordering in the reversed way the π -accepting/ σ -donating capabilities of phosphines. The IR spectra of the tricarbonyl complexes contain the typical three strong to medium absorption bands of a mer CO arrangement in the range of 1957–1790 cm^{-1} . The ν_{CO} frequencies, follow the order $\text{PONOP-}i\text{Pr} < \text{PNP}^{\text{Me}}\text{-}i\text{Pr} \approx \text{PNP-}i\text{Pr} < \text{PNP}(\text{CH}_2)\text{-}i\text{Pr}$ which indicate the increasing electron donor strengths of the PNP ligands, for both Mo and W complexes.

3.5. Conclusions

In summary, it was demonstrated that the solvothermal synthesis technique provides a powerful, simple, and practical synthetic method to afford molybdenum and tungsten PNP pincer carbonyl complexes of the type $[\text{M}(\text{PNP})(\text{CO})_3]$ ($\text{M} = \text{Mo}, \text{W}$) in high isolated yields in a short time. It has to be emphasized that in particular the short reaction times allow the use of thermally more sensitive ligands. As far as W complexes are concerned, these complexes are not readily accessible with conventional methods. Moreover, this study also allows a direct comparison of steric and electronic properties of Mo and W metal PNP pincer complexes.

3.6. Experimental part

The metal precursors hexacarbonyl of molybdenum and tungsten were purchased from commercial vendors. The precursor complexes $[\text{Mo}(\text{CO})_4(\mu\text{-Br})\text{Br}]_2$ and $[\text{W}(\text{CO})_4(\mu\text{-Br})\text{Br}]_2$ were prepared according to the literature.³¹ The IR spectra were recorded on Bruker Tensor 27 spectrometer, in the range between 600 and 4000 cm^{-1} with a resolution of 4 cm^{-1} .*

3.6.1. Syntheses

General synthetic procedure for tricarbonyl molybdenum and tungsten complexes: A suspension of the metal hexacarbonyl (0.60 mmol) and 1 equiv. of the respective PNP ligand (0.60 mmol) in CH_3CN (4 mL) were placed in a 20 mL sealed glass tube and stirred for 2 h at 135 °C (unless otherwise noted) whereupon a clear solution was obtained. The reaction mixture was allowed to cool to room temperature without stirring. In most cases the product was obtained as crystalline material and was decanted and washed with *n*-pentane. In all other cases the solvent was removed

* The same experimental conditions in the following chapters.

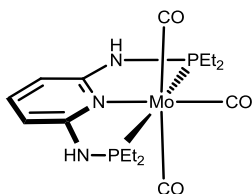
Chapter 3 – Tricarbonyl Molybdenum and Tungsten Complexes

under reduced pressure. The remaining solid was washed with *n*-pentane and dried under vacuum.

Alternative synthetic procedure: Method A: A suspension of $[\text{Mo}(\text{CO})_6]$ (1.0 mmol) in CH_3CN (20 mL) was refluxed for 3 h under an argon atmosphere. The resulting yellow solution was cooled down to room temperature and 1 equiv. of respective PNP ligand (1.0 mmol) in toluene (8 mL) was added and the solution was refluxed for 1-4 days, depending on the ligand. After this period the solvent was evaporated under vacuum and the compound was washed with CH_3CN and *n*-pentane. The compound was dried under vacuum affording a yellow powder.

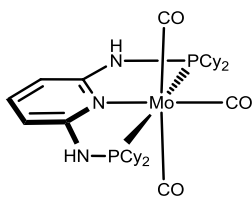
Method B: A solution of $[\text{W}(\text{CO})_4(\mu\text{-Br})\text{Br}]_2$ (1.0 mmol) in CH_2Cl_2 (10 mL) was treated with 0.5 equiv. of PNP ligand (1.0 mmol) and the mixture was stirred for 5 h at room temperature. After removal of the solvent under reduced pressure, a solid was obtained, which was washed with diethyl ether mixture and dried under vacuum yield the $[\text{W}(\text{PNP})(\text{CO})_3\text{Br}]\text{Br}$ compound. The compound is dissolved in THF (15 mL) and stirred in the presence of NaHg (10%) (3.0 mmol) for 8 h at room temperature. The solvent was then removed under reduced pressure. The residue was redissolved in acetone (10 mL), and the solution was filtered through Celite. After removal of the solvent under reduced pressure, a yellow solid was obtained, which was washed twice with diethyl ether (10 mL) and dried under vacuum.

$[\text{Mo}(\text{PNP-Et})(\text{CO})_3]$ (2a)



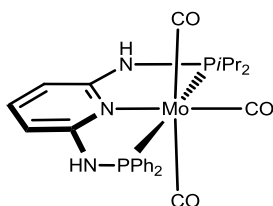
The product was obtained as yellow crystals in 91% yield. Anal. Calcd. for $\text{C}_{16}\text{H}_{25}\text{MoN}_3\text{O}_3\text{P}_2$ (465.30). C, 41.30; H, 5.42; N, 9.03. Found: C, 41.21; H, 5.55; N, 9.11. $^1\text{H NMR}$ (δ , CD_2Cl_2 , 20 °C): 7.12 (t, $J = 7.9$ Hz, 1H, py^4), 6.07 (d, $J = 8.0$ Hz, 2H, $\text{py}^{3,5}$), 5.32 (s, 2H, NH), 2.11-2.06 (m, 4H, CH_2), 2.03-1.97 (m, 4H, CH_2), 1.26-1.13 (m, 12H, CH_3). $^{13}\text{C}\{^1\text{H}\}$ NMR (δ , CD_2Cl_2 , 20 °C): 230.2 (t, $J = 5.2$ Hz, CO), 213.8 (t, $J = 10.5$ Hz, CO), 160.2 (vt, $J = 8.6$ Hz, $\text{py}^{2,6}$), 137.1 (py^4), 97.4 (vt, $J = 2.8$ Hz, $\text{py}^{3,5}$), 28.1 (vt, $J = 10.8$ Hz, CH_2), 7.8 (CH_3). $^{31}\text{P}\{^1\text{H}\}$ NMR (δ , CD_2Cl_2 , 20 °C): 111.3. IR (ATR, cm^{-1}): 1929 (ν_{CO}), 1840 (ν_{CO}), 1780 (ν_{CO}).

[Mo(PNP-Cy)(CO)₃] (2c)



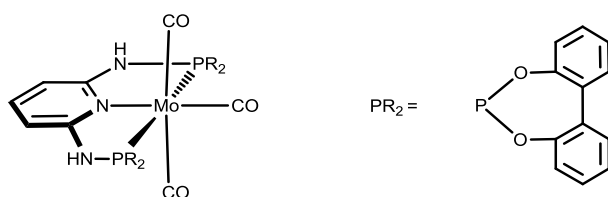
The product was obtained as a yellow solid in 96% yield. Anal. Calcd. for C₃₂H₄₉MoN₃O₃P₂ (681.67). C, 56.38; H, 7.25; N, 6.15. Found: C, 56.21; H, 7.35; N, 6.31. ¹H NMR (δ, CD₂Cl₂, 20 °C): 7.16 (t, J = 7.6 Hz, 1H, py⁴), 6.11 (d, J = 7.8 Hz, 2H, py^{3,5}), 5.32 (s, 2H, NH), 2.14-1.77 (m, 22H, Cy), 1.63-1.19 (m, 22H, Cy). ¹³C{¹H} NMR (δ, CD₂Cl₂, 20 °C): 231.1 (br, CO), 216.4 (t, J = 10.0 Hz, CO), 160.9 (vt, J = 7.0 Hz, py^{2,6}), 137.6 (py⁴), 97.5 (py^{3,5}), 42.9 (vt, J = 8.9 Hz, Cy), 28.8 (d, J = 32.3 Hz, Cy), 27.5 (d, J = 25.6 Hz, Cy), 26.7 (Cy). ³¹P{¹H} NMR (δ, CD₂Cl₂, 20 °C): 122.6. IR (ATR, cm⁻¹): 1941 (ν_{CO}), 1828 (ν_{CO}), 1790 (ν_{CO}).

[Mo(Ph-PNP-*i*Pr)(CO)₃] (2f)



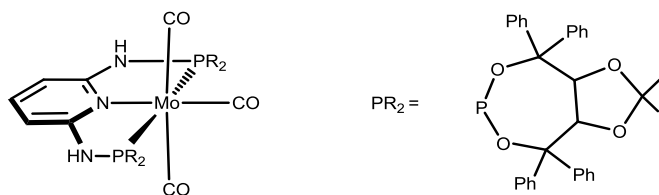
The product was obtained as a yellow solid in 92.7% yield. Anal. Calcd. for C₂₆H₂₉MoN₃O₃P₂ (589.43). C, 52.98; H, 4.96; N, 7.13. Found: C, 52.34; H, 5.09; N, 7.38. ¹H NMR (δ, acetone-*d*₆, 20 °C): 8.16 (d, J = 5.1 Hz, 1H, Ph), 7.73-7.63 (m, 4H, Ph), 7.44-7.30 (m, 6H, Ph, py⁴), 7.21 (dd, J = 10.0 Hz, 5.9 Hz, 2H, NH), 6.43 (d, J = 7.9, 1H, py^{3,5}), 6.27 (d, J = 8.0 Hz, 1H, py^{3,5}), 2.48-2.27 (m, 2H, CH), 1.31 (d, J = 6.9 Hz, 3H, CH₃), 1.24 (dd, J = 7.0 Hz, J = 3.8 Hz, 6H, CH₃), 1.17 (d, J = 7.2 Hz, 3H, CH₃). ¹³C{¹H} NMR (δ, acetone-*d*₆, 20 °C): 229.4 (t, J = 5.3 Hz, CO), 213.8 (t, J = 10.3 Hz, CO), 161.5 (dd, J = 11.8 Hz, J = 4.4 Hz, py^{2,6}), 160.4 (dd, J = 15.2 Hz, J = 4.3 Hz, py^{2,6}), 141.8 (py⁴), 141.2 (py⁴), 137.5 (Ph), 130.5 (vd, J = 14.6 Hz, Ph), 129.2 (vd, J = 1.7 Hz, Ph), 128.0 (vd, J = 9.9 Hz, Ph), 97.8 (d, J = 6.0 Hz, py^{3,5}), 97.7 (d, J = 7.3 Hz, py^{3,5}), 32.1 (d, J = 20.0 Hz, CH), 18.2 (vt, J = 6.9 Hz, CH₃). ³¹P{¹H} NMR (δ, acetone-*d*₆, 20 °C): 132.1 (d, J = 97.6 Hz), 104.7 (d, J = 97.4 Hz). IR (ATR, cm⁻¹): 1956 (ν_{CO}), 1844 (ν_{CO}), 1757 (ν_{CO}).

[Mo(PNP-BIPOL)(CO)₃] (2g)

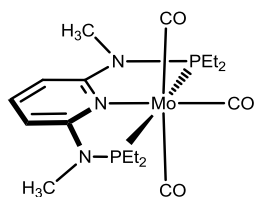


The product was obtained as a yellow solid in 95% yield. Anal. Calcd. for C₃₂H₂₁MoN₃O₇P₂ (717.44). C, 53.57; H, 2.95; N, 5.86. Found: C, 53.51; H, 2.89; N, 5.80. ¹H NMR (δ, acetone-d₆, 20 °C): 8.96 (s, 2H, NH), 7.78 (dd, J = 7.7 Hz, J = 1.7 Hz, 4H, Ph), 7.55-7.48 (m, 5H, Ph, py⁴), 7.44-7.37 (m, 8H, Ph), 6.62 (d, J = 8 Hz, 2H, py^{3,5}). ¹³C{¹H} NMR (δ, acetone-d₆, 20 °C): 224.7 (t, J = 8.5 Hz, CO), 208.4 (t, J = 13.7 Hz, CO), 159.4 (vt, J = 11.4 Hz, py^{2,6}), 150.7 (vt, J = 4.5 Hz, Ph), 139.8 (py⁴), 131.5 (Ph), 130.6 (2Ph), 126.6 (Ph), 123.2 (Ph), 100.7 (py^{3,5}). ³¹P{¹H} NMR (δ, acetone-d₆, 20 °C): 204.8. IR (ATR, cm⁻¹): 1985 (ν_{CO}), 1876 (ν_{CO}).

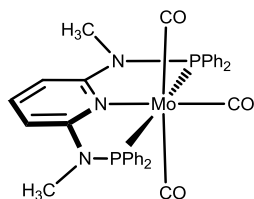
[Mo(PNP-TADDOL)(CO)₃] (2h)



The product was obtained as a yellow solid in 89.6% yield. Anal. Calcd. for C₇₀H₆₁MoN₃O₁₁P₂ (1278.15). C, 65.78; H, 4.81; N, 3.29. Found: C, 65.23; H, 4.37; N, 3.08. ¹H NMR (δ, CD₂Cl₂, 20 °C): 7.57 (d, J = 7.3 Hz, 4H, Ph), 7.44-7.39 (m, 4H, Ph), 7.34 (vt, J = 7.4 Hz, 4H, Ph), 7.30 (vt, J = 7.2 Hz, 2H, Ph), 7.26-7.11 (m, 26H, Ph), 6.90 (t, J = 7.9 Hz, 1H, py⁴), 5.34 (dd, J = 36.4 Hz, 7.9 Hz, 4H, CH^{TAD}), 5.27 (d, J = 8.0, 2H, py^{3,5}), 5.09 (s, 2H, NH), 0.50 (s, 6H, CH₃^{TAD}), 0.40 (s, 6H, CH₃^{TAD}). ¹³C{¹H} NMR (δ, CD₂Cl₂, 20 °C): 221.6 (t, J = 8.1 Hz, CO), 206.7 (t, J = 13.0 Hz, CO), 155.4 (t, J = 10.3 Hz, py^{2,6}), 144.2 (Ph), 141.5 (Ph), 140.9 (Ph), 140.0 (Ph), 136.3 (py⁴), 127.9 (Ph), 127.8 (Ph), 127.6 (Ph), 127.3 (d, J = 12.9 Hz, Ph), 127.1 (Ph), 126.4 (d, J = 10.6 Hz, Ph), 126.2 (Ph), 126.1 (Ph), 126.0 (Ph), 114.2 (CCH₃^{TAD}), 97.6 (py^{3,5}), 87.9 (t, J = 7.9 Hz, C(Ph)₂), 85.9 (C(Ph)₂), 78.7 (d, J = 27.6 Hz, CH^{TAD}), 25.7 (CH₃^{TAD}), 25.3 (CH₃^{TAD}). ³¹P{¹H} NMR (δ, CD₂Cl₂, 20 °C): 172.7. IR (ATR, cm⁻¹): 1980 (ν_{CO}), 1946 (ν_{CO}), 1867 (ν_{CO}).

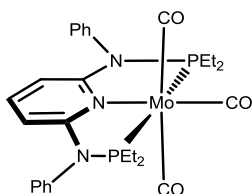
[Mo(PNP^{Me}-Et)(CO)₃] (2i)

The product was obtained as yellow crystals in 91% yield. Anal. Calcd. for C₁₈H₂₉MoN₃O₃P₂ (493.35). C, 43.82; H, 5.92; N, 8.52. Found: C, 43.21; H, 5.44; N, 8.09. ¹H NMR (δ, CD₂Cl₂, 20 °C): 7.32 (tt, J = 8.2 Hz, J = 1.1 Hz, 1H, py⁴), 5.98 (d, J = 8.2 Hz, 2H, py^{3,5}), 2.92 (t, J = 1.7 Hz, 6H, NCH₃), 2.16-2.08 (m, 4H, CH₂), 2.04-1.92 (m, 4H, CH₂), 1.20-1.04 (m, 12H, CH₃). ¹³C{¹H} NMR (δ, CD₂Cl₂, 20 °C): 230.6 (t, J = 5.2 Hz, CO), 214.9 (t, J = 10.7 Hz, CO), 162.1 (vt, J = 10.2 Hz, py^{2,6}), 137.9 (py⁴), 97.4 (vt, J = 2.7 Hz, py^{3,5}), 32.7 (t, J = 1.7 Hz, NCH₃), 27.1 (vt, J = 10.0 Hz, CH₂), 8.1 (t, J = 2.4 Hz, CH₃). ³¹P{¹H} NMR (δ, CD₂Cl₂, 20 °C): 132.3. IR (ATR, cm⁻¹): 1942 (ν_{CO}), 1822 (ν_{CO}), 1806 (ν_{CO}).

[Mo(PNP^{Me}-Ph)(CO)₃] (2k)

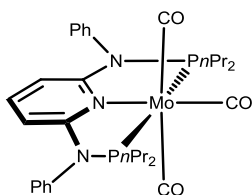
The product was obtained as a yellow solid in 92 % yield. Anal. Calcd. For C₃₄H₂₉N₃O₃P₂Mo (685.51): C, 59.57; H, 4.26; N, 6.13%. Found: C, 59.74; H, 4.19; N, 6.23%. ¹H NMR (δ, CD₂Cl₂, 20 °C): 7.44-7.60 (m, 21H, Ph, py⁴), 6.34 (d, J = 8.2 Hz, 2H, py^{3,5}), 2.99 (s, 6H, NCH₃). ¹³C {¹H} NMR (δ, CD₂Cl₂, 20 °C): 227.8 (t, J = 4.9 Hz, CO), 211.9 (t, J = 9.9 Hz, CO), 161.0-161.1 (m, py^{2,6}), 143.9 (py⁴), 136.3 (vt, J = 5.8 Hz, py^{2,6}), 134.9 (vd, J = 45.5 Hz, Ph¹), 131.8 (Ph⁴), 130.6 (vt, J = 5.2 Hz, Ph^{3,5}), 130.5 (Ph⁴), 129.0 (vd, J = 58.8 Hz, Ph¹), 128.4 (vt, J = 4.9 Hz, Ph^{3,5}), 127.9 (vt, J = 5.4 Hz, Ph^{2,6}), 100.0 (py^{3,5}), 35.7 (NCH₃). ³¹P{¹H} NMR (δ, CD₂Cl₂, 20 °C): 131.0. IR (ATR, cm⁻¹): 1956 (ν_{CO}), 1911 (ν_{CO}), 1850 (ν_{CO}).

[Mo(PNP^{Ph}-Et)(CO)₃] (2l)



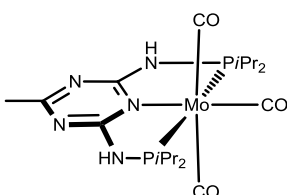
The product was obtained as a yellow-brown solid in 99% yield. Anal. Calcd. for C₂₈H₃₃MoN₃O₃P₂ (617.50). C, 54.46; H, 5.39; N, 6.81. Found: C, 54.50; H, 5.35; N, 6.88. ¹H NMR (δ, CD₂Cl₂, 20 °C): 7.54-7.38 (m, 6H, Ph), 7.27-7.12 (m, 4H, Ph), 6.89 (br, 1H, py⁴), 5.35 (br, 2H, py^{3,5}), 1.98 (br, 8H, CH₂), 1.29 (br, 12H, CH₃). ¹³C{¹H} NMR (δ, CD₂Cl₂, 20 °C): 229.9 (t, J = 5.0 Hz, CO), 214.3 (t, J = 10.5 Hz, CO), 163.5 (vt, J = 10.6 Hz, py^{2,6}), 140.5 (Ph), 136.7 (py⁴), 130.8 (Ph), 130.4 (Ph), 128.3 (Ph), 100.8 (py^{3,5}), 28.3 (vt, J = 9.9 Hz, CH₂), 9.1 (CH₃). ³¹P{¹H} NMR (δ, CD₂Cl₂, 20 °C): 129.5. IR (ATR, cm⁻¹): 1949 (ν_{CO}), 1815 (ν_{CO}).

[Mo(PNP^{Ph}-*n*Pr)(CO)₃] (2m)



The product was obtained as a yellow-brown solid in 97.1% yield. Anal. Calcd. for C₃₂H₄₁MoN₃O₃P₂ (673.59). C, 57.06; H, 6.14; N, 6.24. Found: C, 56.81; H, 5.95; N, 6.02. ¹H NMR (δ, CD₂Cl₂, 20 °C): 7.57-7.36 (m, 6H, Ph), 7.17-7.09 (m, 4H, Ph), 6.84 (t, J = 8.2 Hz, 1H, py⁴), 5.30 (d, J = 8.2 Hz, 2H, py^{3,5}), 2.03-1.68 (m, 8H, CH₂), 1.68-1.49 (m, 8H, CH₂), 1.07-0.96 (m, 12H, CH₃). ¹³C{¹H} NMR (δ, CD₂Cl₂, 20 °C): 229.6 (t, J = 5.1 Hz, CO), 213.8 (t, J = 10.6 Hz, CO), 163.0 (vt, J = 10.9 Hz, py^{2,6}), 140.3 (Ph), 136.3 (py⁴), 130.6 (Ph), 130.1 (Ph), 128.0 (Ph), 100.5 (py^{3,5}), 38.0 (vt, J = 9.7 Hz, CH₂), 18.5 (vt, J = 3.8 Hz, CH₂), 15.7 (vt, J = 8.3 Hz, CH₃). ³¹P{¹H} NMR (δ, CD₂Cl₂, 20 °C): 122.6. IR (ATR, cm⁻¹): 1951 (ν_{CO}), 1857 (ν_{CO}), 1821 (ν_{CO}).

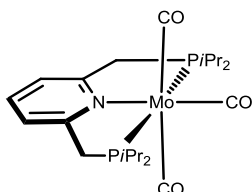
[Mo(Triaz^{Me}-*i*Pr)(CO)₃] (2n)



The product was obtained as a yellow solid in 84.8% yield. Anal. Calcd. for C₁₉H₃₃MoN₅O₃P₂ (539.11). C, 42.46; H, 6.19; N, 13.03. Found: C, 41.71; H, 5.85; N,

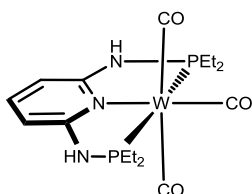
12.83. $^1\text{H NMR}$ (δ , CD_2Cl_2 , $20\text{ }^\circ\text{C}$): 5.96 (s, 2H, NH), 2.37-2.24 (m, 4H, CH), 2.16 (s, 3H, CH_3), 1.18 (ddd, $J = 16.1\text{ Hz}$, $J = 13.5\text{ Hz}$, $J = 7.1\text{ Hz}$, 24H, CH_3). $^{13}\text{C}\{^1\text{H}\}$ NMR (δ , CD_2Cl_2 , $20\text{ }^\circ\text{C}$): 228.9 (t, $J = 5.5\text{ Hz}$, CO), 215.4 (t, $J = 10.1\text{ Hz}$, CO), 174.0 (Triaz⁶), 169.7 (vt, $J = 11.0\text{ Hz}$, Triaz^{2,4}), 31.5 (vt, $J = 9.2\text{ Hz}$, CH), 25.0 (CH_3), 18.4 (vt, $J = 2.7\text{ Hz}$, CH_3), 17.9 (vt, $J = 3.6\text{ Hz}$, CH_3). $^{31}\text{P}\{^1\text{H}\}$ NMR (δ , CD_2Cl_2 , $20\text{ }^\circ\text{C}$): 131.0. IR (ATR, cm^{-1}): 1946 (ν_{CO}), 1822 (ν_{CO}).

[Mo(PNP(CH₂)-*i*Pr)(CO)₃] (2p)



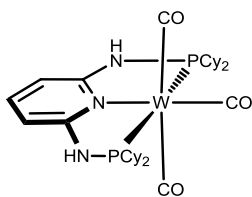
The product was obtained as yellow powder in 91% yield. Anal. Calcd. for $\text{C}_{22}\text{H}_{35}\text{MoNO}_3\text{P}_2$ (519.43). C, 50.87; H, 6.79; N, 2.70. Found: C, 50.34; H, 6.09; N, 2.23. $^1\text{H NMR}$ (δ , CD_2Cl_2 , $20\text{ }^\circ\text{C}$): 7.48 (t, $J = 7.7\text{ Hz}$, 1H, py^4), 7.20 (d, $J = 7.7\text{ Hz}$, 2H, $\text{py}^{3,5}$), 3.51-3.43 (m, 4H, CH_2), 2.41-2.18 (m, 4H, CH), 1.26 (dd, $J = 14.4\text{ Hz}$, $J = 7.0\text{ Hz}$, 12H, CH_3), 1.12 (dd, $J = 14.7$, $J = 7.2\text{ Hz}$, 12H, CH_3). $^{13}\text{C}\{^1\text{H}\}$ NMR (δ , CD_2Cl_2 , $20\text{ }^\circ\text{C}$): 235.9 (t, $J = 5.8\text{ Hz}$, CO), 219.8 (t, $J = 9.5\text{ Hz}$, CO), 163.0 (vt, $J = 5.0\text{ Hz}$, $\text{py}^{2,6}$), 135.7 (py^4), 119.9 (vt, $J = 3.8\text{ Hz}$, $\text{py}^{3,5}$), 42.7 (t, $J = 7.1\text{ Hz}$, CH_2), 28.5 (vt, $J = 8.7\text{ Hz}$, CH), 19.1-18.6 (m, CH_3). $^{31}\text{P}\{^1\text{H}\}$ NMR (δ , CD_2Cl_2 , $20\text{ }^\circ\text{C}$): 81.2. IR (ATR, cm^{-1}): 1928 (ν_{CO}), 1816 (ν_{CO}), 1793 (ν_{CO}).

[W(PNP-Et)(CO)₃] (3a)



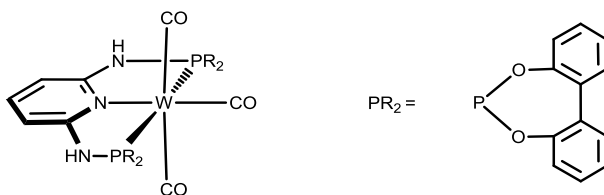
The product was obtained as a yellow solid in 79% yield. Anal. Calcd. for $\text{C}_{16}\text{H}_{25}\text{WN}_3\text{O}_3\text{P}_2$ (553.18). C, 34.74; H, 4.56; N, 7.60. Found: C, 34.61; H, 4.65; N, 7.55. $^1\text{H NMR}$ (δ , CD_2Cl_2 , $20\text{ }^\circ\text{C}$): 7.06 (t, $J = 8.0\text{ Hz}$, 1H, py^4), 6.06 (d, $J = 8.0\text{ Hz}$, 2H, $\text{py}^{3,5}$), 5.63 (s, 2H, NH), 2.18-2.11 (m, 4H, CH_2), 2.02-1.95 (m, 4H, CH_2), 1.15-1.07 (m, 12H, CH_3). $^{13}\text{C}\{^1\text{H}\}$ NMR (δ , CD_2Cl_2 , $20\text{ }^\circ\text{C}$): 222.0 (br, CO), 208.2 (t, $J = 7.5\text{ Hz}$, CO), 161.4 (vt, $J = 8.7\text{ Hz}$, $\text{py}^{2,6}$), 137.0 (py^4), 97.1 (vt, $J = 2.8\text{ Hz}$, $\text{py}^{3,5}$), 28.7 (vt, $J = 13.4\text{ Hz}$, CH_2), 8.1 (CH_3). $^{31}\text{P}\{^1\text{H}\}$ NMR (δ , CD_2Cl_2 , $20\text{ }^\circ\text{C}$): 94.0 ($^1J_{\text{W-P}} = 324.4\text{ Hz}$). IR (ATR, cm^{-1}): 1921 (ν_{CO}), 1834 (ν_{CO}), 1768 (ν_{CO}).

[W(PNP-Cy)(CO)₃] (3c)



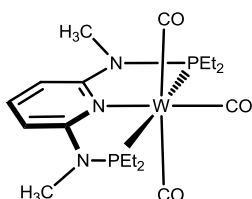
The reaction was performed at 155 °C for 5 h and the product was obtained as yellow crystals in 84% yield. Anal. Calcd. for C₃₂H₄₉WN₃O₃P₂ (769.55). C, 49.95; H, 6.42; N, 5.46. Found: C, 49.80; H, 6.49; N, 5.53. ¹H NMR (δ, acetone-d₆, 20 °C): 7.40 (s, 2H, NH), 7.04 (t, J = 8.4 Hz, 1H, py⁴), 6.19 (d, J = 7.8 Hz, 2H, py^{3,5}), 2.09-1.19 (m, 44H, Cy). ¹³C{¹H} NMR (δ, acetone-d₆, 20 °C): 222.3 (br, CO), 211.3 (t, J = 7.3 Hz, CO), 162.8 (vt, J = 8.5 Hz, py^{2,6}), 137.3 (py⁴), 96.9 (py^{3,5}), 43.5 (vt, J = 12.4 Hz, Cy), 27.3 (vt, J = 5.6 Hz, Cy), 26.9 (vt, J = 5.6 Hz, Cy), 26.4 (Cy). ³¹P{¹H} NMR (δ, acetone-d₆, 20 °C): 109.5 (¹J_{W-P} = 320.3 Hz). IR (ATR, cm⁻¹): 1933 (ν_{CO}), 1807 (ν_{CO}), 1773 (ν_{CO}).

[W(PNP-BIPOL)(CO)₃] (3g)



The product was obtained as yellow solid in 93 % yield. Anal. Calcd. for C₃₂H₂₁WN₃O₇P₂ (805.32). C, 47.73; H, 2.63; N, 5.22. Found: C, 47.60; H, 2.72; N, 5.13. ¹H NMR (δ, acetone-d₆, 20 °C): 9.26 (s, 2H, NH), 7.68 (dd, J = 7.6 Hz, J = 1.6 Hz, 4H, Ph), 7.55-7.47 (m, 5H, Ph, py⁴), 7.45-7.38 (m, 8H, Ph), 6.67 (d, J = 8 Hz, 2H, py^{3,5}). ¹³C{¹H} NMR (δ, acetone-d₆, 20 °C): 215.5 (t, J = 4.3 Hz, CO), 201.4 (t, J = 10.1 Hz, CO), 160.7 (vt, J = 11.5 Hz, py^{2,6}), 150.7 (vt, J = 4.4 Hz, Ph), 140.0 (py⁴), 130.6 (2Ph), 126.7 (Ph), 123.3 (Ph), 100.16 (vt, J = 3.9 Hz, py^{3,5}). ³¹P{¹H} NMR (δ, acetone-d₆, 20 °C): 188.2 (¹J_{W-P} = 494.1 Hz). IR (ATR, cm⁻¹): 1979 (ν_{CO}), 1858 (ν_{CO}).

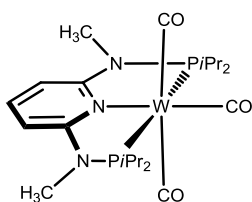
[W(PNP^{Me}-Et)(CO)₃] (3i)



The product was obtained as yellow crystals in 91% yield. Anal. Calcd. for C₁₈H₂₉WN₃O₃P₂ (581.23). C, 37.20; H, 5.03; N, 7.23. Found: C, 36.96; H, 4.85; N,

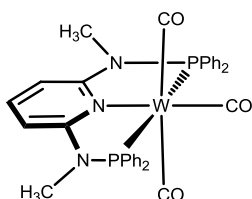
7.01. $^1\text{H NMR}$ (δ , CD_2Cl_2 , $20\text{ }^\circ\text{C}$): 7.34 (tt, $J = 8.2\text{ Hz}$, $J = 1.0\text{ Hz}$, 1H, py^4), 6.00 (d, $J = 8.3\text{ Hz}$, 2H, $\text{py}^{3,5}$), 2.93 (t, $J = 1.9\text{ Hz}$, 6H, NCH_3), 2.29-2.16 (m, 4H, CH_2), 2.13-1.99 (m, 4H, CH_2), 1.15-1.02 (m, 12H, CH_3). $^{13}\text{C}\{^1\text{H}\}$ NMR (δ , CD_2Cl_2 , $20\text{ }^\circ\text{C}$): 222.4 (br, CO), 208.9 (t, $J = 7.7\text{ Hz}$, CO), 163.1 (vt, $J = 10.2\text{ Hz}$, $\text{py}^{2,6}$), 137.6 (py^4), 97.4 (vt, $J = 2.7\text{ Hz}$, $\text{py}^{3,5}$), 32.9 (br, NCCH_3), 27.8 (vt, $J = 12.8\text{ Hz}$, CH_2), 8.3 (t, $J = 1.6\text{ Hz}$, CH_3). $^{31}\text{P}\{^1\text{H}\}$ NMR (δ , CD_2Cl_2 , $20\text{ }^\circ\text{C}$): 115.8 ($^1J_{\text{W-P}} = 329.9\text{ Hz}$). IR (ATR, cm^{-1}): 1934 (ν_{CO}), 1795 (ν_{CO}).

[W(PNP^{Me}-iPr)(CO)₃] (3j)



The product was obtained as yellow needles in 92% yield. Anal. Calcd. for $\text{C}_{22}\text{H}_{37}\text{WN}_3\text{O}_3\text{P}_2 \cdot \text{CH}_3\text{CN}$ (678.40). C, 42.49; H, 5.94; N, 8.26. Found: C, 42.54; H, 6.06; N, 8.23. $^1\text{H NMR}$ (δ , CD_2Cl_2 , $20\text{ }^\circ\text{C}$): 7.44 (t, $J = 6.9\text{ Hz}$, 1H, py^4), 6.07 (d, $J = 8.0\text{ Hz}$, 2H, $\text{py}^{3,5}$), 3.04 (s, 6H, NCH_3), 2.47-2.36 (m, 4H, CH), 1.40-1.30 (m, 12H, CH_3), 1.17-1.02 (m, 12H, CH_3). $^{13}\text{C}\{^1\text{H}\}$ NMR (δ , CD_2Cl_2 , $20\text{ }^\circ\text{C}$): 222.5 (t, $J = 1.7\text{ Hz}$, CO), 211.6 (t, $J = 7.8\text{ Hz}$, CO), 163.5 (vt, $J = 9.3\text{ Hz}$, $\text{py}^{2,6}$), 137.7 (py^4), 96.9 ($\text{py}^{3,5}$), 34.2 (NCH_3), 33.8 (vt, $J = 11.7\text{ Hz}$, CH), 19.6 (vt, $J = 6.1\text{ Hz}$, CH_3), 18.3 (CH_3). $^{31}\text{P}\{^1\text{H}\}$ NMR (δ , CD_2Cl_2 , $20\text{ }^\circ\text{C}$): 144.0 ($^1J_{\text{W-P}} = 326.2\text{ Hz}$). IR (ATR, cm^{-1}): 1928 (ν_{CO}), 1890 (ν_{CO}), 1797 (ν_{CO}).

[W(PNP^{Me}-Ph)(CO)₃] (3k)

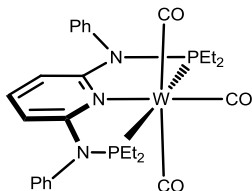


The product was obtained as yellow needles in 95 % yield. Anal. Calcd. for $\text{C}_{34}\text{H}_{29}\text{WN}_3\text{O}_3\text{P}_2 \cdot \text{CH}_3\text{CN}$ (814.46). C, 53.09; H, 3.99; N, 6.88. Found: C, 53.15; H, 4.05; N, 6.92. $^1\text{H NMR}$ (δ , acetone-d_6 , $20\text{ }^\circ\text{C}$): 7.71 (t, $J = 8.4\text{ Hz}$, 1H, py^4), 7.65-7.60 (m, 8H, Ph), 7.54-7.41 (m, 12H, Ph), 6.54 (d, $J = 8.4\text{ Hz}$, 2H, $\text{py}^{3,5}$), 3.07 (t, $J = 2.1\text{ Hz}$, 6H, NCH_3). $^{13}\text{C}\{^1\text{H}\}$ NMR (δ , acetone-d_6 , $20\text{ }^\circ\text{C}$): 221.1 (br, CO), 207.4 (t, $J = 7.0\text{ Hz}$, CO), 163.5 (vt, $J = 11.3\text{ Hz}$, $\text{py}^{2,6}$), 139.1 (py^4), 138.9 (Ph), 138.7 (Ph), 131.7 (vt, $J = 6.4\text{ Hz}$, Ph), 130.4 (s, Ph), 129.2 (vt, $J = 4.9\text{ Hz}$, Ph), 100.4 (vt, $J = 3.3\text{ Hz}$, $\text{py}^{3,5}$), 38.1 (vt, $J =$

Chapter 3 – Tricarbonyl Molybdenum and Tungsten Complexes

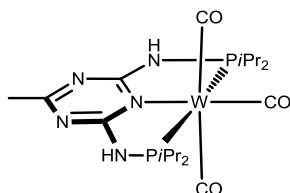
1.7 Hz, NCH₃). **³¹P{¹H} NMR** (δ, acetone-d₆, 20°C): 114.7 (¹J_{w-p} = 342.1 Hz). **IR (ATR, cm⁻¹):** 1954 (ν_{CO}), 1839 (ν_{CO}), 1801 (ν_{CO}).

[W(PNP^{Ph}-Et)(CO)₃] (3l)



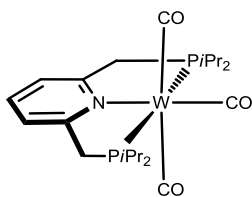
The product obtained were yellow crystals in 94% yield. Anal. Calcd. for C₂₈H₃₃WN₃O₃P₂ (705.38). C, 47.68; H, 4.72; N, 5.96. Found: C, 47.71; H, 4.81; N, 5.92. **¹H NMR** (δ, CD₂Cl₂, 20 °C): 7.62-7.47 (m, 6H, Ph), 7.25-7.19 (m, 4H, Ph), 6.92 (tt, J = 8.3 Hz, J = 1.2 Hz, 1H, py⁴), 5.40 (d, J = 8.3 Hz, 2H, py^{3,5}), 2.17-2.02 (m, 8H, CH₂), 1.37-1.19 (m, 12H, CH₃). **¹³C{¹H} NMR** (δ, CD₂Cl₂, 20 °C): 221.7 (bt, CO), 208.4 (t, J = 7.0 Hz, CO), 164.5 (vt, J = 10.5 Hz, py^{2,6}), 140.7 (Ph), 136.6 (py⁴), 130.7 (Ph), 129.3 (Ph), 128.4 (Ph), 100.8 (py^{3,5}), 29.0 (vt, J = 12.7 Hz, CH₂), 9.4 (s, CH₃). **³¹P{¹H} NMR** (δ, CD₂Cl₂, 20 °C): 112.7 (¹J_{w-p} = 328.6 Hz). **IR (ATR, cm⁻¹):** 1934 (ν_{CO}), 1804 (ν_{CO}).

[W(Triaz^{Me}-iPr)(CO)₃] (3n)



The product was obtained as a yellow solid in 91.8% yield. Anal. Calcd. for C₁₉H₃₃WN₅O₃P₂ (625.28). C, 36.50; H, 5.32; N, 11.20. Found: C, 36.16; H, 5.06; N, 11.02. **¹H NMR** (δ, CD₂Cl₂, 20 °C): 6.35 (s, 2H, NH), 2.41-2.29 (m, 4H, CH), 2.17 (s, 3H, CH₃), 1.17 (ddd, J = 21.2 Hz, J = 16.3 Hz, J = 7.1 Hz, 24H, CH₃). **¹³C{¹H} NMR** (δ, CD₂Cl₂, 20 °C): 220.6 (t, J = 2.1 Hz, CO), 209.2 (t, J = 7.4 Hz, CO), 173.7 (Triaz⁶), 170.8 (vt, J = 10.9 Hz, Triaz^{2,4}), 32.3 (vt, J = 11.7 Hz, CH), 25.0 (CH₃), 18.6 (vt, J = 2.1 Hz, CH₃), 18.2 (vt, J = 3.0 Hz, CH₃). **³¹P{¹H} NMR** (δ, CD₂Cl₂, 20 °C): 113.2 (¹J_{w-p} = 318.9 Hz). **IR (ATR, cm⁻¹):** 1943 (ν_{CO}), 1818 (ν_{CO}).

[W(PNP(CH₂)-iPr)(CO)₃] (3p)



The product was obtained as yellow powder in 87% yield. Anal. Calcd. for C₂₂H₃₅WNO₃P₂ (607.31). C, 43.51; H, 5.81; N, 2.31. Found: C, 43.13; H, 5.22; N, 2.03. ¹H NMR (δ, CD₂Cl₂, 20 °C): 7.52 (t, J = 7.5 Hz, 1H, py⁴), 7.25 (d, J = 7.7 Hz, 2H, py^{3,5}), 3.66-3.58 (m, 4H, CH₂), 2.46-2.24 (m, 4H, CH), 1.25 (dd, J = 14.5 Hz, J = 7.1 Hz, 12H, CH₃), 1.11 (dd, J = 14.9, J = 7.1 Hz, 12H, CH₃). ¹³C{¹H} NMR (δ, CD₂Cl₂, 20 °C): 227.8 (t, J = 3.4 Hz, CO), 215.1 (t, J = 6.8 Hz, CO), 164.3 (vt, J = 5.0 Hz, py^{2,6}), 135.6 (py⁴), 119.7 (vt, J = 3.8 Hz, py^{3,5}), 44.7 (t, J = 9.1 Hz, CH₂), 29.0 (vt, J = 11.1 Hz, CH), 18.9 (CH₃). ³¹P{¹H} NMR (δ, CD₂Cl₂, 20 °C): 67.5 (¹J_{w-p} = 304.3 Hz). IR (ATR, cm⁻¹): 1920 (ν_{CO}), 1808 (ν_{CO}), 1787 (ν_{CO}).

3.6.2. X-ray structure determinations

X-ray diffraction data were collected at *T* = 100 K on a Bruker Kappa APEX-2 CCD diffractometer with an Oxford Cryosystems cooler using graphite-monochromatised Mo-K_α radiation (λ = 0.71073 Å) and fine sliced φ- and ω-scans covering complete spheres of the reciprocal space. After data integration with program SAINT corrections for absorption and detector effects were applied with the program SADABS³² The structures were solved by direct methods (SHELXS97) and refined on F₂ with the program SHELXL97³³ Non-hydrogen atoms were refined anisotropically. Most H atoms were placed in calculated positions and thereafter refined as riding on the parent atoms. All crystal structures were checked with the program PLATON³⁴ Molecular graphics was generated with program MERCURY³⁵.[†]

3.7. References

- [1] E. W. Abel; F. G. A. Stone; *Q. Rev. Chem. Soc.*, **1969**, 23, 325-371.
- [2] Radius, U.; Bickelhaupt, F. M.; Ehlers, A. W.; Goldberg, N.; Hoffmann, R.; *Inorganic Chemistry*, **1998**, 37, 1080-1090.
- [3] Astruc, D.; *Organometallic Chemistry and Catalysis*, **2007**, Springer-Verlag Berlin Heidelberg.

[†] The same experimental conditions in the following chapters.

Chapter 3 – Tricarbonyl Molybdenum and Tungsten Complexes

- [4] Bachert, I.; Bartussek, I.; Braunstein, P.; Guillon, E.; Rose, J.; Kickelbick, G.; *Journal of Organometallic Chemistry*, **1999**, *580*, 257–264.
- [5] Kollár, L.; *Modern Carbonylation Methods*, **2008**, Wiley-VCH KGaA, Weinheim.
- [6] Nakamoto, K.; *Infrared and Raman Spectra of Inorganic and Coordination Compounds, Part B, Applications in Coordination, Organometallic, and Bioinorganic Chemistry*, 6th Edition, **2009**, John Wiley & Sons, Inc., New Jersey.
- [7] a) Van der Boom, M. E.; Milstein, D.; *Chem. Rev.*, **2003**, *103*, 1759-1792; b) Liang, L. C.; *Coord. Chem. Rev.*, **2006**, *250*, 1152-1177; c) Morales-Morales, D.; Jensen, C. M.; *The Chemistry of Pincer Compounds*, **2007**, Elsevier, Amsterdam; d) Bhattacharya, P.; Guan, H.; *Comment. Inorg. Chem.*, **2011**, *32*, 88-112; e) Choi, J.; MacArthur, A. H. R.; Brookhart, M.; Goldman, A. S.; *Chem. Rev.*, **2011**, *111*, 1761-1779; f) Van Koten, G.; Milstein, D.; *Top. Organomet. Chem.*, in *Organometallic Pincer Chemistry*, ed., **2013**, Springer, Berlin; g) Szabo, K. J.; Wendt, O. F.; *Pincer and Pincer-Type Complexes: Applications in Organic Synthesis and Catalysis*, **2014**, Wiley-VCH, Germany.
- [8] Radosevich, A. T.; Melnick, J. G.; Stoian, S. A.; Bacciu, D.; Chen, C.; Foxman, B. M.; Ozerov, O. V.; Nocera, D. G.; *Inorg. Chem.*, **2009**, *48*, 9214-9221.
- [9] Bruneau-Voisine, A.; Wang, D.; Dorcet, V.; Roisnel, T.; Darcel, C.; Sortais, J.; *Journal of Catalysis*, **2017**, *347*, 57-62.
- [10] Kinauer, M.; Scheibel, M. G.; Abbenseth, J.; Heinemann, F. W.; Stollberg, P.; Würtelea, C.; Schneider, S.; *Dalton Trans.*, **2014**, *43*, 4506-4513.
- [11] DeRieux, W. W.; Wong, A.; Schrodi, Y.; *Journal of Organometallic Chemistry*, **2014**, *772-773*, 60-67.
- [12] Raj, J. G. J.; Pathak, D. D.; Kapoor, P. N.; *Journal of Molecular Structure*, **2015**, *1087*, 41-45.
- [13] Gao, Y.; Yang, X.; Shi, Q.; *Inorganica Chimica Acta*, **1995**, *240*, 661-663.
- [14] Mathur, P.; Tauqeer, M.; Torubaev, Y. V.; Shaikh, M. M.; Lahiri, G. K.; Pasynskii, A. A.; Pavlova, A. V.; *Journal of Organometallic Chemistry*, **2014**, *758*, 55-59.
- [15] Ye, Q.; Wu, Q.; Zhao, H.; Song, Y.; Xue, X.; Xiong, R.; *Journal of Organometallic Chemistry*, **2005**, *690*, 286-290.
- [16] Ardon, M.; Hogarth, G.; Ocroft, D. T. W.; *Journal of Organometallic Chemistry*, **2004**, *689*, 2429-2435.
- [17] Tang, L.; Jia, W.; Wang, Z.; Chai, J.; Wang, J.; *Journal of Organometallic Chemistry*, **2001**, *637-639*, 209-215.
- [18] a) Schirmer, W.; Flörke, U.; Haupt, H.-J.; *Z. Anorg. Allg. Chem.* **1987**, *545*, 83-97; b) Schirmer, W.; Flörke, U.; Haupt, H.-J.; *Z. Anorg. Allg. Chem.* **1989**, *574*, 239-255.
- [19] Haenel, M. W.; Hillebrand, S.; Patent No.: US 6,290,926 B1, **2001**.
- [20] Siclovan, O. P.; Angelici, R. J.; *Inorg. Chem.*, **1998**, *37*, 432-444.
- [21] a) Benito-Garagorri, D.; Becker, E.; Wiedermann, J.; Lackner, W.; Pollak, M.; Mereiter, K.; Kisala, J.; Kirchner, K.; *Organometallics*, **2006**, *25*, 1900-1913; b) Benito-Garagorri, D.; Kirchner, K.; *Accounts of Chemical Research*, **2008**, *41*, 201-213.

Chapter 3 – Tricarbonyl Molybdenum and Tungsten Complexes

- [22] Wingard, L. A.; White, P. S.; Templeton, J. L.; *Dalton Trans.*, **2012**, 41, 11438-11448.
- [23] Castro-Rodrigo, R.; Chakraborty, S.; Munjanja, L.; Brennessel, W. W.; Jones, W. D.; *Organometallics*, **2016**, 35, 3124-3131.
- [24] Öztopcu, Ö.; Holzacker, C.; Puchberger, M.; Weil, M.; Mereiter, K.; Veiros, L. F.; Kirchner, K.; *Organometallics*, **2013**, 32, 3042-3052.
- [25] Birdwhistell, K. R.; Schulz, B. E.; Dizon, P. M.; *Inorganic Chemistry Communications*, **2012**, 26, 69-71.
- [26] de Aguiar, S. R. M. M.; Stöger, B.; Pittenauer, E.; Puchberger, M.; Allmaier, G.; Veiros, L. F.; Kirchner, K.; *Journal of Organometallic Chemistry*, **2014**, 760, 74-83.
- [27] Mastalir, M.; de Aguiar, S. R. M. M.; Glatz, M.; Stöger, B.; Kirchner, K.; *Organometallics*, **2016**, 35, 229-232.
- [28] Katritzky, A. R.; Ramsden, C. A.; Joule, J. A.; Zhdankin, V. V.; *Handbook of Heterocyclic Chemistry*, 3rd Edition, **2010**, Elsevier Ltd., Amsterdam.
- [29] Wiedermann, J.; Synthesis and reactivity of molybdenum, iron, and palladium complexes with mono-, bi- and tridentate phosphorus and nitrogen donor ligands, Dissertation, Vienna University of Technology, **2008**.
- [30] a) Van der Boom, M. E.; Milstein, D.; *Chem. Rev.*, **2003**, 103, 1759-1792; b) Vlugt, J. I.; Reek, J. N. H.; *Angew. Chem. Int. Ed.*, **2009**, 48, 8832-8846; c) Schneider, S.; Meiners, J.; Askevold, B.; *Eur. J. Inorg. Chem.*, **2012**, 412-429; d) Wang, Z.; Liu, N.; *Eur. J. Inorg. Chem.*, **2012**, 901-911.
- [31] a) Cotton, A. F.; Falvello, L. R.; Meadows, J. H.; *Inorg. Chem.*, **1985**, 24, 514-517; b) Boyden, J. A.; Colton, R.; *Aust. J. Chem.*, **1968**, 21, 2567-2578; c) Baker, P. K.; Fraser, S. G.; Keys, E. M.; *J. Organomet. Chem.*, **1986**, 309, 319-321.
- [32] Bruker computer programs: APEX2, SAINT, and SADABS; Bruker AXS Inc.: Madison, WI, **2015**.
- [33] Sheldrick, G. M.; *Acta Cryst. A*, **2008**, 64, 112-122.
- [34] Spek, A. L.; *J. Appl. Cryst.*, **2003**, 36, 7-13.
- [35] Macrae, C. F.; Edgington, P. R.; McCabe, P.; Pidcock, E.; Shields, G. P.; Taylor, R.; Towler, M.; van de Streek, J.; *J. Appl. Crystallogr.*, **2006**, 39, 453-457.

Chapter 4

Hydrido Carbonyl

Molybdenum and

Tungsten PNP Pincer

Complexes

Chapter 4 – Hydrido Carbonyl Molybdenum and Tungsten PNP pincer complexes

Transition metal hydrides play a central role in synthetic, structural and catalytic organometallic chemistry. The first transition metal hydride compound was reported by W. Heiber in 1931 when he synthesized $\text{Fe}(\text{CO})_4\text{H}_2$.¹ Although he claimed that the $\text{Fe}(\text{CO})_4\text{H}_2$ contained a Fe–H bond, it was not accepted until 1950s, when the concept of covalent M–H bonds was widely recognized. However, in 1984 a new phase in hydride chemistry was opened with the discovery of Kuba's dihydrogen complex $[\text{W}(\text{H}_2)(\text{CO})_3(\text{PCy}_3)_2]$.²

The methods of preparing transition metal hydrides are organized in protonation, hydrogenation, H atom transfer from the medium, oxidative addition of H_2 on 16-electron complexes, hydrogenolysis of d^0 metal-alkyl complexes by σ -bond metathesis, hydrogenation by $n\text{-Bu}_3\text{SnH}$ involving σ -bond metathesis, decomposition of a ligand and deprotonations of H_2 complexes.³ A wide range of chemical processes, from organometallic catalysis to energy conversion and hydrogen storage applications, are accomplishing through the metal hydrides compounds. Isomerization of olefins, hydrogenation, hydroformylation and hydrosilylation are their most common catalysis.^{4,5}

4.1. Metal-hydrogen bonds

In organometallic chemistry the metal-hydrogen bonds are ubiquitous X-type ligands. They vary enormously in polarization and pK_a and they may be acidic or hydridic depending on the nature of the metal center and on reaction conditions. The most prominent is the terminal hydride ligand. However many complexes are known where the H ligand bridges two or three metals. The small hydride ligand, H^- , acts as a σ donor to the metal center giving a very strong M–H bond.^{5,6}

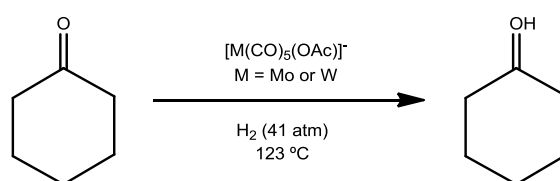
The metal–H distances are typically quite short ranging from 1.5 to about 1.8 Å. However, a hydride ligand is sometimes difficult to be detected via X-ray diffraction due to its small electron density. In the proton NMR, the hydride is normally observed in the range of -5 to -25 ppm due to the proximity to the metal causing a large shielding. Terminal M–H bonds can be observed in the region of 2200-1600 cm^{-1} by infrared spectroscopy. These resonances are sometimes weak or unobservable or coupled to other vibrational modes in the molecule.^{5,6}

4.2. Mo and W hydrides

Molybdenum and tungsten hydride complexes are used as catalyst precursors in homogeneous catalysis for reactions such as hydrogenation of ketones,

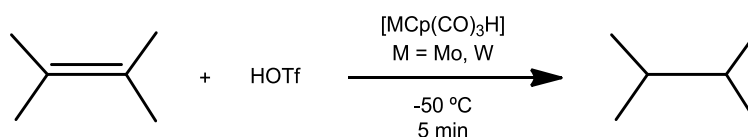
Chapter 4 – Hydrido Carbonyl Molybdenum and Tungsten PNP pincer complexes

hydrosilylation of ketones, hydrolysis reactions, and hydration of nitriles.⁴ Darensbourg and coworkers found that cyclohexanone could be hydrogenated to cyclohexanol by molybdenum and tungsten complexes (5 mol%), with turnover numbers of 3.5 for Mo and 10 for W, after 24 h (Scheme 4.1.). The loss of CO from $[\text{M}(\text{CO})_5(\text{OAc})]^-$ followed by heterolytic cleavage of H_2 would give the anionic hydride $[\text{M}(\text{CO})_5\text{H}]^-$ and HOAc. Insertion of the C=O bond into the M–H bond would give an anionic alkoxide complex that would produce the alcohol upon reaction with HOAc, regenerating $[\text{M}(\text{CO})_5(\text{OAc})]^-$.⁷



Scheme 4.1. Hydrogenation of cyclohexanone catalyzed with Mo and W complexes

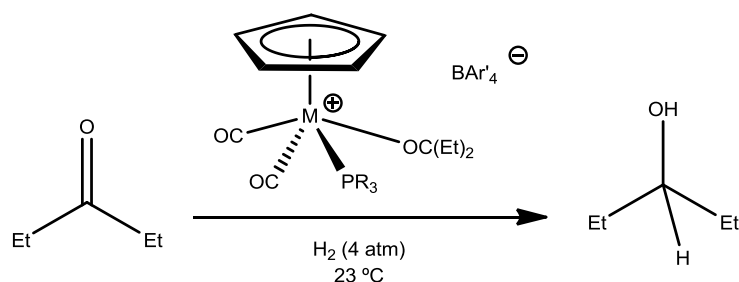
Hydrogenation of C=C bonds through the reaction with triflic acid (HOTf) and metal hydrides, such as $\text{Cp}(\text{CO})_3\text{WH}$, $\text{Cp}^*(\text{CO})_3\text{WH}$, ($\text{Cp}^* = \eta^5\text{-C}_5\text{Me}_5$), $\text{Cp}(\text{CO})_3\text{MoH}$, can be accomplished within minutes at low temperature (Scheme 4.2.). Excellent yields (> 90 %) were obtained for the 1,1-disubstituted, trisubstituted and tetrasubstituted alkenes. However, with styrene, stilbene and related C=C compounds lower yields (around 50 %) were achieved.⁸ The same tungsten hydride complexes can also hydrogenate C=O bonds of ketones in the presence HCF_3SO_3 (HOTf).⁹



Scheme 4.2. Hydrogenation of C=C bonds catalyzed with Mo and W complexes

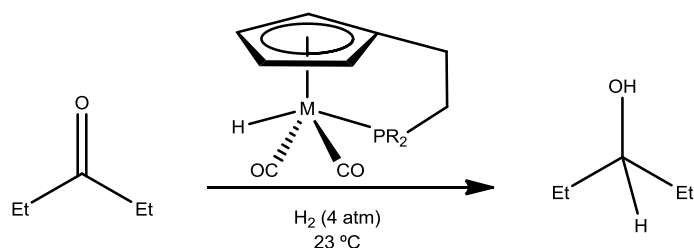
The tungsten and molybdenum ketone complexes $[\text{Cp}(\text{CO})_2(\text{PR}_3)\text{M}(\text{O}=\text{CEt}_2)]^+ \text{BAR}'_4^-$ ($\text{Ar}' = 3,5\text{-bis}(\text{trifluoromethyl})\text{phenyl}$; $\text{R} = \text{Me}, \text{Ph}, \text{Cy}$) catalyze the hydrogenation of $\text{Et}_2\text{C}=\text{O}$ at 23 °C under 4 atm of H_2 (Scheme 4.3.). In the case of the Mo complexes the use of phosphines accelerates the rate of catalysis. The catalysts with more bulky phosphines are faster indicating that steric factors predominate over electronic effects.¹⁰

Chapter 4 – Hydrido Carbonyl Molybdenum and Tungsten PNP pincer complexes



Scheme 4.3. Hydrogenation of $\text{Et}_2\text{C}=\text{O}$ catalyzed with Mo and W complexes

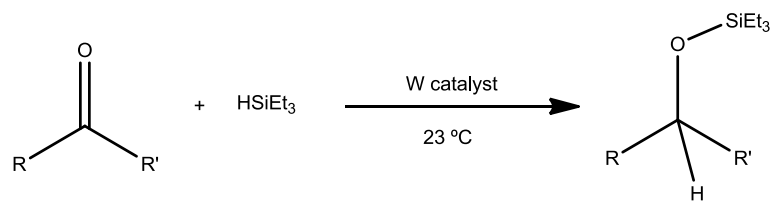
To overcome the problem of dissociation of the phosphine that leads to catalyst deactivation, molybdenum complexes with a two-carbon linkage between the phosphine and cyclopentadienyl ring were synthesized and successfully used in ketone hydrogenation (Scheme 4.4.).¹¹



Scheme 4.4. Hydrogenation of $\text{Et}_2\text{C}=\text{O}$ catalyzed with Mo and W complexes featuring phosphine ligands

Another type of reaction that shares several similarities to catalytic hydrogenations is the hydrosilylation in which a Si-H bond is added across a $\text{C}=\text{C}$ or $\text{C}=\text{O}$ bond. The hydrosilylation of ketones is accomplished with 0.2 mol% of the tungsten catalyst $[\text{WCp}(\text{CO})_2(\text{IMes})(\text{ketone})]^+$ under solvent-free conditions at 23 °C with a turnover frequency of 370 h^{-1} (Scheme 4.5.). The precipitation of the catalyst at the end of the reaction represents an advantage since it can be easily separated from the reaction mixture and recycled, a feature that is characteristic of a heterogeneous catalyst. This catalyst remains active after five cycles of recovery and recycling. The resting state of the catalyst was found to be a mixture of $[\text{CpW}(\text{CO})_2(\text{IMes})(\text{SiEt}_3)\text{H}]^+$ and the dihydride $[\text{CpW}(\text{CO})_2(\text{IMes})(\text{H})_2]^+$.¹² These studies clarified the fundamental reaction pathways and point the way for further development of new classes of catalysts.

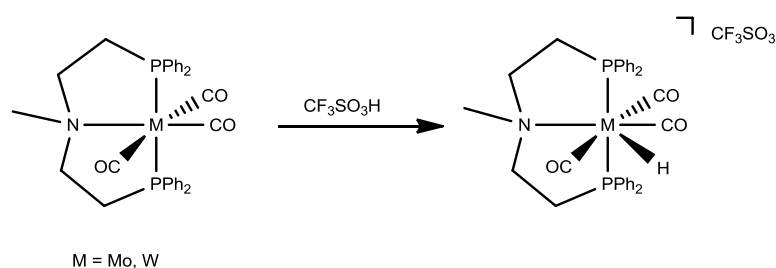
Chapter 4 – Hydrido Carbonyl Molybdenum and Tungsten PNP pincer complexes



Scheme 4.5. Hydrosilylation of ketones by a tungsten complex

4.3. Mo and W pincer hydrides

Similar to tricarbonyl Mo and W complexes described in Chapter 3, only a few examples of Mo and W pincer hydrides complexes are described in the literature. Addition of 1 equiv of triflic acid to either *fac*- or *mer*-isomers of $[M(\text{PNP})(\text{CO})_3]$ (PNP = $\text{H}_3\text{CN}(\text{CH}_2\text{CH}_2\text{PPh}_2)_2$) resulted in the formation of the fluxional seven-coordinate hydride complexes $[M(\text{PNP})(\text{CO})_3\text{H}][\text{CF}_3\text{SO}_3]$ (M = Mo, W) (Scheme 4.6.).¹³

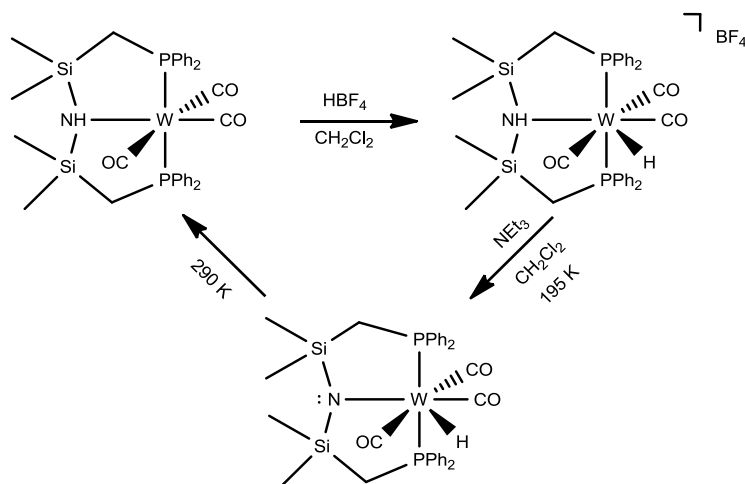


Scheme 4.6. Synthesis of Mo and W hydride PNP pincer complexes with an aliphatic backbone

A few years ago, Templeton and co-workers described the synthesis of a series of hydrido carbonyl tungsten complexes featuring the silazane-based PNP pincer-type ligand $\text{HN}(\text{SiMe}_2\text{CH}_2\text{PPh}_2)_2$.¹⁴ Addition of tetrafluoroboric acid to a CH_2Cl_2 solution of the respective tricarbonyl complex resulted in an immediate color change to pale yellow consistent with protonation at the tungsten center to form the desired W(II) hydride complex (Scheme 4.7.)

The fluxional behavior of seven-coordinate complexes in solution is well-known,^{15,16} since typically none of the idealized geometries such as capped prism, capped octahedron, and pentagonal bipyramid or any of the less symmetrical arrangements are typically characterized by a markedly lower total energy.¹⁷ Hence, interconversions between these various structures are quite facile.

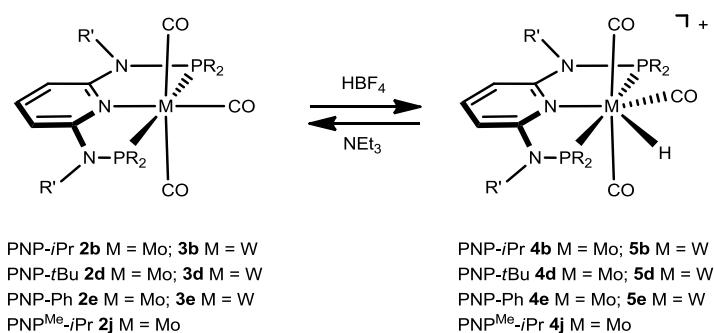
Chapter 4 – Hydrido Carbonyl Molybdenum and Tungsten PNP pincer complexes



Scheme 4.7. Synthesis of tungsten hydride complexes with a silazane-based PNP pincer

Addition of triethylamine to the cationic hydride complex at 195 K resulted in selective kinetic deprotonation of the amine proton to form $W(PNP)(CO)_3H$. The resulting lone pair on the nitrogen atom may have provided some electron density to the tungsten center, but all of the original ligands remained bound to the 18-electron tungsten in the neutral product. When warmed to room temperature, the proton was transferred to the amide nitrogen to reform the thermodynamically favored isomer $W(PNP)(CO)_3$ in a formal reduction to $W(0)$.

In the last years, a series of new hydrido carbonyl complexes featuring PNP pincer ligands based on 2,6-diaminopyridine of the type $[M(PNP)(CO)_3H]^+$ ($M = Mo, W$), were developed by Kirchner and coworkers through the synthesis of $[M(PNP)(CO)_3]$ ($M = Mo, W$) with HBF_4 in CH_2Cl_2 (Scheme 4.8).¹⁸



Scheme 4.8. Synthesis of molybdenum and tungsten hydride complexes with an 2,6-diaminopyridine-based PNP pincer ligand

Chapter 4 – Hydrido Carbonyl Molybdenum and Tungsten PNP pincer complexes

These cationic hepta-coordinate complexes will suffer full reversible protonation upon addition of NEt_3 as base, reforming quantitatively the Mo(0) and W(0) complexes $[\text{M}(\text{PNP})(\text{CO})_3]$. In analogy to Templeton's complexes the Mo and W metal hydrides are acidic¹⁹ and this often gives rise to unique reactivity.⁴

In an indistinguishable approach, Jones's working group research the chemistry of molybdenum and tungsten featuring a PONOP pincer ligand based on a 2,6-dihydroxypyridine scaffold with different phosphine moieties. The molybdenum hydride complex was shown to catalyze the isomerization of 1-hexene to internal isomers under mild conditions.²⁰

4.4. Results and discussion

In order to further develop the chemistry of Mo and W pincer systems with a central pyridine ring donor contains $\text{NR}'\text{PR}_2$ in the two ortho positions, the synthesis of a series of new hydrido carbonyl Mo and W was achieved. Addition of HBF_4 to a CH_2Cl_2 solution of $[\text{M}(\text{PNP})(\text{CO})_3]$ ($\text{M} = \text{Mo}, \text{W}$) resulted in an immediate color change consistent with protonation at the molybdenum and tungsten centers, generating $[\text{Mo}(\text{PNP})(\text{CO})_3\text{H}]\text{BF}_4$ and $[\text{W}(\text{PNP})(\text{CO})_3\text{H}]\text{BF}_4$ complexes, respectively (Figure 4.1.). In the same manner, the Mo(II) and W(II) hydride complexes featuring a CH_2 linker (**4p**, **5p**) were synthesized by protonation of the precursors $[\text{M}(\text{PNP}(\text{CH}_2)\text{-}i\text{Pr})(\text{CO})_3]$ ($\text{M} = \text{Mo}, \text{W}$).

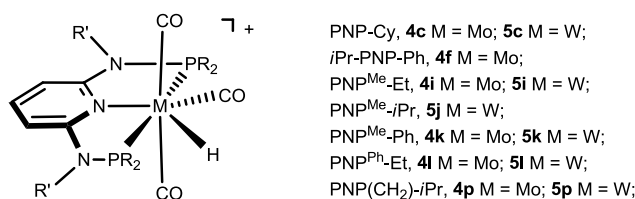


Figure 4.1. Molybdenum and tungsten hydride PNP complexes

All hydride complexes are thermally robust pale yellow solids that are air stable in the solid state but slowly decompose in solution. Characterization was accomplished by elemental analysis and by ^1H , $^{13}\text{C}\{^1\text{H}\}$, and $^{31}\text{P}\{^1\text{H}\}$ NMR and IR spectroscopy, table 4.1, for molybdenum and tungsten complexes respectively.

The IR spectra of these seven-coordinated complexes show the three ν_{CO} bands for a *mer* CO arrangement assignable to one weak symmetric and two strong asymmetric ν_{CO} stretching modes in the range of 2045–1848 cm^{-1} (Table 4.1.). In some

Chapter 4 – Hydrido Carbonyl Molybdenum and Tungsten PNP pincer complexes

cases only two bands are observed since the two strong asymmetric band overlap. The complex $[W(\text{PNP}^{\text{Me}}\text{-}i\text{Pr})(\text{CO})_3\text{H}]^+$ display two sets of resonances in the IR spectrum, which are 81 and 19 cm^{-1} apart, may be due to intermolecular interactions, e.g., $\text{CO}\cdots\text{H-Mo}$ bonds in the solid state. Based on the IR data a rough ordering of the PNP ligands can be made: $\text{PNP}^{\text{Me}}\text{-Ph} < \text{PNP-Ph} < \text{PNP}^{\text{Ph}}\text{-Et} < i\text{Pr-PNP-Ph} < \text{PNP}^{\text{Me}}\text{-Et} < \text{PNP-}i\text{Pr} < \text{PNP-Cy} < \text{PNP}^{\text{Me}}\text{-}i\text{Pr} < \text{PNP-}t\text{Bu} < \text{PNP}(\text{CH}_2)\text{-}i\text{Pr} < \text{PONOP-}i\text{Pr}$. This indicates an increasing electron donor strengths of the PNP ligands for both Mo and W complexes.

Moreover, when compared with the tricarbonyl complexes $[\text{M}(\text{PNP})(\text{CO})_3]$ (M = Mo, W) (see Chapter 3) the hydride complexes display a shift of almost 100 cm^{-1} to higher energy for the three carbonyl frequencies due to a decrease of the π backbonding since the metal center becomes more electropositive by forming the M-H bond. The only exception are Mo and W complexes with the PONOP-*i*Pr ligand where the shift is around 10 cm^{-1} to lower energy.

Table 4.1. Selected $^{31}\text{P}\{^1\text{H}\}$ NMR shifts and IR data of the pincer hydrido carbonyl Mo and W complexes

Ligands	Mo complexes			W complexes		
		$^{31}\text{P}\{^1\text{H}\} / \delta$	IR / cm^{-1} ν_{CO}		$^{31}\text{P}\{^1\text{H}\} / \delta$	IR / cm^{-1} ν_{CO}
(PNP- <i>i</i> Pr)	(4b*)	142.3 121.4	2035, 1923, 1920	(5b*)	125.9 108.6	2027, 1910, 1906
(PNP-Cy)	(4c)	122.2 101.7	2029, 1920	(5c)	104.9 87.6	2023, 1976, 1898
(PNP- <i>t</i> Bu)	(4d*)	158.8 142.8	2019, 1937, 1916	(5d*)	141.1 126.8	2021, 1934, 1897
(PNP-Ph)	(4e*)	111.5 97.8	2042, 1940, 1937	(5e*)	95.5 84.8	2038, 1963, 1918
(<i>i</i> Pr-PNP-Ph)	(4f)	Broad	2038, 1921	(5f)	-	-
(PNP ^{Me} -Et)	(4i)	130.4 115.0	2036, 1914	(5i)	112.6 101.1	2030, 1944, 1902
(PNP ^{Me} - <i>i</i> Pr)	(4j*)	166.1 147.7	2028, 1928, 1910	(5j)	136.6 119.9	2023, 1942 1912, 1893
(PNP ^{Me} -Ph)	(4k)	122.7 109.5	2045, 1939	(5k)	106.2 96.4	2038, 1919
(PNP ^{Ph} -Et)	(4l)	127.5 111.6	2040, 1907, 1889	(5l)	109.5 97.3	2034, 1914
(PONOP- <i>i</i> Pr)	(4o*)	221.12 194.55	1948, 1898, 1848	(5o*)	202.11 181.21	1940, 1919, 1908
(PNP(CH ₂)- <i>i</i> Pr)	(4p)	79.9 64.3	2026, 1905	(5p)	64.1 51.5	2019, 1933, 1887

*Previous prepared in the literature^{18,20}

Chapter 4 – Hydrido Carbonyl Molybdenum and Tungsten PNP pincer complexes

Characteristic features in the $^{13}\text{C}\{^1\text{H}\}$ NMR spectrum comprise two low-field triplet resonances (1:2 ratio) assignable to the carbonyl carbon atoms trans and cis to the pyridine nitrogen, respectively, for molybdenum and tungsten complexes, like it was observed for the analogous tricarbonyl complexes. An upfield is displayed when compared the molybdenum with the tungsten complexes, as well as for the hydrides complexes to the corresponding tricarbonyl complexes.

The presence of the hydride in the coordination sphere influences slightly the acidity of the proton of the NH linker, proven by the shift of the signal in the ^1H NMR comparing between $[\text{MPNP}(\text{CO})_3]$ (Chapter 3) and $[\text{MPNP}(\text{CO})_3\text{H}]^+$.

All complexes exhibit a fluxional behavior that was evident from variable-temperature ^1H and $^{31}\text{P}\{^1\text{H}\}$ NMR.* At room temperature, the ^1H NMR spectrum of Mo and W complexes confirmed the presence of one hydride ligand, which appeared either as triplets or as a not resolved doublet of doublets. As regards the $^{31}\text{P}\{^1\text{H}\}$ NMR, at room temperature present particularly broad peaks signals for molybdenum and tungsten complexes due to their fluxional behavior.

As an example the variable-temperature 400 MHz ^1H NMR spectra of the hydride region (**a**) and the ^{31}P NMR spectra (**b**) of $[\text{W}(\text{PNP}^{\text{Me-}i\text{Pr}})(\text{CO})_3\text{H}]\text{BF}_4$ (**5j**) are shown in Figure 4.2.. At $-40\text{ }^\circ\text{C}$, the hydride resonances appear as a well-resolved doublet of doublets with one large and one small coupling constant of about 21 and 54 Hz, respectively. The hydride signal, at lower temperature constitutes the X part of an AMX spin system, giving rise to a doublet of doublets which, at elevated temperatures in the fast exchange regime, becomes a simple A_2X spin system where the X part exhibits a triplet resonance. However, the $^{31}\text{P}\{^1\text{H}\}$ NMR spectra, at $-40\text{ }^\circ\text{C}$ of $[\text{W}(\text{PNP}^{\text{Me-}i\text{Pr}})(\text{CO})_3\text{H}]\text{BF}_4$ (**5j**) give rise to two doublets with a large geminal coupling constant of about 84 Hz, which is indicative of the phosphorus atoms being in mutually trans positions.

* Due to technical problems the NMR measurements at low temperature were not accessible

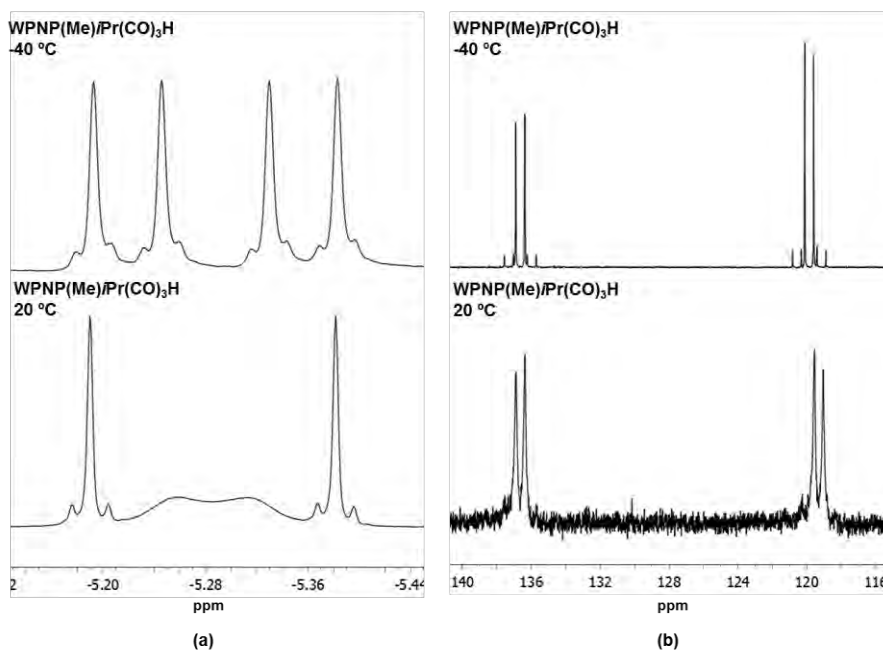


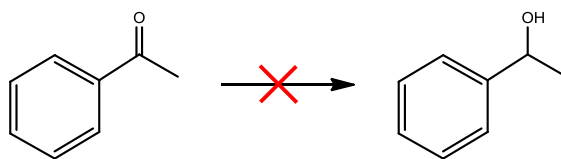
Figure 4.2. Variable-temperature 400 MHz ^1H NMR spectra of the hydride region (a) and the ^{31}P NMR spectra (b) of $[\text{W}(\text{PNP}^{\text{Me}}\text{-iPr})(\text{CO})_3\text{H}]\text{BF}_4$ (**5j**) in CD_2Cl_2

Independently which type of PNP ligand, the synthesis of $[\text{M}(\text{PNP})(\text{CO})_3]$ ($\text{M} = \text{Mo}, \text{W}$) with HBF_4 in CH_2Cl_2 originates the cationic hepta-coordinate complexes of the type $[\text{M}(\text{PNP})(\text{CO})_3\text{H}]^+$ ($\text{M} = \text{Mo}, \text{W}$). These cationic hepta-coordinate complexes upon addition of trimethylamine will full reverse to the $\text{Mo}(0)$ and $\text{W}(0)$ complexes $[\text{M}(\text{PNP})(\text{CO})_3]$. The deprotonation suggest that the hydride moieties present in these complexes are indeed acidic in nature, comparable to example in the literature.

4.4.1. Catalytic applications

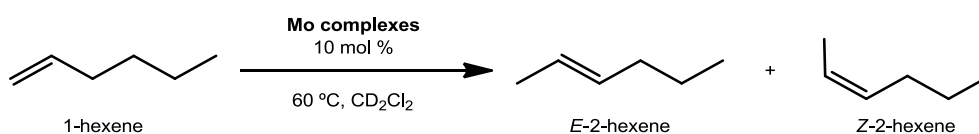
Metal hydrides complexes can accomplish a wide range of chemical process due to their unique reactivity provide special from the acidity of the hydride. Since the hydride moiety present in the molybdenum complexes is quite acidic, speculation that they might act as catalytic agents. These studies indicate that molybdenum hydrides complexes are inactive in the hydrogenation of acetophenone. The study of different solvents, effect of base, reaction time and hydrogen pressure was performed unfortunately no conversion was observed in any of these cases.

Chapter 4 – Hydrido Carbonyl Molybdenum and Tungsten PNP pincer complexes



Scheme 4.9. Hydrogenation of acetophenone with Mo hydride complexes

Catalytic isomerization of terminal alkenes was achieved by the molybdenum hydrido carbonyl complexes. The conversion of 1-hexene to the internal isomers was performed at 60 °C in CD₂Cl₂ with 10 mol % of the catalyst, Scheme 4.10..



Scheme 4.10. Isomerization of 1-hexene with Mo hydride complexes

The internal standard blocks catalytic activity of the Mo complexes so was added only when the reaction is finished. All conversions were measured every hour until 7h and then at 24h from ¹H NMR spectroscopy with 1,3,5-trimethylbenzene as an internal standard (Table 4.2.). The preliminary results show that [Mo(PNP^{Me}-iPr)(CO)₃H]⁺ was the best catalytic agent for the isomerization of 1-hexene to 2-hexenes, probably both E- and Z-isomers. There is no prove of the existence of 3-hexene.

Table 4.2. Conversion at 7h and 24h of the isomerization of 1-hexene to 2-hexene

Catalytic agent (10 mol %)	Conversion (%) (7h)	Conversion (%) (24h)
[Mo(PNP- <i>i</i> Pr)(CO) ₃ H] ⁺ (4b)	47.1	54.6
[Mo(PNP- <i>t</i> Bu)(CO) ₃ H] ⁺ (4b)	2.4	3.1
[Mo(PNP ^{Me} - <i>i</i> Pr)(CO) ₃ H] ⁺ (4d)	93.6	94.2
[Mo(PNP(CH ₂)- <i>i</i> Pr)(CO) ₃ H] ⁺ (4e)	0.0	0.0
[W(PNP- <i>i</i> Pr)(CO) ₃ H] ⁺ (5b)	0.0	0.0

4.5. Conclusions

In resume, the seven-coordinate cationic hydrido carbonyl Mo(II) and W(II) complexes of the type $[M(\text{PNP})(\text{CO})_3\text{H}]^+$ ($M = \text{Mo}, \text{W}$) featuring PNP pincer ligands based on 2,6-diaminopyridine were prepared and fully characterized.

All seven-coordinate complexes exhibit fluxional behavior in solution, since none of the idealized geometries (capped prism, capped octahedron, and pentagonal bipyramid) or any of the less symmetrical arrangements are typically characterized by a markedly lower total energy. The protonation of these complexes is fully reversible, and upon addition of NEt_3 as base the Mo(0) and W(0) complexes $[M(\text{PNP})(\text{CO})_3]$ are re-formed quantitatively. Attempts to perform hydrogenation of acetophenone employing the hydrido Mo complexes as catalytic agents were unsuccessful. However the same complexes were active for isomerization of terminal alkenes. The Mo complex that demonstrated the best results features the N,N'-bis(di-*iso*-propylphosphino)-N,N'-dimethyl-2,6-diaminopyridine ligand ($\text{PNP}^{\text{Me-}/\text{Pr}}$).

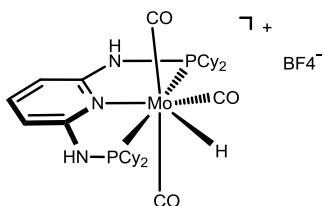
4.6. Experimental part

The syntheses of precursor complexes $[\text{MPNP}(\text{CO})_3]$ ($M = \text{Mo}, \text{W}$) were reported in Chapter 3.

4.6.1. Synthesis

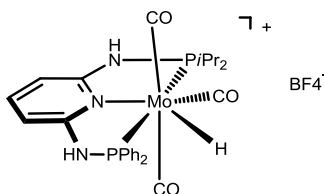
To a solution of $[\text{MPNP}(\text{CO})_3]$ ($M = \text{Mo}, \text{W}$) (0.300 mmol) in CH_2Cl_2 (10 mL) was added HBF_4 (0.400 mmol), the reaction was performed at room temperature. The reaction was stirred for 18 h and after this period the solution was filtered, solvent was removed under vacuum, and the solid was washed twice with Et_2O and *n*-pentane and then dried under vacuum.

[Mo(PNP-Cy)(CO)₃H]BF₄ (4c)



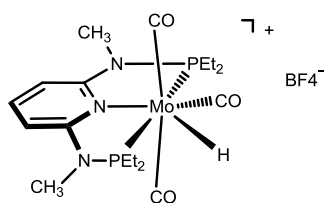
The product was obtained as a pale yellow solid in 92% yield. Anal. Calcd. for C₃₂H₅₀BF₄MoN₃O₃P₂ (769.47). C, 49.95; H, 6.55; N, 5.46. Found: C, 49.26; H, 6.12; N, 5.29. ¹H NMR (δ, CD₂Cl₂, 20 °C): 7.30 (t, J = 7.9 Hz, 1H, py⁴), 6.59 (s, 2H, NH), 6.47 (d, J = 7.9 Hz, 2H, py^{3,5}), 2.21-1.67 (m, 22H, Cy), 1.50-1.18 (m, 22H, Cy), -5.52 (vt, J = 37.2 Hz, 1H, H). ¹³C{¹H} NMR (δ, CD₂Cl₂, 20 °C): 212.2 (br, CO), 206.1 (t, J = 9.5 Hz, CO), 159.3 (dd, J = 10.0 Hz, J = 4.0 Hz, py^{2,6}), 140.9 (py⁴), 100.6 (d, J = 7.6 Hz, py^{3,5}), 41.9 (Cy), 41.5 (Cy), 28.8 (Cy), 28.0 (Cy), 26.9 (Cy), 26.7 (Cy), 26.4 (Cy), 25.8 (Cy). ³¹P{¹H} NMR (δ, CD₂Cl₂, 20 °C): 122.2 (d, J = 63.4 Hz), 101.7 (d, J = 63.2 Hz). IR (ATR, cm⁻¹): 2029 (ν_{CO}), 1920 (ν_{CO}).

[Mo(Ph-PNP-*i*Pr)(CO)₃H]BF₄ (4f)



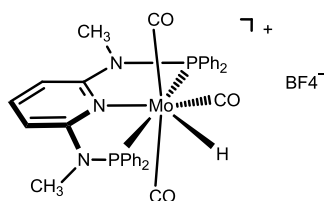
The product was obtained as a pale yellow solid in 94% yield. Anal. Calcd. for C₂₆H₃₀BF₄MoN₃O₃P₂ (677.25). C, 46.11; H, 4.46; N, 6.20. Found: C, 45.88; H, 4.31; N, 6.07. ¹H NMR (δ, CD₂Cl₂, 20 °C): 7.79-7.70 (m, 4H, Ph), 7.63-7.45 (m, 7H, Ph, NH), 7.37 (t, J = 8.0 Hz, 1H, py⁴), 6.93 (s, 1H, NH), 6.72 (d, J = 8.0 Hz, 1H, py^{3,5}), 6.61 (d, J = 8.1 Hz, 1H, py^{3,5}), 2.77-2.56 (m, 2H, CH), 1.41 (d, J = 7.0 Hz, 3H, CH₃), 1.32 (dd, J = 9.7 Hz, J = 7.1 Hz, 6H, CH₃), 1.23 (d, J = 7.1 Hz, 3H, CH₃), -5.07 (dd, J = 39.8 Hz, J = 33.8 Hz, 1H). ¹³C{¹H} NMR (δ, CD₂Cl₂, 20 °C): 212.4 (t, J = 11.8 Hz, CO), 204.5 (t, J = 9.7 Hz, CO), 159.6 (dd, J = 9.7 Hz, J = 4.6 Hz, py^{2,6}), 158.1 (dd, J = 14.0 Hz, J = 4.0 Hz, py^{2,6}), 141.3 (Ph), 135.2 (py⁴), 134.3 (py⁴), 131.8 (Ph), 130.6 (vd, J = 13.3 Hz, Ph), 129.1 (vd, J = 11.4 Hz, Ph), 101.8 (d, J = 7.2 Hz, py^{3,5}), 101.2 (d, J = 8.7 Hz, py^{3,5}), 31.8 (d, J = 25.9 Hz, CH), 18.2 (dd, J = 7.6 Hz, J = 2.9 Hz, CH₃). ³¹P{¹H} NMR (δ, CD₂Cl₂, 20 °C): broad peaks. IR (ATR, cm⁻¹): 2038 (ν_{CO}), 1921 (ν_{CO}).

[Mo(PNP^{Me}-Et)(CO)₃H]BF₄ (4i)



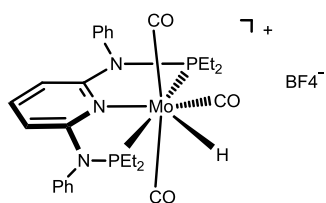
The product was obtained as a pale yellow in 91% yield. Anal. Calcd. for C₁₈H₃₀BF₄MoN₃O₃P₂ (581.08). C, 37.20; H, 5.20; N, 7.23. Found: C, 37.41; H, 5.03; N, 7.08. ¹H NMR (δ, CD₂Cl₂, 20 °C): 7.79 (tt, J = 8.4 Hz, J = 1.2 Hz, 1H, py⁴), 6.47 (d, J = 8.3 Hz, 2H, py^{3,5}), 3.23 (d, J = 4.7 Hz, 6H, NCH₃), 2.64-2.52 (m, 4H, CH₂), 2.46-1.26 (m, 4H, CH₂), 1.33 (dt, J = 19.9 Hz, J = 7.6 Hz, 12H, CH₃), -5.40 (vt, J = 36.8 Hz, H). ¹³C{¹H} NMR (δ, CD₂Cl₂, 20 °C): 212.4 (t, J = 11.6 Hz, CO), 204.2 (t, J = 10.1 Hz, CO), 160.4 (dd, J = 15.3 Hz, J = 3.2 Hz, py^{2,6}), 141.8 (py⁴), 101.1 (d, J = 6.7 Hz, py^{3,5}), 33.7 (t, J = 3.7 Hz, NCH₃), 25.4 (br, CH₂), 7.8 (br, CH₃). ³¹P{¹H} NMR (δ, CD₂Cl₂, 20 °C): 130.4 (d, J = 71.6 Hz), 115.0 (d, J = 71.6 Hz). IR (ATR, cm⁻¹): 2036 (ν_{CO}), 1914 (ν_{CO}).

[Mo(PNP^{Me}-Ph)(CO)₃H]BF₄ (4k)



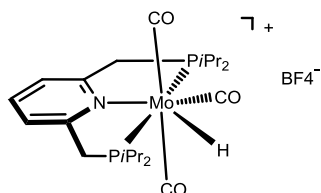
The product was obtained as a pale yellow solid in 96% yield. Anal. Calcd. for C₃₄H₃₀BF₄MoN₃O₃P₂ (773.33). C, 52.81; H, 3.91; N, 5.43. Found: C, 52.51; H, 3.67; N, 5.18. ¹H NMR (δ, CD₂Cl₂, 20 °C): 7.90 (tt, J = 8.4 Hz, J = 1.4 Hz, 1H, py⁴), 7.61-7.56 (m, 8H, Ph), 7.54-7.50 (m, 12H, Ph), 6.66 (d, J = 8.4 Hz, 2H, py^{3,5}), 3.06 (d, J = 5.1 Hz, 6H, NCH₃), -4.59 (vt, J = 36.9 Hz, H). ¹³C{¹H} NMR (δ, CD₂Cl₂, 20 °C): 212.3 (t, J = 11.4 Hz, CO), 203.3 (t, J = 9.4 Hz, CO), 160.1 (dd, J = 17.9 Hz, J = 3.7 Hz, py^{2,6}), 142.7 (py⁴), 135.4 (d, J = 3.0 Hz), 132.4 (Ph), 131.3 (d, J = 12.9 Hz, Ph), 129.7 (d, J = 11.0 Hz, Ph), 102.9 (d, J = 7.4 Hz, py^{3,5}), 37.38 (br, NCH₃). ³¹P{¹H} NMR (δ, CD₂Cl₂, 20 °C): 122.7 (d, J = 85.5 Hz), 109.5 (d, J = 85.5 Hz). IR (ATR, cm⁻¹): 2045 (ν_{CO}), 1939 (ν_{CO}).

[Mo(PNP^{Ph}-Et)(CO)₃H]BF₄ (4l)



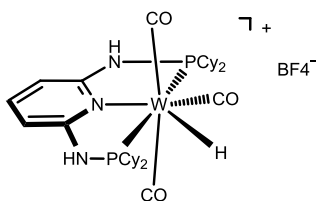
The product was obtained as a pale yellow solid in 89% yield. Anal. Calcd. for C₂₈H₃₄BF₄MoN₃O₃P₂ (705.30). C, 47.68; H, 4.86; N, 5.96. Found: C, 47.40; H, 4.53; N, 5.78. ¹H NMR (δ, CD₂Cl₂, 20 °C): 7.71-7.62 (m, 6H, Ph), 7.31-7.24 (m, 5H, Ph, py⁴), 5.73 (d, J = 8.3 Hz, 2H, py^{3,5}), 2.43-2.19 (m, 8H, CH₂), 1.34 (dt, J = 20.3 Hz, J = 7.5 Hz, 12H, CH₃), -5.25 (t, J = 37.6 Hz, H). ¹³C{¹H} NMR (δ, CD₂Cl₂, 20 °C): 212.2 (t, J = 11.7 Hz, CO), 204.5 (t, J = 10.1 Hz, CO), 161.6 (dd, J = 17.3 Hz, J = 3.6 Hz, py^{2,6}), 140.7 (Ph), 135.8 (py⁴), 131.3 (Ph), 130.0 (d, J = 7.6 Hz, Ph), 129.9 (Ph), 104.2 (d, J = 5.2 Hz, py^{3,5}), 26.3 (d, J = 31.1 Hz, CH₂), 25.6 (d, J = 20.3 Hz, CH₂), 15.1 (CH₃), 8.5 (CH₃). ³¹P{¹H} NMR (δ, CD₂Cl₂, 20 °C): 127.5 (d, J = 94.9 Hz), 111.6 (d, J = 94.8 Hz). IR (ATR, cm⁻¹): 2040 (ν_{CO}), 1907 (ν_{CO}), 1889 (ν_{CO}).

[Mo(PNP(CH₂)-iPr)(CO)₃H]BF₄ (4p)



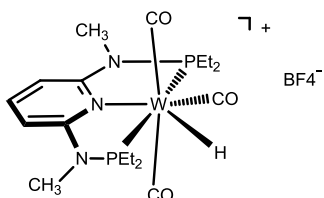
The product was obtained as a pale yellow powder in 95% yield. Anal. Calcd. for C₂₂H₃₆BF₄WNO₃P₂ (607.24). C, 43.51; H, 5.98; N, 2.31. Found: C, 42.54; H, 6.06; N, 2.09. ¹H NMR (δ, CD₂Cl₂, 20 °C): 7.89 (t, J = 7.6 Hz, 1H, py⁴), 7.61 (d, J = 5.7 Hz, 2H, py^{3,5}), 3.83 (s, 2H, CH₂), 3.52 (dd, J = 13.6 Hz, J = 6.7 Hz, 2H, CH₂), 2.61 (vd, J = 38.1 Hz, 4H, CH), 1.47-1.34 (m, 12H, CH₃), 1.23 (dd, J = 20.1, J = 7.1 Hz, 12H, CH₃), -5.43 (dd, J = 41.6 Hz, J = 22.2 Hz, 1H). ¹³C{¹H} NMR (δ, CD₂Cl₂, 20 °C): 213.2 (dd, J = 18.0 Hz, J = 6.6 Hz, CO), 207.5 (t, J = 8.8 Hz, CO), 161.1 (vd, J = 39.2 Hz, py^{2,6}), 140.7 (py⁴), 123.4 (vd, J = 8.5 Hz, py^{3,5}), 40.6 (d, J = 16.8 Hz, CH₂), 38.6 (d, J = 19.8 Hz, CH₂), 27.7 (vt, J = 26.1 Hz, CH), 27.0 (vt, J = 21.2 Hz, CH), 18.7 (CH₃), 18.0 (CH₃). ³¹P{¹H} NMR (δ, CD₂Cl₂, 20 °C): 79.9 (d, J = 72.4 Hz), 64.3 (d, J = 72.5 Hz). IR (ATR, cm⁻¹): 2026 (ν_{CO}), 1905 (ν_{CO}).

[W(PNP-Cy)(CO)₃H]BF₄ (5c)



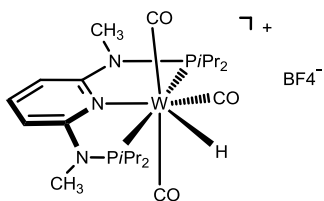
The product was obtained as a pale yellow solid in 89.0% yield. Anal. Calcd. for C₃₅H₅₉BF₄WN₃O₃P₂ (900.44). C, 46.69; H, 6.38; N, 4.67. Found: C, 46.52; H, 6.19; N, 4.33. ¹H NMR (δ, CD₂Cl₂, 20 °C): 7.39 (t, J = 8.0 Hz, 1H, py⁴), 6.83 (s, 1H, NH), 6.76 (s, 1H, NH), 6.54 (d, J = 8.0 Hz, 2H, py^{3,5}), 1.50-1.38 (m, 22H, Cy), 1.34-1.22 (m, 22H, Cy), -5.52 (dd, J = 56.6 Hz, J = 21.6 Hz, 1H, H). ¹³C{¹H} NMR (δ, CD₂Cl₂, 20 °C): 204.8 (dd, J = 12.9 Hz, J = 5.7 Hz, CO), 198.4 (t, J = 7.4 Hz, CO), 159.9 (dd, J = 30.4 Hz, J = 7.4 Hz, py^{2,6}), 141.2 (py⁴), 100.4 (dd, J = 37.4 Hz, J = 6.4 Hz, py^{3,5}), 42.1 (dd, J = 76.7 Hz, J = 28.5 Hz, Cy), 29.0 (vt, J = 74.3 Hz, Cy), 28.1 (d, J = 81.4 Hz, Cy), 26.5 (d, J = 12.4 Hz, Cy), 25.8 (Cy). ³¹P{¹H} NMR (δ, CD₂Cl₂, 20 °C): 104.9 (d, ²J_{pp} = 82.2 Hz, ¹J_{w-p1} = 288.8 Hz, ¹J_{w-p2} = 123.3 Hz), 87.6 (d, ²J_{pp} = 82.3 Hz, ¹J_{w-p1} = 306.7 Hz, ¹J_{w-p2} = 141.9 Hz). IR (ATR, cm⁻¹): 2023 (ν_{CO}), 1976 (ν_{CO}), 1898 (ν_{CO}).

[W(PNP^{Me}-Et)(CO)₃H]BF₄ (5i)



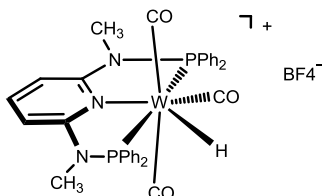
The product was obtained as a pale yellow in 97% yield. Anal. Calcd. for C₁₈H₃₀BF₄WN₃O₃P₂ (669.06). C, 32.31; H, 4.52; N, 6.28. Found: C, 31.98; H, 4.57; N, 6.01. ¹H NMR (δ, CD₂Cl₂, 20 °C): 7.79 (tt, J = 8.3 Hz, J = 1.4 Hz, 1H, py⁴), 6.49 (d, J = 8.3 Hz, 2H, py^{3,5}), 3.22 (s, 6H, NCH₃), 2.72-2.60 (m, 4H, CH₂), 2.56-2.38 (m, 4H, CH₂), 1.31 (dt, J = 19.8 Hz, J = 7.6 Hz, 12H, CH₃), -5.07 (dd, J = 54.6 Hz, J = 22.8 Hz, H). ¹³C{¹H} NMR (δ, CD₂Cl₂, 20 °C): 205.1 (dd, J = 18.3 Hz, J = 2.1 Hz, CO), 196.6 (t, J = 7.8 Hz, CO), 160.9 (dd, J = 14.6 Hz, J = 4.3 Hz, py^{2,6}), 141.8 (py⁴), 101.2 (s, py^{3,5}), 33.8 (d, J = 15.4 Hz, NCH₃), 26.5 (d, J = 35.8 Hz, CH₂), 25.5 (d, J = 30.6 Hz, CH₂), 8.4 (CH₃), 7.7 (CH₃). ³¹P{¹H} NMR (δ, CD₂Cl₂, 20 °C): 112.6 (d, ²J_{pp} = 82.1 Hz, ¹J_{w-p1} = 291.1 Hz, ¹J_{w-p2} = 130.1 Hz), 101.1 (d, ²J_{pp} = 82.1 Hz, ¹J_{w-p1} = 315.9 Hz, ¹J_{w-p2} = 151.1 Hz). IR (ATR, cm⁻¹): 2030 (ν_{CO}), 1944 (ν_{CO}), 1902 (ν_{CO}).

[W(PNP^{Me}-*i*Pr)(CO)₃H]BF₄ (5j)



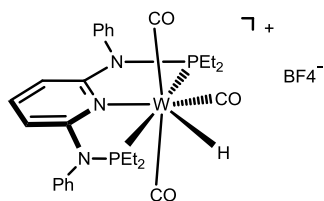
The product was obtained as pale yellow solid in 98.0% yield. Anal. Calcd. for C₂₂H₃₈BF₄WN₃O₃P₂ (725.15). C, 36.44; H, 5.28; N, 5.79. Found: C, 36.66; H, 5.02; N, 5.56. ¹H NMR (δ, CD₂Cl₂, -40 °C): 7.68 (t, J = 8.3 Hz, 1H, py⁴), 6.34 (d, J = 8.4 Hz, 2H, py^{3,5}), 3.10 (t, J = 5.1 Hz, 6H, NCH₃), 2.94-2.74 (m, 4H, CH), 1.38 (ddd, J = 34.8 Hz, J = 19.6 Hz, J = 6.9 Hz, 12H, CH₃), 1.09 (ddd, J = 16.3 Hz, J = 7.0 Hz, J = 1.7 Hz, 12H, CH₃), -5.29 (dd, J = 54.8 Hz, J = 21.2 Hz, 1H, H). ¹³C{¹H} NMR (δ, CD₂Cl₂, 20 °C): 203.2 (br, CO), 196.9 (t, J = 7.5 Hz, CO), 161.6 (dd, J = 12.0 Hz, J = 4.1 Hz, py^{2,6}), 142.0 (py⁴), 100.8 (d, J = 5.2 Hz, py^{3,5}), 35.5 (NCH₃), 33.1 (br, CH), 19.9 (br, CH₃), 19.2 (br, CH₃), 18.2 CH₃). ³¹P{¹H} NMR (δ, CD₂Cl₂, 20 °C): 136.6 (d, J = 83.6 Hz, ¹J_{W-P1} = 297.5 Hz, ¹J_{W-P2} = 130.5 Hz), 119.9 (d, J = 83.5 Hz, ¹J_{W-P1} = 314.5 Hz, ¹J_{W-P2} = 147.3 Hz). IR (ATR, cm⁻¹): 2023 (ν_{CO}), 1942 (ν_{CO}), 1912 (ν_{CO}), 1893 (ν_{CO}).

[W(PNP^{Me}-Ph)(CO)₃H]BF₄ (5k)



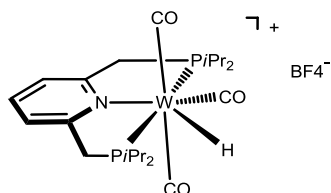
The product was obtained as a pale yellow solid in 95.1 % yield. Anal. Calcd. for C₃₄H₃₀BF₄WN₃O₃P₂ (861.21). C, 47.42; H, 3.51; N, 4.88. Found: C, 47.64; H, 3.26; N, 4.57. ¹H NMR (δ, CD₂Cl₂, 20 °C): 7.91 (tt, J = 8.4 Hz, J = 1.5 Hz, 1H, py⁴), 7.60-7.55 (m, 8H, Ph), 7.53 (br, 12H, Ph), 6.68 (d, J = 8.4 Hz, 2H, py^{3,5}), 3.05 (d, J = 5.3 Hz, 6H, NCH₃), -4.21 (t, J = 39.8 Hz, H). ¹³C{¹H} NMR (δ, CD₂Cl₂, 20 °C): 205.4 (t, J = 9.1 Hz, CO), 196.5 (t, J = 7.1 Hz, CO), 160.4 (d, J = 14.5 Hz, py^{2,6}), 142.5 (py⁴), 132.4 (Ph), 131.3 (Ph), 129.5 (Ph), 103.0 (d, J = 7.0 Hz, py^{3,5}), 37.5 (d, J = 3.1 Hz, NCH₃), 36.8 (d, J = 5.4 Hz, NCH₃). ³¹P{¹H} NMR (δ, CD₂Cl₂, 20 °C): 106.2 (d, ²J_{pp} = 85.9 Hz, ¹J_{W-P1} = 302.0 Hz), 96.4 (d, ²J_{pp} = 83.8 Hz, ¹J_{W-P1} = 329.5 Hz). IR (ATR, cm⁻¹): 2038 (ν_{CO}), 1919 (ν_{CO}).

[W(PNP^{Ph}-Et)(CO)₃H]BF₄ (5l)



The product was obtained as a pale yellow solid in 86% yield. Anal. Calcd. for C₂₈H₃₄BF₄MoN₃O₃P₂ (793.18). C, 42.40; H, 4.32; N, 5.30. Found: C, 42.08; H, 4.17; N, 5.18. ¹H NMR (δ, CD₂Cl₂, 20 °C): 7.58-7.51 (m, 6H, Ph), 7.10-1.05 (m, 4H, Ph), 7.34 (t, J = 7.9 Hz, 1H, py⁴), 5.59 (d, J = 8.3 Hz, 2H, py^{3,5}), 2.33-2.24 (m, 4H, CH₂), 2.19 (br, 4H, CH₂), 1.21-1.11 (m, 6H, CH₃), 1.05 (t, J = 7.0 Hz, 6H, CH₃), -5.08 (dd, J = 55.5 Hz, J = 23.4 Hz, H). ¹³C{¹H} NMR (δ, CD₂Cl₂, 20 °C): 204.8 (dd, J = 10.2 Hz, J = 8.6 Hz, CO), 196.9 (t, J = 7.8 Hz, CO), 162.1 (dd, J = 16.4 Hz, J = 3.9 Hz, py^{2,6}), 140.7 (Ph), 135.8 (py⁴), 131.4 (Ph), 130.0 (Ph), 129.9 (Ph), 104.3 (d, J = 8.9 Hz, py^{3,5}), 27.3 (d, J = 35.8 Hz, CH₂), 26.1 (d, J = 30.6 Hz, CH₂), 9.1 (s, CH₃), 8.5 (s, CH₃). ³¹P{¹H} NMR (δ, CD₂Cl₂, 20 °C): 109.5 (d, ²J_{pp} = 82.9 Hz, ¹J_{w-p1} = 293.8 Hz, ¹J_{w-p2} = 149.5 Hz), 97.3 (d, ²J_{pp} = 83.1 Hz, ¹J_{w-p1} = 315.0 Hz, ¹J_{w-p2} = 147.1 Hz). IR (ATR, cm⁻¹): 2034 (ν_{CO}), 1914 (ν_{CO}).

[W(PNP(CH₂)-iPr)(CO)₃]BF₄ (5p)



The product was obtained as pale yellow solid in 87% yield. Anal. Calcd. for C₂₂H₃₆BF₄WNO₃P₂ (695.12). C, 38.01; H, 5.22; N, 2.02. Found: C, 38.14; H, 5.01; N, 1.96. ¹H NMR (δ, CD₂Cl₂, 20 °C): 7.81 (t, J = 7.8 Hz, 1H, py⁴), 7.54 (d, J = 7.8 Hz, 2H, py^{3,5}), 3.80 (dd, J = 8.8 Hz, J = 6.4 Hz, 4H, CH₂), 2.63-2.43 (m, 4H, CH), 1.28 (ddd, J = 21.3 Hz, J = 16.8 Hz, J = 7.0 Hz, 12H, CH₃), 1.16-1.05 (m, 12H, CH₃), -4.77 (dd, J = 47.1 Hz, J = 21.1 Hz, 1H). ¹³C{¹H} NMR (δ, CD₂Cl₂, 20 °C): 205.7 (dd, J = 17.4 Hz, J = 3.5 Hz, CO), 200.7 (t, J = 6.6 Hz, CO), 162.1 (dd, J = 5.1 Hz, J = 2.9 Hz, py^{2,6}), 161.7 (t, J = 3.9 Hz, py^{2,6}), 140.8 (py⁴), 123.4 (d, J = 8.9 Hz, py^{3,5}), 41.1 (d, J = 21.2 Hz, CH₂), 39.3 (d, J = 23.6 Hz, CH₂), 28.0 (d, J = 28.7 Hz, CH), 27.2 (d, J = 25.2 Hz, CH), 18.8 (CH₃), 18.7 (CH₃), 17.9 (CH₃). ³¹P{¹H} NMR (δ, CD₂Cl₂, 20 °C): 64.1 (d, ²J_{pp} = 69.0 Hz, ¹J_{w-p1} = 266.9 Hz, ¹J_{w-p2} = 128.9 Hz), 51.5 (d, ²J_{pp} = 68.9 Hz, ¹J_{w-p1} = 284.6 Hz, ¹J_{w-p2} = 146.7 Hz). IR (ATR, cm⁻¹): 2019 (ν_{CO}), 1933 (ν_{CO}), 1887 (ν_{CO}).

4.6.2. General procedure for the catalytic applications

Method for hydrogenation reactions: To a solution of the substrate (1 mmol) dissolved under argon in degassed isopropanol (2.5 mL) was added the appropriate catalyst (5%) dissolved in degassed isopropanol (2.5 mL). KO^tBu (4%) was added and the reaction mixture was transferred through a stainless steel capillary into a steel autoclave. The argon gas was then replaced by hydrogen gas (3-5 cycles) and the pressure was set. All hydrogenations were carried out for 18 h at r.t. under hydrogen gas at a pressure of 20 bar. After completion of the reaction, diethyl ether (10 mL) was added and the reaction was quenched by the addition of an aqueous solution of H₃PO₄ (20%). The organic phase was separated, washed with brine, dried over MgSO₄ and filtered through a plug of aluminium oxide.

Method for isomerization reactions: In a Young NMR tube was loaded [Mo(PNP)(CO)₃H]⁺ (0.016 mmol) (10 mol %), 10 equiv. of alkene isomer (0.16 mmol) and 0.5 mL of CD₂Cl₂. The resulting solution was heated at 65 °C in an oil bath, and 1H NMR spectra were recorded periodically to monitor the progress of the reaction. In the end of every result it was had the internal standard 1,3,5-trimethylbenzene (39 mg, 0.16 mmol).

4.7. References

- [1] Hieber, W.; Leutert, F.; *Naturwissenschaften*, **1931**, 19, 360-361.
- [2] Kubas, G. J.; Ryan, R. R.; Swanson, B. I.; Vergamini, P. J.; Wasserman, H. J.; *J. Am. Chem. Soc.*, **1984**, 106, 451-452.
- [3] Astruc, D.; *Organometallic Chemistry and Catalysis*, **2007**, Springer-Verlag Berlin Heidelberg.
- [4] Bullock, R. M.; *Catalysis Without Precious Metals*, **2010**, Wiley-VCH Verlag GmbH & Co. KGaA, Germany.
- [5] Wiedner, E. S.; Chambers, M. B.; Pitman, C. L.; Bullock, R. M.; Miller, A. J. M.; Appel, A. M.; *Chem. Rev.*, **2016**, 116, 8655-8692.
- [6] Crabtree, R. H.; *Encyclopedia of Inorganic Chemistry*, **2006**, John Wiley & Sons, DOI:10.1002/0470862106.ia086.
- [7] Tooley, P.A.; Ovalles, C.; Kao, S.C.; Darensbourg, D.J.; Darensbourg, M.Y.; *J. Am. Chem. Soc.*, **1986**, 108, 5465-5470.
- [8] a) Kursanov, D. N.; Parnes, Z. N.; Loim, N. M.; *Synthesis*, **1974**, 633-651; b) Kursanov, D. N.; Parnes, Z. N.; Kalinkin, M. I.; Loim, N. M.; *Ionic Hydrogenation and Related Reactions*, **1985**, Harwood Academic Publishers, New York.

Chapter 4 – Hydrido Carbonyl Molybdenum and Tungsten PNP pincer complexes

- [9] Song, J. S.; Szalda, D. J.; Bullock, R. M.; Lawrie, C. J. C.; Rodkin, M. A.; Norton, J. R.; *Angew. Chem. Int. Ed. Engl.*, **1992**, *31*, 1233-1235.
- [10] a) Bullock, R. M.; Voges, M. H.; *J. Am. Chem. Soc.*, **2000**, *122*, 12594-12595; b) Voges, M. H.; Bullock, R. M.; *J. Chem. Soc., Dalton Trans.*, **2002**, 759-770.
- [11] a) Bullock, R. M.; Kimmich, B. F. M.; Fagan, P.J.; Hauptman, E.; Patent No.: US 6,613,923 B1, **2003**; b) Kimmich, B. F. M.; Fagan, P. J.; Hauptman, E.; Marshall, W. J.; Bullock, R. M.; *Organometallics*, **2005**, *24*, 6220-6229.
- [12] Dioumaev, V. K.; Bullock, R. M.; *Nature*, **2003**, *424*, 530-532.
- [13] Siclovan, O. P.; Angelici, R.; *J. Inorg. Chem.*, **1998**, *37*, 432-444.
- [14] Wingard, L. A.; White, P. S.; Templeton, J. L.; *Dalton Trans.*, **2012**, *41*, 11438-11448.
- [15] Curtis, M. D.; Shiu, K.-B.; *Inorg. Chem.*, **1985**, *24*, 1213-1218.
- [16] a) Baker, P. K.; Al-Jahdali, M.; Meehan, M. M.; *J. Organomet. Chem.*, **2002**, *648*, 99-108; b) Baker, P. K.; Drew, M. G. B.; Moore, D. S.; *J. Organomet. Chem.*, **2002**, *664*, 45-58.
- [17] a) Hoffmann, R.; Beier, B. F.; Muetterties, E. L.; Rossi, A. R.; *Inorg. Chem.*, **1977**, *16*, 511-522; b) Thompson, H. B.; Bartell, L. S.; *Inorg. Chem.*, **1968**, *7*, 488-491.
- [18] Öztopcu, Ö.; Holzhacker, C.; Puchberger, M.; Weil, M.; Mereiter, K.; Veiros, L. F.; Kirchner, K.; *Organometallics*, **2013**, *32*, 3042-3052.
- [19] Morris, R. H.; *J. Am. Chem. Soc.*, **2014**, *136*, 1948-1959.
- [20] Castro-Rodrigo, R.; Chakraborty, S.; Munjanja, L.; Brennessel, W. W.; Jones, W. D.; *Organometallics*, **2016**, *35*, 3124-3131.

Chapter 5

Halocarbonyl

Molybdenum and

Tungsten PNP Pincer

Complexes

Although metal carbonyl halides are known for a fairly long time, they have become the subject of renewed interest in recent years. The ligand substitution reactions play a fundamental role in organometallic chemistry, because they are systematically involved in the syntheses of complexes and in wide range of catalysis.¹ The halogen derivatives of substituted metal carbonyls are generally prepared either by the reaction of donor species with metal halocarbonyls or by the treatment of halogens with substituted metal carbonyls.² A more detail concept of metal carbonyls compounds is described on the beginning of Chapter 3. However, the presence of strongly electron-withdrawing ligands, such as halogen makes the metal more electropositive upon formation of the metal-halogen bond. The IR measurements supports this statement, since the ν_{CO} absorptions of the complex tends to shift to a higher frequency due to decreasing of metal–CO π -backbonding.³

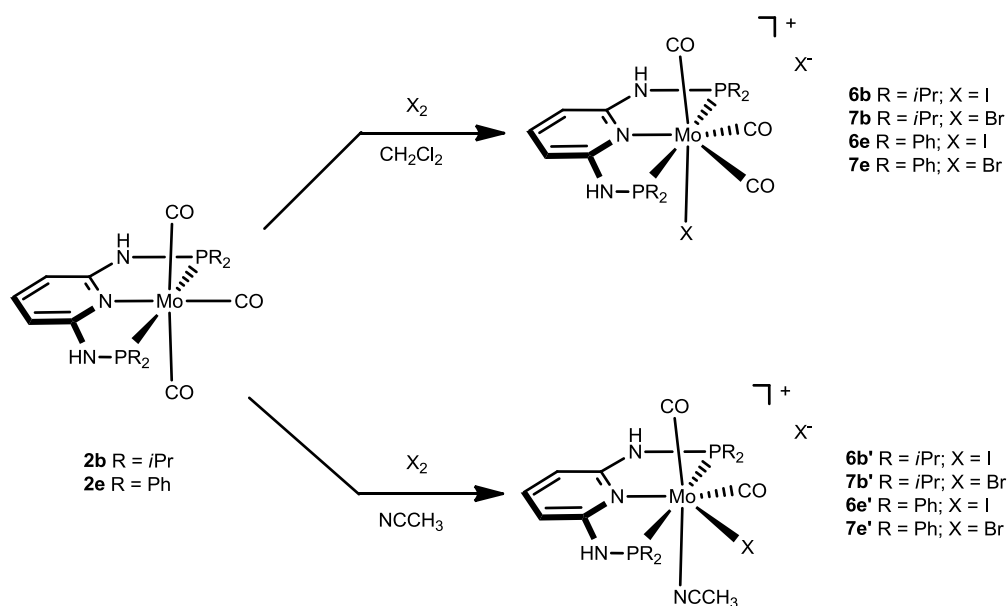
5.1. Molybdenum and tungsten

The synthesis of dihalotetracarbonyls of molybdenum and tungsten by Colton and coworkers, promote the study of a variety of neutral, cationic and anionic halometal carbonyl complexes displaying uncommon oxidation states, geometries and magnetic properties have been synthesized.⁴⁻⁶ In particular, the heptacoordinated halocarbonyl complexes of molybdenum (II) and tungsten (II) have been increasingly important due to the catalytic activity. Seven coordinate halocarbonyl Mo(II) and W(II) complexes of the type $[ML_3(CO)_3X]$ where M = Mo, W; X = Cl, Br, I and L_3 are neutral ($z = 0$) or anionic ($z = -1$) tridentate ligands adopting fac geometries such as Cp, Cp*, trispyrazolylborates, trispyrazolylmethanes, 1,4,7-triazacyclononane, or 1,5,9-triphosphacyclododecane are a common class of compounds. These are typically formed via oxidative addition of X_2 to M(0) complexes $fac-[ML_3(CO)_3]^z$. As L_3 ligands with a mer geometry are concerned such reactions have been rarely studied.⁷

Oxidation to molybdenum (II) and tungsten (II) is most commonly achieved by addition of elemental halogens to zero-valent carbonyl complexes containing at least one non-carbonyl donor ligand.^{8,9} Halogenation by iodine,¹⁰ bromine,¹¹ and chlorine¹² are common in the literature. Oxidative decarboxylation with hydrofluoric acid¹³ or addition of fluoride to a neutral tungsten (II) dicarbonyl complex¹⁴ can provide access to the less common tungsten fluoride complexes. This can be due the much lower electronegativity of the halogens other the fluoride, that the X^- ion has at least modest π -donor ability, in this degree they are more softer bases than F^- .

5.2. Mo and W PNP pincer halocarbonyl complexes

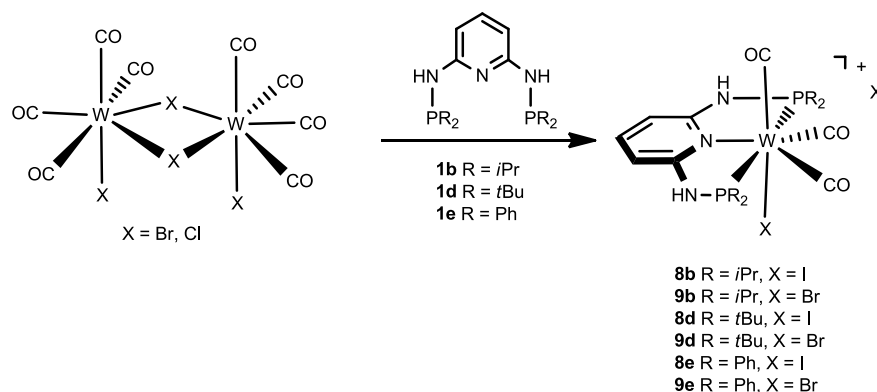
In a fashion way to the Chapters 3 and 4, the chemistry of the Mo and W of PNP pincer halocarbonyl complexes is very limited. In the years of 2006 and 2008, the development of a series of halocarbonyl molybdenum PNP pincer complexes, with a central pyridine ring donor containing NHPR₂ in the two ortho positions, was achieved by the direct oxidation addition of respective tricarbonyl complexes, show on Scheme 5.1..¹⁵



Scheme 5.1. Synthesis of a series of halocarbonyl molybdenum PNP pincer complexes

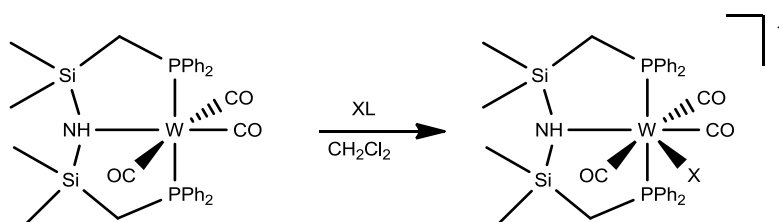
The cationic seven-coordinated species of the type [MoPNP(CO)₃X]X and [MoPNP(CO)₂(CH₃CN)X]X are achieved by adding stoichiometric amounts of X₂ in CH₂Cl₂ or CH₃CN to the precursors [MoPNP(CO)₃] complexes. The analogous tungsten complexes are obtained via the intermediacy of the known dinuclear complex [W(CO)₄(μ-X)X]₂ (X = Br, Cl), prepared in situ from W(CO)₆ and stoichiometric amounts of X₂ in CH₂Cl₂ at -70 °C. Treatment of a solution of [W(CO)₄(μ-X)X]₂ in CH₂Cl₂ at room temperature with the PNP ligands afforded the seven-coordinate tungsten(II) complexes [W(PNP)(CO)₃X]X (X = Br, Cl), Scheme 5.2..

Chapter 5 – Halocarbonyl Molybdenum and Tungsten PNP pincer complexes



Scheme 5.2. Synthesis of a series of halocarbonyl tungsten PNP pincer complexes

This methodology also yields the analogous Mo(0) complexes thus being an alternative method to that described previously. Templeton and coworkers described the synthesis of a series of halocarbonyl tungsten pincer complexes featuring the silazane-based PNP pincer-type ligand $\text{HN}(\text{SiMe}_2\text{CH}_2\text{PPh}_2)_2$.¹⁶



Scheme 5.3. Synthesis of tungsten hydride complexes with a silazane-based PNP pincer

The series of cationic tungsten (II) halide complexes was synthesized, $[\text{W}(\text{PNP})(\text{CO})_3\text{X}]^+$ ($\text{X} = \text{I}, \text{Br}, \text{Cl}, \text{F}$), by various routes, due to the differing reactivities of the halogens.

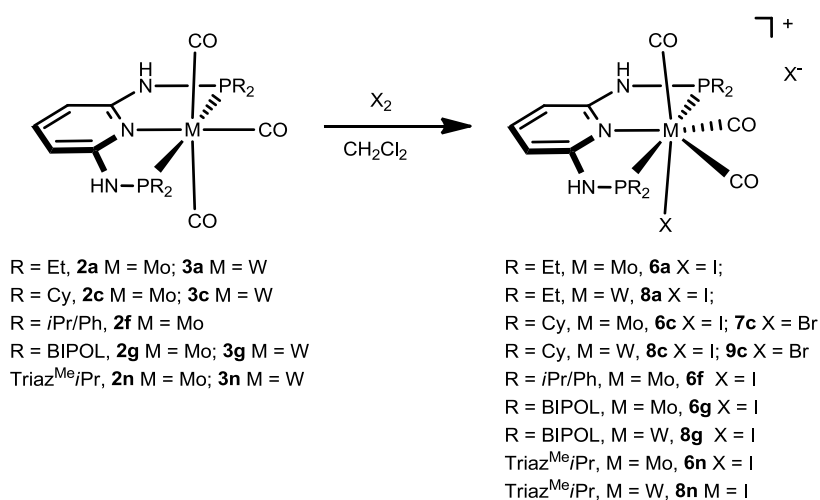
5.3. Results and discussion

A new series of halocarbonyl molybdenum and tungsten PNP complexes was achieved succeeding the exploration of the chemistry of these type of pincer complexes. For the complexes with a central pyridine ring donor contains NHPR_2 in the two ortho positions the reaction of the tricarbonyl PNP complexes $[\text{MPNP}(\text{CO})_3]$ ($\text{M} = \text{Mo}, \text{W}$), with X_2 in CH_2Cl_2 was carried out like is demonstrated in Scheme 5.4..

In general this reaction results in the cationic seven-coordinated molybdenum(II) and tungsten(II) halocarbonyl complexes of the type

Chapter 5 – Halocarbonyl Molybdenum and Tungsten PNP pincer complexes

[Mo(PNP)(CO)₃X]X (X = I, Br). However, in most reactions a mixture of products was achieved impossible to purify due to similar solubility. The same outcome was reached even after several attempts of syntheses with different reactions conditions, taking special consideration in the selection of solvent since one of the CO ligands is labile and easily replace.



Scheme 5.4. Synthesis of the cationic seven-coordinated halocarbonyl Mo and W PNP pincer complexes with NH linkers

Additionally, the complexes with PNP-Et (**6a**, **8a**) and PNP-BIPOL (**6g**, **8g**) ligands show two strong absorption bands in the IR spectra assignable to the symmetric and asymmetric ν_{CO} stretching modes of CO ligands suggesting that complexes of the type [MoPNP(CO)₂I₂] were obtained. Due to their poor solubility full characterization by NMR spectroscopy was precluded.

Complexes **6c-9c** are thermally robust red to yellow solids obtained in 85-89% isolated yield. They are air stable in the solid state but slowly decompose in solution. Characterization was accomplished by combination of ¹H, ¹³C{¹H}, and ³¹P{¹H} NMR spectroscopy, IR spectroscopy, and elemental analysis.* In the ¹³C{¹H} NMR spectrum two low-field triplet resonances (2:1 ratio) were found, assignable to the carbonyl carbon atoms *trans* and *cis* to the pyridine nitrogen (Table 5.1.). In general, compared to the Mo complexes, the NMR signals of the W complexes are typically upfield shifted. The halide ligands do not influence the NMR shifts.

* All complexes in Chapter 5 were characterized by these techniques

Chapter 5 – Halocarbonyl Molybdenum and Tungsten PNP pincer complexes

Table 5.1. Selected $^{13}\text{C}\{^1\text{H}\}$ and $^{31}\text{P}\{^1\text{H}\}$ NMR and IR data of $[\text{M}(\text{PNP-Cy})(\text{CO})_3\text{X}]^+$ (M = Mo, W; X = I, Br)

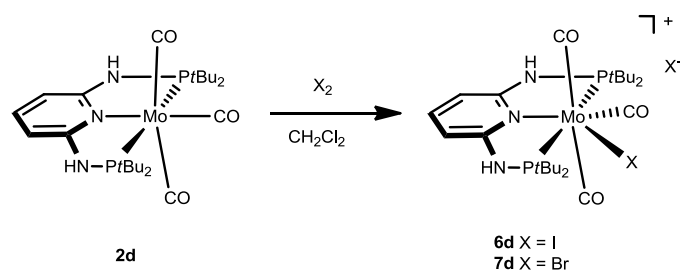
Complexes	$^{13}\text{C}\{^1\text{H}\} / \delta \text{ CO}$	$^{31}\text{P}\{^1\text{H}\} / \delta$	IR / $\text{cm}^{-1} \nu_{\text{CO}}$
$[\text{Mo}(\text{PNP-Cy})(\text{CO})_3\text{I}]^+$ (6c)	232.8, 215.5	109.0	2027, 1964, 1928
$[\text{Mo}(\text{PNP-Cy})(\text{CO})_3\text{Br}]^+$ (7c)	234.8, 218.2	109.6	2037, 1970, 1936
$[\text{W}(\text{PNP-Cy})(\text{CO})_3\text{I}]^+$ (8c)	224.9, 208.7	88.4	2022, 1951, 1915
$[\text{W}(\text{PNP-Cy})(\text{CO})_3\text{Br}]^+$ (9c)	224.3, 212.1	90.7	2024, 1948, 1911

The $^{31}\text{P}\{^1\text{H}\}$ NMR spectra exhibit singlet resonances in the range of 110-87 ppm, where is observed an upfield shift between the molybdenum and the tungsten complexes. The phosphorus resonances (δP) exhibit a slight upfield shift between the complexes with Br or I ligands, probably related to the increasing electronegativity of the halide ligands.

In the ^1H NMR spectrum, is observed a low-field signal assignable to the proton of the NH spacer, that present a higher acidity when compare with the precursor complexes $[\text{MPNP}(\text{CO})_3]$ (M = W, Mo; Chapter 3). The presence of the halogen influences the acidity of the proton for both Mo and W complexes, however the Br ligand promotes a higher effect.

In all complexes, the PNP pincer ligand adopts the typical mer coordination mode with no evidence for any fac isomers. The IR spectra show, in most cases, the typical three strong to medium absorption bands of a mer CO arrangement in the range of 2037-1911 cm^{-1} , assignable to one weaker symmetric and two strong asymmetric ν_{CO} stretching modes. When the respectively halocarbonyl complexes are compare to their precursors, $[\text{M}(\text{PNP})(\text{CO})_3]$ (M = Mo, W) (Chapter 3), there is a shift of almost 100 cm^{-1} to higher energy for the three carbonyl frequencies. This is due to the decrease of the π backbonding since the metal becomes more electropositive by forming the M-X bond. The only exception is the cationic seven-coordinated molybdenum complexes featuring a di-*tert*-butylphosphino, that presents the same geometry then the hydride carbonyl complexes, i. e. the halogen atom is trans to the pyridine nitrogen (Scheme 5.5.). A thermally robust green solid that slowly decompose in solution like the previous complexes.

Chapter 5 – Halocarbonyl Molybdenum and Tungsten PNP pincer complexes



Scheme 5.5. Synthesis of the halocarbonyl molybdenum PNP-*t*Bu pincer complexes

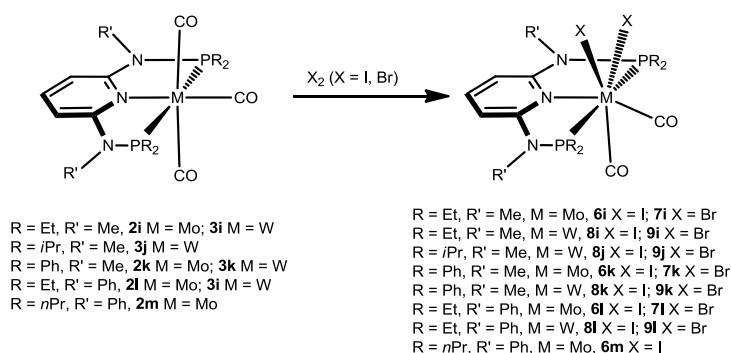
The IR spectra of the $[\text{Mo}(\text{PNP-}t\text{Bu})(\text{CO})_3\text{X}]^+$ ($\text{X} = \text{I}, \text{Br}$) complexes show the three ν_{CO} bands for a mer CO arrangement, assignable to one small symmetric and two strong asymmetric ν_{CO} stretching modes (2070, 1935, 1867 (**6d**), 2029, 1919, 1805 (**7d**)). When compare with the analogous hydride complex $[\text{Mo}(\text{PNP-}t\text{Bu})(\text{CO})_3\text{H}]^+$ in Chapter 4, there is a shift to higher energy, since the metal-halogen bond makes the metal more electropositive.

The $^{13}\text{C}\{^1\text{H}\}$ NMR for these complexes display two low-field triplet resonances (1:2 ratio) at 219.0, 208.2 ppm for **6d** and 220.4, 209.6 ppm for **7d** assignable to the carbonyl carbon atoms trans and cis to the pyridine nitrogen. The $^{31}\text{P}\{^1\text{H}\}$ NMR spectrum of complexes **6d** and **7d** exhibit two doublets at 137.6, 108.2 and 139.8, 113.2, respectively, due to the position of halogen atom, trans to the pyridine nitrogen, that indicate a effected in one of the phosphines making them unequal. There is an upshield compared with the precursor $[\text{Mo}(\text{PNP-}t\text{Bu})(\text{CO})_3]$ (**2d**) (see Chapter 3) and to the analogous $[\text{Mo}(\text{PNP-}t\text{Bu})(\text{CO})_3\text{H}]^+$ (**4d**) (see Chapter 4).

Considering the reactivity of $[\text{M}(\text{PNP})(\text{CO})_3]$ where the PNP ligands contain different PR_2 and NR' units, the addition of X_2 in CH_2Cl_2 yields the neutral seven-coordinated molybdenum(II) and tungsten(II) halocarbonyl complexes of the type $[\text{M}(\text{PNP})(\text{CO})_2\text{X}_2]$ ($\text{M} = \text{Mo}, \text{W}$; $\text{X} = \text{I}, \text{Br}$) shown in Scheme 5.6..

This reaction was independent of the substituents at the P and N sites, respectively, and the chemistry of tungsten strongly parallels that of molybdenum. All complexes are thermally robust red to yellow solids, which are air stable in the solid state but slowly decompose in solution. Due to the poor solubility and thus the low concentration of the some complexes, quaternary carbons could not be detected or were completely precluded, thus solid-state ^{13}C NMR spectra were recorded.

Chapter 5 – Halocarbonyl Molybdenum and Tungsten PNP pincer complexes



Scheme 5.6. Synthesis of the cationic seven-coordinated halocarbonyl Mo and W PNP pincer complexes with NR (R = Me, Ph) linkers

The $^{13}\text{C}\{^1\text{H}\}$ NMR spectra give rise to two characteristic low-field triplet resonances assignable to the carbonyl carbon atoms *trans* and *cis* to the pyridine nitrogen, respectively, for the molybdenum and tungsten complexes (Table 5.2.). The $^{31}\text{P}\{^1\text{H}\}$ NMR spectra exhibit singlet resonances in the range of 141-108 ppm. The pi-accepting/sigma-donating capabilities of phosphines can be studied through the δP shifts, since the nature of the phosphine ligand is the only difference in the series of tricarbonyl complexes following the order $\text{PNP}^{\text{Ph}}\text{-}i\text{Pr} < \text{PNP}^{\text{Me}}\text{-Ph} < \text{PNP}^{\text{Ph}}\text{-Et} < \text{PNP}^{\text{Me}}\text{-Et} < \text{PNP}^{\text{Me}}\text{-}i\text{Pr}$ (Table 5.2.). The phosphorus resonances (δP) exhibit a significant upfield shift on going from Br to I, obviously directly related to the increasing electronegativity of the halide ligands. Both the carbonyl resonances (δCO) and the phosphorus resonances (δP) exhibit a significant upfield shift on going from Mo to W for the two halocarbonyl complexes (Table 5.2.).

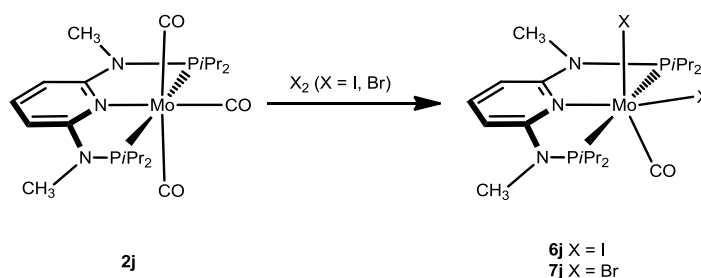
Table 5.2. Selected $^{13}\text{C}\{^1\text{H}\}$ NMR and $^{31}\text{P}\{^1\text{H}\}$ NMR and IR data of the pincer tricarbonyl Mo complexes

Complexes	$^{13}\text{C}\{^1\text{H}\} / \delta$		$^{31}\text{P}\{^1\text{H}\} / \delta$	IR / cm^{-1}	
	CO	CO		ν_{CO}	ν_{CO}
$[\text{Mo}(\text{PNP}^{\text{Me}}\text{-Et})(\text{CO})_2\text{I}_2]$ (6i)	257.9	224.6	135.9	1964	1840
$[\text{Mo}(\text{PNP}^{\text{Me}}\text{-Ph})(\text{CO})_2\text{I}_2]$ (6k)	228.5	218.2	129.3	1946	1870
$[\text{Mo}(\text{PNP}^{\text{Ph}}\text{-Et})(\text{CO})_2\text{I}_2]$ (6l)	258.3	224.3	133.3	1974	1850
$[\text{Mo}(\text{PNP}^{\text{Ph}}\text{-}i\text{Pr})(\text{CO})_2\text{I}_2]$ (6m)	258.3	224.2	127.9	1954	1831
$[\text{W}(\text{PNP}^{\text{Me}}\text{-Et})(\text{CO})_2\text{I}_2]$ (8i)	249.5	207.9	112.8	1953	1828
$[\text{W}(\text{PNP}^{\text{Me}}\text{-}i\text{Pr})(\text{CO})_2\text{I}_2]$ (8j)	225.3	204.2	123.9	1946	1823
$[\text{W}(\text{PNP}^{\text{Me}}\text{-Ph})(\text{CO})_2\text{I}_2]$ (8k)	246.9	222.2	108.0	1952	1850
$[\text{W}(\text{PNP}^{\text{Ph}}\text{-Et})(\text{CO})_2\text{I}_2]$ (8l)	227.6	205.9	109.5	1958	1826

Chapter 5 – Halocarbonyl Molybdenum and Tungsten PNP pincer complexes

The IR spectra show, in most cases, the typical two strong bands in the range of 1979–1815 cm^{-1} (cf. 2143 cm^{-1} in free CO) assignable to one symmetric and one asymmetric ν_{CO} stretching modes, for the mutually *cis* CO ligands. When compare with the analogous bromide complexes $[\text{Mo}(\text{PNP})(\text{CO})_2\text{X}_2]$, there is a shift to higher energy, since the metal-halogen bond makes the metal more electropositive.

The only exception is the $[\text{Mo}(\text{PNP}^{\text{Me}}-i\text{Pr})(\text{CO})_3]$ where instead of $[\text{Mo}(\text{PNP}^{\text{Me}}-i\text{Pr})(\text{CO})_2\text{X}_2]$ ($\text{X} = \text{I}, \text{Br}$) the unusual coordinatively unsaturated six-coordinate complexes $[\text{Mo}(\text{PNP}^{\text{Me}}-i\text{Pr})(\text{CO})\text{X}_2]$ ($\text{X} = \text{I}, \text{Br}$) (**6j**, **7j**) were formed (Scheme 5.7.).



Scheme 5.7. Synthesis of the halocarbonyl molybdenum $\text{PNP}^{\text{Me}}-i\text{Pr}$ pincer complexes

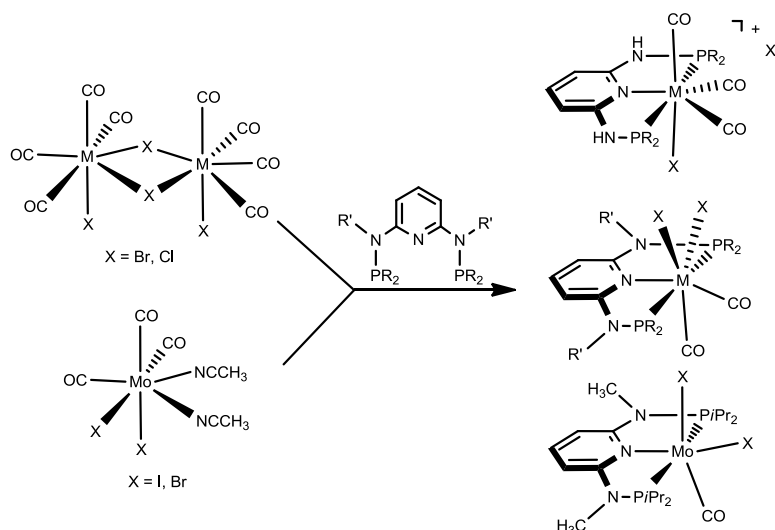
All complexes are thermally robust bluish-green solids, which are air stable in the solid state but slowly decompose in solution and characterization was accomplished with the same techniques described before.

The unusual type $[\text{Mo}(\text{PNP}^{\text{Me}}-i\text{Pr})(\text{CO})\text{X}_2]$ ($\text{X} = \text{I}, \text{Br}$) exhibited one low-field triplet resonances at 247.3 and 247.9 in the $^{13}\text{C}\{^1\text{H}\}$ NMR spectrum, respectively, assignable to the carbon atom of the CO ligand. In the $^{31}\text{P}\{^1\text{H}\}$ NMR spectrum singlets at 190.4 and 195.2 ppm, respectively, are observed, that also line with the increasing electronegativity of the halide ligands. In the IR spectrum the complexes **6j** and **7j** exhibit one strong ν_{CO} band at 1824 and 1816 cm^{-1} , respectively which suggests that Br^- is a better electron donor. For comparison, complexes $[\text{Mo}(\text{PNP}^{\text{Me}}-\text{Ph})(\text{CO})_2\text{X}_2]$ ($\text{X} = \text{I}, \text{Br}$) that displayed to two strong CO stretching due to weaker π -back-bonding interactions and thus the metal center in $[\text{Mo}(\text{PNP}^{\text{Me}}-i\text{Pr})(\text{CO})\text{X}_2]$ seems to be slightly more electron rich than in the seven coordinate complexes $[\text{Mo}(\text{PNP}^{\text{Me}}-\text{Ph})(\text{CO})_2\text{X}_2]$.

Alternatively, the previous complexes were also obtained by reacting the metal precursors $[\text{Mo}(\text{CO})_3(\text{CH}_3\text{CN})_2\text{X}_2]$ ($\text{X} = \text{I}, \text{Br}$) with the PNP pincer ligands. The reaction of $[\text{Mo}(\text{CO})_4(\mu\text{-Cl})\text{Cl}]_2$ in CH_3CN with the respective ligand affords the analogous chlorine complexes $[\text{M}(\text{PNP}^{\text{Me}}-i\text{Pr})(\text{CO})\text{Cl}_2]$ (**10j**) and $[\text{M}(\text{PNP}^{\text{Me}}-\text{Ph})(\text{CO})_2\text{Cl}_2]$ (**10k**).

Chapter 5 – Halocarbonyl Molybdenum and Tungsten PNP pincer complexes

Noteworthy, this methodology also works very well for the synthesis of the bromide complexes.



Scheme 5.8. Alternative methods of synthesis of halocarbonyl Mo and W PNP pincer complexes

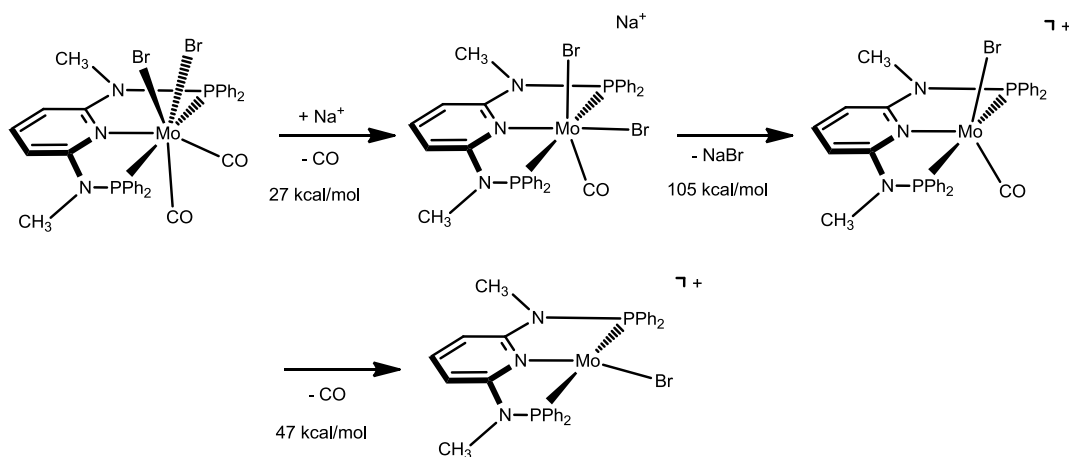
The two chloride complexes $[\text{Mo}(\text{PNP}^{\text{Me}}\text{-}i\text{Pr})(\text{CO})\text{Cl}_2]$ (**10j**) and $[\text{Mo}(\text{PNP}^{\text{Me}}\text{-Ph})(\text{CO})_2\text{Cl}_2]$ (**10k**) behave identical to the analogous iodine and bromine complexes. The phosphorus resonances (δP) of the series of halocarbonyl $\text{PNP}^{\text{Me}}\text{-}i\text{Pr}$ and $\text{PNP}^{\text{Me}}\text{-Ph}$ complexes exhibit a significant upfield shift on going from Cl to Br to I, obviously directly related to the increasing electronegativity of the halide ligands. In the IR spectrum the complex **10j** exhibit one strong ν_{CO} band and the complex **10k** two strong ν_{CO} bands. The complex $[\text{M}(\text{PNP}^{\text{Me}}\text{-Ph})(\text{CO})_2\text{Cl}_2]$ display two sets of resonances in the IR spectrum, which are 26 and 16 cm^{-1} apart, may be due to intermolecular interactions, e.g., $\text{CO}\cdots\text{Cl}\text{-Mo}$ bonds in the solid state.

Moreover, some molybdenum and tungsten complexes were also characterized by means of ESI-MS. This technique enables the detection and the study of reaction substrates and products but also detects short-lived reaction intermediates and decomposition products as they are present in solution. These studies (in the positive and negative ion mode) revealed that complexes with NH linkers in CH_3CN solutions remain largely intact $[\text{M}]^+$. Further abundant fragments are $[\text{M-CO}]^+$ and $[\text{M-2CO}]^+$, where the dissociated suggesting that CO ligands are labile (*vide infra*). In the case of complexes with N-Me and R-Ph linkers in CH_3CN or MeOH solutions in the presence of NaX (X = I, Br, Cl) remain largely intact and fragments of the sodiated complexes $[\text{M+Na}]^+$ or halide adducts $[\text{M+X}]^-$. Further abundant fragments are $[\text{M-X}]^+$ and $[\text{M-X-}$

Chapter 5 – Halocarbonyl Molybdenum and Tungsten PNP pincer complexes

$\text{CO}]^+$ where one halide and CO ligand, respectively, is dissociated suggesting that one halide and one CO ligand are labile (*vide infra*). For the ESI-MS analysis of the exception complexes $[\text{Mo}(\text{PNP}^{\text{Me}}\text{-iPr})(\text{CO})\text{X}_2]$ in CH_3CN and the corresponding sodium halide were subjected to “soft ionization” conditions, in the absence of air signals corresponding to the sodiated complexes $[\text{Mo}(\text{PNP}^{\text{Me}}\text{-iPr})(\text{CO})\text{X}_2]$ ($[\text{M}+\text{Na}]^+$) and also $[\text{Mo}(\text{PNP}^{\text{Me}}\text{-iPr})(\text{CO})\text{X}]^+$ ($[\text{M}-\text{X}]^+$) where one halide ligand is dissociated. The formation of the last fragment is in keeping with the fact that the halide trans to the CO ligand is labile.

An example of this ESI-MS analysis is $[\text{Mo}(\text{PNP}^{\text{Me}}\text{-Ph})(\text{CO})_2\text{Br}_2]$ where under so called “soft ionization” conditions, the most abundant signals observed at m/z is 805.91 which correspond to the sodiated complexes $[\text{Mo}(\text{PNP}^{\text{Me}}\text{-Ph})(\text{CO})\text{Br}_2]$ ($[\text{M}+\text{Na}-\text{CO}]^+$) where one CO ligand is dissociated suggesting that one CO ligand is labile (*vide infra*). Further abundant fragments are $[\text{Mo}(\text{PNP}^{\text{Me}}\text{-Ph})(\text{CO})\text{Br}]^+$ ($[\text{M}-(\text{CO}+\text{NaBr})]^+$) and $[\text{Mo}(\text{PNP}^{\text{Me}}\text{-Ph})\text{Br}]^+$ ($[\text{M}-(2\text{CO}+\text{NaBr})]^+$) as shown in Scheme 5.9..



Scheme 5.9. Fragmentation pattern of $[\text{Mo}(\text{PNP}^{\text{Me}}\text{-Ph})(\text{CO})_2\text{Br}_2]$ complexes observed in the ESI-MS experiments and the DFT calculated energy balance for $\text{X} = \text{Br}$

Corresponding positive-ion ESI full scan mass and MS/MS (low energy CID) spectra of $[\text{Mo}(\text{PNP}^{\text{Me}}\text{-Ph})(\text{CO})_2\text{Br}_2]$ (**7k**) are depicted in Figure 5.1..

Chapter 5 – Halocarbonyl Molybdenum and Tungsten PNP pincer complexes

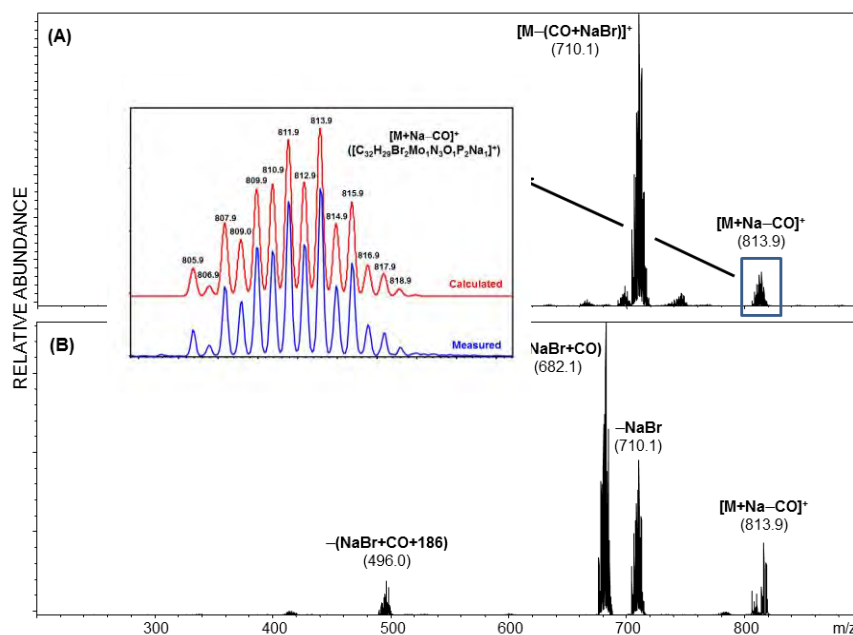


Figure 5.1. Positive-ion ESI mass spectrum of [Mo(PNP^{Me}-Ph)(CO)₂Br₂] (7k) (A) and corresponding MS/MS-spectrum of source-generated [M+Na-CO]⁺ precursor ions (B). Inset: Calculated and measured MS of [M+Na-CO]⁺. In both spectra only signals containing the Mo-isotope of highest abundance (⁹⁸Mo) are annotated

Additionally to the previous characterization, the solid-state structures of **6i**, **7i**, **6j**, **7j**, **6k**, **7k**, **6l**, **8j**, **8k**, **9k**, **8l**, **10j**, **10k** and **8'j** were determined by single-crystal X-ray diffraction. Structural diagrams of a few examples are illustrated in Figures 5.2.-5.6. with selected bond distances given in the captions.

With the exception of **6j**, the coordination geometry around the molybdenum and tungsten complexes may be described as a trigonal mono capped antiprism with one CO as the capping ligand. The crystal structures show the tridentate PNP ligand bound meridionally with two carbonyl and two halide ligands filling the remaining four sites. In the molybdenum complexes **6k** and **6l**, the metal-CO bond lengths in the three complexes average to 1.96 Å (1.92-2.00 Å). The P1-M-P2 angles in the diiodo molybdenum complexes are also hardly affected by the size of the substituents of the phosphorus atoms, being 111.84(2) and 111.98(2)°, respectively. In all complexes the molybdenum center is significantly bent out of the least squares plane defined by the atoms of the pyridine ring.

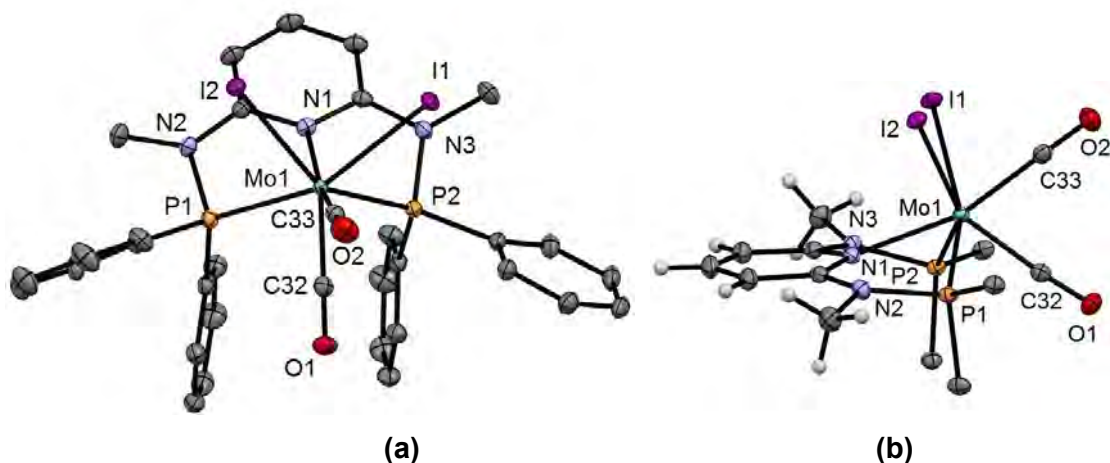


Figure 5.2. (a) Structural view of $[\text{Mo}(\text{PNP}^{\text{Me}}\text{-Ph})(\text{CO})_2\text{I}_2] \cdot \text{CD}_2\text{Cl}_2$ (**6k**· CD_2Cl_2) showing 50% thermal ellipsoids (hydrogen atoms and solvent omitted for clarity). Selected bond lengths (Å) and bond angles (°): Mo1-I1 2.8888(5), Mo1-I2 2.8911(5), Mo1-P1 2.4364(7), Mo1-P2 2.4181(6), Mo-N1 2.276(2), Mo-C32 1.937(2), Mo-C33 1.991(2); P1-Mo1-P2 111.84(2), N1-Mo1-I1 94.11(4), N1-Mo1-I2 88.10(4), N1-Mo1-C32 122.64(7), N1-Mo1-C33 124.49(7), I1-Mo1-I2 82.27(1), C32-Mo1-C33 73.60(8). (b) Side view of **6k** (hydrogen atoms, most phenyl carbon atoms, and solvent omitted for clarity)

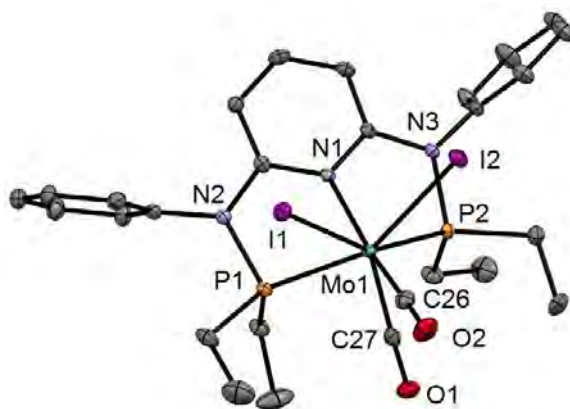


Figure 5.3. Structural view of $[\text{Mo}(\text{PNP}^{\text{Ph}}\text{-Et})(\text{CO})_2\text{I}_2]$ (**6l**) showing 50% thermal ellipsoids (hydrogen atoms and solvent omitted for clarity). Selected bond lengths (Å) and bond angles (°): Mo1-P1 2.4384(8), Mo1-P2 2.4385(7), Mo1-C26 2.002(2), Mo1-C27 1.922(2), Mo1-I1 2.9159(5), Mo1-I2 2.9131(5), P1-Mo1-P2 111.98(2), I1-Mo1-I2 82.89(1), C26-Mo1-C27 72.01(10)

The tungsten complexes, **8j**, **8k** and **8l**, analogous to the molybdenum complexes, have a metal–CO bond lengths in the three complexes average to 1.97 Å (1.93–2.00 Å). The P1–M–P2 angles in the diiodo tungsten complexes are also hardly

Chapter 5 – Halocarbonyl Molybdenum and Tungsten PNP pincer complexes

affected by the size of the substituents of the phosphorus atoms, being 114.97(2), 113.69(1) and 112.93(3), respectively.

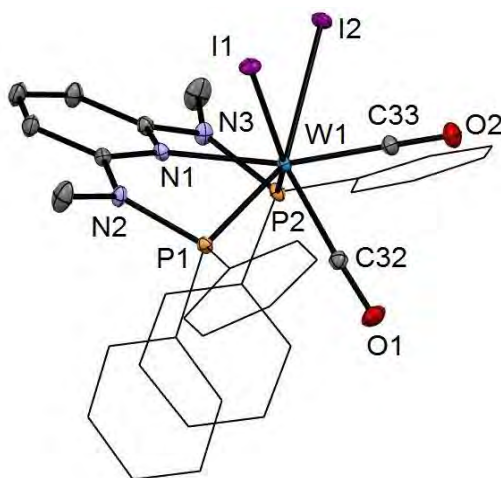


Figure 5.4. Structural view of $[\text{W}(\text{PNP}^{\text{Me}}\text{-Ph})(\text{CO})_2\text{I}_2]$ (**8k**) showing 50% thermal ellipsoids (hydrogen atoms and solvent omitted for clarity). Selected bond lengths (Å) and bond angles ($^\circ$): W1-P1 2.4252(5), W1-P2, 2.4255(5), W1-N1 2.253(1), W1-C32 1.948(2), W1-C33 1.988(2), W1-I1 2.8924(3), W1-I2 2.8958(3), P1-W1-P2 113.69(1), I1-W1-I2 81.15(1), C32-W1-C33 73.46(6)

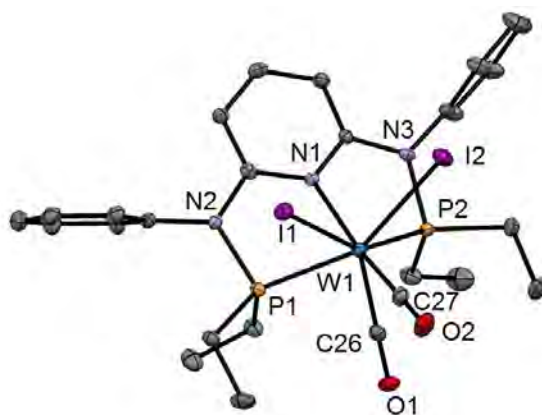


Figure 5.5. Structural view of $[\text{W}(\text{PNP}^{\text{Ph}}\text{-Et})(\text{CO})_2\text{I}_2]$ (**8l**) showing 50% thermal ellipsoids (hydrogen atoms and solvent omitted for clarity). Selected bond lengths (Å) and bond angles ($^\circ$): W1-P1 2.4237(8), W1-P2 2.4322(8), W1-C26 1.932(3), W1-C27 1.997(3), W1-I1 2.9013(3), W1-I2 2.8978(3), P1-W1-P2 112.93(3), I1-W1-I2 81.40(1), C26-W1-C27 72.45(12)

For the series of seven-coordinate neutral halocarbonyl Mo(II) complexes of the type $[\text{Mo}(\text{PNP}^{\text{Me}}\text{-Ph})(\text{CO})_2\text{X}_2]$ (X = I (**6k**), Br (**7k**), and Cl (**10k**)), the coordination geometry around the molybdenum center may be described as a trigonal monocapped

Chapter 5 – Halocarbonyl Molybdenum and Tungsten PNP pincer complexes

antiprism with C32-O1 as capping ligand. The P1-Mo1-P2 angles increases from 111.84(2) to 118.46(3) to 120.18(2)^o, respectively. The corresponding X1-Mo1-X2 and C32-Mo1-C33 angles are essentially independent of the nature of the halide being 82.27(1), 80.56(2) and 81.07(2)^o, and 73.60(8), 74.3(2) and 72.92(7)^o, respectively. The same is accurate for the tungsten complexes [W(PNP^{Me}-Ph)(CO)₂X₂] (X = I (**8k**), Br (**9k**)).

Related with the tricarbonyl molybdenum precursor, **2k**, which possess a distorted octahedron geometry with pyridine and one CO perfectly coplanar, in all the halocarbonyl complexes the molybdenum center is significantly bent out of the least squares plane defined by the atoms of the pyridine ring (N1, C1-C5) by 0.687(3), 0.788(5), and 0.632(3) Å. While Mo-N and Mo-P bonds in all complexes are similar, this deformation leads to a decrease in the intramolecular P-P distance in halocarbonyl complexes and of the P-Mo-P angle from ca. 155° in tricarbonyl precursors to 112-120° in halocarbonyl complexes.

In a related way, a distortion of the Mo coordination has been observed for the six coordinate complexes [Mo(PNP^{Me}-*i*Pr)(CO)X₂] (X = I (**6j**) (Figure 5.6.), Br (**7j**), and Cl (**10j**)), in which the Ph₂ fragment is replaced by the more bulky *i*Pr₂ fragment and the two halogen atoms are in cis/trans-disposition and oriented approximately perpendicular to the P1-P2 vector. In all the complexes, the Mo-N and Mo-P bonds are similar, this deformation leads to a decrease in the intramolecular P-P distance from 4.7 in the tricarbonyl precursor to 4.25 Å in [Mo(PNP^{Me}-*i*Pr)(CO)X₂] complexes and of the P-Mo-P angle from ca. 155° to 126–128°, respectively. This means that the PNP ligand in halocarbonyl complexes are on a transition from meridional to facial coordination that would end with a final ideal P-Mo-P angle of 90°. By a concomitant rotation of the *P/i*Pr₂ fragments about their N-P bonds the space between the *i*Pr₂ fragments on the upper side of the complex above Mo becomes more open, while below it becomes more congested.

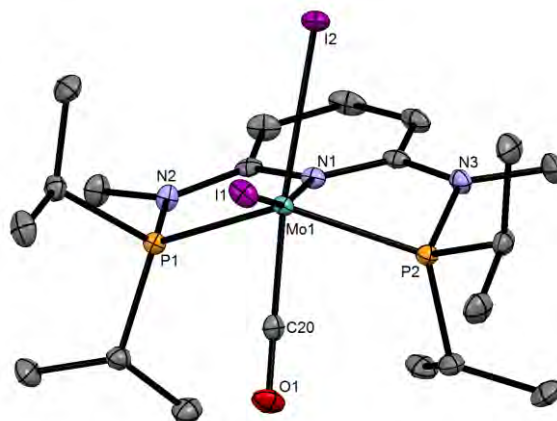


Figure 5.6. Structural view of $[\text{Mo}(\text{PNP}^{\text{Me-}i\text{Pr}})(\text{CO})\text{I}_2]$ (**6j**) showing 50% thermal ellipsoids (H atoms and a second independent complex omitted for clarity). Selected bond lengths (Å) and bond angles ($^\circ$): Mo-N(1) 2.275(2), Mo-C(20) 1.915(3), Mo-P(1) 2.3825(7), Mo-P(2) 2.3764(7), Mo-I(1) 2.7657(3), Mo-I(2) 2.8504(3), P(1)-Mo-P(2) 126.11(2), N(1)-Mo-(1) 74.11(6), N(1)-Mo-P(2) 70.91(6), N(1)-Mo-I(1) 165.50(5), N(1)-Mo-I(2) 79.54(5), N(1)-Mo-C(20) 115.13(9), I(1)-Mo-I(2) 86.36(1), I(1)-Mo-C(20) 79.32(8), I(2)-Mo-C(20) 163.17(7)

The coordination geometry around the molybdenum center, for the complexes $[\text{Mo}(\text{PNP}^{\text{Me-}i\text{Pr}})(\text{CO})\text{X}_2]$ ($\text{X} = \text{I}, \text{Br}, \text{Cl}$) corresponds to a distorted octahedron with the atom pairs P1/P2 N1/X1, and C20/X2. Except for the Mo–halide bond lengths, the bond distances and bond angles and conformations of the three complexes **6j**, **7j**, and **10j**, are very similar and average to Mo–C 1.919 Å, Mo–N 2.270 Å, and Mo–P 2.374 Å.

5.3.1. Reactivity

In all the previous PNP complexes, the modifications of the 2,6-diaminopyridine scaffold by introducing the N-Me and N-Ph instead of N-H linkers conjoined with the modification of the phosphine moieties has a profound impact on the steric and electronic properties of the ligands and consequently also on the stability and reactivity of these metal complexes. Thus far, all complexes with PNP ligands bearing NH moieties, independent of the substituents at the phosphine donor, were generally found to form cationic seven-coordinated species of the type **I** (Figure 5.7.), except for the tert-butyl substitutes in a molybdenum complexes (type **II**). Whereas Mo and W complexes with PNP ligands bearing NR' moieties ($\text{R}' \neq \text{H}$) lead to the formation of neutral dihalo species that are seven-coordinate (type **III**) or in one case with $\text{R} = i\text{Pr}$ and $\text{R}' = \text{Me}$ a six-coordinate complexes (type **IV**).

Chapter 5 – Halocarbonyl Molybdenum and Tungsten PNP pincer complexes

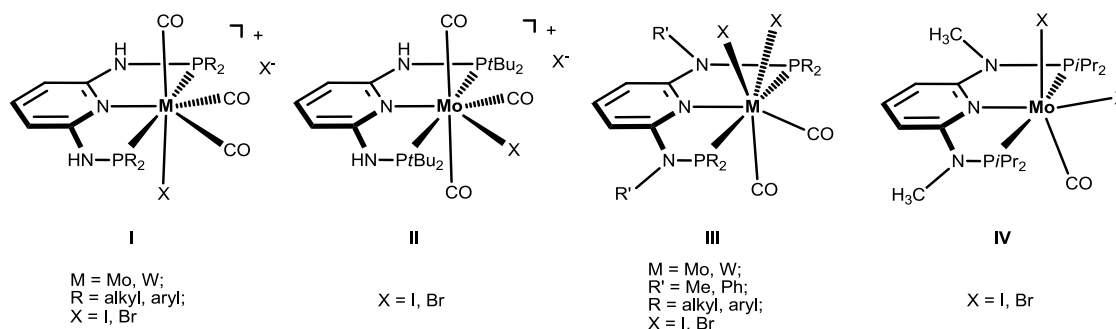
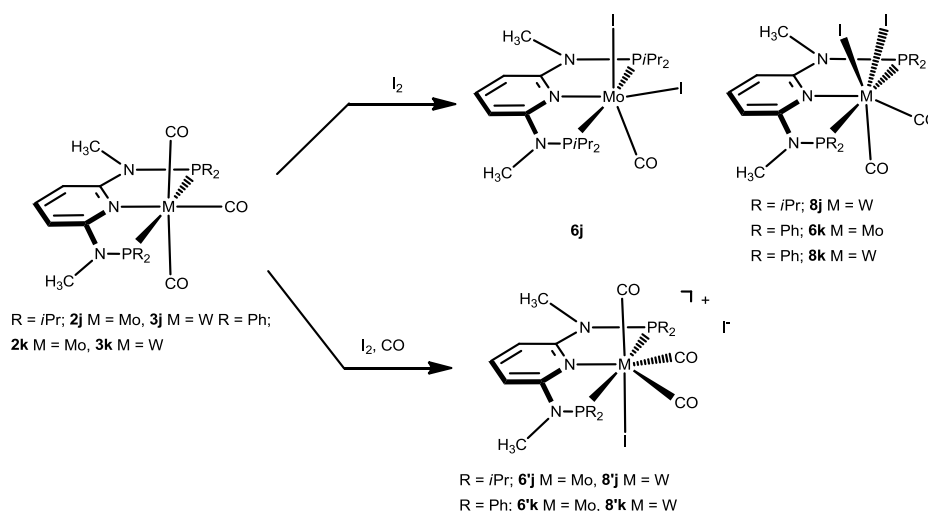


Figure 5.7. Synthesis of seven and six-coordinate iodocarbonyl molybdenum and tungsten complexes

Interestingly, when the oxidative addition of I_2 to $[Mo(PNP^{Me-iPr})(CO)_3]$ (**2j**) and $[W(PNP^{Me-iPr})(CO)_3]$ (**3j**) was performed in the presence of CO in both cases seven-coordinate complexes $[Mo(PNP^{Me-iPr})(CO)_3]I$ (**6'j**) and $[W(PNP^{Me-iPr})(CO)_3]I$ (**8'j**) were formed (Scheme 5.10.). These complexes could be isolated in pure form in 98 and 96% isolated yield. However, in solution in the absence of CO both complexes slowly release CO (about 1 h for Mo, about 3 h for W) and form again the respective neutral six- and seven-coordinate complexes $[Mo(PNP^{Me-iPr})(CO)_2]$ (**6j**) and $[W(PNP^{Me-iPr})(CO)_2]$ (**8j**).



Scheme 5.10. Synthesis of $[MPNP(CO)_3]$ (M = Mo, W) complexes under CO atmosphere

A structural view of complex **8'j** is depicted in Figure 5.8. with selected bond distances and angles given in the caption. The coordination geometry around the molybdenum center corresponds to a distorted capped. The metal-halogen, metal-phosphorus and metal-nitrogen bond length in the complexes $[W(PNP^{Me-iPr})(CO)_2]I$

(8j) and $[\text{W}(\text{PNP}^{\text{Me-}i\text{Pr}})(\text{CO})_3]\text{I}$ (**8'j**) are hardly affected. However the P-Mo-P angles decrease from 150° in the $[\text{W}(\text{PNP}^{\text{Me-}i\text{Pr}})(\text{CO})_3]\text{I}$ to 115° in the $[\text{W}(\text{PNP}^{\text{Me-}i\text{Pr}})(\text{CO})_2\text{I}_2]$.



Figure 5.8. Structural view of $[\text{W}(\text{PNP}^{\text{Me-}i\text{Pr}})(\text{CO})_3]\text{I}$ (**8'j**) showing 50% thermal ellipsoids (hydrogen atoms and solvent omitted for clarity). Selected bond lengths (Å) and bond angles ($^\circ$): W1-I1 2.8835(14), W1-P1 2.5049(13), W1-P2 2.4945(17), W1-N1 2.244(3), W1-C20 1.991(3), W1-C21 1.982(4), W1-C22 2.021(3), P1-W1-P2 $150.32(3)$

Upon treatment of **6j** and **8j** with a halide scavenger (e.g., AgSbF_6) in the presence of CO, $[\text{Mo}(\text{PNP}^{\text{Me-}i\text{Pr}})(\text{CO})_3]$ (**6'j**) and $[\text{W}(\text{PNP}^{\text{Me-}i\text{Pr}})(\text{CO})_3]$ (**8'j**), respectively, are quantitatively formed again. This reaction was performed in CD_2Cl_2 in an NMR tube and monitored by ^1H and $^{31}\text{P}\{^1\text{H}\}$ NMR spectroscopy. Moreover, upon heating **8j** under vacuum no reaction took place and there was no evidence for the formation of $[\text{W}(\text{PNP}^{\text{Me-}i\text{Pr}})(\text{CO})_2]$. Likewise, treatment of **6j** with CO for several hours did not result in the formation of $[\text{Mo}(\text{PNP}^{\text{Me-}i\text{Pr}})(\text{CO})_2\text{I}_2]$.

An extra example was done over time by monitored in the $^{31}\text{P}\{^1\text{H}\}$ NMR spectroscopy the reaction of $[\text{WPNP}^{\text{Me-}i\text{Pr}}\text{-Ph}(\text{CO})_3]$ with iodine in CD_2Cl_2 in an NMR tube (Figure 5.9.). In the beginning the complex $[\text{WPNP}^{\text{Me-}i\text{Pr}}\text{-Ph}(\text{CO})_3]$ exhibit one singlet resonance, upon addition of iodine is observed an extra signals correspondent of $[\text{WPNP}^{\text{Me-}i\text{Pr}}\text{-Ph}(\text{CO})_3]$ at high field. Over time the first signal disappear and a second one appear correspondent to the $[\text{WPNP}^{\text{Me-}i\text{Pr}}\text{-Ph}(\text{CO})_2\text{I}_2]$ at lowfield compared to the $[\text{WPNP}^{\text{Me-}i\text{Pr}}\text{-Ph}(\text{CO})_3]$, until only the final complex $[\text{WPNP}^{\text{Me-}i\text{Pr}}\text{-Ph}(\text{CO})_2\text{I}_2]$ is observed.

Chapter 5 – Halocarbonyl Molybdenum and Tungsten PNP pincer complexes

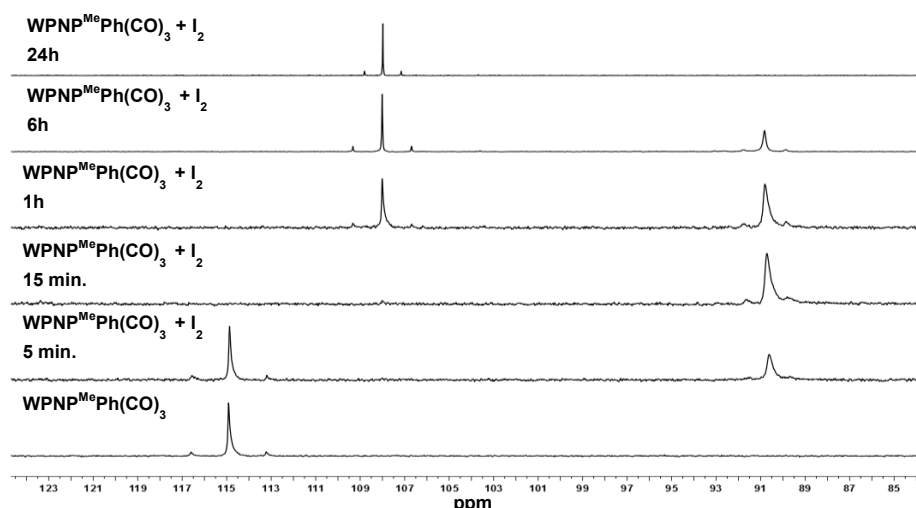
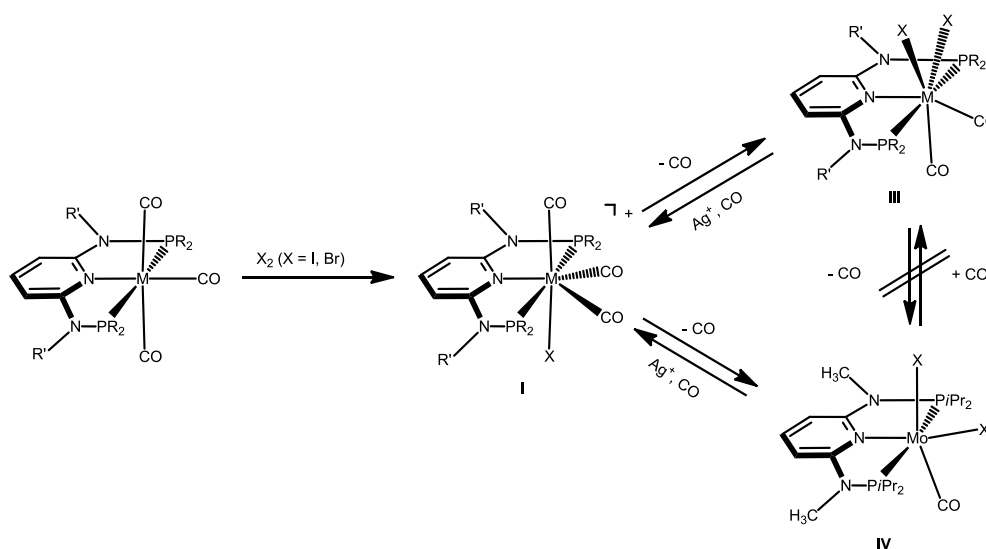


Figure 5.9. Synthesis of $[\text{WPNP}^{\text{Me}}\text{-Ph}(\text{CO})_2]_2$ monitored over time by $^{31}\text{P}\{^1\text{H}\}$ NMR spectroscopy

These experiments clearly suggest that complexes of type **I** are intermediates on the way to complexes of the types **III** and **IV**, but compounds of the type **III** are apparently not intermediates on the way to complexes of the type **IV** (Scheme 5.11.).



Scheme 5.11. Synthesis of seven and six-coordinate halocarbonyl Mo and W

In order to get a better understanding of the mechanism of the above reactions, DFT calculations were performed. First, the free energy values presented in Figure 5.10. indicate that practically all reactions are thermodynamically controlled. The seven-coordinate neutral complexes of type **III** are the most stable species for most

Chapter 5 – Halocarbonyl Molybdenum and Tungsten PNP pincer complexes

combinations of metal and PNP ligand and, thus, are the observed products in most cases.

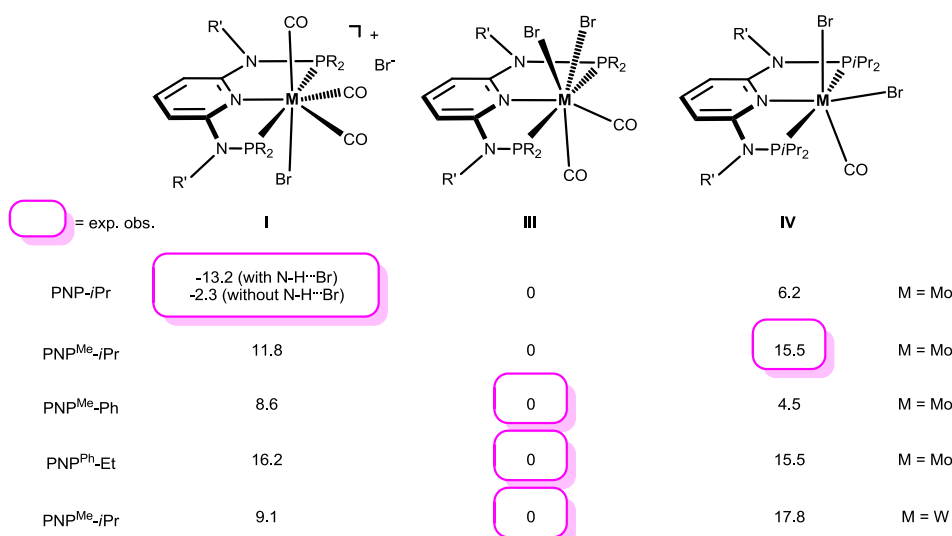


Figure 5.10. DFT calculated free energies (in kcal/mol) of bromocarbonyl complexes referred to $[M(\text{PNP})(\text{CO})_2\text{Br}_2]$ (III)

The cationic complex of type I is obtained in the case of the PNP ligand with a NH linker, in accordance its relative stability calculated by DFT. Interestingly, the existence of an H-bond between the N-H group in the PNP ligand and the bromide counter ion stabilizes the corresponding ion pair by 10.9 kcal/mol.

The special case of the PNP ligands with a NH linker, $[\text{Mo}(\text{PNP-}t\text{Bu})(\text{CO})_3\text{Br}]$, is also under thermodynamic control proven by the free energy values depicted in Figure 5.11.. Unlike the other complexes with NH spacers, the halocarbonyl molybdenum PNP-*t*Bu complexes of type II are the most stable species.

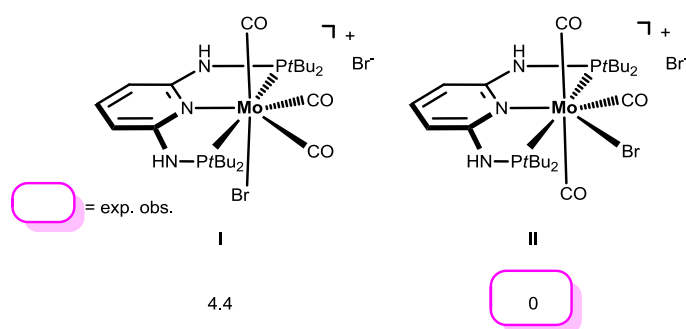


Figure 5.11. DFT calculated free energies (in kcal/mol) of bromocarbonyl complexes referred to $[\text{Mo}(\text{PNP-}t\text{Bu})(\text{CO})_3\text{Br}]$

Chapter 5 – Halocarbonyl Molybdenum and Tungsten PNP pincer complexes

The only abnormality in the free values calculated for the complexes presented in Figure 5.10. corresponds to the Mo complex with $\text{PNP}^{\text{Me-}i\text{Pr}}$. Here, the observed product is the six-coordinated complex with structure **IV** being also the least stable one of all three species with a free energy value 15.5 kcal/mol higher than complex **I**, the most stable one. In this case the product obtained is not the thermodynamic product of the reaction and, thus, we studied the reaction mechanism trying to find a kinetic reason for the formation of complex **IV**. The free energy profiles obtained are represented in Figures 5.12. and 5.13..

The mechanism starts with the ion pair $[\text{Mo}(\text{PNP}^{\text{Me-}i\text{Pr}})(\text{CO})_3\text{Br}]\text{Br}$, i.e., structure **I**, labeled **A** in the profile of Figure 5.12.. Interestingly, this species is observed experimentally if the reaction is performed in the presence of CO. In order to obtain complex $[\text{Mo}(\text{PNP}^{\text{Me-}i\text{Pr}})(\text{CO})\text{Br}_2]$ with structure **IV**, the initial complex (**A**) has to lose two CO ligands and to add one bromide to the metal center. The first step of the mechanism corresponds to loss of the first CO ligand, from **A**. There are two possibilities for that process to occur. The CO ligand lost can be one of the two equatorial CO ligands (the equatorial plane being defined by the PNP ligand) or, alternatively, it can be the axial one, *trans* to the Br-ligand in **A**. Both processes were explored and are represented in Figure 5.12.. Loss of the axial CO leads to complex **B**, and the corresponding barrier has a high value of 30 kcal/mol, corresponding to transition state **TS_{AB}**.

On the other hand, dissociation of one equatorial CO ligand, from **A** to **C**, presents a barrier significantly lower (19 kcal/mol, **TS_{AC}**) and, thus, will be the most favourable process. In the last step, from **D** to **E**,[†] the bromine counter ion coordinates the metal producing the neutral seven-coordinate complex $[\text{Mo}(\text{PNP}^{\text{Me-}i\text{Pr}})(\text{CO})_2\text{Br}_2]$, with structure **III**. This process occurs smoothly with a negligible barrier of only 1 kcal/mol (**TS_{DE}**). In short, formation of **E**, from **A**, is a rather facile process, plausible to happen under the experimental conditions, with an overall barrier of 19 kcal/mol and a favourable free energy balance of $\Delta G = -10$ kcal/mol.

In order to obtain the observed product, $[\text{Mo}(\text{PNP}^{\text{Me-}i\text{Pr}})(\text{CO})\text{Br}_2]$ with structure **IV**, there must be a second CO loss from the metal center and this must happen before bromide coordination, because once the Br^- coordinates the metal, $[\text{Mo}(\text{PNP}^{\text{Me-}i\text{Pr}})(\text{CO})_2\text{Br}_2]$ (**E**, with structure **III**) is formed and this is the thermodynamic product, considerably more stable than the six-coordinate species. Thus, in the reaction path

[†] **D** and **F** are similar to **C** without the neighbour CO molecule.

leading to $[\text{Mo}(\text{PNP}^{\text{Me}}\text{-}i\text{Pr})(\text{CO})\text{Br}_2]$ there will be a second CO loss following the one that yield intermediate **C** in the previous profile.

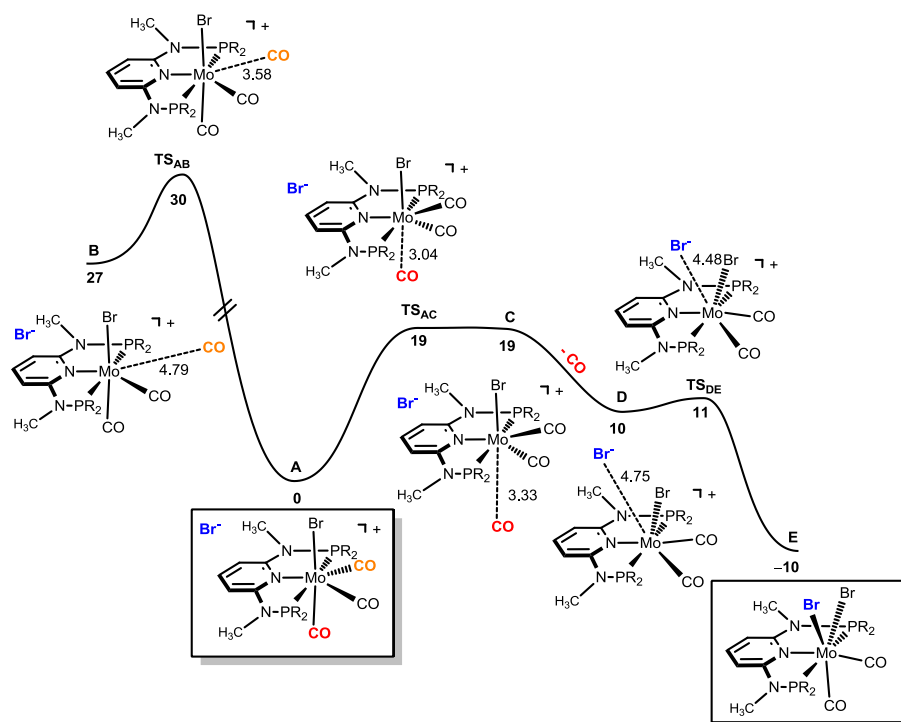


Figure 5.12. Energy profile for the dissociation of CO from $[\text{Mo}(\text{PNP}^{\text{Me}}\text{-}i\text{Pr})(\text{CO})_3\text{Br}]\text{Br}$ (**A**) and formation of seven-coordinate $[\text{Mo}(\text{PNP}^{\text{Me}}\text{-}i\text{Pr})(\text{CO})_2\text{Br}_2]$ (**E**). The free energy values (kcal mol^{-1}) are referred to **A**

The profile for the formation of complex $[\text{Mo}(\text{PNP}^{\text{Me}}\text{-}i\text{Pr})(\text{CO})\text{Br}_2]$ is represented in Figure 5.13.. The path starts with **F**, corresponding to **C** without the free CO molecule. From **F**, loss of another CO ligand leads to **G**, an intermediate with a five-coordinated cationic complex in the ion pair $[\text{Mo}(\text{PNP}^{\text{Me}}\text{-}i\text{Pr})(\text{CO})\text{Br}]\text{Br}$. This process has a high barrier of $\Delta G^\ddagger = 35 \text{ kcal/mol}$ (**TS_{FG}**, relative to **A**) and is clearly unfavourable, from the thermodynamic point of view ($\Delta G = 22 \text{ kcal/mol}$). **G** rearranges to **H** and, in a final step, adds Br^- to yield the product, $[\text{Mo}(\text{PNP}^{\text{Me}}\text{-}i\text{Pr})(\text{CO})\text{Br}_2]$ (**J**).[‡] This is a facile process with barrier of only 1 kcal/mol (**TS_{HI}**) and a free energy balance of $\Delta G = -20 \text{ kcal/mol}$. Overall, the reaction path leading to the 6-coordinate complex **J** presents a barrier of 35 kcal/mol and is endergonic with $\Delta G = 14 \text{ kcal/mol}$.

[‡] **J** and **I** are similar to **C** without the neighbour CO molecule.

Chapter 5 – Halocarbonyl Molybdenum and Tungsten PNP pincer complexes

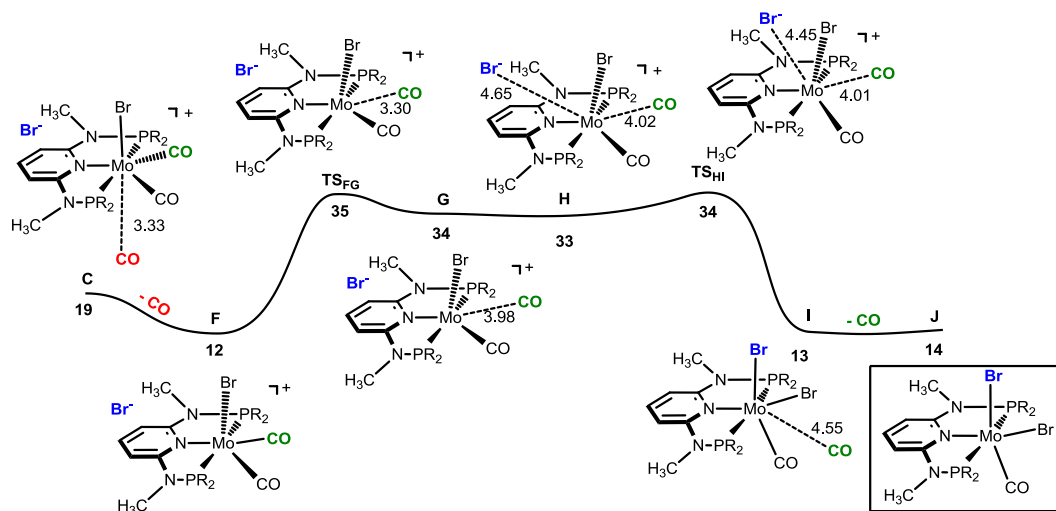


Figure 5.13. Energy profile for the formation of six-coordinate $[\text{Mo}(\text{PNP}^{\text{Me-}i\text{Pr}})(\text{CO})_2\text{Br}]$ (**J**). The free energy values (kcal mol^{-1}) are referred to $[\text{Mo}(\text{PNP}^{\text{Me-}i\text{Pr}})(\text{CO})_3\text{Br}]\text{Br}$ (**A**)

In summary, the conclusions obtained from the DFT mechanistic studies, are that the seven-coordinate complex, $[\text{Mo}(\text{PNP}^{\text{Me-}i\text{Pr}})(\text{CO})_2\text{Br}_2]$ (**E**) with a structure of type **III** should be the thermodynamic as well as the kinetic product. Since **J** is the observed product this means that the reaction must follow an alternative path, not described by the calculations, such as, for example, one involving radical intermediates. This and other possibilities will be the subject of future mechanistic studies. Through DFT calculations it was also possible to evaluate the electronic structure of the unsaturated 16e low spin complex, **7j**. In the frontier orbitals calculated for complex **7j**, one can observe the splitting of the metal d-orbitals that is expected in a distorted octahedral d^4 complex. As expected, all orbitals represented in Figure 5.14. have an important contribution from Mo d-orbitals.

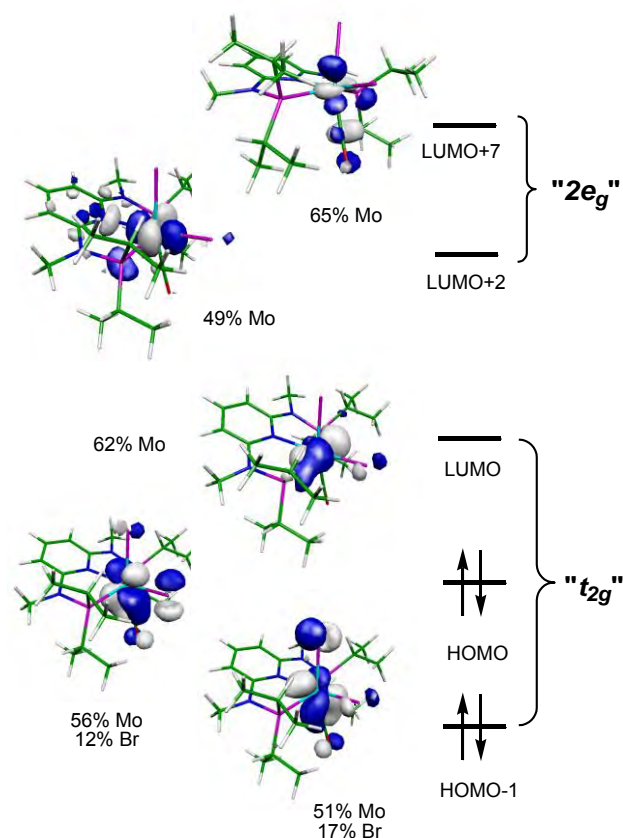


Figure 5.14. Frontier orbitals (d splitting) of $[\text{Mo}(\text{PNP}^{\text{Me-}i\text{Pr}})(\text{CO})\text{Br}_2]$ (**7j**)

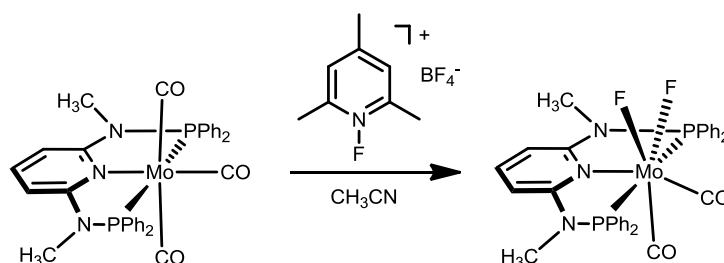
There is a lower energy group of three orbitals that would correspond to the t_{2g} set in a perfect octahedral molecule, and then the two d orbitals pointing directly to the coordinated atoms that would correspond to the $2e_g$ set in a symmetric molecule. In the t_{2g} set the first two orbitals are occupied, being HOMO-1 and HOMO, and show a Mo-Br π^* character indicating that the bromine ligands are acting as π -donors compensating the electron deficiency of the molybdenum center. This is reflected in a significant participation of the Br ligands on the electron density of those orbitals (see Figure 5.14.). In the $2e_g$ set, the x^2-y^2 orbital lies in an equatorial plane defined by the three coordinating atoms of the PNP ligand and by the Br ligand trans to pyridine N-atom, while the z^2 orbital points towards the two axial ligands, the Br-atom and the CO ligand trans to each other.

5.3.2. Fluorine complexes

A small area of investigation in this thesis is the chemistry of carbonyl-containing complexes of Mo and W with a variety of fluorinating agents. The addition of

Chapter 5 – Halocarbonyl Molybdenum and Tungsten PNP pincer complexes

1 equiv. of 1-fluoro-2,4,6-trimethylpyridinium tetrafluoroborate, a reagent acting as net source of “F⁻”, to a solution of [Mo(PNP^{Me}-Ph)(CO)₃] in CH₃CN yielded the analogous fluorine complex [Mo(PNP^{Me}-Ph)(CO)₂F₂] (**11k**) in 93% isolated yield (Scheme 5.12.).



Scheme 5.12. Synthesis of the [Mo(PNP^{Me}-Ph)(CO)₂F₂] complex

The long reaction time required (3 days) and the high yield of this reaction clearly suggest that the BF₄⁻ counterion acts as an additional fluoride source which has indeed precedence in molybdenum and tungsten chemistry.¹⁷ The complex is thermally robust red to yellow solids and characterization was accomplished by elemental analysis and by ¹H, ³¹P{¹H} and ¹³C{¹H} NMR, and IR spectroscopy. Due to the poor solubility and thus the low concentration of the some complexes, quaternary carbons could not be detected or were completely precluded, thus solid-state ¹³C NMR spectra were recorded.

Identical to the other complexes of series PNP^{Me}-Ph, the ¹³C{¹H} NMR spectra give rise to two characteristic low-field triplet resonances assignable to the carbonyl carbon atoms *trans* and *cis* to the pyridine nitrogen, respectively (Table 5.3.).

Table 5.3. Selected ¹³C{¹H} and ³¹P{¹H} NMR and IR data of the [Mo(PNP^{Me}-Ph)(CO)₂(X)₂] complexes

Complexes	¹³ C{ ¹ H} / δ		³¹ P{ ¹ H} / δ	IR / cm ⁻¹	
	CO	CO		ν _{CO}	ν _{CO}
[Mo(PNP ^{Me} -Ph)(CO) ₂ I ₂] (6k)	228.5	218.2	129.3	1946	1870
[Mo(PNP ^{Me} -Ph)(CO) ₂ Br ₂] (7k)	224.8	225.7	133.2	1979	1858
[Mo(PNP ^{Me} -Ph)(CO) ₂ Cl ₂] (10k)	257.6	215.1	135.2	2000	1974
[Mo(PNP ^{Me} -Ph)(CO) ₂ F ₂] (11k)	250.4	214.3	143.7	1977	1880

The ³¹P{¹H} NMR spectra exhibit singlet resonance at 143.7 ppm, exhibit a small downfield shift on going from I to Br to Cl to F, obviously directly related to the increasing electronegativity of the halide ligands. Since the fluorine is much more

Chapter 5 – Halocarbonyl Molybdenum and Tungsten PNP pincer complexes

electronegative than the other halides, it was expected that higher ppm values for the fluorine complex.

The IR spectra show the typical two strong bands assignable to one symmetric and one asymmetric ν_{CO} stretching modes, for the mutually cis CO ligands. The values suggest an ordering of $\text{Cl} > \text{Br} > \text{F} > \text{I}$ for the better electron donors.

The characterization of the fluoride complex by means of ESI-MS detects a different behavior from the other complexes of the same series $[\text{Mo}(\text{PNP}^{\text{Me}}\text{-Ph})(\text{CO})_2\text{X}_2]$. This complex forms after loss of CO and NaF exclusively the cationic fragment $[\text{Mo}(\text{PNP}^{\text{Me}}\text{-Ph})(\text{CO})\text{F}]_2^{2+}$ ($[\text{M}(\text{CO}+\text{NaF})]_2^{2+}$ which is apparently a doubly charged dimer based on isotope spacings (0.5 Da). Higher molecular mass fragments were not observed in this particular case.

Additionally, efforts to characterize this complex by single-crystal X-ray diffraction were unsuccessful. The only achievement was after a few weeks appearing dark red blocks corresponding to the compound $[\text{Mo}_4(\mu_2\text{-O}_2\text{PPh}_2)_4(\mu_3\text{-O})_4\text{O}_4]$, depicted in Figure 5.15., apparently caused by the presence of oxygen. In 1989, Schirmer *et al.* report a chloroform disolvate of the same compound, $[\text{Mo}_4(\mu_2\text{-O}_2\text{PPh}_2)_4(\mu_3\text{-O})_4\text{O}_4] \cdot 2\text{CHCl}_3$, accomplished from the $\text{Mo}(\text{PNP-Ph})(\text{CO})_3$.¹⁸

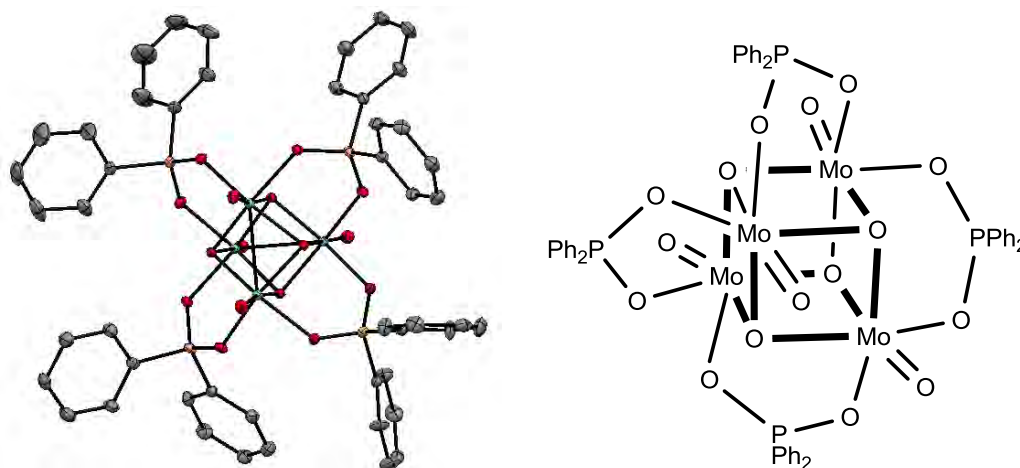


Figure 5.15. Structural view of $[\text{Mo}_4(\mu_2\text{-C}_{12}\text{H}_{10}\text{OP}_2)_4(\mu_3\text{-O})_4\text{O}_4]$, showing 50% thermal ellipsoids (hydrogen atoms and solvent omitted for clarity).

Attempts to obtain the analogous fluorine complex $[\text{Mo}(\text{PNP}^{\text{Me}}\text{-}i\text{Pr})(\text{CO})\text{F}_2]$ (**11j**) upon addition of 1 equiv. of 1-fluoro-2,4,6-trimethylpyridinium as the tetrafluoroborate salt, which is known to act as net source of “F⁺” while the BF_4^- counterion donates fluoride ions,¹⁶ to a solution of $[\text{Mo}(\text{PNP}^{\text{Me}}\text{-}i\text{Pr})(\text{CO})_3]$ in CH_2Cl_2 was unsuccessful.

5.4. Conclusions

A comparative study of a series of halocarbonyl Mo(II) and W(II) complexes of the types $[M(\text{PNP})(\text{CO})_3\text{X}]\text{X}$ and $[M(\text{PNP})(\text{CO})_2\text{X}_2]$ ($M = \text{W}, \text{Mo}; \text{X} = \text{I}, \text{Br}$), featuring PNP pincer ligands based on a 2,6-diaminopyridine scaffold, was carried out. The synthesis of these complexes was accomplished by treatment of $[\text{Mo}(\text{PNP})(\text{CO})_3]$ with stoichiometric amounts of I_2 and Br_2 , respectively. The modification of the PNP ligand by introducing NMe and NPh instead of NH spacers between the aromatic pyridine ring and the P-atoms with concomitant modification of the phosphine moieties changed the steric and electronic properties of the PNP ligand significantly and led to different types of halocarbonyl complexes. While in the case of NH linkers in general cationic seven-coordinate complexes of the type $[M(\text{PNP})(\text{CO})_3\text{X}]^+$ were obtained, with NMe and NPh spacers neutral seven-coordinate complexes of the type $[M(\text{PNP})(\text{CO})_2\text{X}_2]$ were afforded. The only exception is the molybdenum in conjunction with the $\text{PNP}^{\text{Me-}i\text{Pr}}$ ligand, where the coordinatively unsaturated complex $[\text{Mo}(\text{PNP}^{\text{Me-}i\text{Pr}})(\text{CO})\text{X}_2]$ is formed. For the two latter cases, when the reaction is performed in the presence of CO also $[M(\text{PNP})(\text{CO})_3\text{X}]^+$ complexes are formed which slowly lose CO to yield the $[M(\text{PNP})(\text{CO})_2\text{X}_2]$ and $[M(\text{PNP})(\text{CO})\text{X}_2]$, respectively. Upon treatment of $[\text{Mo}(\text{PNP})(\text{CO})\text{I}_2]$ and $[\text{W}(\text{PNP})(\text{CO})_2\text{I}_2]$ with a Ag^+ salt in the presence of CO, $[\text{Mo}(\text{PNP})(\text{CO})_3\text{I}]^+$ and $[\text{W}(\text{PNP})(\text{CO})_3\text{I}]^+$, respectively, are quantitatively formed again. These experiments clearly suggest that complexes of the type $[M(\text{PNP})(\text{CO})_3\text{X}]^+$ are intermediates on the way to complexes of the types $[M(\text{PNP})(\text{CO})_2\text{X}_2]$ and $[M(\text{PNP})(\text{CO})\text{X}_2]$.

In general, the halocarbonyl tungsten chemistry parallels that of molybdenum. The only exception, where the coordinatively unsaturated complex $[\text{Mo}(\text{PNP}^{\text{Me-}i\text{Pr}})(\text{CO})\text{X}_2]$ is formed, was study by DFT mechanistic revealing that the seven-coordinate complexes should be thermodynamic as well as kinetic products. The fact that $[\text{Mo}(\text{PNP}^{\text{Me-}i\text{Pr}})(\text{CO})\text{X}_2]$ is the observed product suggests that the reaction follows an alternative path, for example, one involving radical intermediates. This and other possibilities will be the subject of future mechanistic studies.

5.5. Experimental part

The metal precursors hexacarbonyl of molybdenum and tungsten as well as 1-fluoro-2,4,6-trimethylpyridinium tetrafluoroborate were purchased from commercial vendors. The precursor complexes $[\text{Mo}(\text{NCCH}_3)_2(\text{CO})_3\text{I}_2]$, $[\text{Mo}(\text{NCCH}_3)_2(\text{CO})_3\text{Br}_2]$,

Chapter 5 – Halocarbonyl Molybdenum and Tungsten PNP pincer complexes

$[\text{Mo}(\text{CO})_4(\mu\text{-Br})\text{Br}]_2$, $[\text{Mo}(\text{CO})_4(\mu\text{-Cl})\text{Cl}]_2$ and $[\text{W}(\text{CO})_4(\mu\text{-Br})\text{Br}]_2$ were prepared according to the literature.¹⁹

All solid-state ^{13}C NMR spectra were recorded on a Bruker Avance-300 spectrometer (standard bore), equipped with a 4 mm broad-band MAS probe-head and ZrO_2 rotors. The rotational speed for all experiments was 12 kHz.

All mass spectrometric measurements were performed on an Esquire 3000^{plus} 3D-quadrupole ion trap mass spectrometer (Bruker Daltonics, Bremen, Germany) in positive-ion mode electrospray ionization (ESI-MS). Mass calibration was done with a commercial mixture of perfluorinated trialkyl-triazines (ES Tuning Mix, Agilent Technologies, Santa Clara, CA, USA). All analytes were dissolved in methanol or acetonitrile hypergrade for LCeMS Lichrosolv (Merck, Darmstadt, Germany) to a concentration of roughly 1 mg/mL and doped with sodium halides (Merck, Darmstadt, Germany) to promote $[\text{M} + \text{Na}]^+$ -adduct ion formation of the neutral molybdenum complexes as previously described for titanium and zirconium complexes.^{20,21} Direct infusion experiments were carried out using a Cole Parmer model 74900 syringe pump (Cole Parmer Instruments, Vernon Hills, IL, USA) at a flow rate of 2 $\mu\text{L}/\text{min}$. Full scan and MS2-scans were measured in the mass range m/z 100-1100 with the target mass set to m/z 1000. Further experimental conditions include: dry gas temperature: 150 $^\circ\text{C}$; capillary voltage: -4 kV; skimmer voltage: 40 V; octapole and lens voltages: according to the target mass set. Helium was used as buffer gas for full scans and as collision gas for MS2-scans in the low energy CID mode. The activation and fragmentation width for tandem mass spectrometric (MS/MS) experiments was set to 14 Da to cover the entire isotope cluster for fragmentation. The corresponding fragmentation amplitude ranged from 0.3 to 0.8 V in order to keep a low abundant precursor ion intensity in the resulting spectrum. All mass calculations are based on the lowest mass molybdenum isotope (^{92}Mo -isotope) and tungsten (^{180}W -isotope). Mass spectra and tandem mass spectra were averaged during data acquisition time of 1 to 2 min and one analytical scan consisted of five successive microscans resulting in 50 and 100 analytical scans, respectively, for the final mass spectrum or MS2 spectrum.[§]

5.5.1. Syntheses

General synthetic procedure for halocarbonyl molybdenum and tungsten complexes: To a solution of $[\text{M}(\text{PNP})(\text{CO})_3]$ (M = Mo (**2a-2n**), W (**3a-3n**)) (0.300 mmol)

[§]The same experimental conditions in the following chapters.

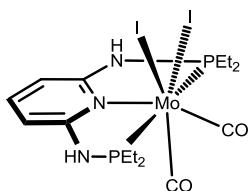
Chapter 5 – Halocarbonyl Molybdenum and Tungsten PNP pincer complexes

in CH_2Cl_2 (10 mL) was added 1 equiv. of I_2 (0.300 mmol). In the case of Br_2 (0.300 mmol), the reaction was performed at $-78\text{ }^\circ\text{C}$ and slowly warmed to room temperature. In both cases, the reaction was stirred for 18 h. After this period the solution was filtered, solvent was removed under vacuum, and the solid was washed twice with Et_2O and *n*-pentane and then dried under vacuum.

Method B: A solution of $[\text{Mo}(\text{CH}_3\text{CN})_2(\text{CO})_3\text{X}_2]$ ($\text{X} = \text{I}, \text{Br}$) (0.300 mmol) in CH_3CN (10 mL) was treated with 1 equiv. of PNP (0.300 mmol). The solution was stirred for 18 h and then filtrated. The product was washed twice with Et_2O and *n*-pentane and then dried under vacuum to yield a powder.

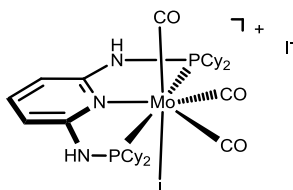
Method C: A solution of $[\text{Mo}(\text{CO})_4(\mu\text{-Br})\text{Br}]_2$ (0.300 mmol) in CH_2Cl_2 (10 mL) was treated with 2 equiv. of PNP (0.600 mmol) and was stirred for 18 h. After this period the solution was filtered, the solvent was removed under reduced pressure, and the remaining solid was washed twice with Et_2O and *n*-pentane.

$[\text{Mo}(\text{PNP-Et})(\text{CO})_2\text{I}_2]$ (6a)



The product was obtained as yellow solid in 96.9% yield. Anal. Calcd. for $\text{C}_{15}\text{H}_{25}\text{I}_2\text{MoN}_3\text{O}_2\text{P}_2$ (691.09). C, 26.07; H, 3.65; N, 6.08. IR (ATR, cm^{-1}): 1967 (ν_{CO}), 1853 (ν_{CO}).

$[\text{Mo}(\text{PNP-Cy})(\text{CO})_3\text{I}]$ (6c)

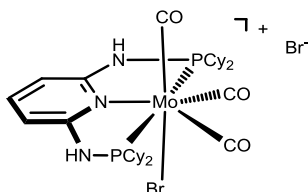


The product was obtained as an orange-red solid in 87% yield. Anal. Calcd. for $\text{C}_{32}\text{H}_{49}\text{I}_2\text{MoN}_3\text{O}_3\text{P}_2$ (935.48): C, 41.09; H, 5.28; N, 4.49. Found: C, 40.98; H, 5.33; N, 4.57. $^1\text{H NMR}$ (δ , CD_2Cl_2 , $20\text{ }^\circ\text{C}$): 7.94 (s, 2H, NH), 7.03 (br, 1H, py^4), 6.98 (br, $\text{py}^{3,5}$), 1.94-1.32 (m, 22H, Cy), 1.28-0.86 (m, 22H, Cy). $^{13}\text{C}\{^1\text{H}\}$ NMR (δ , CD_2Cl_2 , $20\text{ }^\circ\text{C}$): 232.8 (t, $J = 19.5\text{ Hz}$, CO), 215.5 (t, $J = 13.0\text{ Hz}$, CO), 160.2 ($\text{py}^{2,6}$), 142.6 (py^4), 103.0 ($\text{py}^{3,5}$), 42.6 (vt, $J = 10.8\text{ Hz}$, Cy), 41.6 (vt, $J = 11.5\text{ Hz}$, Cy), 30.1-28.1 (Cy), 27.3-26.5 (Cy), 26.1-25.6 (Cy). $^{31}\text{P}\{^1\text{H}\}$ NMR (δ , CD_2Cl_2 , $20\text{ }^\circ\text{C}$): 109.0. IR (ATR, cm^{-1}): 2027 (ν_{CO}),

Chapter 5 – Halocarbonyl Molybdenum and Tungsten PNP pincer complexes

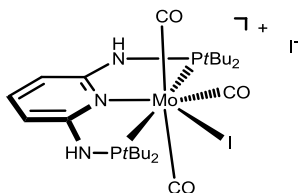
1964 (ν_{CO}), 1928 (ν_{CO}). **ESI-MS (m/z, CH₃CN) positive ion:** 804.0 [M]⁺, 776.0 [M - CO]⁺, 748.1 [M - 2CO]⁺.

[Mo(PNP-Cy)(CO)₃Br]Br (7c)



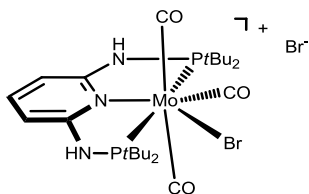
The product was obtained as a yellow solid in 85% yield. Anal. Calcd. for C₃₂H₄₉Br₂MoN₃O₃P₂ (841.48): C, 45.68; H, 5.87; N, 4.99. Found: C, 45.57; H, 5.93; N, 5.20. **¹H NMR (δ, CD₂Cl₂, 20 °C):** 9.03 (s, 2H, NH), 7.20 (br, 3H, py⁴, py^{3,5}), 2.03-1.60 (m, 22H, Cy), 1.48-1.24 (m, 22H, Cy). **¹³C{¹H} NMR (δ, CD₂Cl₂, 20 °C):** 234.8 (t, J = 17.0 Hz, CO), 218.2 (t, J = 13.9 Hz, CO), 160.2 (py^{2,6}), 142.5 (vt, J = 16.6 Hz, py⁴), 102.2 (py^{3,5}), 41.3 (vt, J = 11.7 Hz, Cy), 39.9 (vt, J = 10.7 Hz, Cy), 30.1-28.4 (m, Cy), 28.0-26.6 (m, Cy), 26.5-25.3 (m, Cy). **³¹P{¹H} NMR (δ, CD₂Cl₂, 20 °C):** 109.6. **IR (ATR, cm⁻¹):** 2037 (ν_{CO}), 1970 (ν_{CO}), 1936 (ν_{CO}).

[Mo(PNP-*t*Bu)(CO)₃I]I (6d)



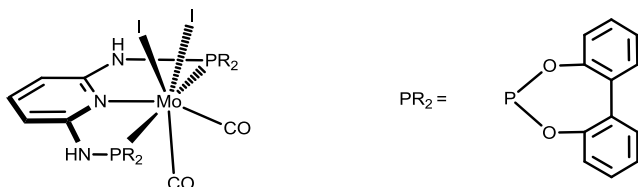
The product was obtained as a green solid in 96% yield. Anal. Calcd. for C₂₄H₄₁I₂MoN₃O₃P₂ (832.98): C, 34.67; H, 4.97; N, 5.77. Found: C, 34.28; H, 4.31; N, 5.46. **¹H NMR (δ, CD₂Cl₂, 20 °C):** 7.58 (t, J = 7.1 Hz, 1H, py⁴), 7.45 (d, J = 7.6 Hz, 1H, py^{3,5}), 7.23 (d, J = 7.6 Hz, 1H, py^{3,5}), 6.71 (d, J = 6.1 Hz, 1H, NH), 6.06 (d, J = 6.6 Hz, 1H, NH), 1.64 (d, J = 14.1 Hz, 18H, CH₃), 1.58 (d, J = 15.0 Hz, 18H, CH₃). **¹³C{¹H} NMR (δ, CD₂Cl₂, 20 °C):** 219.0 (dd, J = 42.2 Hz, J = 7.5 Hz, CO), 208.2 (dd, J = 10.0 Hz, J = 8.0 Hz, CO), 160.5 (dd, J = 6.3 Hz, J = 2.3 Hz, py^{2,6}), 158.9 (dd, J = 6.0 Hz, J = 1.8 Hz, py^{2,6}), 142.8 (py⁴), 104.6 (d, J = 5.7 Hz, py^{3,5}), 104.3 (d, J = 2.8 Hz, py^{3,5}), 45.3 (d, J = 7.4 Hz, C(CH₃)₃), 44.4 (d, J = 11.7 Hz, C(CH₃)₃), 30.1 (d, J = 2.3 Hz, CH₃), 29.5 (d, J = 3.0 Hz, CH₃). **³¹P{¹H} NMR (δ, CD₂Cl₂, 20 °C):** 137.6 (d, J = 50.3 Hz), 108.2 (d, J = 50.3 Hz). **IR (ATR, cm⁻¹):** 2070 (ν_{CO}), 1935 (ν_{CO}), 1867 (ν_{CO}). **ESI-MS (m/z, CH₃CN) positive ion:** 701.0 [M]⁺, 673.0 [M - CO]⁺, 645.0 [M - 2CO]⁺.

[Mo(PNP-*t*Bu)(CO)₃Br]Br (7d)



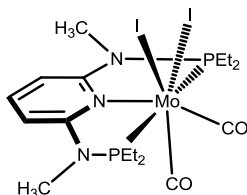
The product was obtained as a green solid in 96% yield. Anal. Calcd. for C₂₄H₄₁Br₂MoN₃O₃P₂ (737.32): C, 39.10; H, 5.60; N, 5.70. Found: C, 39.28; H, 5.27; N, 5.51. ¹H NMR (δ, CD₂Cl₂, 20 °C): 8.30 (br, 1H, py⁴), 7.50 (br, 1H, py^{3,5}), 7.16 (d, J = 4.2 Hz, 1H, py^{3,5}), 6.26 (d, J = 5.4 Hz, 1H, NH), 5.41 (d, J = 8.2 Hz, NH), 1.54 (d, J = 14.6 Hz, 18H, CH₃), 1.43 (br, 18H, CH₃). ¹³C{¹H} NMR (δ, CD₂Cl₂, 20 °C): 220.4 (dd, J = 7.3 Hz, J = 2.1 Hz, CO), 209.6 (dd, J = 13.3 Hz, J = 6.6 Hz, CO), 161.1 (dd, J = 7.1 Hz, J = 3.8 Hz, py^{2,6}), 160.6 (dd, J = 6.7 Hz, J = 2.4 Hz, py^{2,6}), 140.1 (py⁴), 103.8 (d, J = 5.2 Hz, py^{3,5}), 103.5 (d, J = 3.8 Hz, py^{3,5}), 44.6 (d, J = 7.7 Hz, C(CH₃)₃), 44.2 (d, J = 7.4 Hz, C(CH₃)₃), 30.8 (d, J = 7.1 Hz, CH₃), 28.8 (d, J = 10.8 Hz, CH₃). ³¹P{¹H} NMR (δ, CD₂Cl₂, 20 °C): 139.8 (d, J = 43.6 Hz), 113.2 (d, J = 43.6 Hz). IR (ATR, cm⁻¹): 2029 (ν_{CO}), 1919 (ν_{CO}), 1805 (ν_{CO}).

[Mo(PNP-BIPOL)(CO)₂I₂] (6g)



The product was obtained as a yellow solid in 95% yield. Anal. Calcd. for C₃₁H₂₁I₂MoN₃O₆P₂ (944.24). C, 39.43; H, 2.35; N, 4.45. IR (ATR, cm⁻¹): 2008 (ν_{CO}), 1900 (ν_{CO}).

[Mo(PNP^{Me}-Et)(CO)₂I₂] (6i)

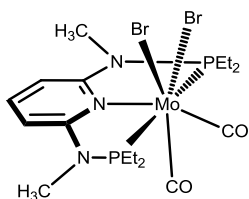


The product was obtained as an orange-red solid in 86% yield. Anal. Calcd. for C₁₇H₂₉I₂MoN₃O₂P₂ (719.15): C, 28.39; H, 4.06; N, 5.84. Found: C, 28.13; H, 3.89; N, 5.67. ¹H NMR (δ, CD₂Cl₂, 20 °C): 7.53 (tt, J = 8.2 Hz, J = 1.1 Hz, 1H, py⁴), 5.99 (d, J = 8.2 Hz, 2H, py^{3,5}), 3.21-3.09 (m, 2H, CH₂), 3.01 (d, J = 4.1 Hz, 6H, NCH₃), 2.59-2.47 (m,

Chapter 5 – Halocarbonyl Molybdenum and Tungsten PNP pincer complexes

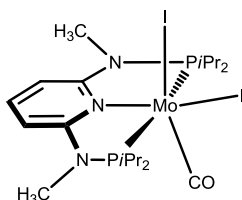
2H, CH₂), 2.26-2.17 (m, 2H, CH₂), 1.98-1.86 (m, 2H, CH₂), 1.09-1.00 (m, 12H, CH₃). ¹³C{¹H} NMR (δ, CD₂Cl₂, 20 °C): 257.9 (t, J = 41.6 Hz, CO), 224.6 (t, J = 8.8 Hz, CO), 161.7 (t, J = 7.5 Hz, py^{2,6}), 143.3 (py⁴), 99.0 (t, J = 1.9 Hz, py^{3,5}), 35.2 (t, J = 3.2 Hz, NCH₃), 24.9-24.4 (m, CH₂), 20.5-19.9 (m, CH₂), 8.9 (t, J = 4.1 Hz, CH₃), 7.1 (t, J = 3.9 Hz, CH₃). ³¹P{¹H} NMR (δ, CD₂Cl₂, 20 °C): 135.9. IR (ATR, 25 °C): 1964 (ν_{CO}), 1840 (ν_{CO}). ESI-MS (m/z, CH₃CN) positive ion: 710.88 [M + Na - CO]⁺, 560.99 [M - (CO + Na)]⁺.

Mo(PNP^{Me}-Et)(CO)₂Br₂ (7i)



The product was obtained as an yellow solid in 84% yield. Anal. Calcd. for C₁₇H₂₉Br₂MoN₃O₃P₂ (624.92): C, 32.66; H, 4.68; N, 6.72. Found: C, 31.28; H, 4.23; N, 6.47. ¹H NMR (δ, CD₂Cl₂, 20 °C): 7.53 (t, J = 8.2 Hz, 1H, py⁴), 6.02 (d, J = 8.2 Hz, 2H, py^{3,5}), 3.02 (d, J = 4.1 Hz, 6H, NCH₃), 2.96-2.86 (m, 2H, CH₂), 2.39-2.27 (m, 2H, CH₂), 2.20-2.09 (m, 2H, CH₂), 1.91-1.80 (m, 2H, CH₂), 1.13-1.05 (m, 6H, CH₃), 1.04-0.97 (m, 6H, CH₃). ¹³C{¹H} NMR (δ, CD₂Cl₂, 20 °C): 263.2 (t, J = 42.9 Hz, CO), 225.8 (t, J = 9.0 Hz, CO), 161.1 (t, J = 7.4 Hz, py^{2,6}), 143.2 (py⁴), 98.9 (t, J = 1.9 Hz, py^{3,5}), 34.9 (t, J = 3.0 Hz, NCH₃), 25.0-24.5 (m, CH₂), 17.9-17.3 (m, CH₂), 8.3 (t, J = 3.9 Hz, CH₃), 7.4 (t, J = 3.9 Hz, CH₃). ³¹P{¹H} NMR (δ, CD₂Cl₂, 20 °C): 140.8. IR (ATR, 25 °C): 1966 (ν_{CO}), 1834 (ν_{CO}).

[Mo(PNP^{Me}-iPr)(CO)I₂] (6j)

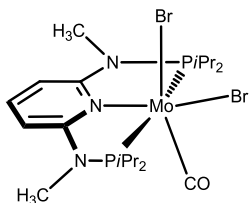


The product was obtained as an green solid in 90% yield. Anal. Calcd. for C₂₀H₃₇I₂MoN₃OP₂ (747.23): C, 32.15; H, 4.99; N, 5.62. Found: C, 32.19; H, 5.09; N, 5.58. ¹H NMR (δ, CD₂Cl₂, 20 °C): 7.66 (t, J = 8.3 Hz, 1H, py), 6.22 (d, J = 8.3 Hz, 2H, py), 3.13 (s, 6H, NCH₃), 2.88-2.79 (m, 2H, CH), 2.52-2.29 (m, 2H, CH), 1.52-1.22 (m, 18H, CH₃), 0.72 (d, J = 6.9 Hz, 3H, CH₃), 0.66 (d, J = 6.9 Hz, 3H, CH₃). ¹³C{¹H} NMR (δ, CD₂Cl₂, 20 °C): 247.3 (t, J = 26.5 Hz, CO), 162.0 (t, J = 7.6 Hz, py^{2,6}), 142.3 (py⁴),

Chapter 5 – Halocarbonyl Molybdenum and Tungsten PNP pincer complexes

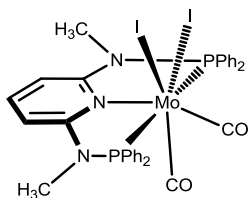
99.1 (py^{3,5}), 34.4 (t, J = 2.7 Hz, NCH₃), 30.2 (d, J = 28.8 Hz, CH), 20.0 (d, J = 18.3 Hz, CH), 19.2 (CH₃), 17.8 (CH₃), 17.7 (CH₃), 16.9 (CH₃). ³¹P{¹H} NMR (δ, CD₂Cl₂, 20 °C): 190.4. IR (ATR, cm⁻¹): 1824 (ν_{CO}). ESI-MS (m/z, CH₃CN, NaI) positive ion: 764.9 [M + Na]⁺, 616.1 [M - I]⁺. In the presence of air: 604.1 [M - (I + CO) + O]⁺, 620.0 [M - (I + CO) + 2O]⁺, 493.1 [M - (2I + CO) + 2O]⁺.

[Mo(PNP^{Me}-iPr)(CO)Br₂] (7j)



The product was obtained as a blue solid in 95% yield. Anal. Calcd. for C₂₀H₃₇Br₂MoN₃OP₂ (653.23): C, 36.77; H, 5.71; N, 6.43. Found: C, 36.65; H, 5.59; N, 6.42. C, 36.77; H, 5.71; N, 6.43. ¹H NMR (δ, CD₂Cl₂, 20 °C): 7.58 (t, J = 8.3 Hz, 1H, py), 6.21 (d, J = 8.0 Hz, 2H, py), 3.14 (s, 6H, NCH₃), 2.89-2.70 (m, 2H, CH), 2.69-2.48 (m, 2H, CH), 1.52 (d, J = 6.9 Hz, 3H, CH₃), 1.45 (d, J = 6.8 Hz, 3H, CH₃), 1.37-1.23 (m, 12H, CH₃), 0.71 (d, J = 7.0 Hz, 3H, CH₃), 0.64 (d, J = 7.0 Hz, 3H, CH₃). ¹³C{¹H} NMR (δ, CD₂Cl₂, 20 °C): 247.9 (t, J = 32.0 Hz, CO), 161.5 (t, J = 8.1 Hz, py^{2,6}), 141.0 (py⁴), 98.2 (py^{3,5}), 34.6 NCH₃), 30.2 (d, J = 29.1 Hz, CH), 20.3 (d, J = 24.5 Hz, (CH₃), 18.2 (CH₃), 17.9 (CH₃), 17.5 (CH₃), 16.3 (CH₃). ³¹P{¹H} NMR (δ, CD₂Cl₂, 20 °C): 195.2. IR (ATR, cm⁻¹): 1816 (ν_{CO}). ESI-MS (m/z, CH₃CN, NaBr) positive ion: 670.0 [M + Na]⁺, 568.1 [M - Br]⁺. In the presence of air: 556.1 [M - (Br + CO) + O]⁺, 572.1 [M - (Br + CO) + 2O]⁺, 493.1 [M - (2Br + CO) + 2O]⁺.

[Mo(PNP^{Me}-Ph)(CO)₂I₂] (6k)

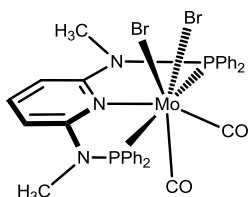


The product was obtained as a red solid in 81% yield. Anal. Calcd. for C₃₃H₂₉I₂N₃O₂P₂Mo (911.31): C, 43.49; H, 3.21; N, 4.61%. Found: C, 43.30; H, 3.18; N, 4.73%. ¹H NMR (δ, CD₂Cl₂, 20 °C): 7.86 (t, J = 8.2 Hz, 1H, py⁴), 7.63 (t, J = 8.2 Hz, 4H, Ph^{2,6}), 7.52 (t, J = 7.0 Hz, 2H, Ph⁴), 7.41 (t, J = 6.9 Hz, 4H, Ph^{2,6}), 7.07 (t, J = 7.2 Hz, 2H, Ph⁴), 6.85 (t, J = 7.1 Hz, 4H, Ph^{3,5}), 6.60 (t, J = 7.3 Hz, 4H, Ph^{3,5}), 6.36 (d, J = 8.2 Hz, 2H, py^{3,5}), 3.14 (s, 6H, NCH₃). ¹³C{¹H} NMR (δ, CD₂Cl₂, 20 °C): 162.1-163.1 (m,

Chapter 5 – Halocarbonyl Molybdenum and Tungsten PNP pincer complexes

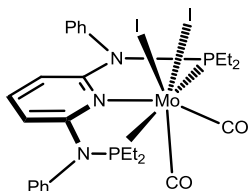
py^{2,6}), 144.8 (py⁴), 138.7 (t, J = 5.7 Hz, py^{2,6}), 132.6 (Ph⁴), 130.6 (t, J = 5.7 Hz, Ph^{3,5}), 130.5 (Ph⁴), 129.0 (t, J = 4.9 Hz, Ph^{3,5}), 128.3 (t, J = 5.5 Hz, Ph^{2,6}), 100.3 (py^{3,5}), 36.1 (NCH₃). The quaternary Ph and CO carbon atoms could not be detected. **¹³C solid-state NMR (δ, 12 kHz, 25 °C):** 228.5 (CO), 218.2 (CO). **³¹P{¹H} NMR (δ, CD₂Cl₂, 20 °C):** 129.3. **IR (ATR, cm⁻¹):** 1946 (ν_{CO}), 1870 (ν_{CO}). **ESI-MS (m/z, CH₃OH, NaI) positive ion:** 901.88 [M + Na - CO]⁺, 751.99 [M - (CO + NaI)]⁺.

Mo(PNP^{Me}-Ph)(CO)₂Br₂ (7k)



The product was obtained as a yellow solid in 84% yield. Anal. Calcd. for C₃₃H₂₉Br₂N₃O₂P₂Mo (817.31): C, 48.50; H, 3.58; N, 5.14%. Found: C, 48.42; H, 3.63; N, 5.06%. **¹H NMR (δ, CD₂Cl₂, 20 °C):** 7.84 (t, J = 7.8 Hz, 1H, py⁴), 7.63 (t, J = 7.4 Hz, 4H, Ph^{2,6}), 7.53 (t, J = 7.2 Hz, 2H, Ph⁴), 7.44 (t, J = 7.1 Hz, 4H, Ph^{2,6}), 7.16 (t, J = 7.2 Hz, 2H, Ph⁴), 6.93 (t, J = 7.2 Hz, 4H, Ph^{3,5}), 6.64 (t, J = 8.0 Hz, 4H, Ph^{3,5}), 6.39 (d, J = 8.0 Hz, 2H, py^{3,5}), 3.11 (s, 6H, NCH₃). **¹³C{¹H} NMR (δ, CD₂Cl₂, 20 °C):** 161.4-161.6 (m, py^{2,6}), 144.6 (py⁴), 137.6 (t, J = 6.0 Hz, py^{2,6}), 135.8 (d, J = 45.9 Hz, Ph¹), 132.2 (Ph⁴), 130.3 (t, J = 4.9 Hz, Ph^{3,5}), 130.2 (Ph⁴), 129.3 (d, J = 56.2 Hz, Ph¹), 128.5 (t, J = 4.8 Hz, Ph^{3,5}), 128.2 (t, J = 5.5 Hz, Ph^{2,6}), 100.1 (py^{3,5}), 35.9 (s, NCH₃). The quaternary CO carbon atoms could not be detected. **¹³C solid-state NMR (δ, 12 kHz, 25 °C):** 244.8 (CO), 225.7 (CO). **³¹P{¹H} NMR (δ, CD₂Cl₂, 20 °C):** 133.2. **IR (ATR, cm⁻¹):** 1979 (ν_{CO}), 1858 (ν_{CO}). **ESI-MS (m/z, CH₃OH, NaBr) positive ion:** 805.91 [M + Na - CO]⁺, 704.00 [M - (CO + NaBr)]⁺.

[Mo(PNP^{Ph}-Et)(CO)₂I₂] (6l)

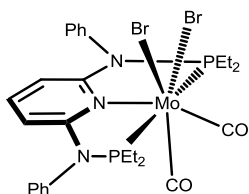


The product was obtained as a yellow solid in 96% yield. Anal. Calcd. for C₂₇H₃₃I₂MoN₃O₂P₂ (843.430): C, 38.46; H, 3.94; N, 4.98%. Found: C, 38.37; H, 4.10; N, 4.88%. **¹H NMR (δ, CD₂Cl₂, 20 °C):** 8.2 (d, J = 6.9 Hz, 2H, Ph), 7.53-7.46 (m, 2H, Ph), 7.45-7.34 (m, 4H, Ph), 7.08 (vt, J = 8.1 Hz, 3H, Ph, py⁴), 5.39 (d, J = 8.1 Hz, 2H, py^{3,5}), 3.22-3.01 (m, 2H, CH₂), 2.49-2.25 (m, 4H, CH₂), 1.98-1.85 (m, 2H, CH₂), 1.17 (dt, J =

Chapter 5 – Halocarbonyl Molybdenum and Tungsten PNP pincer complexes

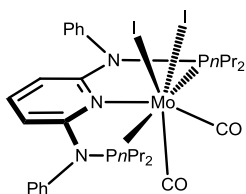
14.2 Hz, $J = 7.4$, 6H, CH₃), 1.10-0.94 (m, 6H, CH₃). ¹³C{¹H} NMR (δ , CD₂Cl₂, 20 °C): 258.3 (t, $J = 4.2$ Hz, CO), 224.3 (t, $J = 4.8$ Hz, CO), 162.6 (vt, $J = 8.2$ Hz, py^{2,6}), 142.4 (Ph), 138.1 (py⁴), 131.1 (Ph), 130.7 (Ph), 129.9 (Ph), 129.6 (Ph), 129.1 (Ph), 101.0 (py^{3,5}), 26.0 (vt, $J = 9.2$ Hz, CH₂) 24.0-23.4 (m, CH₂), 9.1 (CH₃), 7.1 (CH₃). ³¹P{¹H} NMR (δ , CD₂Cl₂, 20 °C): 133.3. IR (ATR, cm⁻¹): 1974 (ν_{CO}), 1850 (ν_{CO}). ESI-MS (m/z , CH₃CN, NaI) positive ion: 861.8 [M + Na]⁺, 833.8 [M + Na - CO]⁺, 711.8 [M - I]⁺, 683.9 [M - (I + CO)]⁺.

[Mo(PNP^{Ph}-Et)(CO)₂Br₂] (7l)



The product was obtained as a yellow solid in 94% yield. Anal. Calcd. for C₂₇H₃₃Br₂MoN₃O₂P₂ (749.30): C, 43.28; H, 4.44; N, 5.61%. Found: C, 43.27; H, 4.53; N, 5.80%. ¹H NMR (δ , CD₂Cl₂, 20 °C): 8.0 (d, $J = 8.0$ Hz, 2H, Ph), 7.51-7.47 (m, 2H, Ph), 7.44-7.36 (m, 4H, Ph), 7.09-7.04 (m, 3H, Ph, py⁴), 5.39 (d, $J = 8.2$ Hz, 2H, py^{3,5}), 2.94-2.82 (m, 2H, CH₂), 2.31-2.23 (m, 4H, CH₂), 1.67-1.54 (m, 2H, CH₂), 1.20-1.12 (m, 6H, CH₃), 1.02-0.93 (m, 6H, CH₃). ¹³C{¹H} NMR (δ , CD₂Cl₂, 20 °C): 263.0 (t, $J = 41.3$ Hz, CO), 225.0 (t, $J = 8.9$ Hz, CO), 161.8 (vt, $J = 8.2$ Hz, py^{2,6}), 142.1 (Ph), 138.0 (vt, $J = 3.3$ Hz, py⁴), 131.1 (Ph), 130.7 (Ph), 129.7 (Ph), 129.1 (Ph), 128.9 (Ph), 100.8 (py^{3,5}), 25.6 (vt, $J = 10.4$ Hz, CH₂) 21.3 (vt, $J = 18.5$ Hz, CH₂), 8.4 (vt, $J = 2.4$ Hz, CH₃), 7.2 (vt, $J = 3.5$ Hz, CH₃). ³¹P{¹H} NMR (δ , CD₂Cl₂, 20 °C): 138.1. IR (ATR, cm⁻¹): 1975 (ν_{CO}), 1848 (ν_{CO}).

[Mo(PNP^{Ph}-*n*Pr)(CO)₂I₂] (6m)

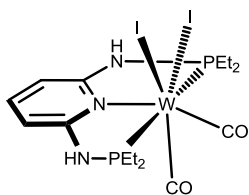


The product was obtained as a yellow-brown solid in 97.2% yield. Anal. Calcd. for C₃₁H₄₁MoN₃O₂P₂ (899.39). C, 41.40; H, 4.59; N, 4.67. Found: C, 41.07; H, 4.13; N, 4.31%. ¹H NMR (δ , CD₂Cl₂, 20 °C): 8.17 (d, $J = 7.2$ Hz, 2H Ph), 7.54-7.47 (m, 2H, Ph), 7.46-7.37 (m, 4H, Ph), 7.10-7.01 (m, 3H, Ph, py⁴), 5.36 (d, $J = 8.1$, 2H, py^{3,5}), 3.15-3.03 (m, 2H, CH₂), 2.36-2.21 (m, 4H, CH₂), 1.82-1.67 (m, 2H, CH₂), 1.63-1.48 (m, 8H, CH₂),

Chapter 5 – Halocarbonyl Molybdenum and Tungsten PNP pincer complexes

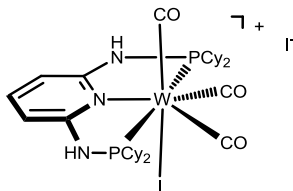
0.97 (vt, $J = 7.2$ Hz, 6H, CH₃), 0.93-0.85 (m, 6H, CH₃). ¹³C{¹H} NMR (δ , CD₂Cl₂, 20 °C): 258.3 (t, $J = 5.6$ Hz, CO), 224.2 (t, $J = 9.2$ Hz, CO), 162.3 (vt, $J = 8.2$ Hz, py^{2,6}), 142.2 (Ph), 138.0 (py⁴), 131.0 (Ph), 130.8 (Ph), 130.0 (Ph), 129.1 (Ph), 128.9 (Ph), 100.8 (py^{3,5}), 36.0 (vt, $J = 9.1$ Hz, CH₂), 32.7 (vt, $J = 18.8$ Hz, CH₂), 18.1 (CH₂), 17.0 (CH₂), 15.6 (vt, $J = 6.3$ Hz, CH₃), 15.5 (vt, $J = 5.3$ Hz, CH₃). ³¹P{¹H} NMR (δ , CD₂Cl₂, 20 °C): 127.9. IR (ATR, cm⁻¹): 1954 (ν_{CO}), 1831 (ν_{CO}). ESI-MS (m/z , CH₃CN, NaI) positive ion: 918.9 [M + Na]⁺, 890.9 [M + Na - CO]⁺, 768.9 [M - I]⁺, 741.0 [M - (I + CO)]⁺.

[W(PNP-Et)(CO)₂I₂] (8a)



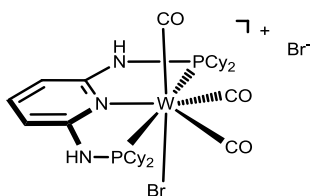
The product was obtained as yellow solid in 88.9% yield. Anal. Calcd. for C₁₅H₂₅I₂WN₃O₂P₂ (778.97). C, 23.13; H, 3.23; N, 5.39. IR (ATR, cm⁻¹): 1963 (ν_{CO}), 1849 (ν_{CO}).

[W(PNP-Cy)(CO)₃I] (8c)



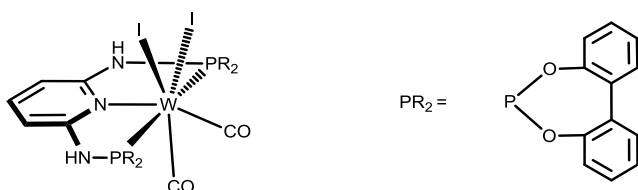
The product was obtained as an orange-red solid in 89% yield. Anal. Calcd. for C₃₂H₄₉I₂WN₃O₂P₂ (1023.36): C, 37.56; H, 4.83; N, 4.11%. Found: C, 37.64; H, 4.88; N, 4.00. ¹H NMR (δ , CD₂Cl₂, 20 °C): 8.25 (s, 2H, NH), 7.31 (t, $J = 7.8$ Hz, 1H, py⁴), 7.20 (d, $J = 7.6$ Hz, 2H, py^{3,5}), 2.00-1.54 (m, 22H, Cy), 1.49-1.20 (m, 22H, Cy). ¹³C{¹H} NMR (δ , CD₂Cl₂, 20 °C): 224.9 (t, $J = 11.1$ Hz, CO), 208.7 (t, $J = 10.7$ Hz, CO), 160.9 (vt, $J = 4.8$ Hz, py^{2,6}), 142.8 (py⁴), 102.2 (py^{3,5}), 41.7 (vt, $J = 11.1$ Hz, Cy), 41.4 (vt, $J = 13.0$ Hz, Cy), 30.2-27.9 (m, Cy), 27.0-26.3 (m, Cy), 25.8-25.5 (m, Cy). ³¹P{¹H} NMR (δ , CD₂Cl₂, 20 °C): 88.4 (¹J_{w-p} = 173.3 Hz). IR (ATR, cm⁻¹): 2022 (ν_{CO}), 1951 (ν_{CO}), 1915 (ν_{CO}). ESI-MS (m/z , CH₃CN) positive ion: 894.0 [M]⁺, 866.0 [M - CO]⁺, 838.1 [M - 2CO]⁺.

[W(PNP-Cy)(CO)₃Br]Br (9c)



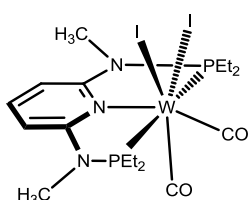
The product was obtained as a yellow-orange solid in 85% yield. Anal. Calcd. for C₃₂H₄₉Br₂WN₃O₂P₂ (929.36): C, 41.36; H, 5.31; N, 4.52%. Found: C, 41.47; H, 5.23; N, 4.60. ¹H NMR (δ, CD₂Cl₂, 20 °C): 9.33 (s, 2H, NH), 7.18 (br, 3H, py⁴, py^{3,5}), 1.97-1.54 (m, 22H, Cy), 1.47-1.18 (m, 22H, Cy). ¹³C{¹H} NMR (δ, CD₂Cl₂, 20 °C): 224.3 (t, J = 10.3 Hz, CO), 212.1 (t, J = 9.8 Hz, CO), 161.1 (vt, J = 4.9 Hz, py^{2,6}), 142.3 (py⁴), 101.7 (py^{3,5}), 41.1 (vt, J = 11.0 Hz, Cy), 39.0 (vt, J = 9.8 Hz, Cy), 29.5-28.7 (m, Cy), 27.6-26.3 (m, Cy), 26.0-25.5 (m, Cy). ³¹P{¹H} NMR (δ, CD₂Cl₂, 20 °C): 90.7 (¹J_{W-P} = 185.4 Hz). IR (ATR, cm⁻¹): 2024 (ν_{CO}), 1948 (ν_{CO}), 1911 (ν_{CO}).

W(PNP-BIPOL)(CO)₂I₂] (8g)



The product was obtained as a yellow solid in 95% yield. Anal. Calcd. for C₃₁H₂₁I₂WN₃O₆P₂ (1031.12). C, 36.07; H, 2.15; N, 4.07. Found: C, 35.87; H, 1.99; N, 3.86. IR (ATR, cm⁻¹): 2003 (ν_{CO}), 1898 (ν_{CO}).

[W(PNP^{Me}-Et)(CO)₂I₂] (8i)

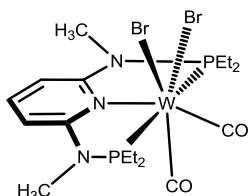


The product was obtained as yellow crystals in 87% yield. Anal. Calcd. for C₁₈H₂₉I₂WN₃O₃P₂ (807.03). C, 25.30; H, 3.62; N, 5.21. Found: C, 25.16; H, 3.33; N, 5.02. ¹H NMR (δ, CD₂Cl₂, 20 °C): 7.80 (tt, J = 8.4 Hz, J = 1.3 Hz, 1H, py⁴), 6.50 (d, J = 8.4 Hz, 2H, py^{3,5}), 3.23 (d, J = 4.8 Hz, 6H, NCH₃), 2.64-2.52 (m, 4H, CH₂), 2.29-2.19 (m, 4H, CH₂), 1.30-1.20 (m, 6H, CH₃), 1.14-1.06 (m, 6H, CH₃). ¹³C{¹H} NMR (δ, CD₂Cl₂, 20 °C): 249.5 (t, J = 30.0 Hz, CO), 207.9 (t, J = 12.7 Hz, CO), 161.6 (vt, J = 7.5 Hz, py^{2,6}), 143.5 (py⁴), 101.7 (d, J = 6.0 Hz, py^{3,5}), 34.6 (t, J = 2.9 Hz, NCCH₃), 23.3 (vt,

Chapter 5 – Halocarbonyl Molybdenum and Tungsten PNP pincer complexes

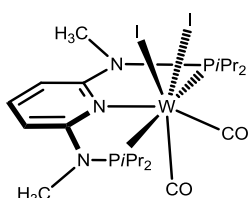
$J = 33.9$ Hz, CH_2), 20.5 (vt, $J = 32.4$ Hz, CH_2), 8.1 (t, $J = 3.8$ Hz, CH_3), 6.5 (t, $J = 3.4$ Hz, CH_3). $^{31}\text{P}\{^1\text{H}\}$ NMR (δ , CD_2Cl_2 , 20 °C): 112.8 ($^1J_{\text{W-P}} = 253.0$ Hz). IR (ATR, cm^{-1}): 1953 (ν_{CO}), 1828 (ν_{CO}).

$[\text{W}(\text{PNP}^{\text{Me}}\text{-Et})(\text{CO})_2\text{Br}_2]$ (9i)



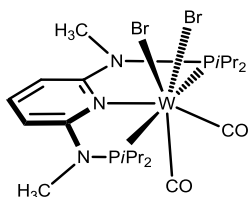
The product was obtained as yellow crystals in 90% yield. Anal. Calcd. for $\text{C}_{18}\text{H}_{29}\text{Br}_2\text{WN}_3\text{O}_3\text{P}_2$ (713.03). C, 28.64; H, 4.10; N, 5.89. Found: C, 38.26; H, 3.99; N, 5.72. ^1H NMR (δ , CD_2Cl_2 , 20 °C): 7.81 (t, $J = 8.4$ Hz, 1H, py^4), 6.52 (d, $J = 8.4$ Hz, 2H, $\text{py}^{3,5}$), 3.22 (d, $J = 3.9$ Hz, 6H, NCH_3), 2.55 - 2.41 (m, 4H, CH_2), 1.97 - 1.81 (m, 4H, CH_2), 1.29 - 1.21 (m, 6H, CH_3), 1.14 - 1.03 (m, 6H, CH_3). $^{13}\text{C}\{^1\text{H}\}$ NMR (δ , CD_2Cl_2 , 20 °C): 257.0 (t, $J = 31.1$ Hz, CO), 211.3 (t, $J = 12.1$ Hz, CO), 162.0 (vt, $J = 7.5$ Hz, $\text{py}^{2,6}$), 143.0 (py^4), 98.9 (br, $\text{py}^{3,5}$), 35.1 (t, $J = 2.6$ Hz, NCCH_3), 25.0 (vt, $J = 27.6$ Hz, CH_2), 20.9 (vt, $J = 35.6$ Hz, CH_2), 8.5 (t, $J = 3.7$ Hz, CH_3), 7.9 (t, $J = 3.5$ Hz, CH_3). $^{31}\text{P}\{^1\text{H}\}$ NMR (δ , CD_2Cl_2 , 20 °C): 118.8 ($^1J_{\text{W-P}} = 249.0$ Hz). IR (ATR, cm^{-1}): 1953 (ν_{CO}), 1819 (ν_{CO}).

$[\text{W}(\text{PNP}^{\text{Me}}\text{-}i\text{Pr})(\text{CO})_2\text{I}_2]$ (8j)



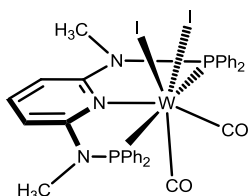
The product was obtained as a yellow solid in 83% yield. Anal. Calcd. for $\text{C}_{21}\text{H}_{37}\text{I}_2\text{WN}_3\text{O}_2\text{P}_2$ (863.14): C, 29.22; H, 4.32; N, 4.87%. Found: C, 29.17; H, 4.40; N, 4.90. ^1H NMR (δ , CD_2Cl_2 , 20 °C): 7.64 (t, $J = 8.3$ Hz, 1H, py^4), 6.06 (d, $J = 8.3$ Hz, 2H, $\text{py}^{3,5}$), 3.98 - 3.71 (m, 2H, CH), 3.21 (d, $J = 3.9$ Hz, 6H, NCH_3), 2.99 - 2.70 (m, 2H, CH), 1.65 (dd, $J = 11.4$ Hz, $J = 7.2$ Hz, 6H, CH_3), 1.58 - 1.29 (m, 12H, CH_3), 1.21 (dd, $J = 12.8$ Hz, $J = 7.4$ Hz, 6H, CH_3). $^{13}\text{C}\{^1\text{H}\}$ NMR (δ , CD_2Cl_2 , 20 °C): 225.3 (t, $J = 13.5$ Hz, CO), 204.2 (br, CO), 162.4 (vt, $J = 7.2$ Hz, $\text{py}^{2,6}$), 143.1 (py^4), 99.0 ($\text{py}^{3,5}$), 38.1 (vt, $J = 9.9$ Hz, CH), 36.6 (t, $J = 3.0$ Hz, NCH_3), 31.0 (vt, $J = 14.4$ Hz, CH), 22.5 (vt, $J = 5.4$ Hz, CH_3), 20.0 (CH_3), 19.8 (vt, $J = 3.1$ Hz, CH_3), 17.6 (CH_3). $^{31}\text{P}\{^1\text{H}\}$ NMR (δ , CD_2Cl_2 , 20 °C): 123.9 ($^1J_{\text{W-P}} = 253.2$ Hz). IR (ATR, cm^{-1}): 1946 (ν_{CO}), 1823 (ν_{CO}). ESI-MS (m/z , CH_3CN , NaI) negative ion: 987.9 [$\text{M} + \text{I}$] $^-$.

[W(PNP^{Me}-iPr)(CO)₂Br₂] (9j)



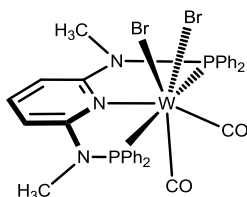
The product was obtained as a yellow solid in 81% yield. Anal. Calcd. for C₂₁H₃₇Br₂WN₃O₂P₂ (769.14): C, 32.79; H, 4.85; N, 5.46%. Found: C, 32.80; H, 4.91; N, 5.53. ¹H NMR (δ, CD₂Cl₂, 20 °C): 7.57 (t, J = 8.2 Hz, 1H, py⁴), 6.04 (d, J = 8.2 Hz, 2H, py^{3,5}), 3.48-3.33 (m, 2H, CH), 3.13 (d, J = 3.9 Hz, 6H, NCH₃), 2.80-2.56 (m, 2H, CH), 1.53 (dd, J = 12.2 Hz, J = 7.2 Hz, 6H, CH₃), 1.39 (dd, J = 20.3 Hz, J = 7.5 Hz, 6H, CH₃), 1.24-1.08 (m, 12H, CH₃). ¹³C{¹H} NMR (δ, CD₂Cl₂, 20 °C): 228.3 (t, J = 11.9 Hz, CO), 210.1 (t, J = 11.0 Hz, CO), 161.8 (vt, J = 6.8 Hz, py^{2,6}), 143.0 (py⁴), 98.9 (py^{3,5}), 37.3 (vt, J = 9.3 Hz, CH), 36.4 (t, J = 2.9 Hz, NCH₃), 28.5 (vt, J = 14.6 Hz, CH), 22.8 (vt, J = 4.5 Hz, CH₃), 19.7 (vt, J = 2.2 Hz, CH₃), 19.4 (CH₃), 17.7 (CH₃). ³¹P{¹H} NMR (δ, CD₂Cl₂, 20 °C): 127.7 (¹J_{w-p} = 246.5 Hz). IR (ATR, cm⁻¹): 1952 (ν_{CO}), 1815 (ν_{CO}).

[W(PNP^{Me}-Ph)(CO)₂I₂] (8k).



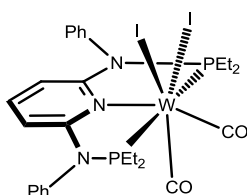
The product was obtained as a yellow solid in 89% yield. Anal. Calcd. for C₃₃H₂₉I₂WN₃O₂P₂ (999.21): C, 39.67; H, 2.93; N, 4.21. Found: C, 39.56; H, 3.03; N, 4.18. ¹H NMR (δ, CD₂Cl₂, 20 °C): 7.81 (t, J = 8.2 Hz, 1H, py⁴), 7.59-7.51 (m, 4H, Ph), 7.43 (t, J = 6.9 Hz, 2H, Ph²), 7.33 (t, J = 7.0 Hz, 4H, Ph), 6.98 (t, J = 7.3 Hz, 2H, Ph), 6.78 (t, J = 6.9 Hz, 4H, Ph), 6.51 (t, J = 8.7 Hz, 4H, Ph), 6.28 (d, J = 8.3 Hz, 2H, py^{3,5}), 3.12 (d, J = 5.0, 6H, NCH₃). ¹³C{¹H} NMR (δ, CD₂Cl₂, 20 °C): 246.9 (t, J = 29.2 Hz, CO), 222.2 (t, J = 7.0 Hz, CO), 163.0 (vt, J = 8.3 Hz, py^{2,6}), 144.0 (Ph), 138.4 (vt, J = 5.9 Hz, py⁴), 132.1 (Ph), 130.1 (vdd, J = 9.4 Hz, J = 4.4 Hz, Ph), 128.3 (vt, J = 5.0 Hz, Ph), 127.8 (vt, J = 5.6 Hz, Ph), 99.7 (py^{3,5}), 36.1 (vt, J = 3.0 Hz, NCH₃). ³¹P{¹H} NMR (δ, CD₂Cl₂, 20 °C): 108.0 (¹J_{w-p} = 266.8 Hz). IR (ATR, cm⁻¹): 1952 (ν_{CO}), 1850 (ν_{CO}). ESI-MS (m/z, CH₃CN, NaI) positive ion: 1019.8 [M + Na]⁺, 991.9 [M + Na - CO]⁺, 869.9 [M - I]⁺, 841.9 [M - (I + CO)]⁺.

[W(PNP^{Me}-Ph)(CO)₂Br₂] (9k)



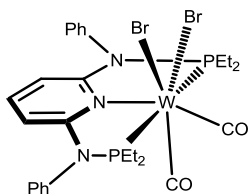
The product was obtained as a yellow solid in 88% yield. Anal. Calcd. For C₃₃H₂₉Br₂WN₃O₂P₂ (905.21): C, 43.79; H, 3.23; N, 4.64. Found: C, 43.88; H, 3.13; N, 4.70. ¹H NMR (δ, CD₂Cl₂, 20 °C): 7.85 (t, J = 8.2 Hz, 1H, py⁴), 7.70-7.55 (m, 4H, Ph), 7.52-7.37 (m, 6H, Ph), 7.15 (t, J = 7.4 Hz, 2H, Ph), 6.94 (t, J = 6.9 Hz, 4H, Ph), 6.61 (t, J = 8.6 Hz, 4H, Ph), 6.38 (d, J = 8.3 Hz, 2H, py^{3,5}), 3.12 (d, J = 5.0 Hz, 6H, NCH₃). ¹³C{¹H} NMR (δ, CD₂Cl₂, 20 °C): 249.0 (t, J = 12.7 Hz, CO), 223.8 (t, J = 9.1 Hz, CO), 162.2 (vt, J = 8.3 Hz, py^{2,6}), 143.8 (Ph), 137.1 (vt, J = 5.8 Hz, py⁴), 131.9 (Ph), 130.6-130.2 (Ph), 128.3 (vt, J = 4.9 Hz, Ph), 127.9 (vt, J = 5.6 Hz, Ph), 99.9 (vt, J = 2.4 Hz, py^{3,5}), 36.1 (vt, J = 2.7 Hz, NCH₃). ³¹P{¹H} NMR (δ, CD₂Cl₂, 20 °C): 112.7 (¹J_{w-p} = 259.6 Hz). IR (ATR, cm⁻¹): 1953 (ν_{CO}), 1859 (ν_{CO}).

[W(PNP^{Ph}-Et)(CO)₂I₂] (8l)



The product was obtained as a yellow solid in 90% yield. Anal. Calcd. for C₂₇H₃₃I₂WN₃O₂P₂ (931.18): C, 34.83; H, 3.57; N, 4.51%. Found: C, 34.90; H, 3.66; N, 4.41. ¹H NMR (δ, CD₂Cl₂, 20 °C): 8.3 (d, J = 7.0 Hz, 2H, Ph), 7.58-7.49 (m, 4H, Ph), 7.45-7.34 (m, 1H, py⁴), 7.28-7.17 (m, 4H, Ph), 5.50 (d, J = 8.1 Hz, 2H, py^{3,5}), 3.38-3.11 (m, 2H, CH₂), 2.66-2.40 (m, 4H, CH₂), 2.19-1.94 (m, 2H, CH₂), 1.37-1.24 (m, 6H, CH₃), 1.16-1.00 (m, 6H, CH₃). ¹³C{¹H} NMR (δ, CD₂Cl₂, 20 °C): 227.6 (t, J = 26.1 Hz, CO), 205.9 (t, J = 13.7 Hz, CO), 163.3 (vt, J = 7.3 Hz, py^{2,6}), 142.1 (Ph), 138.1 (py⁴), 130.8 (Ph), 130.6 (Ph), 129.8 (Ph), 129.5 (Ph), 129.0 (Ph), 100.7 (py^{3,5}), 26.1-25.4 (m, CH₂), 24.0-22.8 (m, CH₂), 9.1 (CH₃), 7.3 (CH₃). ³¹P{¹H} NMR (δ, CD₂Cl₂, 20 °C): 109.5 (¹J_{w-p} = 249.6 Hz). IR (ATR, cm⁻¹): 1958 (ν_{CO}), 1826 (ν_{CO}). ESI-MS (m/z, CH₃CN, NaI) negative ion: 1055.8 [M + I]⁻.

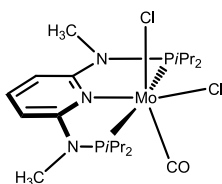
[W(PNP^{Ph}-Et)(CO)₂Br₂] (9i)



The product was obtained as a yellow solid in 88% yield. Anal. Calcd. for C₂₇H₃₃Br₂WN₃O₂P₂ (837.18): C, 38.74; H, 3.97; N, 5.02%. Found: C, 39.00; H, 4.03; N, 5.11. **¹H NMR (δ, CD₂Cl₂, 20 °C):** 8.6 (d, J = 7.0 Hz, 2H, Ph), 7.65-7.47 (m, 4H, Ph), 7.33 (t, J = 3.0 Hz, 1H, py⁴), 7.24-7.16 (m, 4H, Ph), 5.51 (d, J = 8.2 Hz, 2H, py^{3,5}), 3.12-2.86 (m, 2H, CH₂), 2.58-2.27 (m, 4H, CH₂), 2.91-1.62 (m, 2H, CH₂), 1.38-1.18 (m, 6H, CH₃), 1.16-0.99 (m, 6H, CH₃). **¹³C{¹H} NMR (δ, CD₂Cl₂, 20 °C):** 256.4 (t, J = 32.7 Hz, CO), 222.6 (t, J = 18.3 Hz, CO), 162.6 (vt, J = 7.7 Hz, py^{2,6}), 141.9 (Ph), 138.1 (py⁴), 130.9 (Ph), 130.7 (Ph), 129.8 (Ph), 129.1 (Ph), 128.9 (Ph), 100.7 (py^{3,5}), 26.3-24.7 (m, CH₂), 22.4-20.7 (m, CH₂), 8.5 (CH₃), 7.7 (CH₃). **³¹P{¹H} NMR (δ, CD₂Cl₂, 20 °C):** 115.4 (¹J_{W-P} = 243.7 Hz). **IR (ATR, cm⁻¹):** 1952 (ν_{CO}), 1823 (ν_{CO}).

Synthetic procedures of the chloride complexes: A solution of [Mo(CO)₄(μ-Cl)Cl]₂ (0.300 mmol) in CH₂Cl₂ (10 mL) was treated with 2 equiv. of PNP (0.600 mmol) and the solution was stirred for 18 h. After this period the solution was filtered, the solvent was removed under reduced pressure, and the remaining solid was washed twice with Et₂O and *n*-pentane.

[Mo(PNP^{Me}-iPr)(CO)Cl₂] (10j)

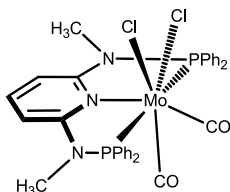


The product was obtained as an blue-green solid in 92% yield. Anal. Calcd. for C₂₀H₃₇Cl₂MoN₃OP₂ (564.33): C, 42.57; H, 6.61; N, 7.45. Found: C, 42.65; H, 6.51; N, 7.55. **¹H NMR (δ, CD₂Cl₂, 20 °C):** 7.58 (t, J = 8.8 Hz, 1H, py), 6.19 (d, J = 7.8 Hz, 2H, py), 3.14 (s, 6H, NCH₃), 2.89-2.74 (m, 2H, CH), 2.76-2.63 (m, 2H, CH), 1.51 (d, J = 6.3 Hz, 3H, CH₃), 1.44 (d, J = 6.3 Hz, 3H, CH₃), 1.30 (m, 12H, CH₃), 0.71 (d, J = 6.7 Hz, 3H, CH₃), 0.65 (d, J = 6.7 Hz, 3H, CH₃). **¹³C{¹H} NMR (δ, CD₂Cl₂, 20 °C):** 248.5 (t, J = 35.2 Hz, CO), 161.3 (t, J = 7.1 Hz, py^{2,6}), 140.8 (py⁴), 97.9 (py^{3,5}), 34.4 (N(CH₃)₂), 30.2 (d, J = 29.93 Hz, CH), 21.3 (d, J = 26.3 Hz, CH), 17.8 (CH₃), 17.6 (CH₃), 17.4 (CH₃), 16.0 (CH₃). **³¹P{¹H} NMR (δ, CD₂Cl₂, 20 °C):** 197.9. **IR (ATR, cm⁻¹):** 1813 (ν_{CO}). **ESI-**

Chapter 5 – Halocarbonyl Molybdenum and Tungsten PNP pincer complexes

MS (m/z, CH₃CN, NaCl) positive ion: 582.1 [M + Na]⁺, 524.1 [M - Cl]⁺. In the presence of air: 512.1 [M - (Cl + CO) + O]⁺, 528.1 [M - (Cl + CO) + 2O]⁺.

[Mo(PNP^{Me}-Ph)(CO)₂Cl₂] (10k)



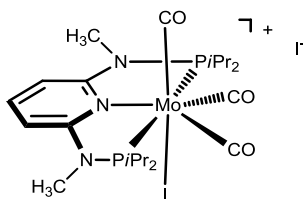
The product was obtained as a yellow solid in 81% yield. Anal. Calcd. for C₃₃H₂₉Cl₂N₃O₂P₂Mo (728.41): C, 54.22; H, 4.01; N, 5.77%. Found: C, 54.10; H, 3.91; N, 5.81%. ¹H NMR (δ, CD₂Cl₂, 20 °C): 7.83 (t, J = 7.6 Hz, 1H, py⁴), 7.67 (t, J = 8.9 Hz, 4H, Ph^{2,6}), 7.54 (t, J = 7.4 Hz, 2H, Ph⁴), 7.45 (t, J = 6.9 Hz, 4H, Ph^{2,6}), 7.24 (t, J = 7.3 Hz, 2H, Ph⁴), 7.00 (t, J = 7.3 Hz, 4H, Ph^{3,5}), 6.69 (t, J = 7.6 Hz, 4H, Ph^{3,5}), 6.40 (d, J = 7.3 Hz, 2H, py^{3,5}), 3.07 (s, 6H, NCH₃). ¹³C{¹H} NMR (δ, CD₂Cl₂, 20 °C): 161.4-161.7 (m, py^{2,6}), 144.3 (py⁴), 136.7 (t, J = 5.9 Hz, py^{2,6}), 132.3 (Ph⁴), 131.12 (t, J = 5.1 Hz, Ph^{3,5}), 130.9 (Ph⁴), 128.9 (t, J = 4.9 Hz, Ph^{3,5}), 128.4 (t, J = 5.4 Hz, Ph^{2,6}), 100.5 (py^{3,5}), 36.2 (NCH₃). The quaternary Ph and CO carbon atoms could not be detected. ¹³C solid-state NMR (δ, 12 kHz, 25 °C): 257.6 (CO), 215.1 (CO). ³¹P{¹H} NMR (δ, CD₂Cl₂, 20 °C): 135.2. IR (ATR, cm⁻¹): 2000 (ν_{CO}), 1974 (ν_{CO}), 1862 (ν_{CO}), 1846 (ν_{CO}). **ESI-MS (m/z, CH₃OH, NaCl) positive ion:** 718.01 [M + Na - CO]⁺, 660.05 [M - (CO + NaCl)]⁺.

General synthetic procedure for the mechanist study of the halocarbonyl molybdenum and tungsten complexes:

Method a) To a solution of [MPNP(CO)₃] (M = Mo, W; 0.300 mmol) in CH₂Cl₂ (10 mL) was added 1 equiv. of I₂ (0.300 mmol) in a CO atmosphere. The reaction was stirred for 18 h and after this period the solution was filtered, solvent was removed under vacuum, and the solid was washed twice with Et₂O and *n*-pentane and then dried under vacuum.

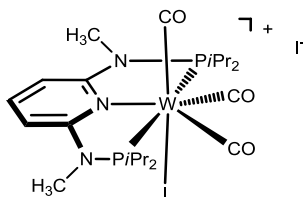
Method b) A solution of [Mo(PNP^{Me}-*i*Pr)(CO)₂Cl₂] and [W(PNP^{Me}-*i*Pr)(CO)₂Cl₂] (0.067 mmol) in CD₂Cl₂ (1 mL) was reacted with AgSbF₆ (0.067 mmol) in a CO atmosphere. The mixture was controlled for 24h by ³¹P{¹H} NMR. NMR spectra of two achieved complexes are identical with those of [M(PNP^{Me}-*i*Pr)(CO)₃]I (M = Mo, W).

[Mo(PNP^{Me}-iPr)(CO)₃]I (6j')



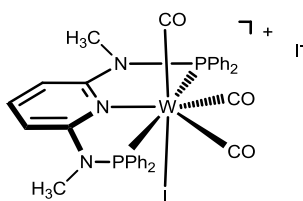
The product was obtained as a red-brown solid in 98% yield. Anal. Calcd. for C₂₂H₃₇I₂MoN₃O₃P₂ (803.27): C, 32.90; H, 4.64; N, 5.23. Found: C, 32.80; H, 4.73; N, 5.29. ¹H NMR (δ, CD₂Cl₂, 20 °C): 7.96 (t, J = 8.3 Hz, 1H, py⁴), 6.63 (d, J = 8.4 Hz, 2H, py^{3,5}), 3.56-3.36 (m, 2H, CH), 3.32 (d, J = 2.7 Hz, 6H, NCH₃), 3.24-3.02 (m, 2H, CH), 1.67-1.57 (m, 6H, CH₃), 1.56-1.42 (m, 12H, CH₃), 1.28-1.13 (m, 6H, CH₃). ¹³C{¹H} NMR (δ, CD₂Cl₂, 20 °C): 231.9 (br, CO), 213.8 (t, J = 13.8 Hz, CO), 161.3 (vt, J = 6.1 Hz, py^{2,6}), 144.3 (py⁴), 102.9 (py^{3,5}), 36.9 (br, CH), 32.7-31.7 (CH), 30.6 (t, J = 10.8 Hz, NCH₃), 21.9 (CH₃), 19.9 (CH₃), 19.0 (CH₃), 18.9 (CH₃). ³¹P{¹H} NMR (δ, CD₂Cl₂, 20 °C): 137.1. IR (ATR, cm⁻¹): 2027 (ν_{CO}), 1971 (ν_{CO}), 1938 (ν_{CO}).

[W(PNP^{Me}-iPr)(CO)₃]I (6k')



The product was obtained as a red-brown solid in 96% yield. Anal. Calcd. for C₂₂H₃₇I₂WN₃O₃P₂ (891.15): C, 29.65; H, 4.19; N, 4.72%. Found: C, 29.57; H, 4.20; N, 4.83. ¹H NMR (δ, CD₂Cl₂, 20 °C): 7.95 (dt, J = 8.4 Hz, J = 1.2 Hz, 1H, py⁴), 6.66 (d, J = 8.4 Hz, 2H, py^{3,5}), 3.53-3.35 (m, 2H, CH), 3.29 (t, J = 2.7 Hz, 6H, NCH₃), 3.25-3.05 (m, 2H, CH), 1.64-1.36 (m, 18H, CH₃), 1.24-1.06 (m, 6H, CH₃). ¹³C{¹H} NMR (δ, CD₂Cl₂, 20 °C): 255.2 (t, J = 25.9 Hz, CO), 207.2 (t, J = 11.0 Hz, CO), 162.8 (br, py^{2,6}), 146.1 (py⁴), 103.2 (py^{3,5}), 37.5 (br, NCH₃), 31.3 (CH), 31.1 (CH), 19.5 (CH₃), 19.2 (CH₃), 17.6 (CH₃), 17.4 (CH₃). ³¹P{¹H} NMR (δ, CD₂Cl₂, 20 °C): 117.4 (br). IR (ATR, cm⁻¹): 2020 (ν_{CO}), 1955 (ν_{CO}), 1915 (ν_{CO}).

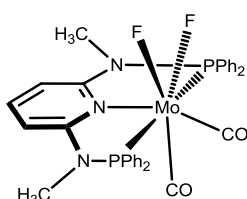
[W(PNP^{Me}-Ph)(CO)₃Ir] (8k')



The product was obtained as a red-brown solid in 96.8% yield. ¹H NMR (δ, CD₂Cl₂, 20 °C): 8.11 (t, J = 8.4 Hz, 1H, py⁴), 7.67-7.28 (m, 20H, Ph), 6.92 (d, J = 8.4 Hz, 2H, py^{3,5}), 3.21 (s, 6H, NCH₃). ¹³C{¹H} NMR (δ, CD₂Cl₂, 20 °C): 222.3 (t, J = 11.3 Hz, CO), 206.5 (t, J = 14.8 Hz, CO), 160.6 (vt, J = 9.1 Hz, py^{2,6}), 145.1 (Ph), 138.4 (vt, J = 5.8 Hz, py⁴), 133.3 (vt, J = 5.7 Hz, Ph), 133.0 (vd, J = 7.1 Hz, Ph), 131.5 (vt, J = 5.9 Hz, Ph), 129.8 (vt, J = 5.5 Hz, Ph), 128.7 (vt, J = 5.9 Hz, Ph), 104.7 (py^{3,5}), 39.4 (NCH₃). ³¹P{¹H} NMR (δ, CD₂Cl₂, 20 °C): 90.6 (¹J_{W-P} = 194.1 Hz). IR (ATR, cm⁻¹): 2033 (ν_{CO}), 1963 (ν_{CO}), 1934 (ν_{CO}).

Synthetic procedures of the fluorine complexes: To a solution of [MoPNP(CO)₃] (0.300 mmol) in CH₃CN (10 mL) 1 equiv. of 1-fluoro-2,4,6-trimethylpyridinium tetrafluoroborate (0.300 mmol) was added. The solution was stirred for 3 days. After this period the solution was filtered, the solvent was then removed under vacuum, and the remaining orange solid was washed twice with Et₂O and n-pentane and dried under vacuum.

[Mo(PNP^{Me}-Ph)(CO)₂F₂] (11k)



The product was obtained as an orange solid in 93% yield. Anal. Calcd. for C₃₃H₂₉F₂N₃O₂P₂Mo (695.50): C, 56.99; H, 4.20; N, 6.04%. Found: C, 57.15; H, 4.26; N, 6.11%. ¹H NMR (δ, CD₃CN, 20 °C): 7.98 (t, J = 8.1 Hz, 1H, py⁴), 7.58 (dd, J = 14.2, 6.9 Hz, 4H, Ph^{2,6}), 7.11-7.49 (m, 8H, Ph⁴, Ph^{2,6}), 7.01 (t, J = 7.2 Hz, 4H, Ph^{3,5}), 6.66 (d, J = 8.3 Hz, 2H, py^{3,5}), 6.37 (dd, J = 10.8 Hz, 7.7 Hz, 4H, Ph^{3,5}), 2.54 (s, 6H, NCH₃). ¹³C solid-state NMR (δ, 12 kHz, 25 °C): 250.4 (CO), 214.3 (CO). ³¹P{¹H} NMR (δ, CD₃CN, 20 °C): 143.7 (t, ²J_{PF} = 41.7 Hz). IR (ATR, cm⁻¹): 1977 (ν_{CO}), 1880 (ν_{CO}). ESI-MS (m/z, CH₃OH, NaF) positive ion: 644.08 [M - (CO + NaF)]⁺.

5.5.2. Computational details

All calculations were performed using the Gaussian 09 software package,²² without symmetry constraints. The optimized geometry and the relative stability of all the complexes with different PNP ligands for the two metal atoms ($M = \text{Mo}$ and W), presented in Figure 5.10. and 5.11., were obtained with the B3LYP functional.²³ This functional includes a mixture of Hartree–Fock²⁴ exchange with DFT²⁵ exchange–correlation, given by Becke’s three parameter functional with the Lee, Yang and Parr correlation functional, which includes both local and non-local terms. The basis set used (basis b1) consisted of the Stuttgart/Dresden ECP (SDD) basis set²⁶ to describe the electrons of the metal atoms, and a standard 6-31g(d,p) basis set²⁷ for all other atoms. The electronic energies (E_{b1}) obtained at the B3LYP/b1 level of theory were converted to free energy at 298.15 K and 1 atm (G_{b1}) by using zero point energy and thermal energy corrections based on structural and vibration frequency data calculated at the same level. G_{b1} represents the free energy values shown in Figure 5.10. and 5.11..

The mechanism for the formation of the Mo complexes with the PNP^{Me}-iPr ligand, represented in the profiles of Figure 5.12. and 5.13., was obtained with an improved methodology. The geometry of all the species were optimized with the PBE0 functional and a basis set (basis b1’) equivalent to b1 but with an f-polarization function added to describe the electrons of the Mo atom.²⁸ The PBE0 functional uses a hybrid generalized gradient approximation (GGA), including 25% mixture of Hartree–Fock exchange with DFT exchange–correlation, given by Perdew, Burke and Ernzerhof functional (PBE),²⁹ and proved to describe well weak interactions,³⁰ such as the ones that may exist in a transition state. Transition state optimizations were performed with the Synchronous Transit-Guided Quasi-Newton (STQN) Method developed by Schlegel *et al.*,³¹ following extensive searches of the potential energy surface.

Frequency calculations were performed to confirm the nature of the stationary points, yielding one imaginary frequency for the transition states and none for the minima. Each transition state was further confirmed by following its vibrational mode downhill on both sides and obtaining the minima presented on the energy profiles. The electronic energies ($E_{b1'}$) obtained at the PBE0/b1’ level of theory were converted to free energy at 298.15 K and 1 atm ($G_{b1'}$) by using zero point energy and thermal energy corrections based on structural and vibration frequency data calculated at the same level.

Single point energy calculations were performed using the M06 functional and an improved basis set (basis b2), with the geometries optimized at the PBE0/b1’ level.

Chapter 5 – Halocarbonyl Molybdenum and Tungsten PNP pincer complexes

Basis b2 consisted of a 3-21G basis set³² with an added f-polarization function for Mo23 and a standard 6-311++G(d,p) basis set³³ for the rest of the elements. The M06 functional is a hybrid meta-GGA functional developed by Truhlar and Zhao,³⁴ and it was shown to perform very well for the kinetics of transition metal molecules, providing a good description of weak and long range interactions.³⁵ Solvent effects (CH₂Cl₂) were considered in all calculations (geometry optimizations included) using the Polarizable Continuum Model (PCM) initially devised by Tomasi and coworkers³⁶ with radii and non-electrostatic terms of the SMD solvation model, developed by Truhlar *et al.*³⁷ The free energy values presented in the profiles (G_{b2}^{soln}) were derived from the electronic energy values obtained at the M06/b2//PBE0/b1' level (E_{b2}^{soln}) according to the following expression: $G_{b2}^{soln} = E_{b2}^{soln} + G_{b1'} - E_{b1'}$.^{**}

5.6. References

- [1] Wilkinson, G.; Stone, F. G. A.; Abel, E. W.; Eds. *Comprehensive Organometallic Chemistry*, **1982**, Pergamon: Oxford, U.K..
- [2] Gutmann, V.; Halogen chemistry, Vol. 3, **1967**, Academic Press, London
- [3] a) Astruc, D.; *Organometallic Chemistry and Catalysis*, **2007**, Springer-Verlag Berlin Heidelberg; b) Nakamoto, K.; *Infrared and Raman Spectra of Inorganic and Coordination Compounds, Part B, Applications in Coordination, Organometallic, and Bioinorganic Chemistry*, 6th Edition, **2009**, John Wiley & Sons, Inc., Hoboken, New Jersey.
- [4] Colton R.; Tomkins, I. B.; *Aust. J. Chem.*, **1966**, *19*, 1143-1146; 1966, *19*, 1519.
- [5] Nyholm, R. S.; Snow M. R.; Stiddard, M. H. B.; *J. Chem. Soc.*, **1965**, 6570-6575.
- [6] Nigam, H. L.; Nyholm R. S.; Stiddard, M. H. B.; *J. Chem. Soc.*, **1960**, 1803-1806.
- [7] a) Dilsky, S.; *J. Organomet. Chem.*, **2007**, *692*, 2887-2896; b) Song, L. C.; Zhang, L. Y.; Hu, Q. M. Huang, X.-Y.; *Inorg. Chim. Acta*, **1995**, *230*, 127-131; c) Curtis M. D.; Shiu, K.; *Inorg. Chem.*, **1985**, *24*, 1213-1218; d) Schwarz, C. L.; Bullock, R. M.; Creutz, C.; *J. Am. Chem. Soc.*, **1991**, *113*, 1225-1236; e) Chaudhuri, P.; Wieghardt, K.; Tsai Y. H.; Krüger, C.; *Inorg. Chem.*, **1984**, *23*, 427-432; f) Baker, K. P.; *Adv. Organomet. Chem.*, **1996**, *40*, 45-115; g) Edwards, P. G.; Fleming J. S.; Liyanage, S. S.; *Inorg. Chem.*, **1996**, *35*, 4563-4568; h) Coles, S. J.; Edwards, P. G.; Fleming J. S.; Hursthouse, M. B.; *J. Chem. Soc., Dalton Trans.*, **1995**, 4091-4097; i) Planinic, P.; Meider, H.; *Polyhedron*, **1990**, *9*, 1099-1105.
- [8] Shiu, K.; Liou, K.; *Organometallics*, **1990**, *9*, 669-675.
- [9] Moss, J. R.; Shaw, B. L.; *J. Chem. Soc. (A)*, **1970**, 595-601.
- [10] King, R. B.; *Inorg. Chem.*, **1964**, *3*, 1039-1041.

^{**} The same experimental conditions in the following chapters.

Chapter 5 – Halocarbonyl Molybdenum and Tungsten PNP pincer complexes

- [11] Filippou, A. C.; Gruenleitner, W.; *J. Organomet. Chem.*, **1990**, 398, 99-115.
- [12] Anker, M. W.; Colton, R.; Tomkins, I. B.; *Aust. J. Chem.*, **1967**, 20, 9-12.
- [13] Backes-Dahmann, G.; Wieghardt, K.; *Inorg. Chem.*, **1985**, 24, 4049-4054.
- [14] Burgmayer, S. J. N.; Templeton, J. L.; *Inorg. Chem.*, **1985**, 24, 2224-2230.
- [15] a) Benito-Garagorri, D.; Becker, E.; Wiedermann, J.; Lackner, W.; Pollak, M.; Mereiter, K.; Kisala, J.; Kirchner, K.; *Organometallics*, **2006**, 25, 1900-1913; b) Benito-Garagorri, D.; Kirchner, K.; *Accounts of Chemical Research*, **2008**, 41, 201-213.
- [16] Wingard, L. A.; White, P. S.; Templeton, J. L.; *Dalton Trans.*, **2012**, 41, 11438-11448.
- [17] Bendix, J.; Bøgevig, A.; *Inorg. Chem.*, **1998**, 37, 5992-6001.
- [18] Schirmer, W.; Flörke, U.; Haupt, H.-J. *Z. Anorg. Allg. Chem.* **1989**, 574, 239-255.
- [19] a) Cotton, A. F.; Falvello, L. R.; Meadows, J. H.; *Inorg. Chem.*, **1985**, 24, 514-517; b) Boyden, J. A.; Colton, R.; *Aust. J. Chem.*, **1968**, 21, 2567-2571; c) Baker, P. K.; Fraser, S. G.; Keys, E. M.; *J. Organomet. Chem.*, **1986**, 309, 319-321.
- [20] Maurer, C.; Pittenauer, E.; Du, V.A.; Allmaier, G.; Schubert, U.; *Dalton Trans.*, **2012**, 41, 2346-2353.
- [21] Maurer, C.; Pittenauer, E.; Puchberger, M.; Allmaier, G.; Schubert, U.; *Chem-PlusChem*, **2013**, 78, 343-351.
- [22] Frisch, M. J.; Trucks, G. W.; Schlegel, H. B.; Scuseria, G. E.; Robb, M. A.; Cheeseman, J. R.; Scalmani, G.; Barone, V.; Mennucci, B.; Petersson, G. A.; Nakatsuji, H.; Caricato, M.; Li, X.; Hratchian, H. P.; Izmaylov, A. F.; Bloino, J.; Zheng, G.; Sonnenberg, J. L.; Hada, M.; Ehara, M.; Toyota, K.; Fukuda, R.; Hasegawa, J.; Ishida, M.; Nakajima, T.; Honda, Y.; Kitao, O.; Nakai, H.; Vreven, T.; Montgomery Jr., J. A.; Peralta, J. E.; Ogliaro, F.; Bearpark, M.; Heyd, J. J.; Brothers, E.; Kudin, K. N.; Staroverov, V. N.; Kobayashi, R.; Normand, J.; Raghavachari, K.; Rendell, A.; Burant, J. C.; Iyengar, S. S.; Tomasi, J.; Cossi, M.; Rega, N.; Millam, J. M.; Klene, M.; Knox, J. E.; Cross, J. B.; Bakken, V.; Adamo, C.; Jaramillo, J.; Gomperts, R.; Stratmann, R. E.; Yazyev, O.; Austin, A. J.; Cammi, R.; Pomelli, C.; Ochterski, J. W.; Martin, R. L.; Morokuma, K.; Zakrzewski, V. G.; Voth, G. A.; Salvador, P.; Dannenberg, J. J.; Dapprich, S.; Daniels, A. D.; Farkas, Ö.; Foresman, J. B.; Ortiz, J. V.; Cioslowski, J.; Fox, D. J.; *Gaussian 09, Revision A.02*, Gaussian, Inc., **2009**, Wallingford CT.
- [23] a) Becke, A. D.; *J. Chem. Phys.*, **1993**, 98, 5648-5652; b) Miehlich, B.; Savin, A.; Stoll H.; Preuss, H.; *Chem. Phys. Lett.*, **1989**, 157, 200-206; c) Lee, C.; Yang W.; Parr, G.; *Phys. Rev. B: Condens. Matter*, **1988**, 37, 785-789.
- [24] Hehre, W. J.; Radom, L.; Schleyer P. V. R.; Pople J. A.; *Ab Initio Molecular Orbital Theory*, **1986**, John Wiley & Sons, New York, 1986.
- [25] Parr R. G.; Yang, W.; *Density Functional Theory of Atoms and Molecules*, **1989**, Oxford University Press, New York.
- [26] a) Haeusermann, U.; Dolg, M.; Stoll H.; Preuss, H.; *Mol. Phys.*, **1993**, 78, 1211-1224; b) Kuechle, W.; Dolg, M.; Stoll H.; Preuss, H.; *J. Chem. Phys.*, **1994**, 100, 7535-7542; c)

Chapter 5 – Halocarbonyl Molybdenum and Tungsten PNP pincer complexes

- Leininger, T.; Nicklass, A.; Stoll, H.; Dolg M.; Schwerdtfeger, P.; *J. Chem. Phys.*, **1996**, *105*, 1052-1059.
- [27] a) Ditchfield, R.; Hehre W. J.; Pople, J. A.; *J. Chem. Phys.*, **1971**, *54*, 724-728; b) Hehre, W. J.; Ditchfield R.; Pople, J. A.; *J. Chem. Phys.*, **1972**, *56*, 2257-2261; c) Hariharan P. C.; Pople, J. A.; *Mol. Phys.*, **1974**, *27*, 209-214; d) Gordon, M. S.; *Chem. Phys. Lett.*, **1980**, *76*, 163-167; e) Hariharan P. C.; Pople, J. A.; *Theor. Chim. Acta*, **1973**, *28*, 213-222.
- [28] Ehlers, A. W.; Böhme, M.; Dapprich, S.; Gobbi, A.; Höllwarth, A.; Jonas, V.; Köhler, K. F.; Stegmann, R.; Veldkamp A.; Frenking, G.; *Chem. Phys. Lett.*, **1993**, *208*, 111-208.
- [29] a) Perdew, J. P.; Burke K.; Ernzerhof, M.; *Phys. Rev. Lett.*, **1997**, *78*, 1396; b) Perdew, J. P.; *Phys. Rev. B: Condens. Matter*, **1986**, *33*, 8822-8824.
- [30] Zhao, Y.; Truhlar, D. G.; *J. Chem. Theory Comput.*, **2005**, *1*, 415-432.
- [31] a) Peng, C.; Yayala, P.; Schlegel, H. B.; Frisch, M. J.; *J. Comput. Chem.*, **1996**, *17*, 49-56; b) Peng C.; Schlegel, H. B.; *Isr. J. Chem.*, **1993**, *33*, 449-454.
- [32] a) Binkley, J. S.; Pople J. A.; Hehre, W. J.; *J. Am. Chem. Soc.*, **1980**, *102*, 939-947; b) Dobbs, K. D.; Hehre, W. J.; *J. Comput. Chem.*, **1986**, *7*, 359-378; c) Dobbs, K. D.; Hehre, W. J.; *J. Comput. Chem.*, **1987**, *8*, 880-893; d) Dobbs, K. D.; Hehre, W. J.; *J. Comput. Chem.*, **1987**, *8*, 861-879; e) Gordon, M. S.; Binkley, J. S.; Pople, J. A.; Pietro W. J.; Hehre, W. J.; *J. Am. Chem. Soc.*, **1982**, *104*, 2797-2803; f) Pietro, W. J.; Francl, M. M.; Hehre, W. J.; DeFrees, D. J.; Pople, J. A.; Binkley, J. S.; *J. Am. Chem. Soc.*, **1982**, *104*, 5039-5048.
- [33] a) McClean, A. D.; Chandler, G. S.; *J. Chem. Phys.*, **1980**, *72*, 5639-5648; b) Krishnan, R.; Binkley, J. S.; Seeger, R.; Pople, J. A.; *J. Chem. Phys.*, **1980**, *72*, 650-654; c) Wachters, A. J. H.; *J. Chem. Phys.*, **1970**, *52*, 1033-1036; d) Hay, P. J.; *J. Chem. Phys.*, **1977**, *66*, 4377-4384; e) Raghavachari, K.; Trucks, G. W.; *J. Chem. Phys.*, **1989**, *91*, 1062-1065; f) Binning Jr., R. C; Curtiss, L. A.; *J. Comput. Chem.*, **1990**, *11*, 1206-1216; g) McGrath, M. P.; Radom, L.; *J. Chem. Phys.*, **1991**, *94*, 511-516; h) Clark, T.; Chandrasekhar, J.; Spitznagel, G. W. Schleyer, P. V. R.; *J. Comput. Chem.*, **1983**, *4*, 294-301; i) Frisch, M. J.; Pople, J. A.; Binkley, J. S.; *J. Chem. Phys.*, **1984**, *80*, 3265-3269.
- [34] Zhao, Y.; Truhlar, D. G.; *Theor. Chem. Acc.*, **2008**, *120*, 215-241.
- [35] a) Zhao, Y.; Truhlar, D. G.; *Acc. Chem. Res.*, **2008**, *41*, 157-167; b) Zhao, Y.; Truhlar, D. G.; *Chem. Phys. Lett.*, **2011**, *502*, 1-144.
- [36] a) Cancès, M. T.; Mennucci, B.; Tomasi, J.; *J. Chem. Phys.*, **1997**, *107*, 3032-3041; b) Cossi, M.; Barone, V.; Mennucci, B.; Tomasi, J.; *Chem. Phys. Lett.*, **1998**, *286*, 253-417; c) Mennucci, B.; Tomasi, J.; *J. Chem. Phys.*, **1997**, *106*, 5151-5158; d) Tomasi, J.; Mennucci, B.; Cammi, R.; *Chem. Rev.*, **2005**, *105*, 2999-3094.
- [37] Marenich, A. V.; Cramer, C. J.; Truhlar, D. G.; *J. Phys. Chem. B*, **2009**, *113*, 6378-6396.

5.7. Annex

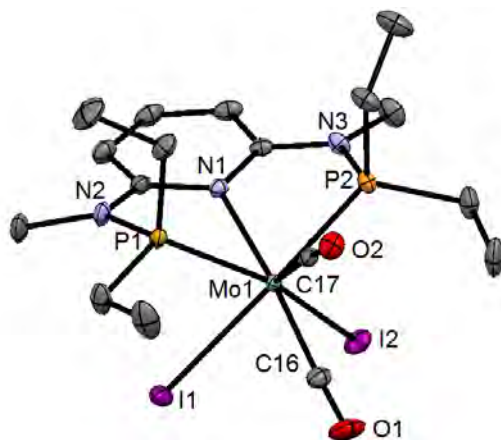


Figure 5.16. Structural view of $[\text{Mo}(\text{PNP}^{\text{Me-Et}})(\text{CO})_2\text{I}_2]$ (**6i**) showing 50% thermal ellipsoids (hydrogen atoms and solvent molecules omitted for clarity). Selected bond lengths (Å) and bond angles (°): Mo1-I1 2.9186(2), Mo1-I2 2.8966(2), Mo1-P1 2.4126(5), Mo1-P2 2.4171(4), Mo-N1 2.279(1), Mo-C16 1.985(2), Mo-C17 1.922(2); P1-Mo1-P2 113.42(2), N1-Mo1-I1 91.59(4), N1-Mo1-I2 89.90(4), N1-Mo1-C32 118.55(6), N1-Mo1-C33 168.85(7), I1-Mo1-I2 81.92(1), C32-Mo1-C33 72.59(8)

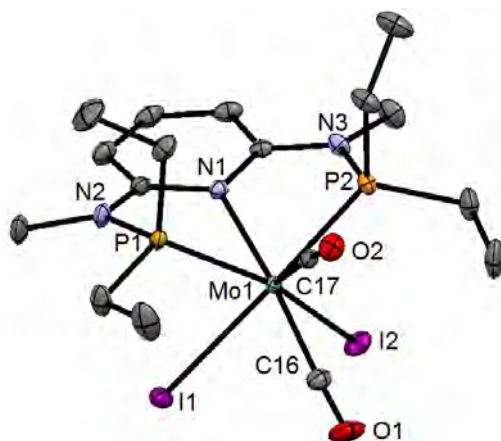


Figure 5.17. Structural view of $[\text{Mo}(\text{PNP}^{\text{Me-Et}})(\text{CO})_2\text{Br}_2]$ (**7i**) showing 50% thermal ellipsoids (hydrogen atoms and solvent molecules omitted for clarity). Selected bond lengths (Å) and bond angles (°): Mo1-Br1 2.697(2), Mo1-Br2 2.689(2), Mo1-P1 2.426(2), Mo1-P2 2.433(2), Mo-N1 2.270(3), Mo-C32 1.931(3), Mo-C33 1.983(3); P1-Mo1-P2 115.23(3), N1-Mo1-Br1 91.94(7), N1-Mo1-Br2 89.05(7), N1-Mo1-C32 120.1(1), N1-Mo1-C33 167.9(1), Br1-Mo1-Br2 82.57(1), C32-Mo1-C33 72.0(1)

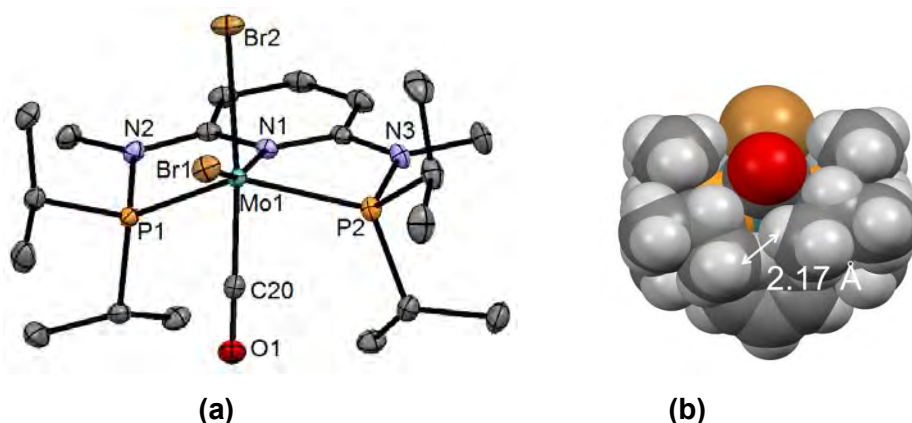


Figure 5.18. (a) Structural view of $[\text{Mo}(\text{PNP}^{\text{Me-}i\text{Pr}})(\text{CO})\text{Br}_2]$ (**7j**) showing 50% thermal ellipsoids (H atoms omitted for clarity). Selected bond lengths (Å) and bond angles ($^\circ$): Mo-N(1) 2.2665(12), Mo-C(20) 1.9209(15), Mo-P(1) 2.3847(4), Mo-P(2) 2.3620(4), Mo-Br(1) 2.5494(2), Mo-Br(2) 2.6301(3); P(1)-Mo-P(2) 128.01(2), N(1)-Mo-P(1) 72.13(3), N(1)-Mo-P(2) 73.97(3), N(1)-Mo-Br(1) 163.60(3), N(1)-Mo-Br(2) 78.98(3), N(1)-Mo-C(20) 115.05(5), Br(1)-Mo-Br(2) 84.79(1), Br(1)-Mo-C(20) 81.26(4), Br(2)-Mo-C(20) 165.88(4). Space filling representation to illustrate crowding. Viewed down the O1-C20-Mo1-Br2 axis revealing a relatively close contact between *iPr* moieties of the $\text{PNP}^{\text{Me-}i\text{Pr}}$ ligand

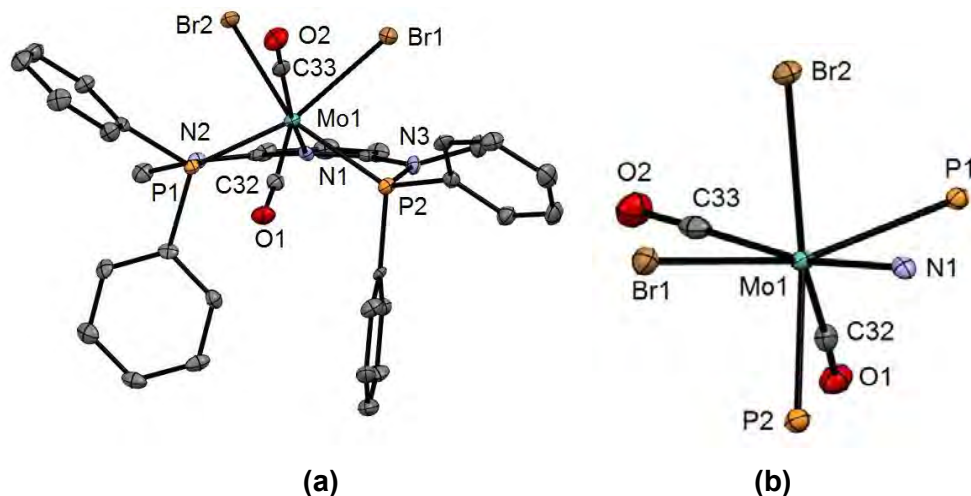


Figure 5.19. (a) Structural view of $[\text{Mo}(\text{PNP}^{\text{Me-Ph}})(\text{CO})_2\text{Br}_2] \cdot 3\text{CDCl}_3$ (**7k**· 3CDCl_3) showing 50% thermal ellipsoids (hydrogen atoms and solvent molecules omitted for clarity). Selected bond lengths (Å) and bond angles ($^\circ$): Mo1-Br1 2.6887(6), Mo1-Br2 2.6537(5), Mo1-P1 2.429(1), Mo1-P2 2.422(1), Mo-N1 2.249(3), Mo-C32 1.929(4), Mo-C33 2.016(4); P1-Mo1-P2 118.46(3), N1-Mo1-Br1 92.01(8), N1-Mo1-Br2 87.46(7), N1-Mo1-C32 120.5(2), N1-Mo1-C33 165.2(2), Br1-Mo1-Br2 80.56(2), C32-Mo1-C33 74.3(2). (b) Structural view of the inner coordination sphere of **7b** emphasizing the capped-trigonal-prism description (Br2 caps the quadrilateral face)

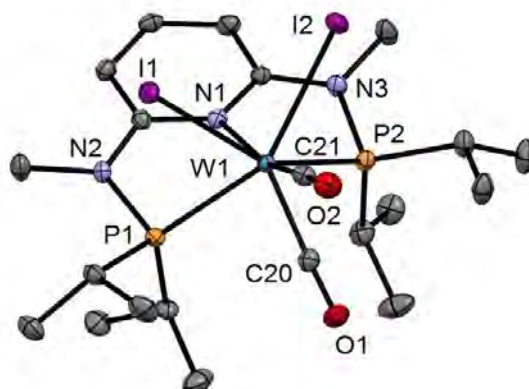


Figure 5.20. Structural view of $[W(\text{PNP}^{\text{Me-}i\text{Pr}})(\text{CO})_2\text{I}_2]$ (**8j**) showing 50% thermal ellipsoids (hydrogen atoms and solvent omitted for clarity). Selected bond lengths (Å) and bond angles ($^\circ$): W1-I1 2.9255(2), W1-I2 2.8999(2), W1-N1 2.2553(18), W1-P1 2.4616(7), W1-P2 2.4594(6), W1-C20 1.940(3), W1-C21 1.982(2), I1-W1-I2 79.855(5), P1-W1-P2 114.97(2), C20-W1-C21 69.54(10)

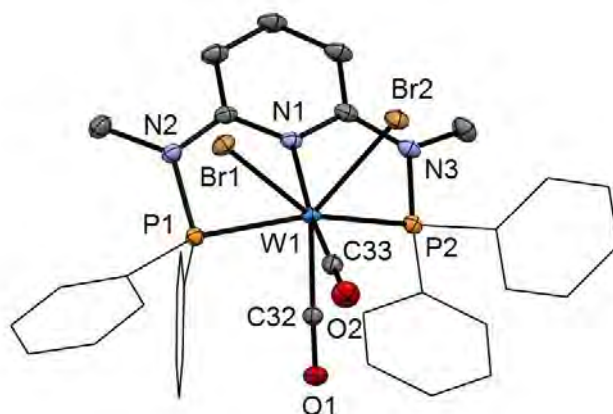


Figure 5.21. Structural view of $[W(\text{PNP}^{\text{Me-Ph}})(\text{CO})_2\text{Br}_2]$ (**9k**) showing 50% thermal ellipsoids (hydrogen atoms and solvent omitted for clarity). Selected bond lengths (Å) and bond angles ($^\circ$): W1-P1 2.4190(7), W1-P2 2.4203(8), W1-N1 2.240(2), W1-C32 1.953(2), W1-C33 1.984(2), W1-Br1 2.6871(3), W1-Br2 2.6444(3), P1-W1-P2 120.44(2), Br1-W1-Br2 79.43(1), C32-W1-C33 73.44(9)

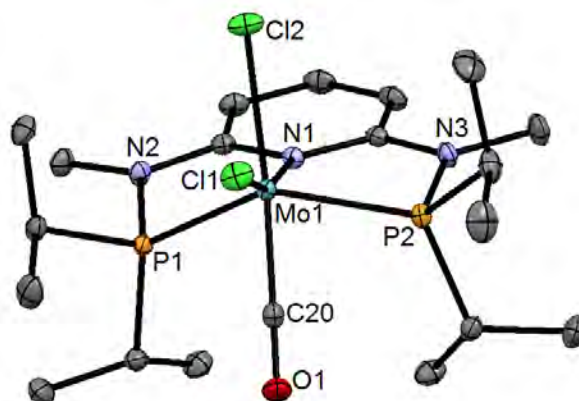


Figure 5.22. Structural view of $[\text{Mo}(\text{PNP}^{\text{Me-}i\text{Pr}})(\text{CO})\text{Cl}_2]$ (**10j**) showing 50% thermal ellipsoids (H atoms omitted for clarity). Selected bond lengths (Å) and bond angles (°): Mo-N(1) 2.2691(8), Mo-C(20) 1.9208(10), Mo-P(1) 2.3783(3), Mo-P(2) 2.3579(3), Mo-Cl(1) 2.4052(2), Mo-Cl(2) 2.4792(3); P(1)-Mo-P(2) 128.03(1), N(1)-Mo-P(1) 72.20(2), N(1)-Mo-P(2) 73.65(2), N(1)-Mo-Cl(1) 163.04(2), N(1)-Mo-Cl(2) 79.27(2), N(1)-Mo-C(20) 114.82(4), Cl(1)-Mo-Cl(2) 83.88(1), Cl(1)-Mo-C(20) 82.07(3), Cl(2)-Mo-C(20) 165.87(3)

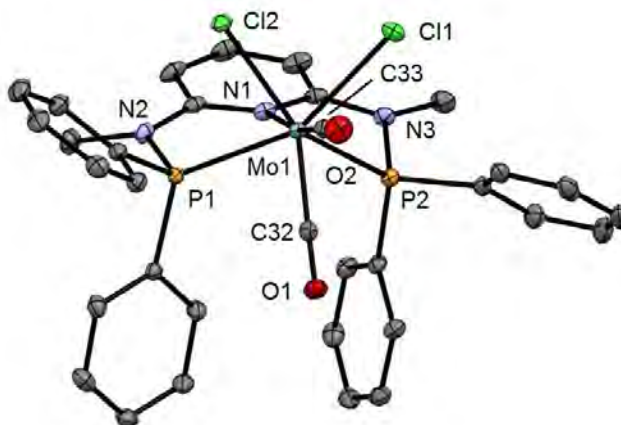


Figure 5.23. Structural view of $[\text{Mo}(\text{PNP}^{\text{Me-Ph}})(\text{CO})_2\text{Cl}_2] \cdot 1.5\text{CD}_2\text{Cl}_2$ (**10k**· $1.5\text{CD}_2\text{Cl}_2$) showing 50% thermal ellipsoids (hydrogen atoms and solvent molecules omitted for clarity). Selected bond lengths (Å) and bond angles (°): Mo1-Cl1 2.5424(7), Mo1-Cl2 2.5031(8), Mo1-P1 2.4253(9), Mo1-P2 2.4259(8), Mo-N1 2.248(1), Mo-C32 1.950(2), Mo-C33 1.990(2); P1-Mo1-P2 120.18(2), N1-Mo1-Cl1 92.20(4), N1-Mo1-Cl2 86.96(3), N1-Mo1-C33 117.00(6), N1-Mo1-C32 169.96(6), Cl1-Mo1-Cl2 81.07(2), C32-Mo1-C33 72.92(7)

Chapter 6

Mono Oxo

Molybdenum(IV) PNP

Pincer Complexes

Complexes with M=O bonds exhibit very different reactivities depending on the nature of the transition metal. The early transition metals are very oxophilic and form M=O bonds that are not very reactive called **oxides**. On the other hand, **metal-oxo** complexes are late transition metals form labile M=O bonds because of the repulsion between the filled *d* metal orbitals and *p* oxygen orbitals. They are often obtain by transfer of an oxygen atom onto a transition metal using an oxygen atom donor such as H₂O₂ or from O₂. These complexes are key species that are important from a theoretical point of view, in biochemistry, organic synthesis and catalysis of metathesis, dimerization, polymerization and oxidation of olefins.¹

6.1. Metal-oxo complexes

An important feature in the structure of M=O complexes is the duality of behavior concerning the number of electrons given to the metal. Indeed, if the metal center is electron deficient the O donates 4 electrons (**a**). On the other hand, if the metal already has 18 valence electrons, the O donates only 2 electrons (**b**).

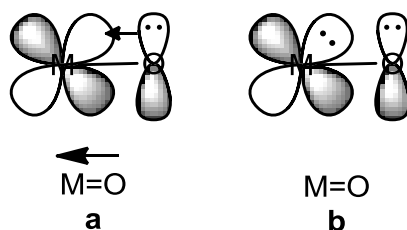


Figure 6.1. Coordination between metal and oxygen

The larger electronegativity of oxygen causes a polarity of the bonds with a metal, $M^{\delta+}=O^{\delta-}$, consequence of the strong polarization is the lack of such a double bond in early transition metal (groups 3 to 5), lanthanide and actinide complexes because of systematic M-O-M bridging. On the other hand, the later transition metals, where the number of d-electrons is larger, there is a repulsion between these filled d-non-bonding orbitals and the non-bonding orbitals of the heteroatom. The consequence is that M=O bonds are unstable at the right of the iron column. Between these two sides of the periodic table, the most stable metal-oxo (M=O) complexes are found along a diagonal from V to Os with the most common ones from Mo.

The M=O complexes are most often d^0 -complexes, i.e., they do not have non-bonding electrons that would have to face the non-bonding oxygen π lone pairs. Some

d^2 -complexes are known, however, and even some d^4 -ones, but not in octahedral geometry because the latter would maximize this destabilization.^{1,2}

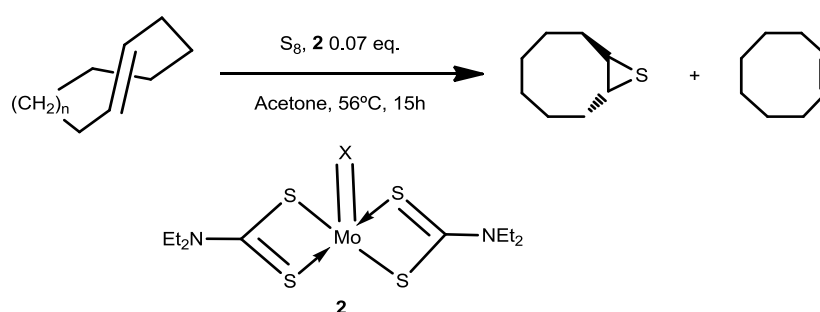
6.2. Molybdenum oxo complexes

The chemistry of molybdenum in its higher oxidation states is dominated by oxo-species which may have terminal oxide, bridging oxide or both. A feature of the oxo-species is multiple bonding from oxide to molybdenum which gives rise to a strong characteristic infrared absorption at 900-1000 cm^{-1} .^{1,2}

Mo(IV) complexes featuring a mono oxo unit comprise an important class of compounds.^{3,4} On the one hand, besides of being intrinsically interesting,⁵ such complexes are well documented to act as catalysts for various oxidation processes involving, for instance molecular oxygen.⁶ They are also known to generate hydrogen from water⁷ and are applied in several catalytic reactions such as hydrosilylation⁸ and sulfur transfer to alkenes and allenes.⁹

Moreover, Nature efficiently utilizes the Mo=O unit to achieve difficult multielectron redox catalysis with oxotransferases, which catalyze oxygen atom transfer to and from substrates.¹⁰⁻¹² Accordingly, many mono oxo Mo(IV) compounds are intensively studied with dithiolene-type ligands as mimics for this class of enzymes.¹³⁻¹⁶ High valent Mo=O or M \equiv O species are often generated accidentally by trace amounts of O₂ or water contaminations due to the high affinity of molybdenum towards oxygen.

One catalytic application of molybdenum oxo compounds is the episulfidation of (*E*)-cyclooctene and (*E*)-cyclononene achieved with elemental sulfur (Scheme 6.1).¹⁷



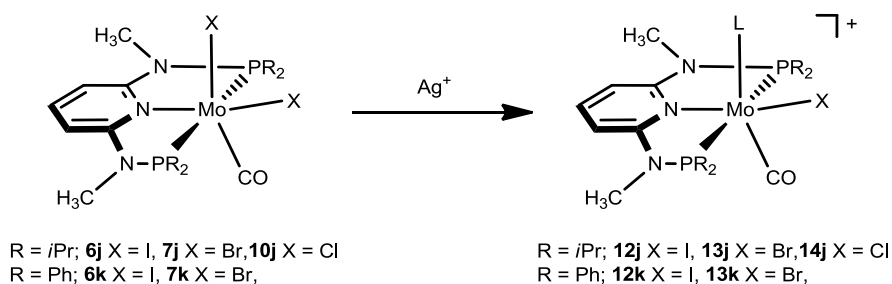
Scheme 6.1. Catalytic sulfur-transfer reaction with (*E*)-cyclooctene and (*E*)-cyclononene

Another example is the activation of molecular oxygen forming a monooxo peroxo Mo(VI) compound. This is achieved with mono oxo Mo(IV) compounds that

contain a bis(β -ketiminato) ligand. This research, reported by Mösch-Zanetti and coworkers, represents a new entry into molybdenum peroxo derivatives.¹⁸

6.3. Results and discussion

Treating of the $[\text{Mo}(\text{PNP}^{\text{Me}}-i\text{Pr})(\text{CO})(\text{X})_2]$ ($\text{X} = \text{I}$ (**6j**), Br (**7j**), Cl (**10j**)) and $[\text{Mo}(\text{PNP}^{\text{Me}}-\text{Ph})(\text{CO})_2(\text{X})_2]$ ($\text{X} = \text{I}$ (**6k**), Br (**7k**)) (Chapter 5) with silver salt (AgSbF_6 or AgCF_3SO_3) in a coordinating solvent such as CH_3CN , THF or Acetone led to the immediate precipitation of AgX (Scheme 6.2.). Subsequent the formation of the bluish-green cationic 16e-complexes $[\text{Mo}(\text{PNP}^{\text{Me}}-i\text{Pr})(\text{CO})(\text{L})(\text{X})]^+$ ($\text{L} = \text{solvent}$; $\text{X} = \text{I}, \text{Br}, \text{Cl}$) was achieved, although the complexes with the $\text{PNP}^{\text{Me}}-\text{Ph}$ ligand provide different compounds.



Scheme 6.2. Synthesis of cationic complexes $[\text{Mo}(\text{PNP}^{\text{Me}}-\text{R})(\text{CO})(\text{L})(\text{X})]^+$ ($\text{R} = i\text{Pr}, \text{Ph}$; $\text{L} = \text{CH}_3\text{CN}, \text{THF}, \text{Acetone}$; $\text{X} = \text{I}, \text{Br}, \text{Cl}$) upon halide abstraction with Ag^+ salts

All complexes are thermally stable both in the solid state and in solution if air is excluded but readily decompose in the presence of oxygen to give several as yet not identified (oxidation) products. The use of non-coordinated solvents such as CH_2Cl_2 also promotes the formation of secondary products. The sensitivity towards oxygen in comparison to precursor complexes may be due to the liability of these complexes which are actually latent 14e systems.

Characterization was accomplished by elemental analysis and by ^1H , $^{13}\text{C}\{^1\text{H}\}$ and $^{31}\text{P}\{^1\text{H}\}$ NMR, IR spectroscopy and elemental analysis. The $^{13}\text{C}\{^1\text{H}\}$ NMR spectrum of **12j**, **13j** and **14j** exhibit the characteristic low-field resonances of the CO ligand as poorly-resolved broad signals at 250.0, 230.1 and 235.0 ppm, respectively. In the $^{31}\text{P}\{^1\text{H}\}$ NMR spectrum of these complexes singlets at 183.3, 179.4 and 186.0 ppm were observed. Due to the decreased electron donor strengths of the molybdenum center, in the cationic complexes **12j**, **13j** and **14j** the CO stretching frequencies are

shifted to higher wavenumbers (1832, 1840 and 1836 cm^{-1}) as compared to those of the neutral compounds **6j**, **7j** and **10j**.

Attempts to crystallize the cationic molybdenum complexes were not so successful. The complex **12j** only provide amorphous crystals, while the complexes **13j** and **14j** from CH_3CN solutions gave large and highly solvated but very unstable crystals for which only a poor crystal structure model could be derived. Even so, it was possible to identify that the coordinated acetonitrile molecule in trans disposition to CO. However if the complex **14j** is crystalized from a THF solution, the CH_3CN ligand was replaced by a THF molecule and the crystal of $[\text{Mo}(\text{PNP}^{\text{Me-}i\text{Pr}})(\text{CO})(\text{THF})\text{Cl}]\text{SbF}_6$ (**14j'**) was obtained (Figure 6.2).¹⁹ This complex features essentially the same coordination geometry like the dihalogenide precursors **6j**, **7j**, and **10j**. Thus, all bond distances involving Mo except for the Mo–OTHF agree within 0.02 Å with those of **10j**, and also bond angles, the distance P1–P2, and other geometric parameters are in good agreement with halocarbonyl precursors.

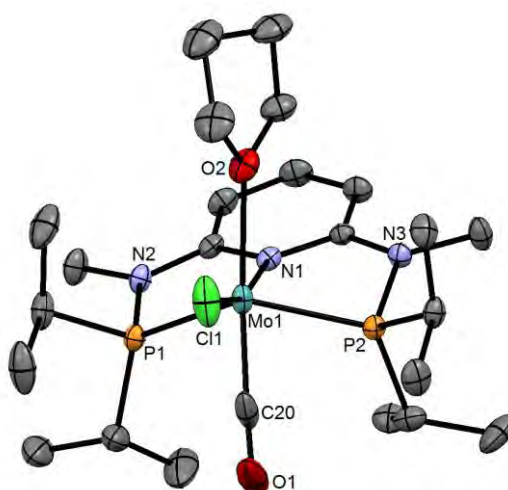


Figure 6.2. Structural view of $[\text{Mo}(\text{PNP}^{\text{Me-}i\text{Pr}})(\text{CO})(\text{THF})\text{Cl}]\text{SbF}_6$ (**14j'**) showing 50% thermal ellipsoids (H atoms and SbF_6^- anion omitted for clarity). Selected bond lengths (Å) and bond angles ($^\circ$): Mo–N(1) 2.260(2), Mo–C(20) 1.913(4), Mo–P(1) 2.3853(9), Mo–P(2) 2.3717(8), Mo–Cl(1) 2.3966(8), Mo–O(2) 2.312(3), P(1)–Mo–P(2) 125.66(4), N(1)–Mo–P(1) 73.80(6), N(1)–Mo–P(2) 71.82(6), N(1)–Mo–Cl(1) 162.97(9), N(1)–Mo–O(2) 80.18(9), N(1)–Mo–C(20) 113.20(14), Cl(1)–Mo–O(2) 83.09(7), Cl(1)–Mo–C(20) 83.79(13), O(2)–Mo–C(20) 165.21(13)

Remembering that the ESI-MS is a technique that enables not only the detection and the study of reaction substrates and products but also short-lived reaction intermediates and decomposition products as they are present in solution. As shown in the Chapter 5, the solutions of **6j**, **7j** and **10j** in CH_3CN and the corresponding

sodium halide in the absence of air signals corresponding to the sodiated complexes $[\text{Mo}(\text{PNP}^{\text{Me}}-i\text{Pr})(\text{CO})\text{X}_2] ([\text{M} + \text{Na}]^+)$ and also $[\text{Mo}(\text{PNP}^{\text{Me}}-i\text{Pr})(\text{CO})\text{X}]^+ ([\text{M} - \text{X}]^+)$ where one halide ligand is dissociated.

However, in the presence of air not only the cationic specie $[\text{Mo}(\text{PNP}^{\text{Me}}-i\text{Pr})(\text{CO})\text{X}]^+ (\mathbf{A}, [\text{M} - \text{X}]^+)$ was detected but additional species which no longer feature a CO ligand, but contain instead one oxygen atom $[\text{Mo}(\text{PNP}^{\text{Me}}-i\text{Pr})(\text{O})\text{X}]^+ (\mathbf{B}, [\text{M} - \text{X} - \text{CO} + \text{O}]^+)$ and two oxygen atoms $[\text{Mo}(\text{PNP}^{\text{Me}}-i\text{Pr})(\text{O})_2\text{X}]^+ (\mathbf{C}$ or $\mathbf{D}, [\text{M} - \text{X} - \text{CO} + 2\text{O}]^+)$, Figure 6.3..

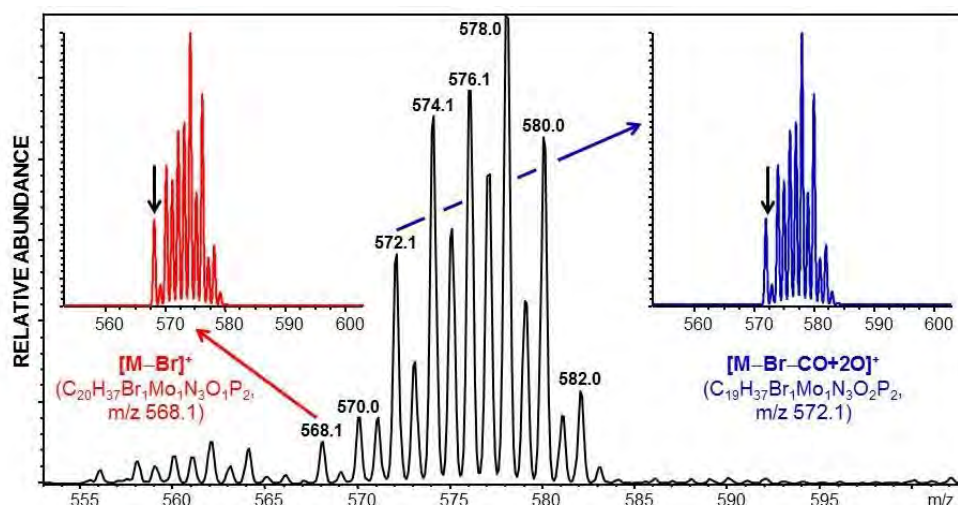


Figure 6.3. Positive-ion ESI-MS of $[\text{Mo}(\text{PNP}^{\text{Me}}-i\text{Pr})(\text{CO})\text{Br}_2]$ in CH_3CN covering the mass region of the $[\text{M} - \text{Br}]^+$ and the $[\text{M} - \text{Br} - \text{CO} + 2\text{O}]^+$ fragments. Insets show the isotope pattern match for $[\text{Mo}(\text{PNP}^{\text{Me}}-i\text{Pr})(\text{CO})\text{Br}]^+ ([\text{M} - \text{Br}]^+)$ and $[\text{Mo}(\text{PNP}^{\text{Me}}-i\text{Pr})(\text{O})_2\text{Br}]^+ ([\text{M} - \text{Br} - \text{CO} + 2\text{O}]^+)$

Additionally, for $\text{X} = \text{I}$ and Br a different dioxo species with the general formula $[\text{Mo}(\text{PNP}^{\text{Me}}-i\text{Pr})(\text{O})_2]^+ (\mathbf{E}, [\text{M} - 2\text{X} + 2\text{O}]^+)$ was detected, presumably due to loss of an iodine and bromine radical, respectively. It is interesting to mention that in the case of $[\text{Mo}(\text{PNP}^{\text{Me}}-i\text{Pr})(\text{CO})\text{I}_2]$ all dioxygen containing fragments as well as the cationic specie were vanished after 24 h to yield among several intractable species the doubly oxidized both protonated and sodiated PNP^{Me}-*i*Pr ligand (m/z 402.2 and 424.2), while the signal of the mono oxo species **B** remained. Positive ion ESI full scan mass spectra is depicted in Figure 6.4..

Identical results are observed for the measurements of the cationic PNP complexes **12j**, **13j** and **14j**, as expected since during reaction was detected several not identified oxidation products in the presence of oxygen.

Chapter 6 – Mono Oxo Molybdenum(IV) PNP Pincer Complexes

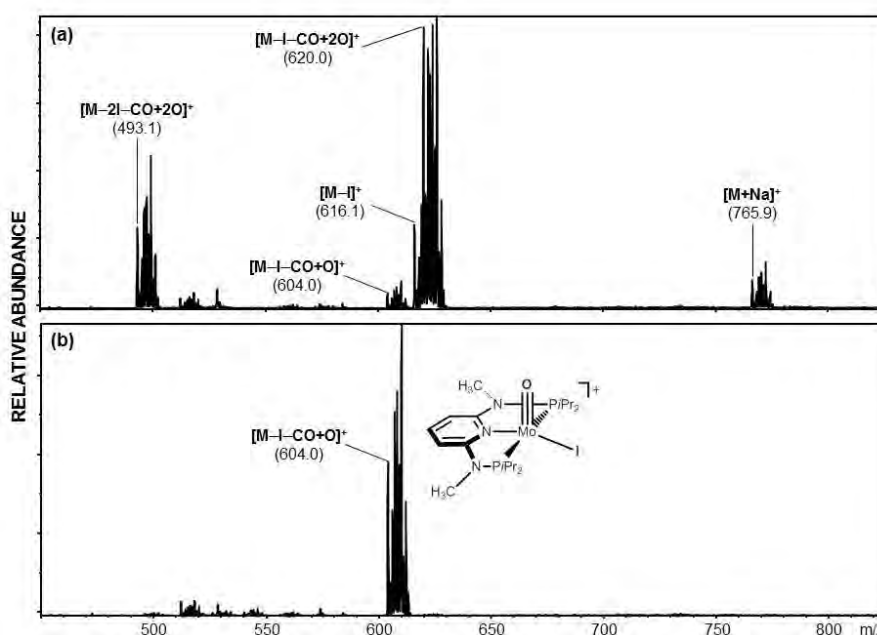
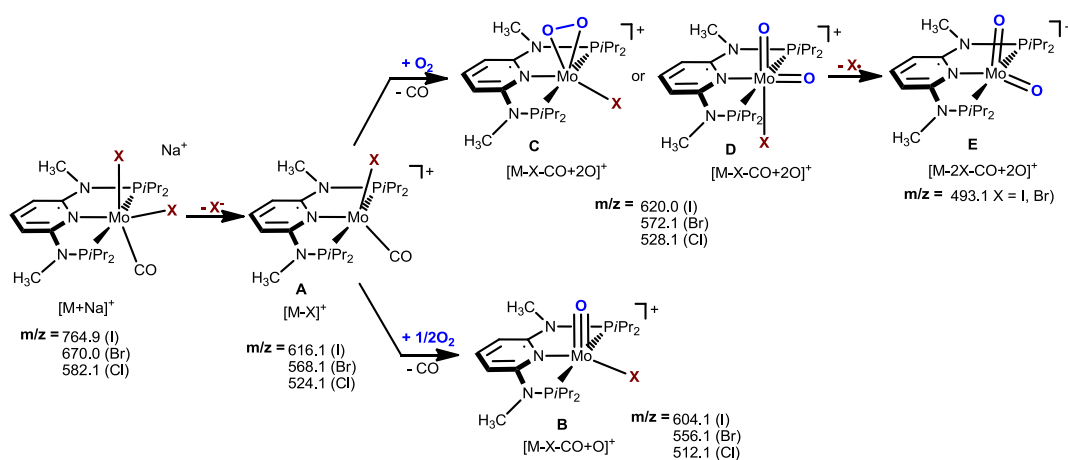


Figure 6.4. (a) Positive-ion full scan ESI-MS of $[\text{Mo}(\text{PNP}^{\text{Me-}i\text{Pr}})(\text{CO})\text{I}_2]$ (**6j**) in CH_3CN in the presence of air after 15 min (b) and after 24 h

Possible structures based on their m/z values are shown in Scheme 6.3.. The formation of **A** is in keeping with the fact that the halide trans to the CO ligand is labile, like is observed experimental. The stability of $[\text{M} - \text{X} - \text{CO} + 2\text{O}]^+$ (**C** or **D**) was further tested in CID (MS/MS) experiments revealing that no O_2 release took place. This observation seems to support the formation of a cis dioxo Mo(VI) complex (**D**) rather than a molybdenum species with a κ^2 -bound O_2 ligand (**C**).



Scheme 6.3. Fragmentation pathways of $[\text{Mo}(\text{PNP}^{\text{Me-}i\text{Pr}})(\text{CO})\text{X}_2]$ in CH_3CN in the presence of molecular oxygen as established by ESI MS experiments. Structural suggestions are based on DFT calculations

Chapter 6 – Mono Oxo Molybdenum(IV) PNP Pincer Complexes

The DFT calculations, employing the cationic complex $[\text{Mo}(\text{PNP}^{\text{Me}}\text{-}i\text{Pr})(\text{CO})\text{Br}]^+$ (**A**) as model system, supports the ESI-MS measurements. The optimized structures and the free energy balances for the reaction steps are depicted in Figure 6.5. The highly unsaturated 14e species $[\text{Mo}(\text{PNP}^{\text{Me}}\text{-}i\text{Pr})(\text{CO})\text{Br}]^+$ is almost equally stable in the triplet state, **3A**, and in the singlet state, **1A** ($\Delta G = 1.8 \text{ kcal mol}^{-1}$). Addition of oxygen to any of those species would lead to the cationic mono oxo Mo(IV) complex $[\text{Mo}(\text{PNP}^{\text{Me}}\text{-}i\text{Pr})(\text{O})(\text{Br})]^+$ (**B**) or to the dioxygen Mo(IV) and Mo(VI) species $[\text{Mo}(\text{PNP}^{\text{Me}}\text{-}i\text{Pr})(\kappa^2\text{-O}_2)(\text{Br})]^+$ (**C**) or *cis*- $[\text{Mo}(\text{PNP}^{\text{Me}}\text{-}i\text{Pr})(\text{O})_2(\text{Br})]^+$ (**1D**), respectively. Complex **C** is slightly more stable in the triplet state (**3C**), while the opposite is observed for the mono oxo species, where **1B** is significantly more stable than **3B** (by $18.5 \text{ kcal mol}^{-1}$). All O_2 addition steps are thermodynamically strongly favored. **1B** and **1D** are the most stable products for each O -stoichiometry, the corresponding reactions being exergonic by 59.9 and $85.9 \text{ kcal mol}^{-1}$, respectively. Also, given the stability differences, the $\kappa^2\text{-O}_2$ species **C** are probably intermediates in the formation of **1D** as the dioxo product.

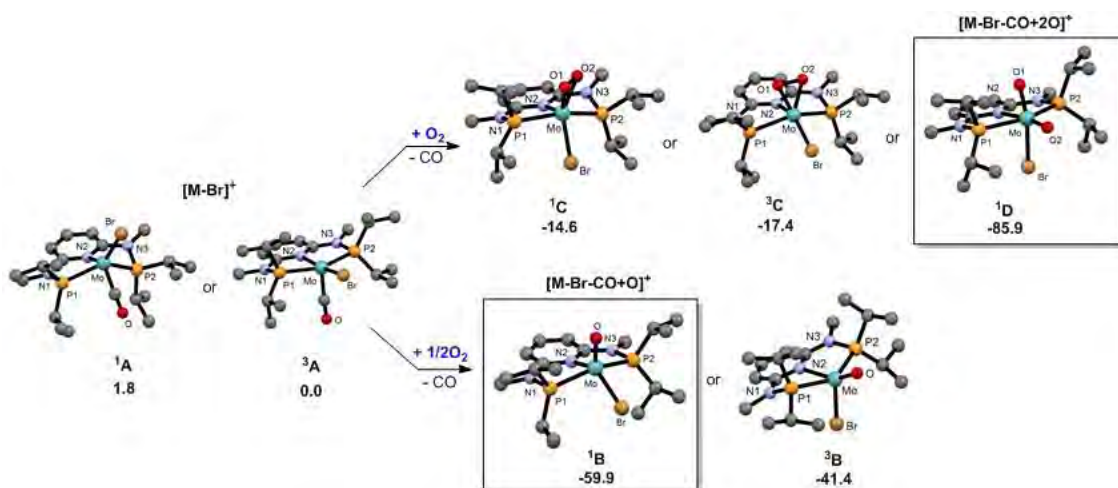


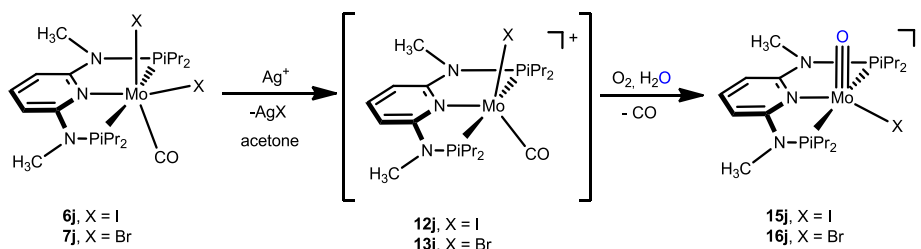
Figure 6.5. Reactions of $[\text{Mo}(\text{PNP}^{\text{Me}}\text{-}i\text{Pr})(\text{CO})\text{Br}]^+$ (**A**) in the presence of air based on ESI-MS experiments and DFT/B3LYP calculations (free energies in kcal mol^{-1})

Accordingly, based on the ESI-MS measurements and the DFT calculations is possible that the predominant **1B** and **1D** are formed if complexes $[\text{Mo}(\text{PNP}^{\text{Me}}\text{-}i\text{Pr})(\text{CO})\text{X}]^+$ are exposed to air, however a full study is extremely necessary. It has to be noted that a related mono oxo Mo(IV) PCP pincer complex was recently formed as side product while synthesizing a Mo(IV) PCP nitride complex.²⁰ Molybdenum complexes with the *cis*- $[\text{MoO}_2]^{2+}$ core, on the other hand, are very common which have found wide applications in organic synthesis due to their oxidation properties.²¹

6.3.1. Mono oxo molybdenum complexes

The preliminary ESI-MS studies and DFT/B3LYP calculations of complexes $[\text{Mo}(\text{PNP}^{\text{Me}}-i\text{Pr})(\text{CO})\text{X}_2]$ (**6j**, **7j**) readily form, *via* the cationic fragments $[\text{Mo}(\text{PNP}^{\text{Me}}-i\text{Pr})(\text{CO})\text{X}]^+$ (**12j**, **13j**), in apparently parallel pathways mono oxo complexes and the presumably dioxo species. It was not clear whether the source of oxygen was molecular oxygen from air, traces of water in the solvent, or both.

The synthesis of cationic coordinately unsaturated mono oxo Mo (IV) complexes of the type $[\text{Mo}(\text{PNP}^{\text{Me}}-i\text{Pr})(\text{O})\text{X}]^+$ (**15j**, **16j**) was achieved after a full research on the reactions condition, i.e. different solvents, times of reactions, different oxygen sources, etc. Ultimately, the oxo complexes are formed through an interplay between water and molecular oxygen, from the $[\text{Mo}(\text{PNP}^{\text{Me}}-i\text{Pr})(\text{CO})\text{X}]^+$ (**12j**, **13j**) prepared *in situ* by reacting $[\text{Mo}(\text{PNP}^{\text{Me}}-i\text{Pr})(\text{CO})\text{X}_2]$ (**6j**, **7j**) with silver salt, or direct form the isolated intermediates (Scheme 6.4.).



Scheme 6.4. Synthesis of mono oxo Mo(IV) complexes

When a solution of $[\text{Mo}(\text{PNP}^{\text{Me}}-i\text{Pr})(\text{CO})\text{X}]^+$ (**12j**, **13j**) in acetone, prepared *in situ* by reacting $[\text{Mo}(\text{PNP}^{\text{Me}}-i\text{Pr})(\text{CO})\text{X}_2]$ (**6j**, **7j**) with AgSbF_6 followed by removal of AgX , is exposed shortly to air and subsequently treated with an excess of water, the cationic mono oxo complexes $[\text{Mo}(\text{PNP}^{\text{Me}}-i\text{Pr})(\text{O})\text{X}]^+$ (**15j**, **16j**) are afforded in 72 and 66% isolated yields. These complexes were characterized by a combination of elemental analysis, ^1H , $^{13}\text{C}\{^1\text{H}\}$, and $^{31}\text{P}\{^1\text{H}\}$ NMR, IR and ESI-MS. Characteristic are the $\text{Mo}\equiv\text{O}$ stretching frequencies at 955 and 940 cm^{-1} , respectively. In the ESI-MS the most abundant signals are observed at m/z 604.1 and 556.1, respectively, which correspond to the intact complexes ($[\text{M}]^+$).

NMR and IR monitoring of the reaction with **6j** after addition of the halide scavenger revealed the immediate formation of **12j**. This intermediate gives rise to a signal at 183.3 ppm in the $^{31}\text{P}\{^1\text{H}\}$ NMR spectrum and exhibits one strong ν_{CO} band at 1832 cm^{-1} (*cf* 1824 cm^{-1} in **6j**). Upon admission of air and addition of water, a new resonance at 149.2 ppm was observed due to the formation of **15j**. In addition, small

Chapter 6 – Mono Oxo Molybdenum(IV) PNP Pincer Complexes

amounts (ca 8%) of the known tricarbonyl complex $[\text{Mo}(\text{PNP}^{\text{Me-}i\text{Pr}})(\text{CO})_3\text{I}]^{+\ast}$ are formed as side product due to reaction of **12j** with CO, which is released during the oxidation process. Another two extra compounds are found in small quantities (ca 10%) at 78.9 and 73.7 ppm. The same observations are found for the complex **16j**.

The solid state structure of **15j** was determined by single-crystal X-ray diffraction and is depicted in Figure 6.6.. This complex **15j** is best described as having a pseudo square pyramidal structure. The Mo1-O1 bond distance of 1.663(2) Å comparatively short but in the typical range for a $\text{Mo}\equiv\text{O}$ triple bond.^{13b,15,22-24}

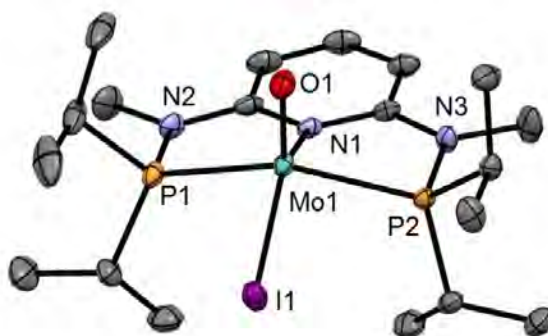


Figure 6.6. Structural diagram of $[\text{Mo}(\text{PNP}^{\text{Me-}i\text{Pr}})(\text{O})\text{I}]\text{SbF}_6$ (**15j**) showing 50%-ellipsoids (hydrogen atoms and SbF_6^- counterion omitted for clarity). Selected bond distances and angles (Å, deg): Mo1-O1 1.663(2), Mo1-N1 2.143(2), Mo1-P2 2.4413(8), Mo1-P1 2.4455(8), Mo1-I1 2.7359(4), O1-Mo1-N1 108.67(11), O1-Mo1-P2 104.89(8), O1-Mo1-P1-107.02(8), P2-Mo1-P1 144.81(3), O1-Mo1-I1 108.40(9), N1-Mo1-I1 142.92(6)

In the several attempts to crystallize the $[\text{Mo}(\text{PNP}^{\text{Me-}i\text{Pr}})(\text{O})\text{X}]^+$ (**15j**) complex, another compound was formed in CHCl_3 (Figure 6.7.) that correspond to the observed $^{31}\text{P}\{^1\text{H}\}$ NMR peak at 73.7 ppm. Unfortunately, the analogous bromide complex was not successful crystallize.

* Illustrated in chapter 5

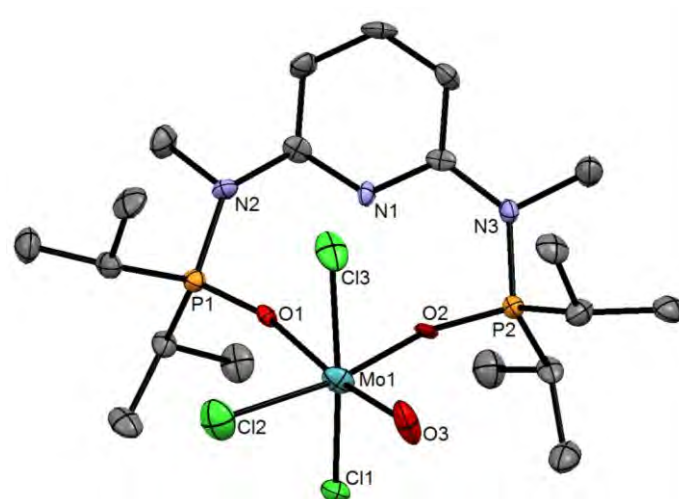


Figure 6.7. Structural diagram of $[\text{Mo}(\text{PONOP}^{\text{Me}}\text{-}i\text{Pr})(\text{O})\text{Cl}_3]\text{SbF}_6$ (**15j'**) showing 50%-ellipsoids (hydrogen atoms and SbF_6^- counterion omitted for clarity). Selected bond distances and angles (\AA , deg): Mo1-O1 2.212(4), Mo1-O2 2.078(4), Mo1-O3 1.724(5), Mo1-Cl1 2.369(2), Mo1-Cl2 2.287(2), Mo1-Cl3 2.368(2), Cl1-Mo1-Cl3 166.79(7), O1-Mo1-O2 76.0(2), Cl2-Mo1-O3 100.3(2), Cl3-Mo1-O3 96.1(2)

Concerning the frontier orbitals of **15j** (Figure 6.8.), the pattern obtained is typical of a d^2 -metal complex with a square planar (SP) geometry.²¹ The HOMO can be seen as the xy orbital (the z axis being defined by the Mo–O bond) and the LUMO is mostly centered in the ligand pyridine ring. The two following orbitals (LUMO+1 and LUMO+2) are based on metal yz and xz , respectively (see Figure 6.9). Those are Mo–O π^* orbitals and, thus, are the two empty antibonding counterparts of π -donation from the oxo ligand to the metal, indicating a Mo \equiv O triple bond. Finally, the two upper orbitals in Figure 6.8. are based on the metal z^2 and x^2-y^2 .

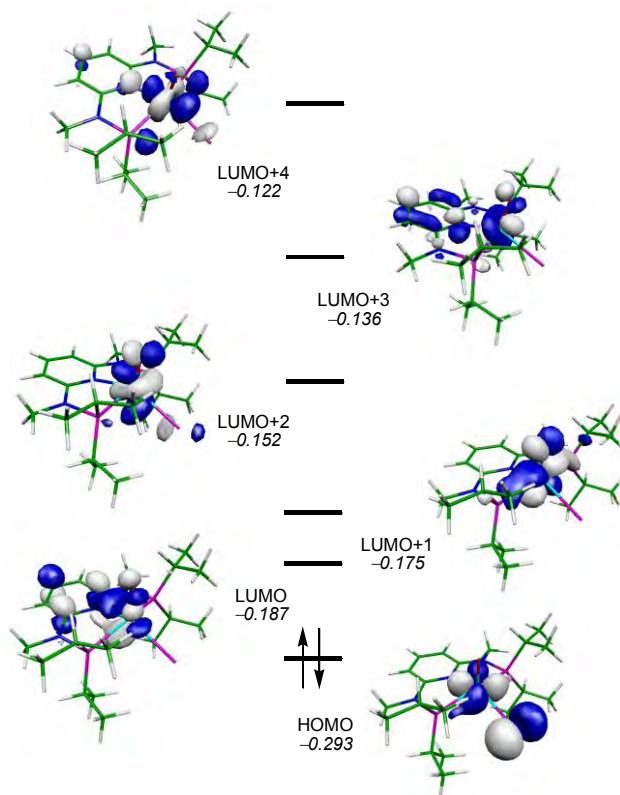


Figure 6.8. Frontier orbitals (*d*-splitting) of $[\text{Mo}(\text{PNP}^{\text{Me-}i\text{Pr}}(\text{O}))\text{I}]^+$ (**15j**). Orbital energy values in atomic units

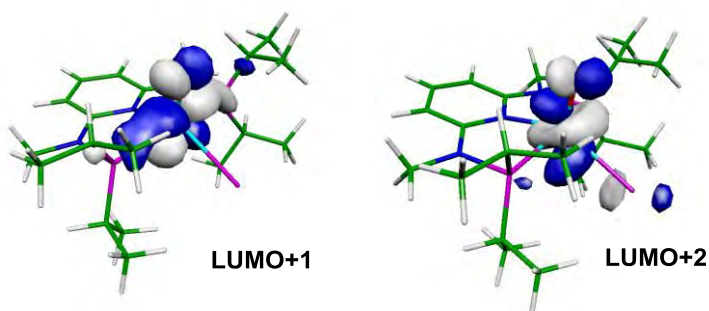


Figure 6.9. Mo–O π^* orbitals of complex $[\text{Mo}(\text{PNP}^{\text{Me-}i\text{Pr}}(\text{O}))\text{I}]^+$ (**15j**)

In order to evaluate the role of H_2O or O_2 as a source of oxygen, solutions of **6j** in CH_3CN were subjected to ESI-MS analysis in the positive ion mode in the presence of H_2^{18}O and $^{18}\text{O}_2$, respectively (Figure 6.10., for simulated spectra see Figure 6.11.). In the case of H_2^{18}O a significantly higher amount of ^{18}O was incorporated compared to $^{18}\text{O}_2$ (rough estimation 90% vs 50%). There was little $^{18}\text{O}/^{16}\text{O}$ isotope back exchange

Chapter 6 – Mono Oxo Molybdenum(IV) PNP Pincer Complexes

observed in the case of water due to the higher concentration of H_2^{18}O present in contrast to $^{18}\text{O}_2$ in air.

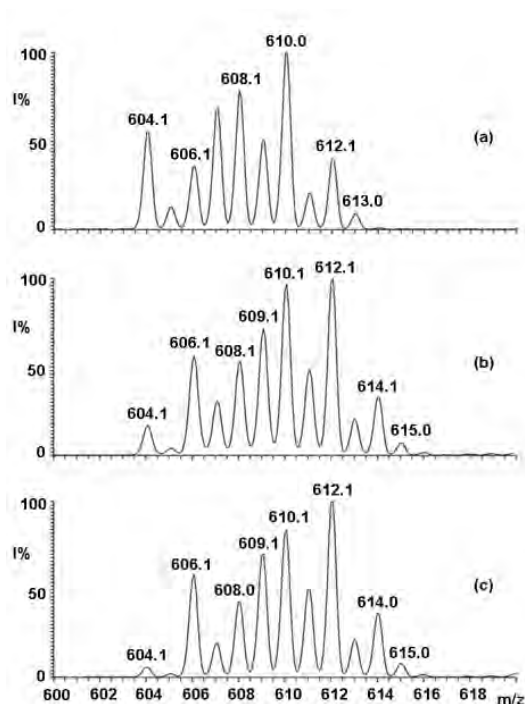


Figure 6.10. Part of the positive-ion ESI-MS spectra of $[\text{Mo}(\text{PNP}^{\text{Me-}i\text{Pr}})(\text{CO})\text{I}_2]$ (**6j**) in CH_3CN : (a) in the presence of air, (b) in the presence of $^{18}\text{O}_2$, (c), in the presence of H_2^{18}O

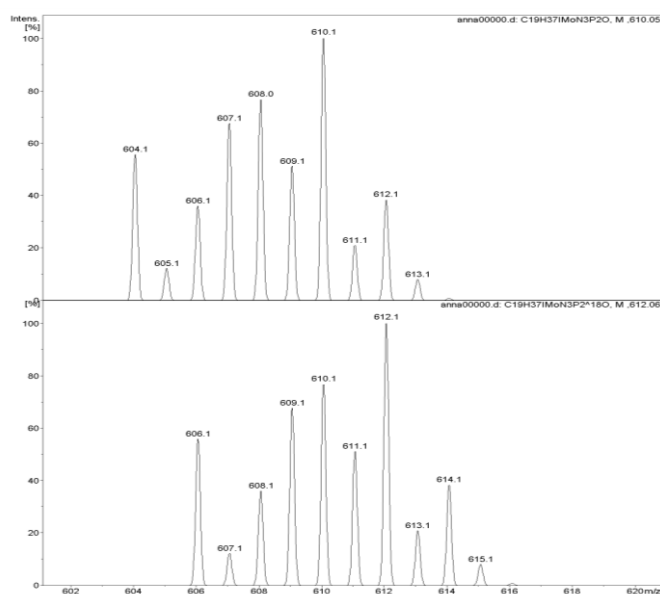
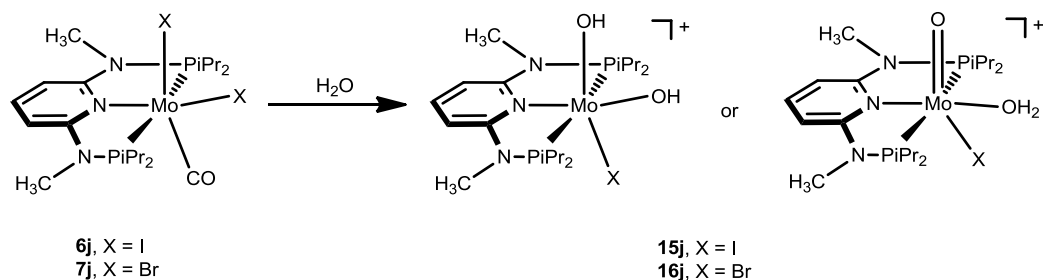


Figure 6.11. Expected isotopic pattern from the simulated spectra of $[\text{Mo}(\text{PNP}^{\text{Me-}i\text{Pr}})(\text{O})\text{I}_2]^+$ (**13j**): $\text{C}_{19}\text{H}_{37}\text{IMoN}_3\text{OP}_2$ (upper spectrum) and $\text{C}_{19}\text{H}_{37}\text{IMoN}_3^{18}\text{OP}_2$ (lower spectrum)

Chapter 6 – Mono Oxo Molybdenum(IV) PNP Pincer Complexes

In an attempt to get further mechanistic insights, in particular the role of water, the reaction of $[\text{Mo}(\text{PNP}^{\text{Me-}i\text{Pr}})(\text{CO})\text{X}_2]$ ($\text{X} = \text{I}, \text{Br}$) with water in the absence of oxygen was performed. Complexes which were tentatively assigned as *bis* hydroxo $[\text{Mo}(\text{PNP}^{\text{Me-}i\text{Pr}})(\text{OH})_2\text{X}]^+$ or mono oxo aquo $[\text{Mo}(\text{PNP}^{\text{Me-}i\text{Pr}})(\text{H}_2\text{O})(\text{O})\text{X}]^+$ (**15j** and **16j**) were obtained but could not be unequivocally characterized and obtained in pure form (Scheme 6.5.). Attempts to crystallize any of these complexes were unsuccessful.



Scheme 6.5. Reaction of $[\text{Mo}(\text{PNP}^{\text{Me-}i\text{Pr}})(\text{CO})\text{X}_2]$ ($\text{X} = \text{I}, \text{Br}$) with water

From IR spectroscopy it was apparent that the carbonyl ligand was no longer present. In the $^{31}\text{P}\{^1\text{H}\}$ NMR spectrum of singlets were observed suggesting that the phosphines are equivalent and that the oxidation state of the metal is Mo(II) or Mo(IV). The ^1H NMR spectrum shows two signals at 14.21, 8.84 ppm (**15j**) and 14.18, 9.54 ppm (**16j**) which disappeared upon addition of D_2O consistent with an OD^- or a D_2O exchange.

The molybdenum complexes were also characterized by means of ESI-MS. This study revealed that under so called “soft ionization” conditions the most abundant signals are observed at m/z 604.1 and 555.9 which correspond to the oxo complexes $[\text{Mo}(\text{PNP}^{\text{Me-}i\text{Pr}})(\text{CO})\text{X}]^+$ ($\text{X} = \text{I}, \text{Br}$). Moreover, a fragment with m/z 525.9 for both complexes was detected which may correspond to a $[\text{Mo}(\text{ONO}^{\text{Me-}i\text{Pr}})(\text{O})\text{OH}]^+$ fragment with no halide being coordinated and both phosphine moieties being oxidized to $\text{R}_2\text{P}=\text{O}$ units. Further fragmentation also reveals the loss of m/z 134 which indeed corresponds to a $\text{R}_2\text{P}=\text{O}$ unit.

Based on our observation a mechanistic of formation of the mono-oxo complex was studied with DFT calculations and the resulting free energy profiles are represented in Figures 6.12. and 6.13..

Chapter 6 – Mono Oxo Molybdenum(IV) PNP Pincer Complexes

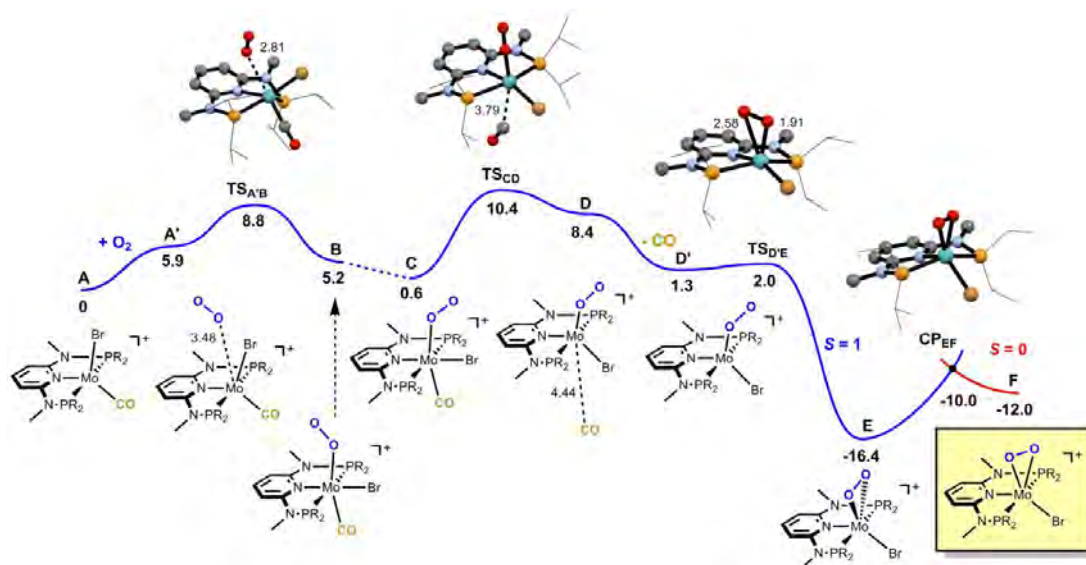


Figure 6.12. Free energy profile calculated for the oxidation of complex **A**. The free energy values (kcal/mol) are referred to the initial reactants (**A** + O₂) and relevant distances (Å) are presented

The mechanism starts with intermediate **13j** (**A** in the profile), formed after Br⁻ removal from the initial reactant, **7j**. Dissociation of the CO ligand directly from **13j** proved to be unfavorable, with $\Delta G = 34$ kcal/mol. Alternatively, O₂ coordination to **A** is a rather facile process. The reaction proceeds along the spin triplet Potential Energy Surface (PES), O₂ being a triplet, and starts with **A'**, the pair of reactants, **13j** and O₂, producing a superoxo complex, **B**, with O₂ and CO occupying opposite coordination positions, and Br *trans* to the pyridine N-atom. The energy barrier is 8.8 kcal/mol (TS_{A'B}) and after re-orientation of the O₂ ligand, from **B** to **C**, the process is practically thermoneutral with respect to the initial reagents (**C** is only 0.6 kcal/mol less stable than the separated reactants, **A**). In the transition state, TS_{A'B}, the new Mo–O bond is only incipient with a distance of 2.81 Å, still far from the coordination distance of 2.05 Å, observed in **B**.

The second part of the mechanism corresponds to CO dissociation. Loss of the CO ligand, from **C**, has a barrier of 9.8 kcal/mol (TS_{CD}) and yields a coordinatively unsaturated species, with the O₂ ligand and the halide, beside the PNP ligand, in **D** and **D'**. The transition state, TS_{CD}, is a late one with a Mo–C(CO) separation of 3.79 Å, and the entire process, from **C** to **D'**, is again essentially thermoneutral ($\Delta G = 0.7$ kcal/mol).

From **D'** there is coordination of the dangling O-atom with formation of a peroxide κ^2 -O₂ ligand, corresponding to an oxidative addition, with the metal changing from Mo(II) in **D'** and in the previous species, to Mo(IV) in **E**. This is a very easy

Chapter 6 – Mono Oxo Molybdenum(IV) PNP Pincer Complexes

process with a barrier of only 0.7 kcal/mol ($TS_{D/E}$) and, in the transition state, the new Mo–O bond is still far from being formed with a distance of 2.58 Å, significantly longer than the Mo–O bonds in **E** ($d = 1.97$ Å). Formation of the peroxide complex is thermodynamically favorable, **E** being 16.4 kcal/mol more stable than the initial reagents.

The reaction path proceeds, from **E** to **F**, with a change in spin state, from triplet ($S = 1$) to singlet ($S = 0$). That corresponds to a “spin-forbidden” or “non-adiabatic” reaction and, thus, its profile goes through a minimum-energy crossing point (MECP) of the two potential energy surfaces (PES) involved.²⁵ In this MECP both the energy as well as the geometry of the molecule are the same in the two surfaces. Once that point is reached, following the reaction coordinate, there is a given probability for the system to change spin state and hop from one PES to the other and, thus, give rise to the “spin-forbidden” reaction.²⁶ The barrier calculated for the spin change of **E** is only 6.4 kcal/mol ($CP_{E/F}$) but the spin singlet intermediate, **F**, is 4.4 kcal/mol less stable than its high spin counterpart, and, thus this corresponds to a rather facile but noticeably endergonic step.

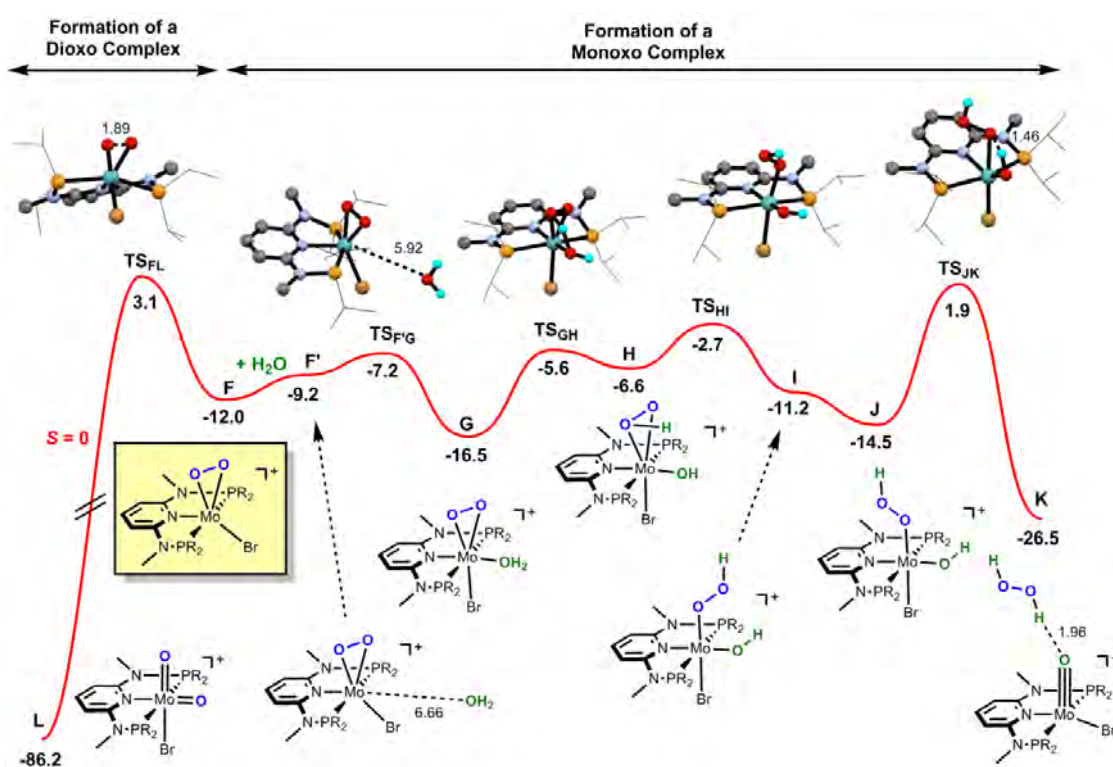


Figure 6.13. Free energy profile calculated for the competitive formation of mono- and dioxo complexes **K** and **L**, respectively. The free energy values (kcal/mol) are referred to the initial reactants (**A** + O_2) and relevant distances (Å) are presented

Following intermediate **F**, the reaction profile proceeds along the spin singlet PES and is depicted in Figure 6.13.. There are two alternative paths. In one case, there is scission of the O–O bond in **F** (marked in Figure 6.13.) originating another oxidative addition process that leads to the di-oxo Mo(VI) complex **L**. This is a single-step process represented on the left side of the profile in Figure 6.13., being highly exergonic as the product, **L**, is 86.2 kcal/mol more stable than the initial reagents (**A**). The barrier associated with this step is 15.1 kcal/mol and, in the corresponding transition state, **TS_{FL}**, the O–O is already clearly elongated ($d_{\text{O-O}} = 1.89 \text{ \AA}$), when compared to the distance present in intermediate **F** ($d_{\text{O-O}} = 1.47 \text{ \AA}$).

Alternatively, there may be water addition to **F** in the four-step process represented to the right of that intermediate in the profile of Figure 6.13. Coordination of water to **F** is a facile process with a barrier of only 4.8 kcal/mol. The corresponding transition state, **TS_{FG}**, is an early one with the incoming water molecule quite remote from the metal centre ($d_{\text{Mo-O}} = 5.92 \text{ \AA}$), but the process is exergonic since the resulting water adduct (**G**) is 7.3 kcal/mol more stable than the pair $\text{H}_2\text{O} + [\text{Mo}(\text{PNP}^{\text{Me-}i\text{Pr}})(\kappa^2\text{-O}_2)(\text{Br})]^+$ (in **F'**). In **G**, there is a pseudo-octahedral coordination around the metal with the O_2 and the halide in opposite positions, and the water *trans* to pyridine N-atom.

From **G** to **H** there is H-transfer from the water to the O_2 ligand, transforming the peroxide into a hydroperoxide $\kappa^2\text{-OOH}$ ligand. This process has a barrier of 10.9 kcal/mol and is clearly endergonic ($\Delta G = 9.9 \text{ kcal/mol}$). In the transition state, **TS_{GH}**, the new O–H bond is almost formed ($d = 1.14 \text{ \AA}$) while the former one, H–O (water) is practically broken ($d = 1.32 \text{ \AA}$).

From **H** to **I** the hydroperoxide goes from $\kappa^2\text{-}$ to $\kappa^1\text{-}$ coordination with the breaking of one Mo–O bond in a facile process with a barrier of 3.9 kcal/mol. In the corresponding transition state, **TS_{HI}**, the Mo–O distance (2.68 \AA) is already 0.46 \AA longer than the one existing in the $\kappa^2\text{-HOO}$ intermediate, **H**.

From **I** to **J** there is a re-orientation of the $\kappa^1\text{-HOO}$ ligand and, then in a final step takes place H-transfer from the hydroxo ligand to the second O-atom in HCOO, forming hydrogen peroxide and the mono-oxo complex, $[\text{Mo}(\text{PNP}^{\text{Me-}i\text{Pr}})(\text{O})(\text{Br})]^+$, in **K**. In the corresponding transition state, **TS_{JK}**, the new O–H bond is still far from formed ($d = 1.46 \text{ \AA}$) and the H–O(OH) bond is practically intact ($d = 1.07 \text{ \AA}$), only 0.1 \AA longer than the one present in intermediate **J**. Also, in **TS_{JK}**, the OOH ligand is starting to decoordinate, the Mo–O distance being 0.33 \AA longer than the one existing in **J**, in the process that will lead to the release of one H_2O_2 molecule, in **K**. This last step has a barrier of 16.4 kcal/mol and is clearly exergonic with $\Delta G = -12.0 \text{ kcal/mol}$, resulting in a final product 26.5 kcal/mol more stable than **A**.

In the formation of the mono-oxo complex (from **F** to **K**) the less stable transition state is the last one, **TS_{JK}**, with a free energy 1.9 kcal/mol above the initial reactants. On the other hand, **TS_{FL}**, the transition state associated with the formation of the di-oxo product (from **F** to **L**) has an energy of 3.1 kcal/mol, relative to **A**. Although the difference between the total barriers of the two paths is only 1.2 kcal/mol and, thus, they can be considered competitive, formation of the mono-oxo complex $[\text{Mo}(\text{PNP}^{\text{Me-}i\text{Pr}})(\text{O})(\text{Br})]^+$, in **K**, following water addition to the intermediate with a κ^2 -peroxide ligand (**F**) is slightly more favorable than O–O splitting with formation of the corresponding di-oxo species $[\text{Mo}(\text{PNP}^{\text{Me-}i\text{Pr}})(\text{O})_2(\text{Br})]^+$ (**L**). Importantly, in the calculated mechanism the O-ligand in the final complex is originated from the incoming water molecule, in agreement with the experimental results obtain with H_2^{18}O .

6.4. Conclusions

In sum, we have prepared and fully characterized new cationic Mo pincer complexes of the type $[\text{Mo}(\text{PNP}^{\text{Me-}i\text{Pr}})(\text{CO})\text{X}]^+$ ($\text{X} = \text{I}, \text{Br}, \text{Cl}$) featuring the PNP pincer ligand N,N'-bis(diisopropylphosphino)-N,N'-dimethyl-2,6-diaminopyridine ($\text{PNP}^{\text{Me-}i\text{Pr}}$).

The preliminary ESI MS studies and DFT/B3LYP calculations support that one halide ligand in $[\text{Mo}(\text{PNP}^{\text{Me-}i\text{Pr}})(\text{CO})\text{X}_2]$ is labile to give the cationic formally 14e fragments $[\text{Mo}(\text{PNP}^{\text{Me-}i\text{Pr}})(\text{CO})\text{X}]^+$ which are able to react with molecular oxygen in parallel pathways to yield mono and dioxo Mo(IV) and Mo(VI) species. A detailed experimental and theoretical study in order to establish the nature of these oxygen containing molybdenum species and the mechanisms of the corresponding reactions are currently underway and results will be reported in due course.

The new cationic mono oxo Mo (IV) PNP complexes of the type $[\text{Mo}(\text{PNP}^{\text{Me-}i\text{Pr}})(\text{O})\text{X}]^+$ ($\text{X} = \text{I}, \text{Br}$). These compounds are coordinatively unsaturated and feature a strong Mo–O triple bond. The bonding mode of the oxo ligand is as also supported by DFT calculations. The formation of these complexes requires the interplay between water and molecular oxygen. ESI MS measurements with ^{18}O labeled water (H_2^{18}O) and molecular oxygen ($^{18}\text{O}_2$) reveal that the oxygen of the $\text{Mo}\equiv\text{O}$ unit is originated from water. The X-ray structure of $[\text{Mo}(\text{PNP}^{\text{Me-}i\text{Pr}})(\text{O})]\text{SbF}_6$ is presented. Currently detailed experimental and theoretical studies are underway in order to establish a reasonable mechanism for the formation of mono as well as dioxo molybdenum complexes and to explain the $^{18}\text{O}/^{16}\text{O}$ isotope scrambling.

6.5. Experimental part

The precursor complexes $[\text{Mo}(\text{PNP}^{\text{Me-}i\text{Pr}})(\text{CO})(\text{X})_2]$ ($\text{X} = \text{Br}, \text{I}, \text{Cl}$) were prepared according to Chapter 5.

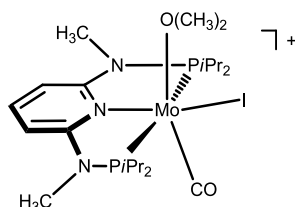
6.5.1. Syntheses

Synthesis of the cationic metal complexes: A solution of $[\text{Mo}(\text{PNP}^{\text{Me-}i\text{Pr}})(\text{CO})(\text{X})_2]$ ($\text{X} = \text{I}, \text{Br}, \text{Cl}$; 0.46 mmol) in CH_3CN , THF or Acetone (10 mL) was reacted with AgSbF_6 or AgCF_3SO_3 (0.46 mmol) and the mixture was stirred for 16 h. After filtration over glass wool and Celite, the solvent was removed under reduced pressure and a blue-green solid was obtained which was washed twice with diethyl ether (10 mL) and dried under vacuum.

Synthesis of the oxo-metal complexes: A solution of $[\text{Mo}(\text{PNP}^{\text{Me-}i\text{Pr}})(\text{CO})\text{X}_2]$ (0.15 mmol) in acetone (10 mL) was reacted with AgSbF_6 (0.15 mmol) and the mixture was stirred for 4 h. After filtration over glass wool and Celite, the solution was exposed to air for 2 min and an excess of H_2O (3 mL, 0.17 mol) was added. 30 minutes later the solution was filtrated over glass wool and Celite and the solvent was removed under reduced pressure and a green solid was washed twice *n*-pentane and then dried under vacuum.

Synthesis of the aquo-metal complexes: A solution of $[\text{Mo}(\text{PNP}^{\text{Me-}i\text{Pr}})(\text{CO})(\text{X})_2]$ ($\text{X} = \text{I}, \text{Br}$; 0.46 mmol) in acetone was reacted with H_2O (3 mL) and the mixture was stirred for 3h. After filtration over glass wool and Celite, the solvent was removed under reduced pressure and a blue-green solid was obtained which was washed twice with diethyl ether (10 mL) and dried under vacuum.

$[\text{Mo}(\text{PNP}^{\text{Me-}i\text{Pr}})(\text{CO})(\text{O}(\text{CH}_3)_2)]\text{SbF}_6$ (12j).

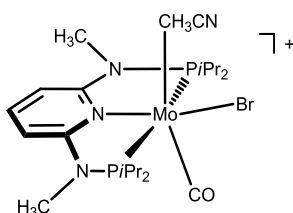


The product was obtained as a green solid in 81.2% (SbF_6); 85.6% (OTf) yield. Anal. Calcd. for $\text{C}_{23}\text{H}_{44}\text{F}_6\text{IMoN}_3\text{O}_2\text{P}_2$ (915.18) (SbF_6): C, 30.18; H, 4.85; N, 4.59. Found: C, 31.20; H, 4.43; N, 4.12. Anal. Calcd. for $\text{C}_{24}\text{H}_{44}\text{F}_3\text{IMoN}_3\text{O}_5\text{P}_2\text{S}$ (828.50) (OTf): C, 34.79; H, 5.35; N, 3.87. Found: C, 33.57; H, 5.01; N, 3.29. $^1\text{H NMR}$ (δ , CD_2Cl_2 , 20 °C): 7.73 (t, $J = 8.2$ Hz, 1H, py^4), 6.33 (d, $J = 8.3$ Hz, 2H, $\text{py}^{3,5}$), 3.13 (d, $J = 3.9$ Hz, 6H, NCH_3),

Chapter 6 – Mono Oxo Molybdenum(IV) PNP Pincer Complexes

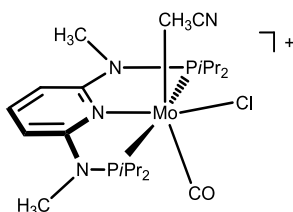
2.90-2.70 (m, 2H, CH), 2.69-2.49 (m, 2H, CH), 1.52-1.36 (m, 6H, CH₃), 1.32-1.12 (m, 12H, CH₃), 0.70-0.56 (m, 6H, CH₃). **¹³C{¹H} NMR (δ, CD₂Cl₂, 20 °C):** 250.0 (t, *J* = 30.0 Hz, CO), 161.1 (vt, *J* = 8.4 Hz, py^{2,6}), 142.0 (py⁴), 99.0 (py^{3,5}), 34.1 (t, *J* = 3.6 Hz, NCH₃), 29.9-29.1 (CH), 22.1-21.3 (CH), 17.4 (vt, *J* = 2.9 Hz, CH₃), 17.2 (CH₃), 16.5 (CH₃), 16.4 (vt, *J* = 4.1 Hz, CH₃). **³¹P{¹H} NMR (δ, CD₂Cl₂, 20 °C):** 183.3. **IR (ATR, cm⁻¹):** 1832 (ν_{CO}).

Mo(PNP^{Me}-iPr)(CO)(CH₃CN)Br]SbF₆ (13j)



The product was obtained as a green solid in 90.0% yield. Anal. Calcd. for C₂₂H₄₀F₆BrMoN₄OP₂Sb (850.14): C, 31.08; H, 4.74; N, 6.59. Found: C, 31.12; H, 4.81; N, 6.62. **¹H NMR (δ, CD₂Cl₂, 20 °C):** 7.65 (t, *J* = 8.0 Hz, 1H, py⁴), 6.40 (d, *J* = 7.5 Hz, 2H, py^{3,5}), 3.12 (s, 6H, NCH₃), 2.80 (br, 2H, CH), 2.67 (br, 2H, CH), 2.20 (s, 3H, NCCH₃), 1.36-1.24 (m, 12H, CH₃), 1.15-1.03 (m, 12H, CH₃). **¹³C{¹H} NMR (δ, CD₂Cl₂, 20 °C):** 230.1 (br, CO), 162.1 (t, *J* = 6.4 Hz, py^{2,6}), 143.6 (py⁴), 132.4 (NCCH₃), 99.0 (py^{3,5}), 34.6 (NCH₃), 30.7 (d, *J* = 27.0 Hz, CH), 22.1 (d, *J* = 20.1 Hz, CH₃), 17.5 (CH₃), 17.2 (CH₃), 17.3 (CH₃), 15.7 (NCCH₃). **³¹P{¹H} NMR (δ, CD₂Cl₂, 20 °C):** 179.4. **IR (ATR, cm⁻¹):** 2279 (ν_{CN}), 1840 (ν_{CO}). **ESI-MS (m/z, CH₃CN) positive ion:** 568.1 [M - Br]⁺.

[Mo(PNP^{Me}-iPr)(CO)(CH₃CN)Cl]SbF₆ (14j)

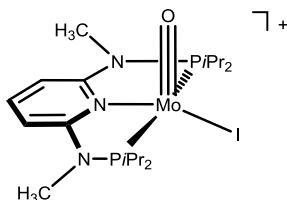


The product was obtained as a green solid in 90.0% yield. Anal. Calcd for C₂₂H₄₀ClF₆MoN₄OP₂Sb (806.67): C, 32.80; H, 5.00; N, 6.95. Found: C, 32.85; H, 4.89; N, 7.02. **¹H NMR (δ, CDCl₃, 20 °C):** 7.79 (t, *J* = 8.1 Hz, 1H, py), 6.48 (d, *J* = 8.1 Hz, 2H, py), 3.65 (s, 6H, NCH₃), 3.26 (br, 2H, CH), 2.85 (br, 2H, CH), 2.23 (s, 3H, NCCH₃), 1.49-1.35 (m, 12H, CH₃), 1.21-1.11 (m, 12H, CH₃). **¹³C{¹H} NMR (δ, CD₂Cl₂, 20 °C):** 235.0 (br, CO), 162.0 (t, *J* = 7.8 Hz, py^{2,6}), 143.7 (py⁴), 130.0 (NCCH₃), 99.8 (py^{3,5}), 35.2 (NCH₃), 30.7 (d, *J* = 23.6 Hz, CH), 22.5 (d, *J* = 28.8 Hz, CH), 18.0 (CH₃), 17.9

Chapter 6 – Mono Oxo Molybdenum(IV) PNP Pincer Complexes

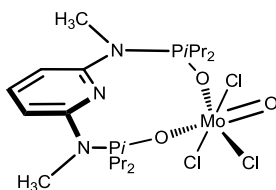
(CH₃), 17.7 (CH₃), 16.1 (CH₃), 15.5 (NCCH₃). ³¹P{¹H} NMR (δ, CD₂Cl₂, 20 °C): 186.0. IR (ATR, cm⁻¹): 2277 (ν_{CN}), 1836 (ν_{CO}). ESI-MS (m/z, CH₃CN) positive ion: 582.1 [M - Cl]⁺.

[Mo(PNP^{Me}-iPr)(O)I]SbF₆ (15j)



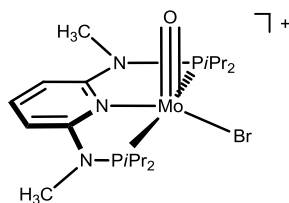
The product was obtained as a green solid in 72.0% yield. Anal. Calcd for C₁₉H₃₇I₁F₆MoN₃OP₂Sb (844.08): C, 27.04; H, 4.43; N, 4.98. Found: C, 26.76; H, 4.12; N, 4.66. ¹H NMR (δ, CD₂Cl₂, 20 °C): 8.05 (tt, *J* = 8.5 Hz, *J* = 1.2 Hz, 1H, py⁴), 6.60 (d, *J* = 8.5 Hz, 2H, py^{3,5}), 3.49-3.33 (m, 2H, CH), 3.33-3.28 (m, 6H, NCH₃), 3.16-2.94 (m, 2H, CH), 1.71-1.53 (m, 6H, CH₃), 1.50-1.36 (m, 6H, CH₃), 1.31-1.17 (m, 6H, CH₃), 0.79-0.63 (m, 6H, CH₃). ¹³C{¹H} NMR (δ, CD₂Cl₂, 20 °C): 165.3 (vt, *J* = 7.4 Hz, py^{2,6}), 148.1 (py⁴), 100.9 (vt, *J* = 3.0 Hz, py^{3,5}), 36.0 (NCH₃), 28.2 (t, *J* = 11.6 Hz, CH), 23.5 (t, *J* = 9.9 Hz, CH), 18.0 (vt, *J* = 5.4 Hz, CH₃), 17.4 (vt, *J* = 2.3 Hz, CH₃), 17.1 (CH₃), 16.6 (CH₃). ³¹P{¹H} NMR (δ, CD₂Cl₂, 20 °C): 149.2. IR (ATR, cm⁻¹): 955 (ν_{M=O}). ESI MS (m/z, CH₃CN) positive ion: [M]⁺ 603.9.

[Mo(PONOP^{Me}-iPr)(O)Cl₃]SbF₆ (15j')



The product was obtained as a red solid. ¹H NMR (δ, CD₂Cl₂, 20 °C): 7.95 (t, *J* = 8.6 Hz, 1H, py⁴), 7.02 (d, *J* = 8.5 Hz, 2H, py^{3,5}), 3.10 (d, *J* = 7.2 Hz, 6H, NCH₃), 2.59-2.37 (m, 4H, CH), 1.38-1.15 (m, 24H, CH₃). ³¹P{¹H} NMR (δ, CD₂Cl₂, 20 °C): 73.7.

[Mo(PNP^{Me}-iPr)(O)Br]SbF₆ (16j)



The product was obtained as a green solid in 66.0% yield. Anal. Calcd for C₁₉H₃₇BrF₆MoN₃OP₂Sb (797.08): C, 28.63; H, 4.68; N, 5.27. Found: C, 29.02; H, 4.43; N, 4.99. ¹H NMR (δ, CD₂Cl₂, 20 °C): 8.06 (t, *J* = 8.2 Hz, 1H, py⁴), 6.63 (d, *J* = 8.3 Hz, 2H, py^{3,5}), 3.32 (s, 6H, NCH₃), 2.88-2.74 (m, 2H, CH), 2.68-2.56 (m, 4H, CH), 1.76-1.46 (m, 12H, CH₃), 1.44-0.96 (m, 12H, CH₃). ¹³C{¹H} NMR (δ, CD₂Cl₂, 20 °C): 161.9 (vt, *J* = 7.0 Hz, py^{2,6}), 146.6 (py⁴), 101.7 (vt, *J* = 2.6 Hz, py^{3,5}), 36.6 (NCH₃), 31.6 (t, *J* = 12.8 Hz, CH), 29.8 (t, *J* = 8.6 Hz, CH), 20.2 (CH₃), 19.4 (br, CH₃), 18.6 (vt, *J* = 5.8 Hz, CH₃), 17.2 (CH₃). ³¹P{¹H} NMR (δ, CD₂Cl₂, 20 °C): 145.2. IR (ATR, cm⁻¹): 940 (ν_{M=O}). ESI MS (*m/z*, CH₃CN) positive ion: [M]⁺ 555.9.

[Mo(PNP^{Me}-iPr)I(L)_n] (17j)

The product was obtained as a green solid in 68.0% yield. ¹H NMR (δ, CD₂Cl₂, 20 °C): 14.21 (br, 1H), 8.84 (br, 1H), 7.90 (t, *J* = 8.2 Hz, 1H, py⁴), 6.49 (d, *J* = 8.0 Hz, 2H, py^{3,5}), 3.31 (s, 6H, NCH₃), 2.90-2.72 (m, 2H, CH), 2.52-2.34 (m, 2H, CH), 1.66 (dd, *J* = 16.4 Hz, *J* = 7.3 Hz, 12H, CH₃), 1.51-1.23 (m, 12H, CH₃). ¹³C{¹H} NMR (δ, CD₂Cl₂, 20 °C): 161.6 (vt, *J* = 6.3 Hz, py^{2,6}), 144.7 (py⁴), 100.5 (br, py^{3,5}), 36.8 (NCH₃), 36.8 (br, CH), 28.2 (br, CH), 19.8 (br, CH₃), 19.2 (br, CH₃), 18.7 (br, CH₃), 17.7 (br, CH₃). ³¹P{¹H} NMR (δ, CD₂Cl₂, 20 °C): 129.2. ESI MS (*m/z*, CH₃CN) positive ion: [M] 604.1 and [M] 525.9.

[Mo(PNP^{Me}-iPr)Br(L)_n] (18j)

The product was obtained as a green solid in 64.0% yield. ¹H NMR (δ, CD₂Cl₂, 20 °C): 14.18 (br, 1H), 9.54 (br, 1H), 7.70 (t, *J* = 8.4 Hz, 1H, py⁴), 6.31 (d, *J* = 8.4 Hz, 2H, py^{3,5}), 3.14 (br, 6H, NCH₃), 3.02-2.92 (m, 2H, CH), 2.76-2.62 (m, 2H, CH), 1.64-1.42 (m, 12H, CH₃), 1.26-0.90 (m, 12H, CH₃). ¹³C{¹H} NMR (δ, CD₂Cl₂, 20 °C): 161.1 (vt, *J* = 6.5 Hz, py^{2,6}), 143.3 (py⁴), 99.8 (t, *J* = 2.5 Hz, py^{3,5}), 36.7 (NCH₃), 33.0 (br, CH), 28.1 (br, CH), 19.5 (br, CH₃), 19.0 (br, CH₃), 17.8 (br, CH₃), 17.3 (br, CH₃). ³¹P{¹H} NMR (δ, CD₂Cl₂, 20 °C): 128.2. ESI MS (*m/z*, CH₃CN) positive ion: [M] 555.9 and [M] 525.9.

6.6. References

- [1] Astruc, D.; *Organometallic Chemistry and Catalysis*, **2007**, Springer-Verlag Berlin Heidelberg.
- [2] IMOA, "International molybdenum association", <http://www.imoa.info/molybdenum-uses/molybdenum-chemistry-uses/molybdenum-oxidation-states.php>, **2017**
- [3] Nugent, W. A.; Mayer, J. M.; *Metal-Ligand Multiple Bonds*; **1988**, Wiley: New York.
- [4] a) Holm, R. H.; *Chem. Rev.*, **1987**, *87*, 1401-1449; b) Holm, R. H.; *Coord. Chem. Rev.*, **1990**, *100*, 183-221; c) Enemark, J. H.; Young, C. G.; *Adv. Inorg. Chem.*, **1994**, *40*, 1-88; d) Enemark, J. H.; Cooney, J. J. A.; Wang, J. J.; Holm, R. H.; *Chem. Rev.*, **2004**, *104*, 1175-1200.
- [5] Some examples of mono oxo Mo(IV) complexes: a) Lanthier, E.; Bendix, J.; Reber, C.; *Dalton Trans.*, **2010**, *39*, 3695-3705; b) Bendix, J.; Bøgevig, A.; *Inorg. Chem.*, **1998**, *37*, 5992-6001; c) Boyd, I. W.; Spence, J. T.; *Inorg. Chem.*, **1982**, *21*, 1602-1606.
- [6] a) Dupé, A.; Judmaier, M. E.; Belaj, F.; Zangger, K.; Mösch-Zanetti, N. C.; *Dalton Trans.*, **2015**, *44*, 20514-20522; b) Lyashenko, G.; Saischek, G.; Pal, A.; Herbst-Irmer, R.; Mösch-Zanetti, N. C.; *Chem. Commun.*, **2007**, 701-703.
- [7] a) Karunadasa, H. I.; Chang, C. J.; Long, J. R.; *Nature*, **2010**, *464*, 1329-1333; b) Sundstrom, E. J.; Yang, X.; Thoi, V. S.; Karunadasa, H. I.; Chang, C. J.; Long, J. R.; Head-Gordon, M.; *J. Am. Chem. Soc.*, **2012**, *134*, 5233-5242.
- [8] Ziegler, J. E.; Du, G.; Fanwick, P. E.; Abu-Omar, M. M.; *Inorg. Chem.*, **2009**, *48*, 11290-11296.
- [9] Adam, W.; Bargon, R. M.; Schenk, W. A.; *J. Am. Chem. Soc.*, **2003**, *125*, 3871-3876.
- [10] a) Brondino, C. D.; Rivas, M. G.; Romão, M. J.; Moura, J. J. G.; Moura, I.; *Acc. Chem. Res.*, **2006**, *39*, 788-796; b) Romão, M. J.; *Dalton Trans.*, **2009**, 4053-4068; c) Hille, R.; *Dalton Trans.*, **2013**, *42*, 3029-3042; d) Hille, R.; *Chem Rev*, **1996**, *96*, 2757-2816.
- [11] Kaufmann, H. L.; Carroll, P. J.; Burgmayer, S. J. N.; *Inorg. Chem.*, **1999**, *38*, 2600-2606.
- [12] a) Goddard, C. A.; Holm, R. H.; *Inorg. Chem.*, **1999**, *38*, 5389-5398; b) Sung, K. M.; Holm, R. H.; *J. Am. Chem. Soc.*, **2001**, *123*, 1931-1943; c) Lim, B. S.; Holm, R. H.; *J. Am. Chem. Soc.*, **2001**, *123*, 1920-1930.
- [13] a) Sugimoto, H.; Siren, K.; Tsukube, H.; Tanaka, K.; *Eur. J. Inorg. Chem.*, **2003**, 2633-2638; b) Sugimoto, H.; Harihara, M.; Shiro, M.; Sugimoto, K.; Tanaka, K.; Miyake, H.; Tsukube, H.; *Inorg. Chem.*, **2005**, *44*, 6386-6392; c) Sugimoto, H.; Suyama, K.; Sugimoto, K.; Miyake, H.; Takahashi, I.; Hirota, S.; Itoh, S.; *Inorg. Chem.*, **2008**, *47*, 10150-10157.
- [14] Seo, J.; Williard, P. G.; Kim, E.; *Inorg. Chem.*, **2013**, *52*, 8706-8712.
- [15] Baba, K.; Okamura, T.; Suzuki, C.; Yamamoto, H.; Yamamoto, T.; Ohama, M.; Ueyama, N.; *Inorg. Chem.*, **2006**, *45*, 894-901.
- [16] Majumdar, A.; Mitra, J.; Pal, K.; Sarkar, S.; *Inorg. Chem.*, **2008**, *47*, 5360-5364.
- [17] Adam, W.; Bargon, R. M.; *Chem. Commun.*, **2001**, 1910-1911.

Chapter 6 – Mono Oxo Molybdenum(IV) PNP Pincer Complexes

- [18] Lyashenko, G.; Saischek, G.; Pal, A.; Herbst-Irmer, R.; Mösch-Zanetti, N. C.; *Chem. Commun.*, **2007**, 701-703.
- [19] de Aguiar, S. R. M. M.; Öztopcu, Ö.; Stöger, B.; Mereiter, K.; Veiros, L. F.; Pittenauer, E.; Allmaier, G.; Kirchner, K.; *Dalton Trans.*, **2014**, 43, 14669-14679.
- [20] Hebden, T. J.; Schrock, R. R.; Takase, M. K.; Müller, P.; *Chem. Commun.*, **2012**, 48, 1851-1853.
- [21] Kühn, F. E.; Santos, A. M.; Abrantes, M.; *Chem. Rev.*, **2006**, 106, 2455-2475.
- [22] Mayer, J. M.; *Inorg. Chem.*, **1988**, 27, 3899-3903.
- [23] Donahue, J. P.; Goldsmith, C. R.; Nadiminti, U.; Holm, R. H.; *J. Am. Chem. Soc.*, **1998**, 120, 12869-12881.
- [24] Coucouvanis, D.; Hadjikyriacou, A.; Toupadakis, A.; Koo, S.-M.; Draganjac, M.; *Inorg. Chem.*, **1991**, 30, 754-767.
- [25] For excellent reviews on MECP and their location for transition metal complexes, see: a) Harvey, J. N.; Poli, R.; Smith, K. M.; *Coord. Chem. Rev.*, **2003**, 347, 238-239; b) Poli, R.; Harvey, J. N.; *Chem. Soc. Rev.*, **2003**, 32, 1-8.
- [26] Harvey, J. N.; *Phys. Chem. Chem. Phys.*, **2007**, 9, 331-343.

Chapter 7

Molybdenum(III) PNP

Pincer Complexes

Chapter 7 – Molybdenum(III) PNP Pincer Complexes

Although transition metal carbonyl complexes are well-known, a more frequently applied synthetic procedure involves transition metal halides or oxides, synthesized a huge amount of complexes.¹

The halides of molybdenum play an increasing role in the chemistry primarily because of their use as starting materials for a wide range of chemical reactions and preparations. A variety of methods are used to prepare the molybdenum fluorine, chlorides, bromides and iodides compounds in their di-, tri-, penta-, and hexavalent states. Another type of halide precursors are the oxide halides, sulphide-halides and selenide-halides of molybdenum.²

7.1. Molybdenum and tungsten PNP pincer halides

Walton and co-workers described the synthesis of the first molybdenum complex containing the 2,6-bis(dicyclohexylphosphinomethyl)pyridine ligand (PNP). The reaction of $K_4Mo_2Cl_8$, afford the dinuclear molybdenum complex $[Mo_2Cl_4(PNP)(HPCy_2)]$ Figure 7.1..³

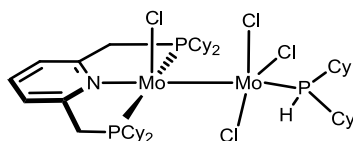
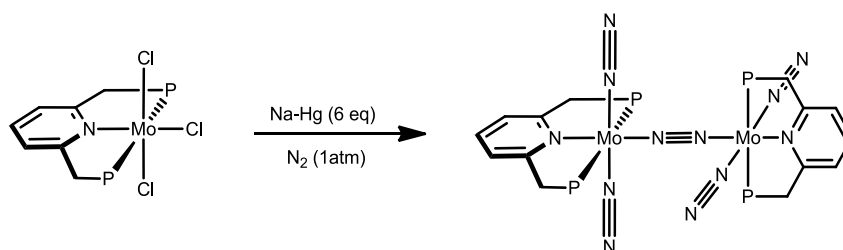


Figure 7.1. The dinuclear molybdenum complex $[Mo_2Cl_4(PNP)(HPCy_2)]$

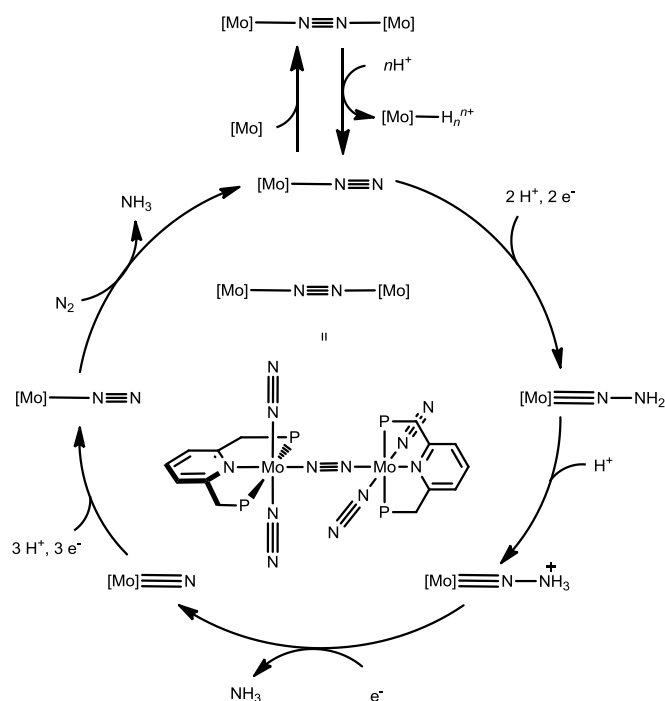
In 2011, Nishibayashi and coworkers reported a diamagnetic dinitrogen-bridged dimolybdenum pincer complex $[Mo_2(N_2)_2(PNP)]_2(\mu-N_2)$ by treatment of $[MoCl_3(PNP)]$ (PNP = 2,6-bis(di-tertbutylphosphinomethyl) pyridine with 6 equiv. of Na–Hg in THF at room temperature for 12 h under an atmospheric pressure of dinitrogen (Scheme 7.1.).⁴



Scheme 7.1. Synthesis of cationic complexes

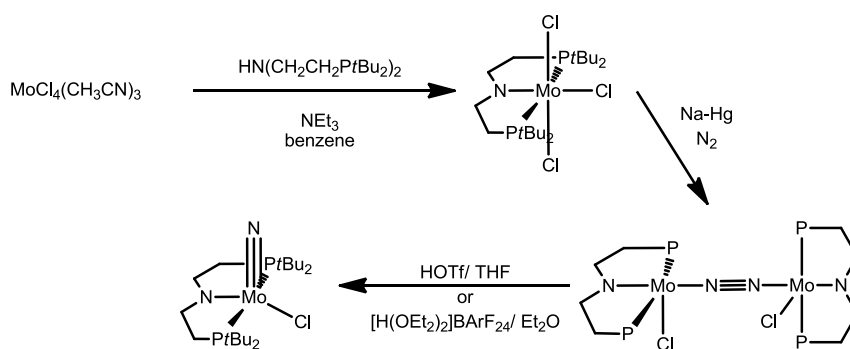
Chapter 7 – Molybdenum(III) PNP Pincer Complexes

This complex works as an effective catalyst for the reduction of dinitrogen to ammonia with 23 equiv. of ammonia being produced with the catalyst (12 equiv. of ammonia are produced based on the molybdenum atom of the catalyst) (Scheme 7.2.).



Scheme 7.2. Reaction pathway for catalytic conversion of dinitrogen into ammonia in the presence of Mo catalyst

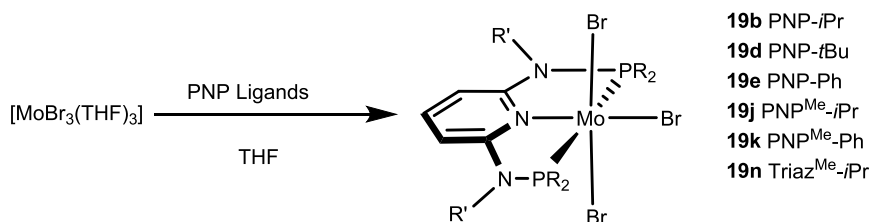
Another example of N_2 splitting catalyzed by a pincer complex was reported in 2017 by Schneider and coworkers. The new molybdenum PNP pincer complex (PNP = $\text{N}(\text{CH}_2\text{CH}_2\text{P}^t\text{Bu}_2)_2$) was achieved by reduction of the molybdenum(IV) complex $[\text{MoCl}_3(\text{PNP})]$ with Na/Hg (2 equiv) in THF at room temperature under N_2 (Scheme 7.3.).⁵



Scheme 7.3. Dinitrogen splitting with Mo pincer complex

7.2. Results and discussion

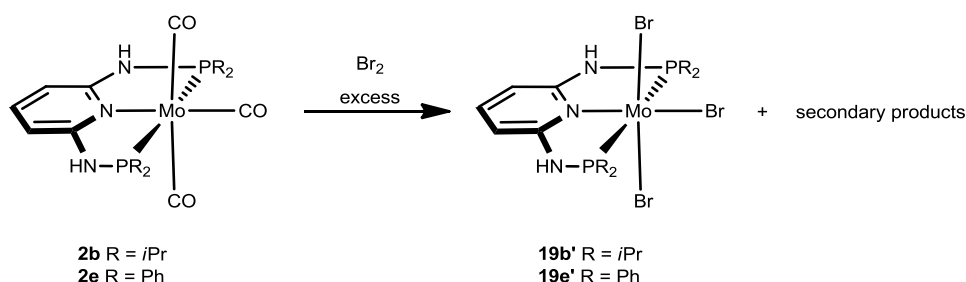
The synthesis of a series of new halide Mo(III) complexes with a central pyridine ring donor contains $\text{NR}'\text{PR}_2$ in the two ortho positions, was achieved by the addition of the PNP ligands to the metal precursor $[\text{MoBr}_3(\text{THF})_3]$ in THF. This resulted in the tribromide molybdenum complexes of the type $[\text{Mo}(\text{PNP})\text{Br}_3]$ shown in Scheme 7.4..



Scheme 7.4. Synthesis of $[\text{MPNP}(\text{Br})_3]$ ($\text{M} = \text{Mo}, \text{W}$) complexes

The six-coordinate 15e complexes are thermally robust red to orange solids, in 81-91% isolated yield, which are air stable in the solid state but slowly decompose in solution. All complexes display large paramagnetic shifted so very broad ^1H NMR signals and no detection was found in the $^{31}\text{P}\{^1\text{H}\}$ NMR. However, they exhibit solution magnetic moments in the range of 3.9-4.2 μ_{B} (Evans method, in acetone) in agreement with a d^3 high-spin electron configuration.

Alternatively, $[\text{Mo}(\text{PNP})\text{Br}_3]$ complexes are obtained by the oxidation of the tricarbonyl complexes $[\text{Mo}(\text{PNP})(\text{CO})_3]$ with an excess of Br_2 (Chapter 3). Unfortunately this reaction afforded also several as yet intractable side products making it difficult to obtain pure complexes (Scheme 7.5.).

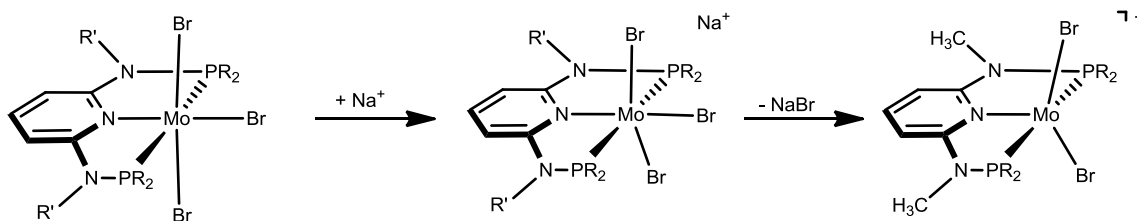


Scheme 7.5. Synthesis of $[\text{MPNP}(\text{Br})_3]$ ($\text{M} = \text{Mo}, \text{W}$) complexes under reflux conditions

The Mo(III) complexes were also characterized by means of ESI-MS. These studies (in the positive and negative ion mode) revealed that complexes in CH_3CN

Chapter 7 – Molybdenum(III) PNP Pincer Complexes

solutions in the presence of NaBr remain largely intact and fragments of the sodiated complexes $[M+Na]^+$. Further abundant fragments are $[M-(Na+Br)]^+$ where one halide is dissociated more easily (Scheme 7.6.).



Scheme 7.6. Fragmentation pattern of $[Mo(PNP)Br_3]$ complexes observed in the ESI-MS experiments

For the ESI-MS analysis of Mo (III) complexes **19b'** and **19e'** in CH_3CN and the corresponding sodium halide were subjected to “soft ionization” conditions, signals corresponding to the sodiated complexes ($[M+Na]^+$) and also ($[M+(Na+Br)-H]^+$) for **19b'** and the extra ($[M+(Na+2Br)-2H]^+$) for **19e'**. These measurements suggest that the secondary products corresponding to the complexes $[Mo(PNP)Br_4]$ and $[Mo(PNP)Br_5]$ probably with 4-bromopyridine and 3,5-dibromopyridine in the frame of the PNP pincer ligands.

In addition to spectroscopic characterization, the solid-state structures of **19b**, **19j** and **19n** were determined by single-crystal X-ray diffraction. Structural views are depicted in Figures 7.2.-7.4. with selected bond distances given in the captions.

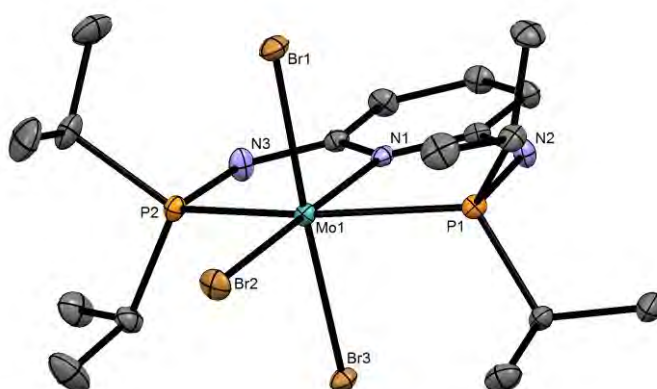


Figure 7.2. Structural view of $[Mo(PNP-*i*Pr)Br_3]$ (**19b**) showing 50% thermal ellipsoids (hydrogen atoms and solvent omitted for clarity). Selected bond lengths (Å) and bond angles (°): Mo1-P1 2.5170(7), Mo1-P2 2.5221(7), Mo1-Br1 2.5405(4), Mo1-Br2 2.5256(3), Mo1-Br3 2.5807(3), P1-Mo1-P2 156.20(2), N1-Mo1-Br2 178.79(6), Br1-Mo1-Br3 176.63(1)

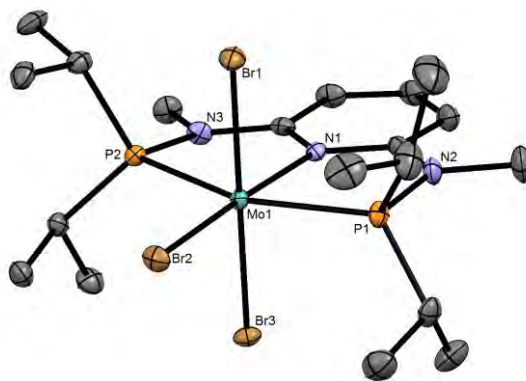


Figure 7.3. Structural view of $[\text{Mo}(\text{PNP}^{\text{Me-}i\text{Pr}})\text{Br}_2]$ (**19j**) showing 50% thermal ellipsoids (hydrogen atoms and solvent omitted for clarity). Selected bond lengths (Å) and bond angles ($^\circ$): Mo1-P1 2.5141(8), Mo1-P2 2.5194(8), Mo1-Br1 2.5531(4), Mo1-Br2 2.5463(4), Mo1-Br3 2.5637(4), P1-Mo1-P2 156.62(3), N1-Mo1-Br2 177.44(6), Br1-Mo1-Br3 175.94(1)

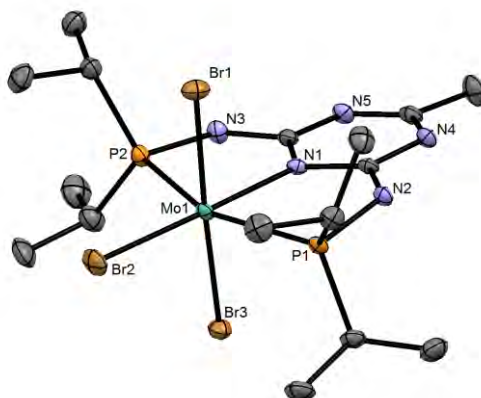


Figure 7.4. Structural view of $[\text{Mo}(\text{Triaz}^{\text{Me-}i\text{Pr}})\text{Br}_2]$ (**19n**) showing 50% thermal ellipsoids (hydrogen atoms and solvent omitted for clarity). Selected bond lengths (Å) and bond angles ($^\circ$): Mo1-P1 2.5303(7), Mo1-P2 2.5221(7), Mo1-Br1 2.5509(4), Mo1-Br2 2.5404(4), Mo1-Br3 2.5570(4), P1-Mo1-P2 153.72(2), N1-Mo1-Br2 178.52(5), Br1-Mo1-Br3 176.14(1)

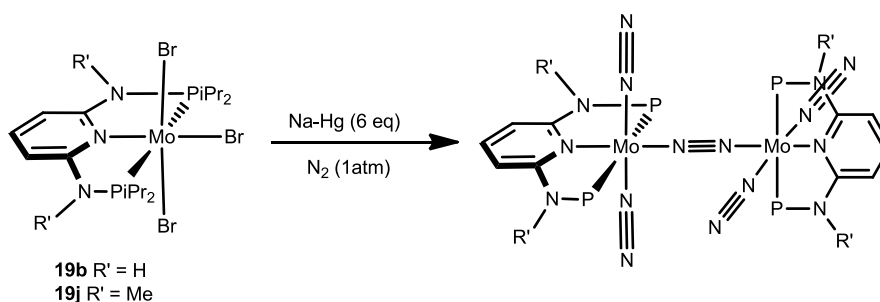
The structures show a distorted-octahedral trivalent molybdenum center surrounded by three meridionally placed donor atoms of the PNP ligand. The three bromide atoms occupy the three remaining positions. In all complexes the trans-Br–M–Br angles deviate from linearity being $176.63(1)^\circ$, $175.94(1)^\circ$ and $176.14(1)^\circ$, respectively, and are contracted towards the pyridine ring. The same pattern is observed for the P–M–P angles which are $156.20(2)^\circ$, $156.62(3)^\circ$ and $153.72(2)^\circ$, respectively.

For comparison, in analogous tricarbonyl complexes $[\text{Mo}(\text{PNP})(\text{CO})_3]$ (**2b**, **2j**), behave similar for the P1–Mo–P2 angles that hardly affected by the size of the

Chapter 7 – Molybdenum(III) PNP Pincer Complexes

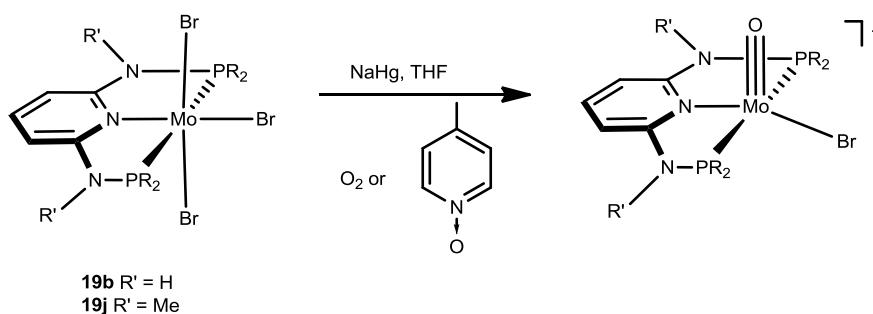
substituents of the phosphorus atoms. Though, the $C_{CO}-Mo-C_{CO}$ and the $Br-Mo-Br$ angles are different, while CO ligands trans to one another deviate significantly from 180° and typically vary strongly with the bulkiness of the PR_2 moiety, the Br ligands almost don't deviate from a straight angle.

Attempts of reduction of the Mo(III) halides complexes with NaHg in THF under nitrogen atmosphere were unsuccessful (Scheme 7.7.). Several reducing agents such as C_8K , sodium naphthalenide or magnesium were tested yielding in all cases mixtures of intractable paramagnetic materials.



Scheme 7.7. Synthesis of $[Mo_2(N_2)_2(PNP)]_2(\mu-N_2)$ complexes

In addition, the Mo(III) complexes were treated with NaHg in THF in the presence of O_2 or pyridine-N-oxide to obtain mono oxo complexes (Scheme 7.8.). Unfortunately the complexes were not achieved, there is no visible color change of the reaction and NMR measurements shows a mix of compounds.



Scheme 7.8. Attempted synthesis of $[MoPNP(O)(Br)]^+$

7.3. Conclusions

In this Chapter, the synthesis of several Mo(III) PNP pincer complexes of the type $[Mo(PNP)Br_3]$ was achieved. Preliminary studies of reduction of the

molybdenum(III) halides complexes with different reducing agents under nitrogen atmosphere were unsuccessful. Identical results with an oxygen source to prepare the mono oxo complexes failed.

7.4. Experimental part

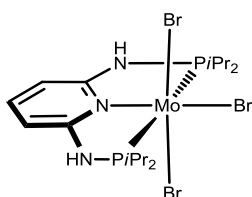
The precursor complex $[\text{Mo}(\text{Br})_3(\text{THF})_3]$ was prepared according to the literature.⁶

7.4.1. Synthesis

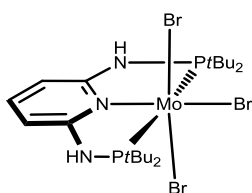
General synthetic procedure for molybdenum (III) complexes: To a solution of $[\text{MoBr}_3(\text{THF})_3]$ (0.300 mmol) in THF (10 mL) was added 1 equiv. of ligand (0.300 mmol). The reaction was stirred for 18 h. After this period the solution was filtered, solvent was removed under vacuum, and the solid was washed twice with Et_2O and *n*-pentane and then dried under vacuum.

Alternative synthetic procedure: A solution of $[\text{MoPNP}(\text{CO})_3]$ (0.300 mmol) in CH_2Cl_2 (10 mL) was cooled down to $-78\text{ }^\circ\text{C}$ and excess of Br_2 was added. The solution was slowly warmed to room temperature and stirred for 18 h. After this period the solution was filtered, solvent was removed under vacuum, and the solid was washed twice with Et_2O and *n*-pentane and then dried under vacuum.

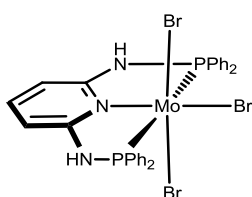
$[\text{Mo}(\text{PNP-}i\text{Pr})\text{Br}_3]$ (19b)



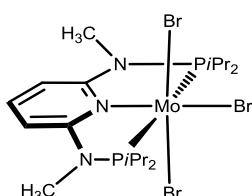
The product was obtained as a yellow-orange solid in 87% yield. Anal. Calcd. for $\text{C}_{17}\text{H}_{33}\text{Br}_3\text{MoN}_3\text{P}_2$ (677.08): C, 30.16; H, 4.91; N, 6.21. Found: C, 29.88; H, 4.53; N, 5.97. $\mu_{\text{eff}} = 3.9(9)\text{ }\mu\text{B}$ (Acetone, Evans method). **ESI-MS (m/z , CH_3CN) positive ion:** 695.0 $[\text{M}+\text{Na}]^+$, 593.0 $[\text{M} - (\text{Na} + \text{Br})]^+$.

[Mo(PNP-*t*Bu)Br₃] (19d)

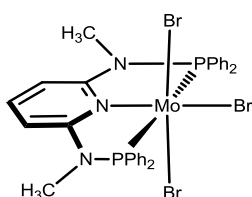
The product was obtained as a yellow-orange solid in 81% yield. Anal. Calcd. for C₂₁H₄₁Br₃MoN₃P₂ (733.19): C, 34.40; H, 5.64; N, 5.73. Found: C, 34.12; H, 5.23; N, 5.51. $\mu_{\text{eff}} = 4.0(4) \mu\text{B}$ (Acetone, Evans method). **ESI-MS (m/z, CH₃CN) positive ion:** 755.3 [M+Na]⁺, 648.1 [M - (Na + Br)]⁺.

[Mo(PNP-Ph)Br₃] (19e)

The product was obtained as a yellow-orange solid in 84% yield. Anal. Calcd. for C₂₉H₂₅Br₃MoN₃P₂ (813.15): C, 42.83; H, 3.10; N, 5.17. Found: C, 42.48; H, 2.98; N, 4.86. $\mu_{\text{eff}} = 3.9(7) \mu\text{B}$ (Acetone, Evans method). **ESI-MS (m/z, CH₃CN) positive ion:** 831.2 [M+Na]⁺, 729.0 [M - (Na + Br)]⁺.

[Mo(PNP^{Me}-*i*Pr)Br₃] (19j)

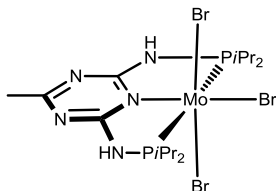
The product was obtained as a yellow-orange solid in 82% yield. Anal. Calcd. for C₁₉H₃₇Br₃MoN₃P₂ (705.14): C, 32.36; H, 5.29; N, 5.96. Found: C, 31.96; H, 5.03; N, 5.59. $\mu_{\text{eff}} = 4.1(2) \mu\text{B}$ (Acetone, Evans method). **ESI-MS (m/z, CH₃CN) positive ion:** 723.1 [M+Na]⁺, 619.0 [M - (Na + Br)]⁺.

[Mo(PNP^{Me}-Ph)Br₃] (19k)

Chapter 7 – Molybdenum(III) PNP Pincer Complexes

The product was obtained as a yellow-orange solid in 89% yield. Anal. Calcd. for $C_{31}H_{29}Br_3MoN_3P_2$ (841.20): C, 44.26; H, 3.47; N, 5.00. Found: C, 44.02; H, 3.14; N, 4.76. $\mu_{\text{eff}} = 4.0(1) \mu\text{B}$ (Acetone, Evans method). **ESI-MS (m/z, CH₃CN) positive ion:** 859.3 [M+Na]⁺, 757.1 [M - (Na +Br)]⁺.

[Mo(Triaz^{Me}-iPr)Br₃] (19n)



The product was obtained as a yellow-orange solid in 83% yield. Anal. Calcd. for $C_{16}H_{33}Br_3MoN_5P_2$ (693.09): C, 27.73; H, 4.80; N, 10.10. Found: C, 27.41; H, 4.29; N, 4.56. $\mu_{\text{eff}} = 4.2(1) \mu\text{B}$ (Acetone, Evans method). **ESI-MS (m/z, CH₃CN) positive ion:** 711.2 [M+Na]⁺, 607.0 [M - (Na +Br)]⁺.

7.5. References

- [1] Astruc, D.; *Organometallic Chemistry and Catalysis*, **2007**, Springer-Verlag Berlin Heidelberg.
- [2] Gutmann, V.; *Halogen Chemistry*, Vol. 3, **1967**, Academic Press, London and New York.
- [3] Lang, H.; Fanwick, P. E.; Walton, R. A.; *Inorganica Chimica Acta*, **2002**, 329, 1-8.
- [4] Arashiba, K.; Miyake, Y.; Nishibayashi, Y.; *Nature Chemistry*, **2011**, 3, 120-125.
- [5] Silantyev, G. A.; Förster, M.; Schluschaß, B.; Abbenseth, J.; Würtele, C.; Volkmann, C.; Holthausen, M. C.; Schneider, S.; *Angew. Chem. Int. Ed.*, **2017**, 56, 1-6.
- [6] Owens, B. E.; Poli, R.; Rheingold, A. L.; *Inorg. Chem.*, **1989**, 28, 1456-1562.

Chapter 8

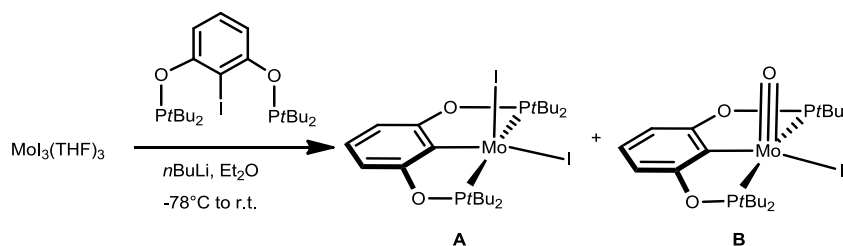
PNP versus PCP Pincer

Complexes

Chapter 8 – PNP vs PCP Pincer Complexes

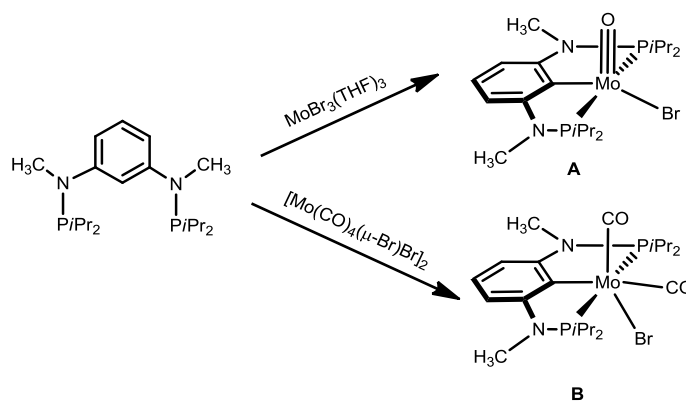
Pincer complexes play a particular almost privileged role, which have received tremendous attention among the many types of transition metal complexes found in the literature. Most conventional are still pincer systems with phosphine donors tethered to an aromatic benzene backbone, so called PCP pincer ligands.^{1,2} Shaw and co-workers³ synthesized the first PCP pincer complexes in the mid-1970s, like it as introduce in the first Chapter.

Over the years, the very well known PCP pincer ligand continues to gain a vast attention, with both precious and non-precious metals. Surprisingly, the chemistry of group 6 PCP complex is still hardly explored, the first and only molybdenum PCP complex was prepared through lithiation of 1-iodo-2,6-[OP(*t*-Bu)₂]₂C₆H₃ and reaction of that lithium reagent with MoI₃(THF)₃ to give [Mo(PCP)(I)₂] (A) (Scheme 8.1).⁴ However this compound A was obtained in the modest yield (46%) since a diamagnetic impurity was present (10-15%), which was proposed to be the Mo(IV) oxo complex (B).



Scheme 8.1. Synthesis of Mo(III) and Mo(IV) POCOP pincer complexes

In 2016, Kirchner and coworkers synthesized two diamagnetic molybdenum pincer complexes [Mo(PCP^{Me}-*i*Pr)(O)Br] and [Mo(PCP^{Me}-*i*Pr)(CO)₂Br] (Scheme 8.2.), from molybdenum precursors [Mo(Br)₃(THF)₃] and [Mo(CO)₄(μ-Br)Br]₂, respectively.⁵



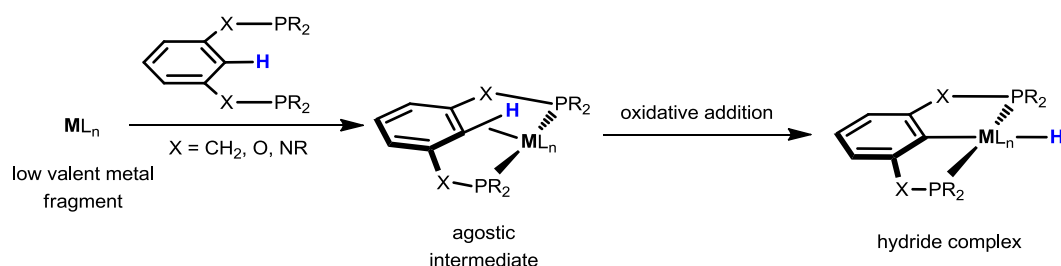
Scheme 8.2. Synthesis of Mo(III) and Mo(IV) PCP pincer complexes

Curiously, there is no more information in literature of PCP complexes with the rest of the non-precious metals of group 6.

8.1. Pincer complexes with agostic interaction

As electron rich low-valent late transition metal PCP pincer complexes are concerned a common synthetic approach goes through oxidative addition.* This pathway leads to the formation of PCP hydride complexes that can involve an intramolecular, directed C-H bond activation of the P(CH)P ligand followed by an oxidative addition of the C-H bond (Scheme 8.3).^{6,7}

This method is associated with a formal two electron oxidation of the metal center. The oxidative addition step seems to require pre-coordination of the C-H bond, *i.e.*, the formation of an agostic intermediate or, at least, transition state.^{8,9}



Scheme 8.3. General synthesis of transition metal PCP pincer complexes

In a few cases, as yet limited to the precious metals Ru, Rh, and Ir, such intermediates were detected and even isolated and structurally characterized (Figure 8.1.). Furthermore, other types of pincer complexes, featuring for example NCN ligands, also follow the same process, presenting the agostic interaction.¹⁰⁻¹⁷

* Discussed in Chapter 1

Chapter 8 – PNP vs PCP Pincer Complexes

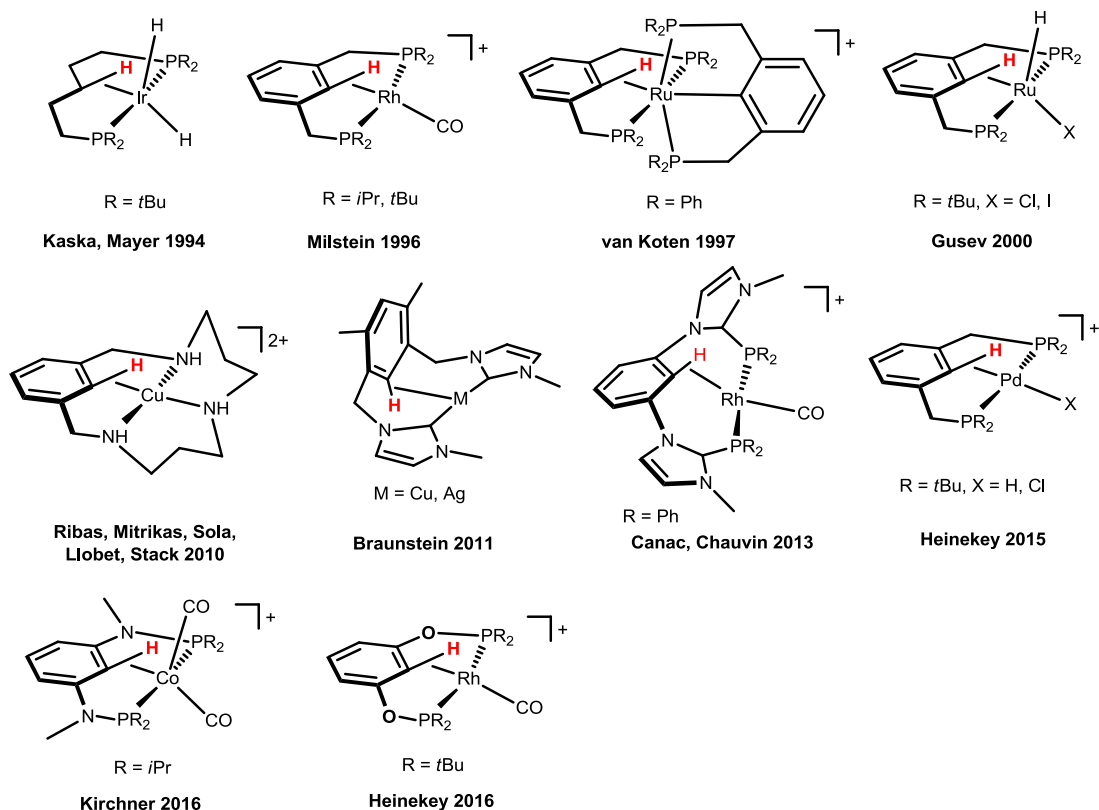
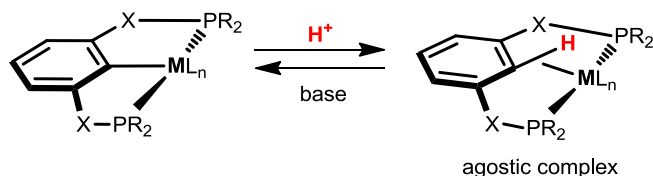


Figure 8.1. Examples of PCP and related pincer complexes featuring a C-H agnostic interaction

Complexes with η^2 -C-H agnostic arene bonds, however, could be derived via alternative routes.¹⁸⁻²¹ An example is the synthesis of an agostic Co(I) complex *via* protonation of the coordinated PCP ligand in $[\text{Co}(\text{PCP}^{\text{Me-}i\text{Pr}})(\text{CO})_2]$ (Scheme 8.4).²⁰ Similar reactions were also reported for Rh(I) and Pd(II) complexes.^{10a,17,21}



Scheme 8.4. Examples of PCP and related pincer complexes featuring a C-H agnostic interaction

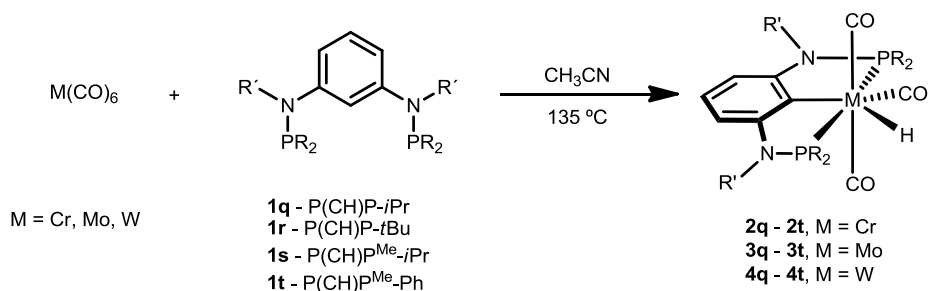
8.2. Results and discussion

Throughout this research, the chemistry of group 6 with pincer ligands, PNP, based on a 2,6-diaminopyridine scaffold with some modification on the amino group and with different phosphine moieties, was explored and perceived. Nonetheless, a

Chapter 8 – PNP vs PCP Pincer Complexes

study with the analogous PCP pincer ligands with a 1,3-diaminobenzene scaffold is inevitable, special since the group six PCP pincer complexes are scarce.

Adopting an identical methodology of the tricarbonyl complexes of the type $[M(\text{PNP})(\text{CO})_3]$ ($M = \text{Mo}, \text{W}$) (Chapter 3),²² a suspension of hexacarbonyl complexes $M(\text{CO})_6$ ($M = \text{Cr}, \text{Mo}, \text{W}$) and PCP ligands **1q-1t** in CH_3CN was placed in a sealed microwave glass tube and stirred for 5 h at 150°C (Scheme 8.5.).



Scheme 8.5. Synthesis of $[\text{MPCP}(\text{CO})_3\text{H}]$ ($M = \text{Cr}, \text{Mo}, \text{W}$) complexes

Surprisingly, the desirable hydridocarbonyl complexes of the type $[\text{M}(\text{PCP})(\text{CO})_3\text{H}]$ ($M = \text{Cr}, \text{Mo}, \text{W}$) was not accomplished with the PCP pincer ligands. The achieved products were of the type $[\text{M}(\text{PCP})(\text{CO})_5]$ ($M = \text{Cr}, \text{Mo}, \text{W}$), connected to the metal center only through one of the phosphine arms of the pincer ligands. To confirm this, one example the $[\text{Mo}(\text{PCP-}t\text{Bu})(\text{CO})_5]$ **3r** complex was characterized. The $^{31}\text{P}\{^1\text{H}\}$ NMR spectra exhibit two doublets which proves only one phosphorus atoms is bond to the metal. Both the $^{13}\text{C}\{^1\text{H}\}$ NMR spectra at downfield and several bands in IR show the presence of five CO ligands coordinated to the metal.

In addition to spectroscopic characterization, the solid-state structure was determined by single-crystal X-ray diffraction. Structural views depicted in Figures 8.2. shows that molybdenum only coordinates to a phosphorus atom of the pincer ligand.

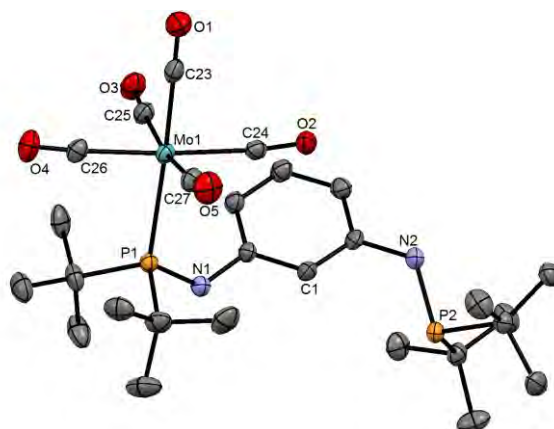
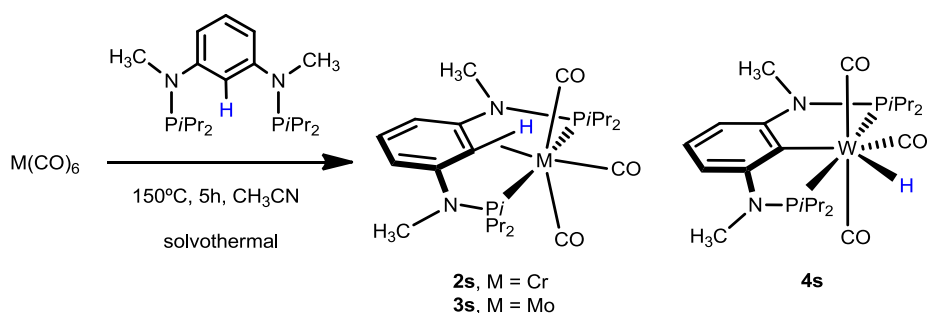


Figure 8.2. Structural view of $[\text{Mo}(\text{P}(\text{CH})\text{P}-t\text{Bu})(\text{CO})_5]$ (**3r**) showing 50% thermal ellipsoids (most H atoms omitted for clarity)

The only exception is the case of the ligand *N,N'*-bis(di-*iso*-propylphosphino)-*N,N'*-dimethyl-1,3-diaminobenzene ($\text{P}(\text{CH})\text{P}^{\text{Me-}i\text{Pr}}$) that for Cr and Mo, the tricarbonyl complexes $[\text{Cr}(\text{P}(\text{CH})\text{P}^{\text{Me-}i\text{Pr}})(\text{CO})_3]$ (**2s**) and $[\text{Mo}(\text{P}(\text{CH})\text{P}^{\text{Me-}i\text{Pr}})(\text{CO})_3]$ (**3s**) were isolated in 96 and 98% isolated yield (Scheme 8.6.). While with W the seven coordinate hydridocarbonyl complex, of the type $[\text{W}(\text{PCP}^{\text{Me-}i\text{Pr}})(\text{CO})_3(\text{H})]$ (**4s**) was obtained in 95% isolated yield. Complexes **2s** and **3s** feature an $\eta^2\text{-C}_{\text{aryl}}\text{-H}$ agostic bond, while **4s** contains strong W-C and W-H σ -bonds as a result of an oxidative addition.

All thermal robust complexes were fully characterized by a combination of ^1H , $^{13}\text{C}\{^1\text{H}\}$, ^{13}C and $^{31}\text{P}\{^1\text{H}\}$ NMR spectroscopy, IR, ESI MS, and elemental analysis. Additionally, all complexes were characterized by X-ray crystallography.



Scheme 8.6. Synthesis of the Cr, Mo and W Complexes **2s-4s**

An important feature of the ^1H NMR spectra of **2s** and **3s** is the high-field shift of the proton attached to the *ipso*-carbon giving rise to triplets at -2.06 and 1.23 ppm, respectively. The latter is superimposed with the signals of the CH_3 groups of the *iPr* moieties and was derived from ^1H - ^{13}C correlation spectra.

Chapter 8 – PNP vs PCP Pincer Complexes

In the $^{13}\text{C}\{^1\text{H}\}$ NMR spectra the *ipso*-carbon atom exhibits a triplet at 71.5 ($J_{\text{CP}} = 6.3$ Hz) and 72.3 ppm ($J_{\text{CP}} = 4.6$ Hz), respectively (*cf* 105.0 ppm in the free $\text{P}(\text{CH})\text{P}^{\text{Me}}\text{-iPr}$ ligand, Figure 8.3.). Proton-coupled ^{13}C NMR data of **2s** and **3s** reveal relatively low $^1J_{\text{HC}}$ coupling constants of 124.9 and 126.0 Hz, respectively, as compared to about 160 and 157 Hz for the other aromatic C-H bonds in the $\text{P}(\text{CH})\text{P}^{\text{Me}}\text{-iPr}$ ligand, which is characteristic for a strong C-H metal interaction.

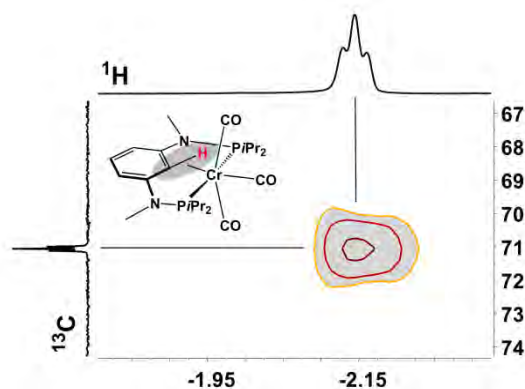


Figure 8.3. Section of the ^1H - ^{13}C HSQC spectrum of **2s** in CD_2Cl_2 exhibiting a cross-peak between the agostic H1 and C1 atoms

The three CO ligands give rise to three low-field resonances as triplets centered at 238.0, 227.9, and 226.8 ppm for **2s**, and 232.4, 219.6, and 216.4 ppm for **3s**, corresponding to the carbonyl carbon atoms on trans and two cis to the benzene C1.

The $^{31}\text{P}\{^1\text{H}\}$ NMR spectra exhibit singlet resonances at 165.5 ppm for $[\text{CrP}(\text{CH})\text{P}^{\text{Me}}\text{-iPr}(\text{CO})_3]$ (**2s**) and 149.7 ppm for the complex $[\text{Mo}(\text{P}(\text{CH})\text{P}^{\text{Me}}\text{-iPr})(\text{CO})_3]$ (**3s**), which means the metal increases the electron density on phosphorus, and thus results in an upfield shift.

Both the carbonyl resonances (δ_{CO}) and the phosphorus resonances (δ_{P}) exhibit a significant upfield shift on going from Cr to Mo.

In the IR complex **2s** exhibits only two bands at 1933 and 1821 cm^{-1} assignable to the symmetric and the two superimposed asymmetric CO stretching frequencies, while complex **3s** shows the expected three strong ν_{CO} bands at 1942, 1839, and 1823 cm^{-1} .

As complex **4s** is concerned, this complex is fluxional in solution at room temperature which is well known for seven-coordinate complexes group six metals, since none of the idealized geometries such as capped prism, capped octahedron, and pentagonal bipyramid, nor any of less symmetrical arrangements are typically

Chapter 8 – PNP vs PCP Pincer Complexes

characterized by a markedly lower total energy.²³⁻²⁶ Hence, interconversions between these various structures are quite facile. Accordingly, the ^1H and ^{31}P NMR resonances are not well resolved at room temperature so they were recorded at -40°C . In ^1H NMR spectrum the hydride resonance appears as a well-resolved doublet of doublet at -5.65 ppm with one large and one small coupling constant of 56.4 and 21.1 Hz. The $^{31}\text{P}\{^1\text{H}\}$ NMR spectrum gives rise to two doublets centered at 138.3 and 120.8 ppm with a large geminal coupling constant of 89.0 Hz which is indicative for the phosphorus atoms being in a mutual *trans* position. The tungsten–phosphorus coupling was observed as a doublet satellite due to ^{183}W , 14% abundant with $I = 1/2$ superimposed over the dominant singlet. In the $^{13}\text{C}\{^1\text{H}\}$ NMR spectrum the most noticeable resonances are two low-field resonances of the carbonyl carbon atoms *trans* and *cis* to the *ipso* carbon observed as two triplets in a $1:2$ ratio. The IR spectrum shows three strong to medium absorption ν_{CO} bands of the symmetric and the two asymmetric vibration modes which is typical for a *mer* CO arrangement.

Compared with the analogous PNP pincer tungsten complex, $[\text{W}(\text{PNP}^{\text{Me}}-i\text{Pr})(\text{CO})_3\text{H}]^+$ (**5j**), the presence of the very electronegative heteroatom nitrogen in the pincer ligand withdraws electron density from the metal making it more electropositive. The IR measurements and $^{13}\text{C}\{^1\text{H}\}$ NMR spectrum show in table 8.1. supports this statement.

Table 8.1. Selected $^{13}\text{C}\{^1\text{H}\}$ and $^{31}\text{P}\{^1\text{H}\}$ NMR and IR data of PCP and PNP pincer W complexes

Complexes	$^{13}\text{C}\{^1\text{H}\} / \delta$	$^{31}\text{P}\{^1\text{H}\} / \delta$	IR / cm^{-1}
$[\text{W}(\text{PCP}^{\text{Me}}-i\text{Pr})(\text{CO})_3\text{H}]$ (4s)	207.8 200.6	138.3 120.8	1991, 1909, 1860
$[\text{W}(\text{PNP}^{\text{Me}}-i\text{Pr})(\text{CO})_3\text{H}]^+$ (5j)	210.8 205.4	166.1 147.7	2028, 1928, 1910

Structural views of **2s** and **3s** are depicted in Figures 8.4. and 8.5. with selected bond distances given in the caption. The overall geometry about the Cr and Mo centers is best described as distorted octahedron where the three carbonyl ligands and the agostic $\eta^2\text{-C}_{\text{aryl}}\text{-H}$ bond define the equatorial plane and the phosphine moieties the axial positions. The P1-M-P2 and *trans*- $\text{C}_{\text{CO}}\text{-M-C}_{\text{CO}}$ bond angles are $155.46(2)$ and $161.92(8)^\circ$ (**2s**), and $151.90(1)$ and $159.98(4)^\circ$ (**3s**), respectively. The distance between the *ipso*-carbon and the Cr and Mo atoms is relatively long ($2.323(2)$ and $2.433(1)$ Å) relative to regular Cr and Mo-carbon σ -bonds (the Cr-C bond in

Chapter 8 – PNP vs PCP Pincer Complexes

[CrCp(NO)(NiPr₂)(CH₂SiMe₃)] is 2.111(2) Å,²⁸ the Mo-C bond distance in [Mo(POCOP-*t*Bu)(N)(I)][Na(15-crown-5)] is 2.167(3) Å⁴). The H(1) atom (which was located in difference Fourier maps and refined freely) interacts with the Cr and Mo centers (1.89(2) and 2.11(2) Å) which was also evident from the ¹H NMR spectra of **2s** and **3s**. It is noteworthy that this hydrogen is severely removed from the aromatic plane by ca. 32 and 28° (*cf* in related Ru, Rh, and Pd complexes this angle is in the range of 14-30°,^{10-17,21} while in Co²⁰ it is 35°). The C1-H1 bond length of 1.00(2) Å is in the range observed in X-ray diffraction measurements for unactivated hydrocarbons (e.g., 1.08 Å in C₆H₆).

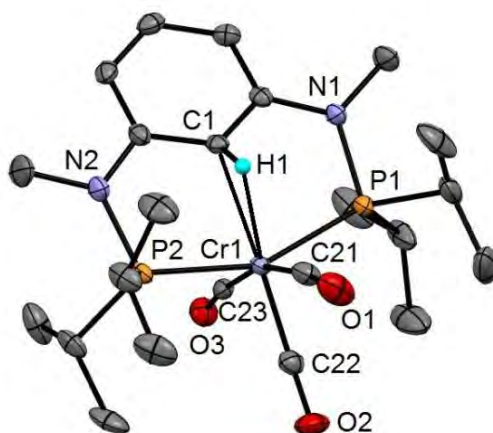


Figure 8.4. Structural view of [Cr(P(CH)P^{Me-Pr})(CO)₃] (**2s**) showing 50% thermal ellipsoids (most H atoms omitted for clarity). Selected bond lengths (Å) and bond angles (°): Cr1-P1 2.3280(7), Cr1-P2 2.3411(7), Cr1-C1 2.323(2), Cr1-H1 1.89(2), Cr1-C21 1.871(2), Cr1-C22 1.821(2), Cr1-C23 1.868(2), C1-H1 1.00(2), P1-Cr1-P2 155.46(2), C1-Cr1-C21 108.24(8), C1-Cr1-C22 171.95(7), C1-Cr1-C23 89.83(7), C1-Cr1-H1 24.9(6), C21-Cr1-C22 79.73(9), C21-Cr1-C23 161.92(8), C22-Cr1-C23 82.21(8)

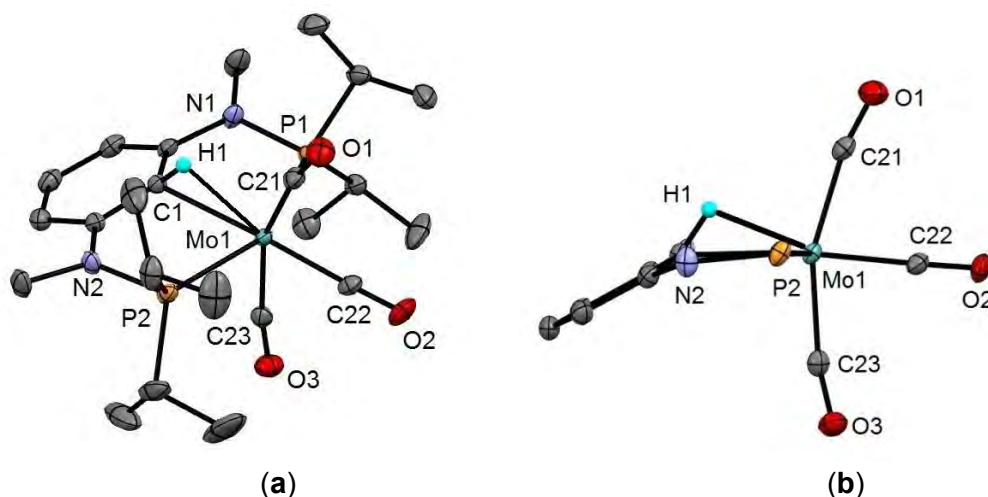


Figure 8.5. (a) Structural view of [Mo(P(CH)P^{Me-/iPr})(CO)₃] (**3s**) showing 50% thermal ellipsoids (most H atoms omitted for clarity). (b) Side view of **2** displaying the orientation of the aryl ring and H1. Selected bond lengths (Å) and bond angles (°): Mo1-P1 2.4558(4), Mo1-P2 2.4592(4), Mo1-C1 2.433(1), Mo1-C21 2.015(1), Mo1-C22 1.946(1), Mo1-C23 2.012(1), Mo1-H1 2.11(2), C1-H1 1.00(2), P1-Mo1-P2 151.90(1), C21-Mo1-C22 78.78(4), C21-Mo1-C23 159.98(4), C22-Mo1-C23 81.32(4), C1-Mo1-H1 24.0(4)

The molecular structure of **4s** is shown in Figure 8.6. with selected bond distances given in the caption. The coordination geometry around the tungsten center corresponds to a distorted capped octahedron, in which a hydride ligand occupies the capping position of an octahedral face. The W-C1 σ -bond is 2.266(4) Å.

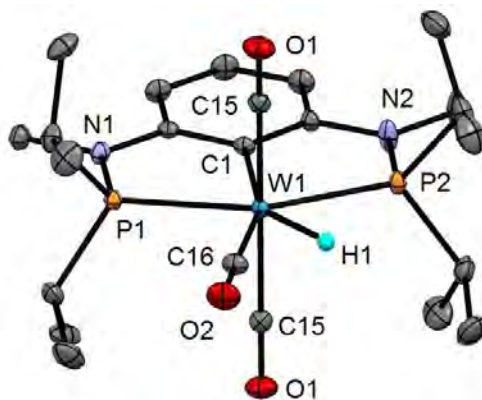


Figure 8.6. Structural view of [W(PCP^{Me-/iPr})(CO)₃(H)] (**4s**) showing 50% thermal ellipsoids (most H atoms omitted for clarity). Selected bond lengths (Å) and bond angles (°): W1-P1 2.497(2), W1-P2 2.480(3), W1-C1 2.266(4), W1-C15 2.040(3), W1-C16 2.039(5), W1-H1 1.64(2), P1-W1-P2 150.47(2), C15-W1-C15 173.27(4), C15-W1-C16 86.69(3), C1-W1-C16 161.30(8)

The carbonyl *trans* to carbon C1 was pushed toward one of the phosphine ligands to accommodate the hydride ligand H1. The hydride to carbonyl C16 atom distance is 1.72 Å. However, the almost linear attachment of the equatorial carbonyl group W1-C16-O2 of 177.8° does not indicate a significant bonding interaction between the hydride and the adjacent carbonyl C atom. A ^1H - ^{13}C correlation spectrum also shows only a weak interaction. The structure of this complex is very similar to those of the previously reported cationic molybdenum and tungsten hydrido carbonyl complexes $[\text{M}(\text{PNP})(\text{CO})_3\text{H}]^+$ (M = Mo, W) featuring neutral PNP pincer ligands based in the 2,6-diaminopyridine scaffold, in Chapter 4.²⁵

ESI-MS studies (in the negative ion mode) of complexes **2s-4s** in CH_3CN solutions revealed that under these reaction conditions these complexes are readily deprotonated and fragments of the anionic complexes $[\text{M}(\text{PCP}^{\text{Me-}i\text{Pr}})(\text{CO})_3]^-$ ($[\text{M-H}]^-$) were observed at m/z 503.2 (based on the ^{52}Cr -isotope, the most abundant one), 543.1 (based on the ^{92}Mo -isotope, the first one), and 633.2 (based on the ^{182}W -isotope, the first abundant one), respectively. Further abundant fragments are exclusively detected at m/z 475.2, 515.2, and 633.2, respectively, as a result of CO loss from **4s** ($[\text{M-H-CO}]^-$). A representative negative ion ESI mass spectrum of $[\text{Mo}(\text{PCP}^{\text{Me-}i\text{Pr}})(\text{CO})_3]^-$ is depicted in Figure 8.7. showing the isotopic pattern of the $[\text{M-H}]^-$ ion in comparison with the theoretical pattern, which turned out to correlate quite well.

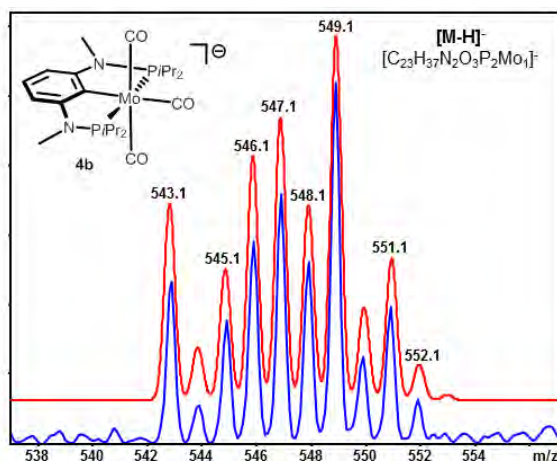


Figure 8.7. Negative-ion ESI MS of $[\text{Mo}(\text{P}(\text{CH})\text{P}^{\text{Me-}i\text{Pr}})(\text{CO})_3]$ (**3s**) in CH_3CN showing the calculated and measured isotopic pattern of the anionic fragment $[\text{Mo}(\text{P}(\text{CH})\text{P}^{\text{Me-}i\text{Pr}})(\text{CO})_3]^-$ ($[\text{M-H}]^-$)

8.2.1. Mechanist study

The nature of the interaction between the C1-H1 bond and the Mo-atom in complex **3s** was investigated by means of DFT calculations. The relevant Wiberg indices (WI)²⁸ indicate the formation of weak Mo-C and Mo-H bonds, with WI = 0.19 and 0.07, respectively, suggesting the existence of an agostic C-H...Mo bond. As a consequence, there is a clear weakening of the C-H bond, much longer (1.12 Å) and weak (WI = 0.74) than the remaining C_{aryl}-H bonds (1.08-1.09 Å and WI = 0.91). Moreover, the HOMO-4 of complex **3s** (Figure 8.8.) represents clearly a Mo-C1 σ bonding interaction resulting from back donation from a Mo d -orbital to the C-H σ^* -orbital, being characteristic of an agostic bond. The frontier orbitals of complex **3s** are presented in Figure 8.9..

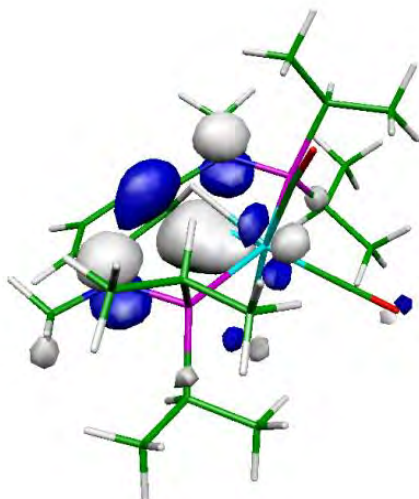


Figure 8.8. HOMO-4 of complex **3s** (1.6 eV below the HOMO)

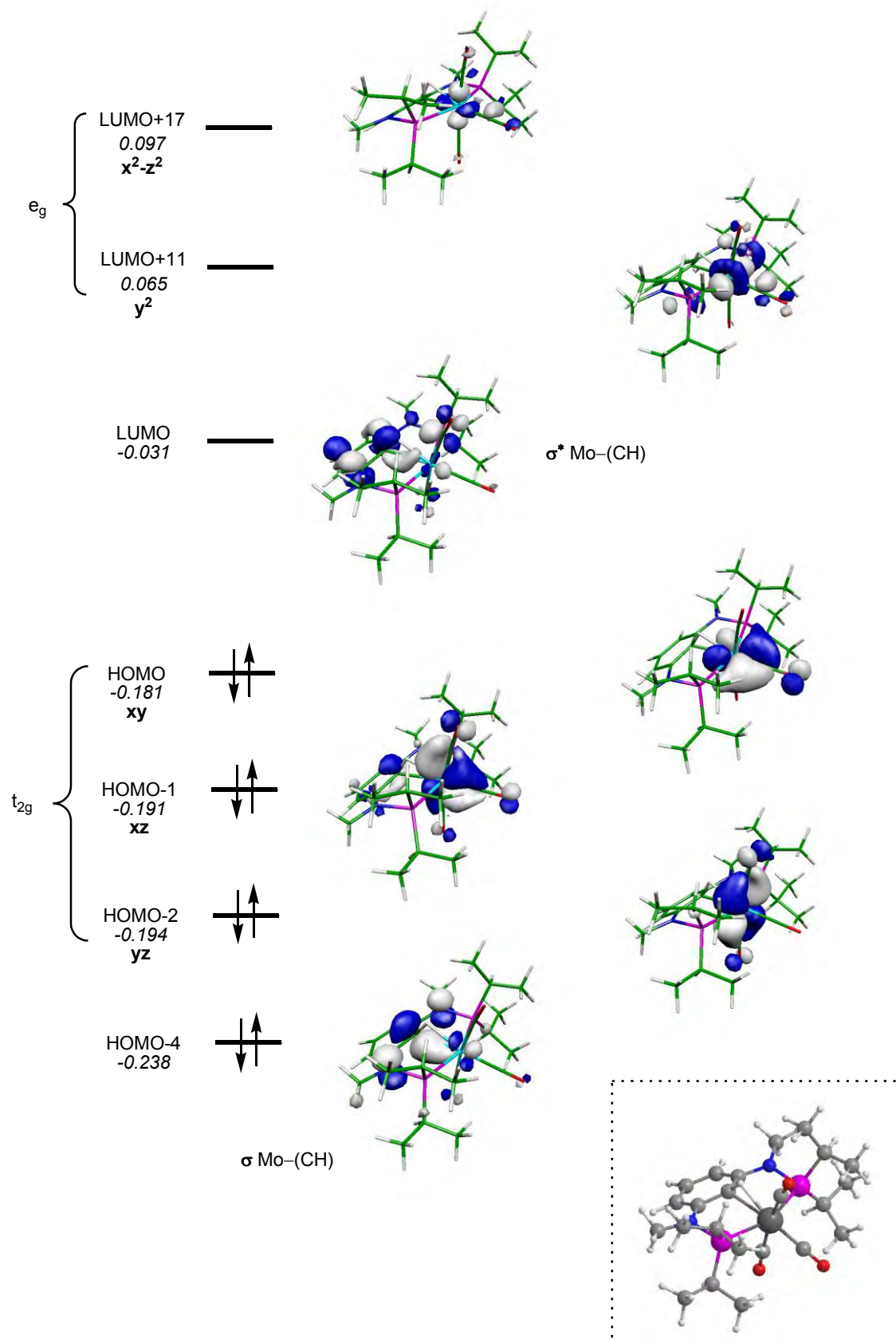


Figure 8.9. Frontier orbitals of complex **3s** (d -splitting). Energy values in atomic units (italics)

Chapter 8 – PNP vs PCP Pincer Complexes

A reaction pathway for the formation of hydride complexes was also investigated by DFT calculations in order to get insights why they are formed for $M = W$, but not in the case of Cr and Mo . The free energy profiles obtained for the $C_{\text{aryl}}\text{-H}$ oxidative addition in the cases of Mo and W are represented in Figure 8.10..

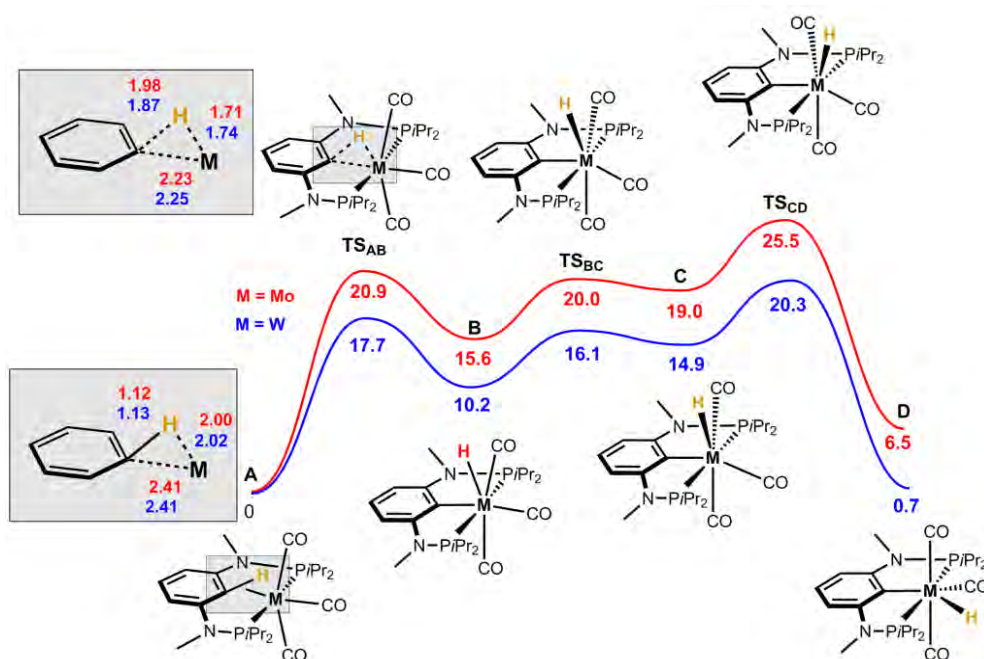


Figure 8.10. Free energy profiles (in kcal/mol) for the oxidative addition of the arene C–H bond in complexes **3s** and **4s** (bond distance in Å)

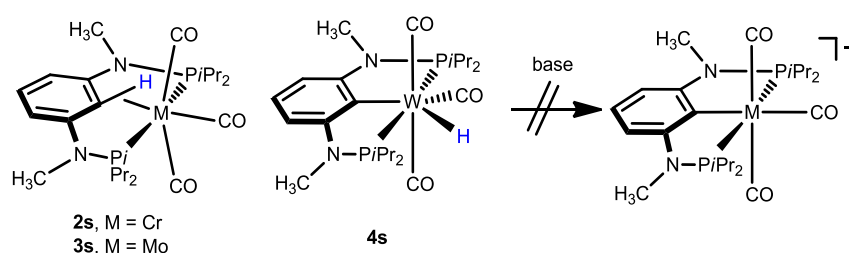
The mechanism obtained starts with cleavage of the agostic C–H bond in the initial complexes (**A**, in Figure 8.10.), leading to hydride seven-coordinated intermediates (**B**). In **B**, the geometry is capped octahedral with the hydride ligand capping a face defined by C_{aryl} , C_{CO} and one P-atom. C–H oxidative addition is an accessible process, with barriers of 18 and 21 kcal/mol, for W and Mo , respectively, but the hydride intermediates, **B**, are clearly less stable than the initial agostic species: $\Delta G = 10$ kcal/mol (W) and 16 kcal/mol (Mo). The following step, from **B** to **C**, corresponds to a re-orientation of the hydride and the nearby CO ligand, with the hydride moving between adjacent $C_{\text{aryl}}\text{-C}_{\text{CO}}\text{-P}$ faces of the capped octahedron. The process has small barriers of 6 kcal/mol (W) and 4 kcal/mol (Mo) and is unfavorable from the thermodynamic point of view, with $\Delta G = 5$ kcal/mol (W) and 3 kcal/mol (Mo). In the final step, from **C** to **D**, the structure of the complexes relaxes to the one observed in complex **3**, with the hydride ligand capping a $C_{\text{CO}}\text{-C}_{\text{CO}}\text{-P}$ face of the capped octahedron, in an orientation close to the mean plan defined by the two P-atoms the

C_{aryl} and its *trans* CO ligand. This final step has barriers of 5-6 kcal/mol and is clearly exergonic with $\Delta G = -14$ kcal/mol (W) and -12 kcal/mol (Mo).

Overall, the mechanisms calculated for the two metal atoms parallel each other. In both cases, the highest barrier corresponds to the last step and the values obtained (26 kcal/mol for Mo and 20 kcal/mol for W, relative to the initial reagent) are in accordance with the experimental conditions. However, the reaction is endergonic and, thus, thermodynamically unfavorable in the case of Mo, with $\Delta G = 7$ kcal/mol, while in the case of W it is essentially thermoneutral ($\Delta G = 1$ kcal/mol). This is in accordance with the formation of the hydride complex for $M = W$ and not for $M = Mo$. The reason for the different reactivity observed can be traced to the M-H bond strength. In fact, in the hydride species **D**, the M-H is considerably stronger for the W species than for Mo complex, as indicated by the corresponding Wiberg indices: WI = 0.51 (W) and 0.46 (Mo).²⁹

8.2.2. Reactivity

The agostic C-H arene bond in several Rh(I) and Co(I) was shown to be acidic and could be readily deprotonated in the presence of even comparatively weak bases such as pyridine or NEt_3 to give the respective PCP complexes.^{9a,19} In the case of Cr and Mo complexes **2s** and **3s**, even in the presence of strong bases such as NaH, *n*BuLi, and KO^tBu, no deprotonation was observed to afford anionic tricarbonyl complexes of the type $[M(PCP^{Me-iPr})(CO)_3]^-$ (Scheme 8.7.).

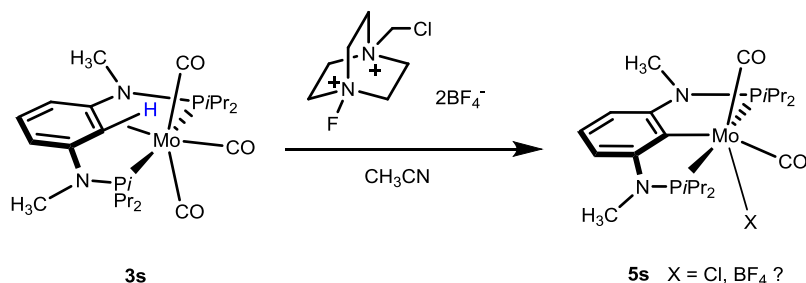


Scheme 8.7. Synthesis of desprotonation the Cr, Mo and W complexes

Likewise, also the hydrido carbonyl complex **4s** did not react with bases, which strongly contrasts the behavior of the cationic hydrido carbonyl Mo and W complexes $[M(PNP)(CO)_3H]^+$ (Chapter 4) where deprotonation took place readily.²⁵ Contrarily, in the presence of strong acids such as HBF_4 , CF_3SO_3H , and CF_3COOH decomposition to intractable materials took place.

Chapter 8 – PNP vs PCP Pincer Complexes

Additional, synthetic approach through oxidative addition to achieved the $[\text{Mo}(\text{PNP})(\text{CO})_2\text{X}]$ ($\text{X} = \text{I}, \text{Br}$) complexes was not successful. The only successful reaction is of the molybdenum pincer complex with selectfluor display in Scheme 8.8..



Scheme 8.8. Reaction of **3s** with selectfluor

Due to the solubility of the selectfluor the reaction is solvent depend, only occurring in CH_3CN to yield the dicarbonyl complexes of the type $[\text{Mo}(\text{PCP}^{\text{Me-}i\text{Pr}})(\text{CO})_2]^+$.

The NMR characterization of complex **5s** shows no evidence for the proton attached to the *ipso*-carbon. The ^1H NMR spectra neither the proton on C1 or hydride resonances appears. In the $^{13}\text{C}\{^1\text{H}\}$ NMR spectrum the *ipso*-carbon atom exhibits a triplet at 123.4 ppm, downfield from both the PCHP ligand and the **3s** precursor, proving the existence of a normal metal-carbon bond. It is also visible two low-field resonances of the carbonyl carbon atoms *trans* and *cis* to the benzene C1 observed as two triplets in a 1:1 ratio. The $^{31}\text{P}\{^1\text{H}\}$ NMR spectra exhibit singlet resonance at 135.9 ppm shifted upfield from the corresponding precursor (149.7 ppm, **3s**), which means the metal increases the electron density on phosphorus. The $^{19}\text{F}\{^1\text{H}\}$ NMR at -151.6 ppm corresponding to the BF_4^- anion but there was no evidence of a fluoride ligand being coordinated to the molybdenum. In the IR complex **5s** exhibits two bands assignable to the symmetric and the asymmetric CO stretching frequencies which is characteristic of two CO ligands being *cis* to one another.

8.3. Conclusions

The reaction of hexacarbonyl group six complexes with the P(CH)P pincer ligand N,N'-bis(di-*iso*-propylphosphino)-N,N'-dimethyl-1,3-diaminobenzene was investigated with the objective to obtain hydridocarbonyl M(II) complexes of the type $[\text{M}(\text{PCP}^{\text{Me-}i\text{Pr}})(\text{CO})_3\text{H}]$. In the case of Cr and Mo, the agostic complexes $[\text{Cr}(\text{P}(\text{CH})\text{P}^{\text{Me-}i\text{Pr}})$

Chapter 8 – PNP vs PCP Pincer Complexes

$i\text{Pr})(\text{CO})_3]$ (**2s**) and $[\text{Mo}(\text{P}(\text{CH})\text{P}^{\text{Me}}-i\text{Pr})(\text{CO})_3]$ (**3s**) were formed and no C-H bond cleavage took place, while with tungsten the expected seven coordinate hydrido carbonyl W(II) complex of $[\text{W}(\text{PCP}^{\text{Me}}-i\text{Pr})(\text{CO})_3\text{H}]$ (**4s**) was formed. DFT mechanistic studies corroborate the experimental observations and indicate that the M-H bond strength grows in the order Cr-H < Mo-H < W-H, explaining the preference for the hydride complex only in the case of W. Complexes **2s** - **4s**, even in the presence of strong bases such as NaH, $n\text{BuLi}$, and $\text{KO}t\text{Bu}$, could not be deprotonated to afford anionic tricarbonyl complexes of the type $[\text{M}(\text{PCP}^{\text{Me}}-i\text{Pr})(\text{CO})_3]^-$.

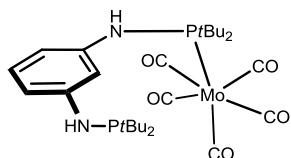
8.4. Experimental Part

The ligand N,N'-bis(di-*iso*-propylphosphino)-N,N'-dimethyl-1,3-diaminobenzene ($\text{P}(\text{CH})\text{P}^{\text{Me}}-i\text{Pr}$) was prepared according to the literature.³⁰

8.4.1. Syntheses

A suspension of the metal hexacarbonyl (0.60 mmol) and 1 equiv. of the respective $\text{P}(\text{CH})\text{P}$ ligand (0.60 mmol) in CH_3CN (4 mL) were placed in a 20 mL sealed glass tube and stirred for 2 h at 135°C (unless otherwise noted, see information below) whereupon a clear solution was obtained. The reaction mixture was allowed to cool to room temperature without stirring. In most cases the product was obtained as crystalline material and was decanted and washed with *n*-pentane. In all other cases the solvent was removed under reduced pressure. The remaining solid was washed with *n*-pentane and dried under vacuum.

$[\text{Mo}(\text{P}(\text{CH})\text{P}-t\text{Bu})(\text{CO})_5]$ (**3r**)

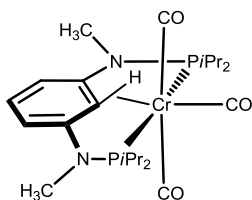


The product was obtained as yellow oil in 96% yield. $^1\text{H NMR}$ (δ , CD_2Cl_2 , 20°C): 6.92 (t, $J = 8.0$ Hz, 1H, Ph), 6.76 (d, $J = 19.1$ Hz, 1H, Ph), 6.59 (s, 1H, Ph), 6.38 (d, $J = 7.8$ Hz), 3.99 (d, $J = 10.5$ Hz, NH), 3.79 (d, $J = 4.6$ Hz, NH), 1.30 (dd, $J = 13.4$, $J = 2.5$ Hz, CH_3), 1.03 (dd, $J = 11.8$, $J = 2.5$ Hz). $^{13}\text{C}\{^1\text{H}\}$ NMR (δ , CD_2Cl_2 , 20°C): 209.6 (d, $J = 25.7$ Hz, CO), 205.9 (d, $J = 8.7$ Hz, CO), 205.8 (d, $J = 8.5$ Hz, CO), 202.9 (CO), 149.8 (dd, $J = 17.3$ Hz, $J = 10.3$ Hz, Ph), 144.3 (dd, $J = 4.5$ Hz, $J = 3.6$ Hz, Ph), 128.6 (t, $J = 9.0$ Hz, Ph), 114.2 (d, $J = 3.0$ Hz, Ph), 111.8 (dd, $J = 9.5$ Hz, 3.1 Hz, Ph), 110.3 (d, $J =$

Chapter 8 – PNP vs PCP Pincer Complexes

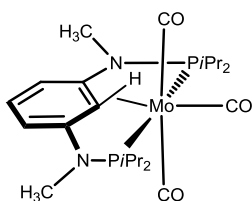
15.4 Hz, Ph), 38.7 (d, $J = 10.9$, $J = 5.7$ Hz, CCH_3), 33.3 (dd, $J = 20.0$ Hz, $J = 2.3$ Hz, CCH_3), 28.3 (d, $J = 7.0$ Hz, CH_3), 27.1 (dd, $J = 15.2$ Hz, $J = 10.0$ Hz, CH_3). $^{31}\text{P}\{^1\text{H}\}$ NMR (δ , CD_2Cl_2 , 20 °C): 125.4(d, $J = 37.8$ Hz), 57.9 (d, $J = 58.7$ Hz).

[Cr(P(CH)P^{Me}-iPr)(CO)₃] (2s)



The product was obtained as red needles in 96% yield. Anal. Calcd. For $\text{C}_{23}\text{H}_{38}\text{CrN}_2\text{O}_3\text{P}_2$ (504.51): C, 54.76; H, 7.59; N, 5.55. Found: C, 54.56; H, 7.67; N, 5.73. ^1H NMR (δ , CD_2Cl_2 , 20 °C): 7.09 (t, $J = 7.9$ Hz, 1H, Ph^4), 6.12 (d, $J = 8.0$ Hz, 2H, $\text{Ph}^{3,5}$), 2.87 (s, 6H, NCH_3), 2.52-2.42 (m, 2H, CH), 2.42-2.30 (m, 2H, CH), 1.28 (dd, $J = 16.3$ Hz, $J = 6.8$ Hz, 7H, CH_3), 1.20-1.09 (m, 12H, CH_3), 1.04 (dd, $J = 14.1$ Hz, $J = 6.9$ Hz, 6H, CH_3), -2.15 (t, $J = 6.2$ Hz, 1H, Ph^1). $^{13}\text{C}\{^1\text{H}\}$ NMR (δ , CD_2Cl_2 , 20 °C): 238.0 (t, $J = 8.1$ Hz, CO), 227.9 (t, $J = 13.1$ Hz, CO), 226.8 (t, $J = 16.2$ Hz, CO), 164.5-164.0 (m, $\text{Ph}^{2,6}$), 132.6 (Ph^4), 103.3-102.9 (m, $\text{Ph}^{3,5}$), 71.1 (t, $J = 6.3$ Hz, Ph^1), 33.9 (d, $J = 15.7$ Hz, CH), 33.0 (d, $J = 5.4$ Hz, NCH_3), 31.6 (d, $J = 20.8$ Hz, CH), 18.6-18.4 (m, CH_3), 18.1 (CH_3), 17.6-17.4 (m, CH_3). ^{13}C NMR (δ , CD_2Cl_2 , 20 °C): 164.5-164.0 (m, $\text{Ph}^{2,6}$), 132.6 (d, $J = 157.2$ Hz, Ph^4), 103.1 (d, $J = 160.7$ Hz, $\text{Ph}^{3,5}$), 71.1 (d, $J = 124.9$ Hz, Ph^1). $^{31}\text{P}\{^1\text{H}\}$ NMR (δ , CD_2Cl_2 , 20 °C): 165.5. IR (ATR, cm^{-1}): 1933 (ν_{CO}), 1821 (ν_{CO}). ESI-MS (m/z , CH_3CN) negative ion: 503.2 [M-H] $^-$, 475.2 M-H-CO] $^-$.

[Mo(P(CH)P^{Me}-iPr)(CO)₃] (3s)

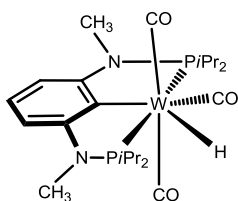


The product was obtained as orange needles in 98% yield. Anal. Calcd. For $\text{C}_{23}\text{H}_{38}\text{MoN}_2\text{O}_3\text{P}_2$ (548.48): C, 50.37; H, 6.98; N, 5.11. Found: C, 50.34; H, 7.14; N, 5.13. ^1H NMR (δ , CD_2Cl_2 , 20 °C): 7.13 (tt, $J = 8.1$ Hz, $J = 1.1$ Hz, 1H, Ph^4), 6.18 (dd, $J = 8.1$ Hz, $J = 1.7$ Hz, 2H, $\text{Ph}^{3,5}$), 2.92-2.85 (m, 6H, NCH_3), 2.50-2.38 (m, 2H, CH), 2.36-2.24 (m, 2H, CH), 1.27-1.20 (m, 7H, CH_3 , Ph^1), 1.15-1.05 (m, 12H, CH_3), 0.97-0.90 (m, 6H, CH_3). $^{13}\text{C}\{^1\text{H}\}$ NMR (δ , CD_2Cl_2 , 20 °C): 232.4 (t, $J = 5.8$ Hz, CO), 219.6 (t, $J = 8.5$ Hz, CO), 216.4 (t, $J = 10.3$ Hz, CO), 164.1 (vt, $J = 9.9$ Hz, $\text{Ph}^{2,6}$), 133.4 (Ph^4), 104.6 (t,

Chapter 8 – PNP vs PCP Pincer Complexes

$J = 3.3$ Hz, $\text{Ph}^{3,5}$), 72.8 (t, $J = 4.6$ Hz, Ph^1), 33.7-33.2 (m, CH, NCH_3), 31.1 (vt, $J = 10.8$ Hz, CH), 19.1 (vt, $J = 7.1$ Hz, CH_3), 18.4 (vd, $J = 4.5$ Hz, CH_3), 18.1 (vt, $J = 6.2$ Hz, CH_3). ^{13}C NMR (δ , CD_2Cl_2 , 20 °C): 164.2-163.8 (m, $\text{Ph}^{2,6}$), 133.4 (d, $J = 157.4$ Hz, Ph^4), 104.5 (d, $J = 161.0$ Hz, $\text{Ph}^{3,5}$), 72.7 (d, $J = 126.0$ Hz, Ph^1). $^{31}\text{P}\{^1\text{H}\}$ NMR (δ , CD_2Cl_2 , 20 °C): 149.7. IR (ATR, cm^{-1}): 1942 (ν_{CO}), 1839 (ν_{CO}), 1823 (ν_{CO}). ESI-MS (m/z , CH_3CN) negative ion: 543.1 $[\text{M}-\text{H}]^-$, 515.1 $[\text{M}-\text{H}-\text{CO}]^-$.

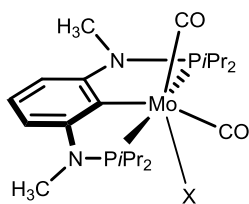
$[\text{W}(\text{PCP}^{\text{Me}}-\text{iPr})(\text{H})(\text{CO})_3]$ (4s)



The product was obtained as yellow-green needles in 95% yield. Anal. Calcd. For $\text{C}_{23}\text{H}_{38}\text{N}_2\text{O}_3\text{P}_2\text{W}$ (636.36): C, 43.41; H, 6.02; N, 4.40. Found: C, 43.38; H, 6.12; N, 4.51. ^1H NMR (δ , CD_2Cl_2 , -40 °C): 6.83 (t, $J = 7.9$ Hz, 1H, Ph^4), 5.99 (d, $J = 8.0$ Hz, 2H, $\text{Ph}^{3,5}$), 2.83 (dd, $J = 7.6$ Hz, $J = 5.5$ Hz, 6H, NCH_3), 2.65-2.32 (m, 4H, CH), 1.21 (ddd, $J = 38.2$ Hz, $J = 17.5$ Hz, $J = 6.9$ Hz, 12H, CH_3), 0.92 (dd, $J = 14.7$ Hz, $J = 7.1$ Hz, $J = 1.7$ Hz, 12H, CH_3), -5.75 (dd, $J = 56.4$ Hz, $J = 21.1$ Hz, 1H). $^{13}\text{C}\{^1\text{H}\}$ NMR (δ , CD_2Cl_2 , 20 °C): 207.8 (vt, CO), 200.6 (t, $J = 7.9$ Hz, CO), 158.6 (dd, $J = 52.7$ Hz, $J = 24.5$ Hz, $\text{Ph}^{2,6}$), 130.9 (t, $J = 10.0$ Hz, Ph^1), 125.3 (Ph^4), 101.6 ($\text{Ph}^{3,5}$), 34.1-32.5 (NCH_3 , CH), 20.6 (CH_3), 19.7 (CH_3), 18.4 (CH_3). ^{13}C NMR (δ , CD_2Cl_2 , 20 °C): 159.1-158.2 (m, $\text{Ph}^{2,6}$), 131.1-130.8 (m, Ph^1), 125.3 (d, $J = 156.8$ Hz, Ph^4), 101.5 (d, $J = 156.5$ Hz, $\text{Ph}^{3,5}$). $^{31}\text{P}\{^1\text{H}\}$ NMR (δ , CD_2Cl_2 , -40 °C): 138.3 (d, $J = 89.0$ Hz, $^1J_{\text{W-P}} = 311.2$ Hz), 120.8 (d, $J = 89.0$ Hz, $^1J_{\text{W-P}} = 322.2$ Hz). IR (ATR, cm^{-1}): 1991 (ν_{CO}), 1909 (ν_{CO}), 1860 (ν_{CO}). ESI-MS (m/z , CH_3CN) negative ion: 633.2 $[\text{M}-\text{H}]^-$, 605.2 $[\text{M}-\text{H}-\text{CO}]^-$.

To a solution of the **3s** (0.60 mmol) in CH_3CN (10 mL) 1 equiv. of selectfluor (0.60 mmol) was added and the solution was stirred for 3 days. After this period the solution was filtered, the solvent was then removed under vacuum, and the remaining yellow solid was washed twice with Et_2O and n-pentane and dried under vacuum.

[Mo(PCP^{Me}-iPr)(CO)₂(X)] (5s)



X = Cl, BF₄ ?

The product was obtained as yellow powder 86% yield. ¹H NMR (δ, CD₃CN, 20 °C): 7.17 (tt, J = 8.0 Hz, J = 1.3 Hz, 1H, Ph⁴), 6.30 (d, J = 8.0 Hz, J = 1.7 Hz, 2H, Ph^{3,5}), 3.03 (t, J = 2.8 Hz, 6H, NCH₃), 2.79-2.70 (m, 2H, CH), 2.69-2.58 (m, 2H, CH), 1.27 (dd, J = 16.2 Hz, J = 7.2 Hz, 6H, CH₃), 1.25-1.19 (m, 12H, CH₃), 1.13 (dd, J = 16.5 Hz, 7.1 Hz, 6H, CH₃). ¹³C{¹H} NMR (δ, CD₃CN, 20 °C): 256.0 (t, J = 15.5 Hz, CO), 230.3 (t, J = 13.2 Hz, CO), 162.0 (vt, J = 11.4 Hz, Ph^{2,6}), 132.7 (Ph⁴), 123.4 (t, J = 7.3 Hz, Ph¹), 105.2 (t, J = 4.6 Hz, Ph^{3,5}), 35.3 (vt, J = 2.4 Hz, NCH₃), 32.0 (vt, J = 11.6 Hz, CH), 31.0 (vt, J = 7.4 Hz, CH), 19.9 (vd, J = 23.9 Hz, CH₃), 19.7 (vt, J = 3.0 Hz, CH₃), 19.2 (vt, J = 3.3 Hz, CH₃). ³¹P{¹H} NMR (δ, CD₃CN, 20 °C): 135.9. ¹⁹F{¹H} NMR (δ, CD₃CN, 20 °C): -151.6. IR (ATR, cm⁻¹): 1935 (ν_{CO}), 1719 (ν_{CO}).

8.5. References

- [1] Coining of the name “pincer”: van Koten, G. *Pure Appl. Chem.*, **1989**, *61*, 1681-1694.
- [2] For reviews on pincer complexes, see: a) Gossage, R. A.; van de Kuil, L. A.; van Koten, G. *Acc. Chem. Res.*, **1998**, *31*, 423-431; b) Albrecht, M.; Van Koten, G.; *Angew. Chem., Int. Ed.*, **2001**, *40*, 3750-3781; c) Van der Boom, M. E.; Milstein, D.; *Chem. Rev.*, **2003**, *103*, 1759-1792; d) Singleton, J. T.; *Tetrahedron*, **2003**, *59*, 1837-1857; e) Morales-Morales, D.; *Rev. Soc. Quím. Méx.*, **2004**, *48*, 338-346; f) Liang, L. C.; *Coord. Chem. Rev.*, **2006**, *250*, 1152-1177; g) Nishiyama, H.; *Chem. Soc. Rev.*, **2007**, *36*, 1133-1141; h) Morales-Morales, D.; Jensen, C. M.; *The Chemistry of Pincer Compounds*, **2007**, Elsevier, Amsterdam; i) Benito-Garagorri, D.; Kirchner, K.; *Acc. Chem. Res.*, **2008**, *41*, 201-213; j) Bhattacharya, P.; Guan, H.; *Comment, Inorg. Chem.*, **2011**, *32*, 88-112; k) Choi, J.; MacArthur, A. H. R.; Brookhart, M.; Goldman, A. S.; *Chem. Rev.*, **2011**, *111*, 1761-1779; l) Selander, N.; Szabo, K. J.; *J. Chem. Rev.*, **2011**, *111*, 2048-2076; m) Schneider, S.; Meiners, J.; Askevold, B.; *Eur. J. Inorg. Chem.*, **2012**, 412-429; n) Van Koten, G.; Milstein, D.; *Top. Organomet. Chem., in Organometallic Pincer Chemistry*, ed., **2013**, Springer, Berlin; (o) Szabo, K. J.; Wendt, O. F.; *Pincer and Pincer-Type Complexes: Applications in Organic Synthesis and Catalysis*, **2014**, Wiley-VCH, Germany; p) Asay, M.; Morales-Morales D.; *Dalton Trans.*, **2015**, *44*, 17432-17447; q) Murugesan, S.; Kirchner, K.; *Dalton Trans.*, **2016**, *45*, 416-439; r) Koten, G. V.; Gossage,

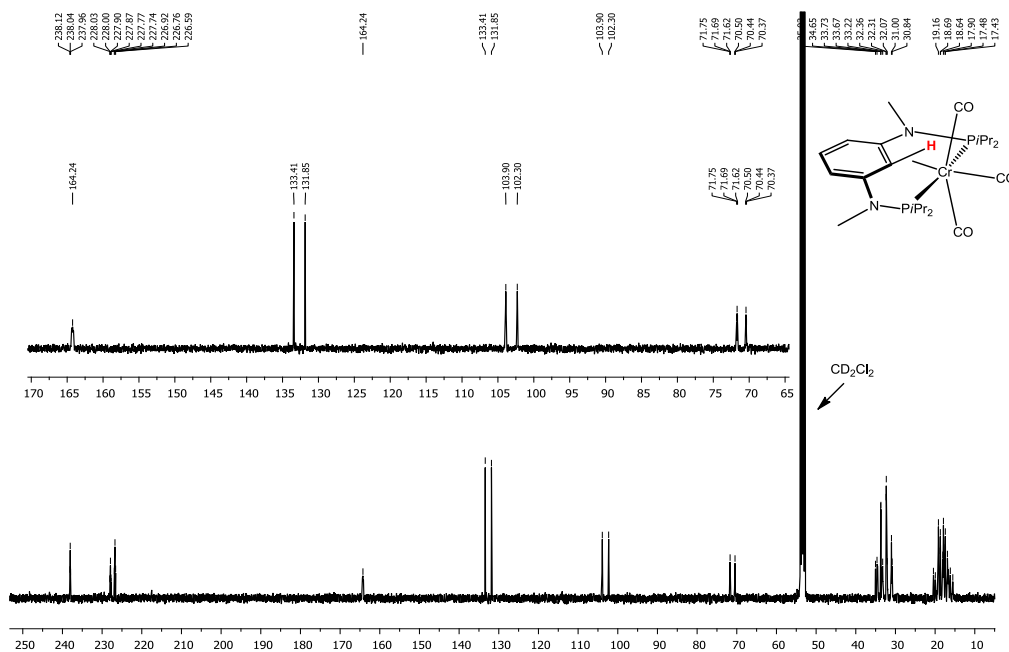
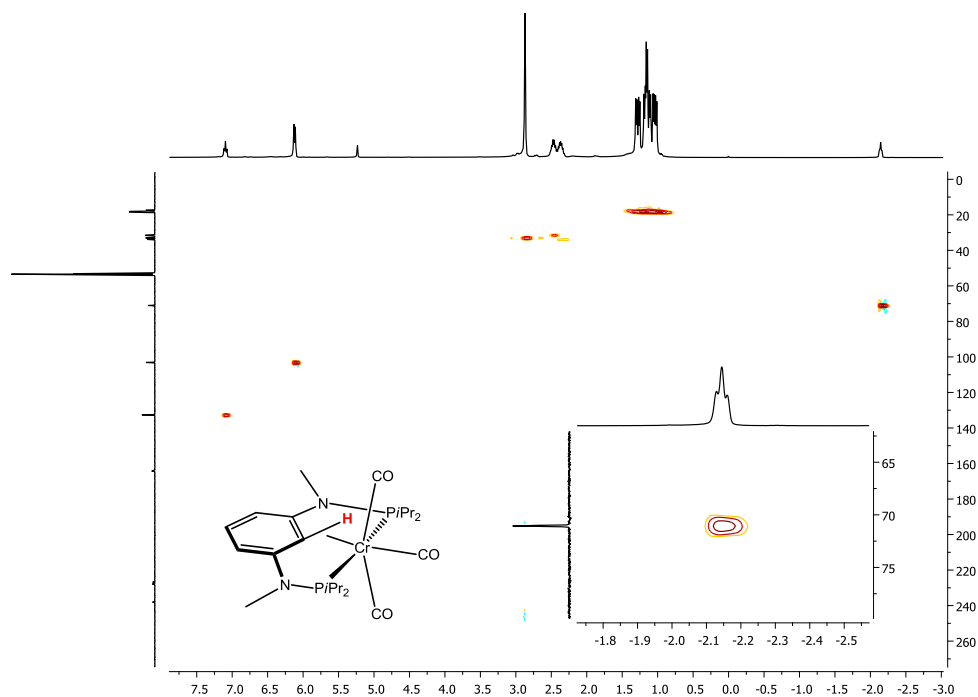
Chapter 8 – PNP vs PCP Pincer Complexes

- R. A.; *Top. Organomet. Chem.*, in *The Privileged Pincer-Metal Platform: Coordination Chemistry & Applications*, ed., **2016**, Springer, Berlin.
- [3] Moulton, C. J.; Shaw, B. L.; *J. Chem. Soc., Dalton. Trans.*, **1976**, 1020-1024.
- [4] Hebden, T. J.; Schrock, R. R.; Takase, M. K.; Mueller, P.; *Chem. Comm.*, **2012**, *48*, 1851-1853.
- [5] Murugesan, S.; "Synthesis and Reactivity of Nickel, Cobalt, and Molybdenum PCP Pincer Complexes", Dissertation, Vienna University of Technology, **2016**.
- [6] For recent reviews on C-H activation and functionalization, see: a) Jia, C.; Kitamura, T.; Fujiwara, Y.; *Acc. Chem. Res.*, **2001**, *34*, 633-639; b) Ritleng, V.; Sirlin, C.; Pfeffer, M.; *Chem. Rev.*, **2002**, *102*, 1731-1770; c) Colby, D. A.; Bergman, R. G.; Ellman, J. A.; *Chem. Rev.*, **2010**, *110*, 624-655; d) Arockiam, P. B.; Bruneau, C.; Dixneuf, P. H.; *Chem. Rev.*, **2012**, *112*, 5879-5918; e) Lewis, J. C.; Bergman, R. G.; Ellman, J. A.; *Acc. Chem. Res.*, **2008**, *41*, 1013-1025; f) Gaillard, S.; Cazin, C. S. J.; Nolan, S. P.; *Acc. Chem. Res.*, **2012**, *45*, 778-787; g) Li, B.; Dixneuf, P. H.; *Chem. Soc. Rev.*, **2013**, *42*, 5744-5767; h) Wencel-Delord, J.; Dröge, T.; Liu, F.; Glorius, F.; *Chem. Soc. Rev.*, **2011**, *40*, 4740-4761.
- [7] a) Shilov, A. E.; Shul'pin, G. B.; *Chem. Rev.*, **1997**, *97*, 2879-2932; b) Labinger, J. A.; Bercaw, J. E.; *Nature*, **2002**, *417*, 507-514; c) Sakaki, S.; *Top. Organomet. Chem.*, **2005**, *12*, 31-78.
- [8] For the central role of agostic interactions in C-H activations, see: a) Hall, C.; Perutz, R. N.; *Chem. Rev.*, **1996**, *96*, 3125-3146; b) Crabtree, R. H.; *J. Organomet. Chem.*, **2004**, *689*, 4083-4091; c) Rybtchinski, B.; Cohen, R.; Ben-David, Y.; Martin, J. M. L.; Milstein, D.; *J. Am. Chem. Soc.*, **2003**, *125*, 11041-11050; d) Jones, W. D.; *Inorg. Chem.*, **2005**, *44*, 4475-4484; e) Bernskoetter, W. H.; Schauer, C. K.; Goldberg, K. I.; Brookhart, M.; *Science*, **2009**, *326*, 553-556.
- [9] Lepetit, C.; Poater, J.; Alikhani, M. E.; Silvi, B.; Canac, Y.; Contreras-García, J.; Sola, M.; Chauvin, R.; *Inorg. Chem.*, **2015**, *54*, 2960-2969.
- [10] a) Vigalok, A.; Uzan, O.; Shimon, L. J. W.; Ben-David, Y.; Martin, J. L.; Milstein, D.; *J. Am. Chem. Soc.*, **1998**, *120*, 12539-12544; b) Vigalok, A.; Rybtchinski, B.; Shimon, L. J. W.; Ben-David, Y.; Milstein, D.; *Organometallics*, **1999**, *18*, 895-905; c) Montag, M.; Schwartsburd, L.; Cohen, R.; Leitius, G.; Ben-David, Y.; Martin, J. M. L.; Milstein, D.; *Angew. Chem., Int. Ed.*; **2007**, *46*, 1901-1904; d) Frech, C. M.; Shimon, L. J. W.; Milstein, D.; *Organometallics*, **2009**, *28*, 1900-1908; e) Montag, M.; Efremenko, I.; Cohen, R.; Shimon, L. J. W.; Leitius, G.; Diskin-Posner, Y.; Ben-David, Y.; Salem, H.; Martin, J. M. L.; Milstein, D.; *Chem. - Eur. J.*, **2010**, *16*, 328-353.
- [11] Albeniz, A. C.; Schulte, G.; Crabtree, R. H.; *Organometallics*, **1992**, *11*, 242-249.
- [12] a) Dani, P.; Karlen, T.; Gossage, R. A.; Smeets, W. J. J.; Spek, A. L.; van Koten, G.; *J. Am. Chem. Soc.*, **1997**, *119*, 11317-11318; b) Dani, P.; Toorneman, M. A. M.; van Klink, G. P. M.; van Koten, G.; *Organometallics*, **2000**, *19*, 5287-5296.
- [13] McLoughlin, M. A.; Flesher, Kaska, W. C.; Mayer, H. A.; *Organometallics*, **1994**, *13*, 3816-3822.

Chapter 8 – PNP vs PCP Pincer Complexes

- [14] van der Boom, M. E.; Iron, M. A.; Atasoylu, O.; Shimon, L. J.W.; Rozenberg, H.; Ben-David, Y.; Konstantinovski, L.; Martin, J. M. L.; Milstein, D.; *Inorg. Chim. Acta*, **2004**, *357*, 1854-1864.
- [15] Gusev, D. G.; Madott, M.; Dolgushin, F. M.; Lyssenko, K. A.; Antipin, M. Yu.; *Organometallics*, **2000**, *19*, 1734-1739.
- [16] Barthes, C.; Lepetit, C.; Canac, Y.; Duhayon, C.; Zargarian, D.; Chauvin, R.; *Inorg. Chem.*, **2013**, *52*, 48-58.
- [17] Connelly, S. J.; Chanez, A. G.; Kaminsky, W.; Heinekey, D. M.; *Angew. Chem., Int. Ed.*; **2015**, *54*, 5915-5918.
- [18] Liu, X.; Pattacini, R.; Deglmann, P.; Braunstein, P.; *Organometallics*, **2011**, *30*, 3302-3310.
- [19] Ribas, X.; Calle, C.; Poater, A.; Casitas, A.; Gomez, L.; Xifra, R.; Parella, T.; Benet-Buchholz, J.; Schweiger, A.; Mitrikas, G.; Sola, M.; Llobet, A.; Stack, T. D. P.; *J. Am. Chem. Soc.*, **2010**, *132*, 12299-12306.
- [20] Murugesan, S.; Stöger, B.; Pittenauer, E.; Allmaier, G.; Veiros, L. F.; Kirchner, K.; *Angew. Chem., Int. Ed.*; **2016**, *55*, 3045-3048.
- [21] Cherry, S. D. T.; Kaminsky, W.; Heinekey, D. M.; *Organometallics*, **2016**, *35*, 2165-2169.
- [22] Mastalir, M.; de Aguiar, S. R. M. M.; Glatz, M.; Stöger, B.; Kirchner, K.; *Organometallics*, **2016**, *35*, 229-232.
- [23] Curtis, M. D.; Shiu, K.-B.; *Inorg. Chem.*, **1985**, *24*, 1213-1218.
- [24] a) Baker, P. K.; Al-Jahdali, M.; Meehan, M. M. J.; *Organomet. Chem.*, **2002**, *648*, 99-108;
b) Baker, P. K.; Drew, M. G. B.; Moore, D. S. J.; *Organomet. Chem.*, **2002**, *664*, 45-58.
- [25] Öztopcu, Ö.; Holzhacker, C.; Puchberger, M.; Weil, M.; Mereiter, K.; Veiros, L. F.; Kirchner, K.; *Organometallics*, **2013**, *32*, 3042-3052.
- [26] a) Hoffmann, R.; Beier, B. F.; Muetterties, E. L.; Rossi, A. R.; *Inorg. Chem.*, **1977**, *16*, 511-522; b) Thompson, H. B.; Bartell, L. S.; *Inorg. Chem.*, **1968**, *7*, 488-491.
- [27] Kuzelka, J.; Legzdins, P.; Rettig, S. J.; Smith, K. M.; *Organometallics*, **1997**, *16*, 3569-3571.
- [28] a) Wiberg, K. B.; *Tetrahedron*, **1968**, *24*, 1083-1096.; b) Wiberg indices are electronic parameters related to the electron density in between two atoms, which scale as bond strength indicators. They can be obtained from a natural population analysis.
- [29] For the equivalent Cr complex, the Cr-H Wiberg index is 0.34.
- [30] Murugesan, S.; Stöger, B.; Carvalho, M. D.; Ferreira, L. P.; Pittenauer, E.; Allmaier, G.; Veiros, L. F.; Kirchner, K.; *Organometallics*, **2014**, *33*, 6132-6140.

8.6. Annex

 ^{13}C NMR, no decoupling (400 MHz, CD_2Cl_2)Figure 8.12. ^{13}C NMR spectrum of complex **2s** ^1H - ^{13}C HSQC NMR (400 MHz, CD_2Cl_2)Figure 8.13. ^1H - ^{13}C HSQC NMR spectrum of complex **2s**

Chapter 8 – PNP vs PCP Pincer Complexes

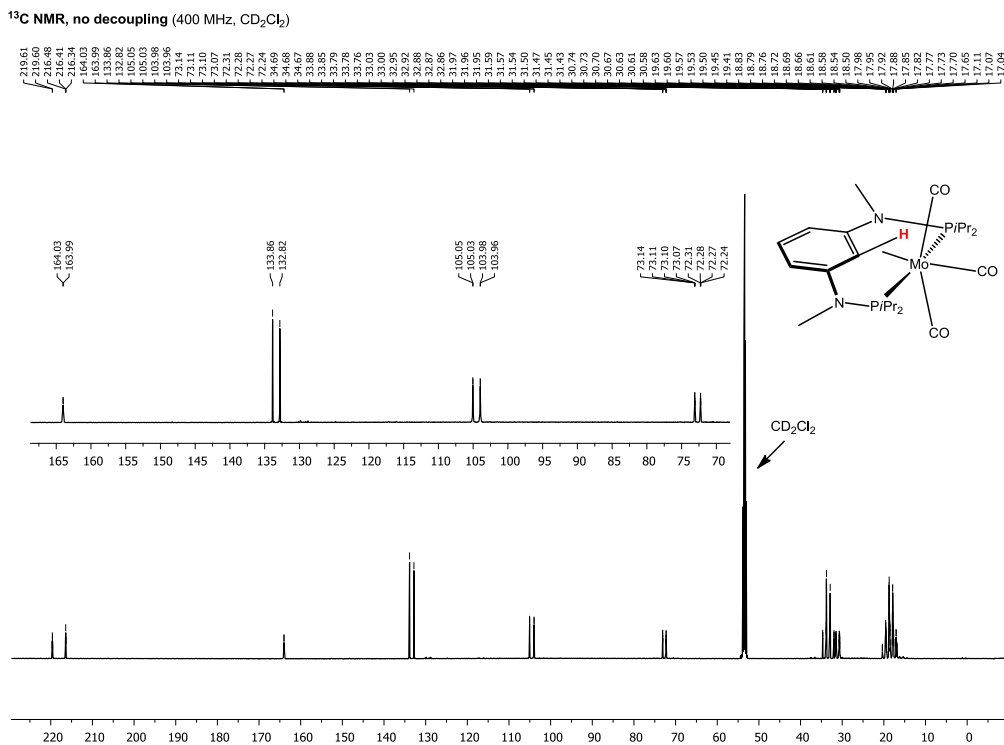


Figure 8.14. ¹³C NMR spectrum of complex **3s**

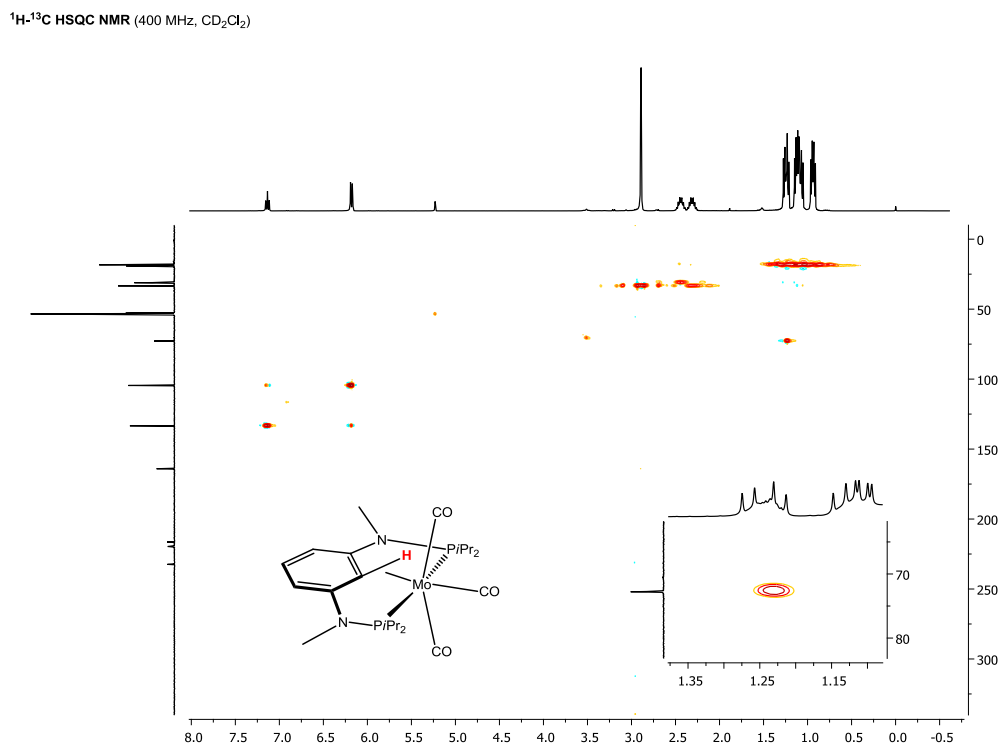


Figure 8.15. ¹H-¹³C HSQC NMR spectrum of complex **3s**

Chapter 8 – PNP vs PCP Pincer Complexes

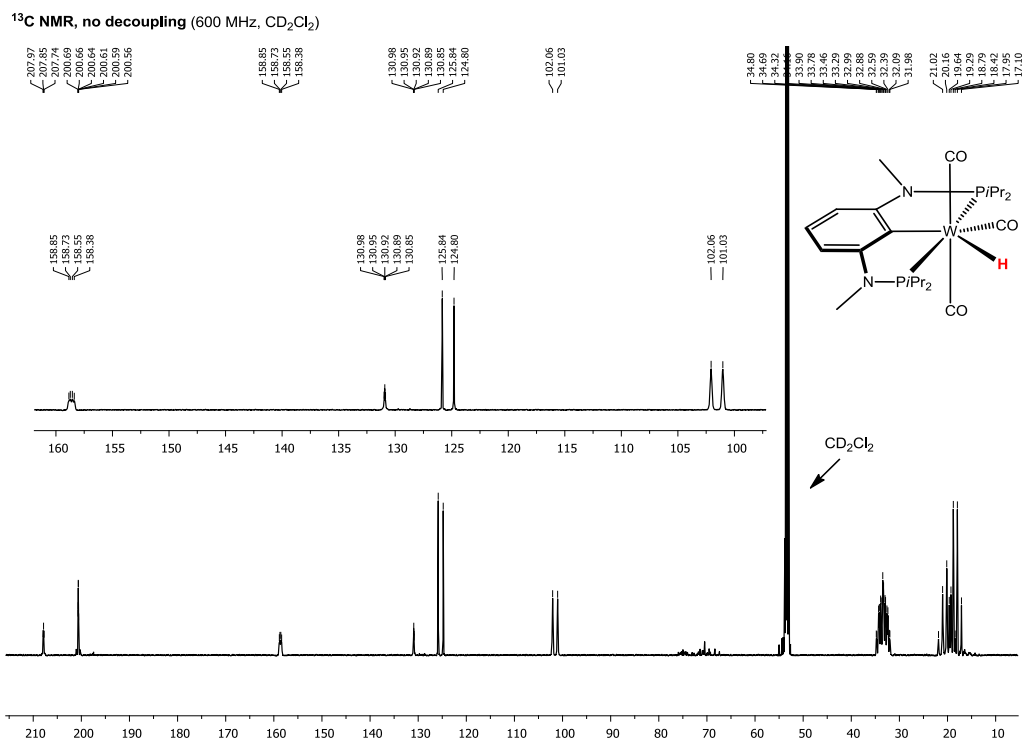


Figure 8.16. ¹³C NMR spectrum of complex 4s

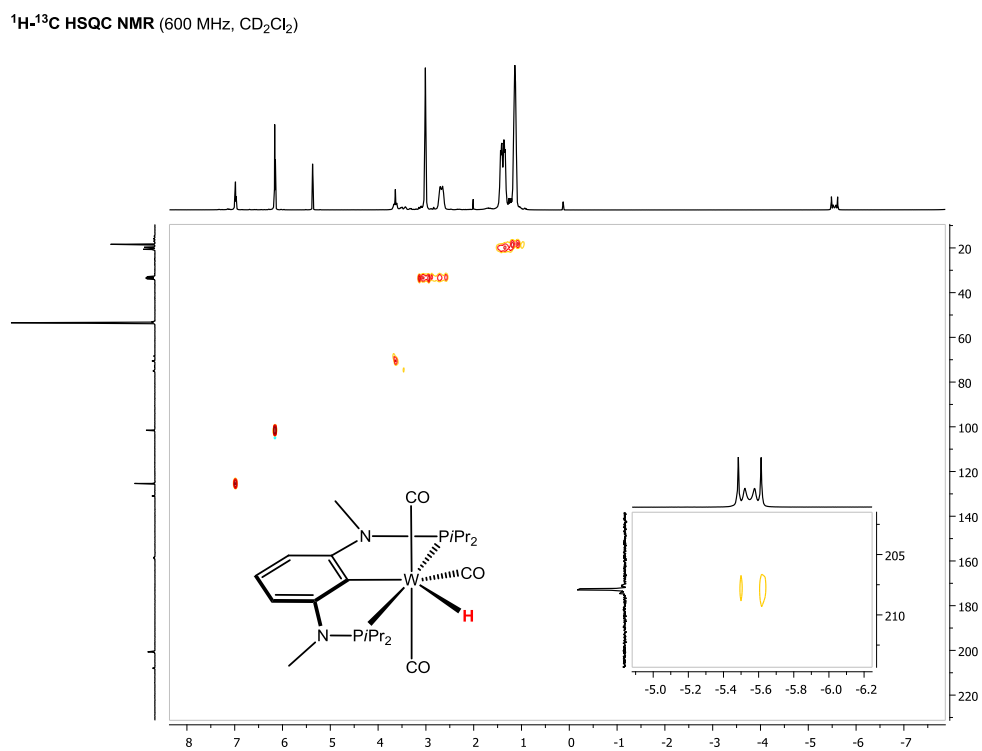


Figure 8.17. ¹H-¹³C HSQC NMR spectrum of complex 4s

Chapter 9

Curriculum Vitae

Sara Aguiar

Curriculum Vitae

Giessaufgasse 1 Top 14
1050 Vienna
0043 660 2942306
saramotaaguiar@hotmail.com

Personal information

Full name **Sara Raquel Mota Merelo de Aguiar**

Nationality Portuguese

Academic degrees

- 08/2013-07/2017 Ph.D. in Chemistry, Vienna University of Technology (TU Wien), Vienna, Austria
Thesis: “Molybdenum and Tungsten PNP Pincer Complexes”, at the Institute of Applied Synthetic Chemistry, Group of Prof. Kirchner
- 09/2009-12/2011 MSc in Chemistry - accredited with Euromaster Label, Faculty of Sciences of the University of Lisbon (FCUL), Lisbon, Portugal
Thesis: “Corrosion processes in materials for biomedical applications and bacterial growth in artificial saliva”, at the Centre of Chemistry and Biochemistry (CQB) University of Lisbon, Group of Prof. Boavida and Prof. Almeida
- 10/2003 – 02/2009 Degree in Chemistry - accredited with Eurobachelor Label, Faculty of Sciences of the University of Lisbon (FCUL), Lisbon, Portugal
Thesis: “The inhibitory effect of *Plectranthus barbatus* and *Plectranthus ecklonii* species and rosmarinic acid on the viability, glucosyltransferase activity and biofilm formation of *Streptococcus sobrinus*”, at the Centre of Chemistry and Biochemistry (CQB) University of Lisbon, Group of Prof. Lino

Chapter 9 – *Curriculum Vitae*

Professional experience

- 2013-ongoing Project Assistant at the Vienna University of Technology (TU Wien), Group of Prof. Kirchner
- 2012 Research Fellowship for Masters (BI) under the Strategic Project (PEst-OE/QUI/UI100/2011-2012) at Center for Structural Chemistry (CQE) of the Higher Technical Institute (IST), Group of Prof. Martins
- 2008-2009 Scholarship research (BII) from FCT, Strategic Project (PTDC/QUI/71576/2006) at Centre of Chemistry and Biochemistry (CQB) of the Faculty of Sciences of the University of Lisbon (FCUL), Group of Prof. Calhorda

Technical skills and competences

- 2016 Course, "Project Management"
- 2014 Course, "Electron Microscopy "
- 2012 Course, "Modern Methods of Structure Elucidation", at the Higher Technical Institute (IST).
- 2009 Course "Molecular Mechanism of Drugs", September, 2009, at the Faculty of Sciences of the University of Lisbon (FCUL).
- 2007 Project Collaborator "Marcas das Ciências e das Técnicas", 2007, at the Faculty of Sciences of the University of Lisbon (FCUL).
- 2007 Course "Técnicas Quirópticas em Química Orgânica" March 2007, at the Faculty of Sciences of the University of Lisbon (FCUL).

Work related skills **Techniques:** NMR, IR, UV/VIS, XRD, TEM, Electrochemical Techniques (potentiodynamic polarization, OCP and CV), basic knowledge of MS, HPLC and GC.

Chapter 9 – *Curriculum Vitae*

Computer skills and competences Average knowledge level of a user under Windows and Linux operating systems and programs microsoft office, mestrec, mercury, origin and knowledge of programming languages FORTRAN 90 and C + +

Organisational skills and competences Supervision of Teams competing in the Junior Olympics in Chemistry, April 2008 – Faculty of Sciences of the University of Lisbon (FCUL),

Languages

Portuguese (mother tongue), English (C2), German (A2), French (A2), Spanish (A1)

Other Reports

1. Report of the Research Fellowship, entitled “Synthesis of new organometallic complexes immobilization in clays and MCM-41”, at the Centre of Chemistry and Biochemistry (CQB) of the Faculty of Sciences of the University of Lisbon (FCUL), Group of Prof. Calhorda, 2010
2. Report of the Research Fellowship, entitled “Syntheses and reactivity of new complexes supported by N-heterocyclic carbene (NHC) ligands”, at the Center for Structural Chemistry (CQE) of the Higher Technical Institute (IST), Group of Prof. Martins, 2012

Chapter 9 – Curriculum Vitae

Publications

1. Sara R. M. M. de Aguiar, Özgür Öztopcu, Anna Troiani, Giulia de Petris, Matthias Weil, Ernst Pittenauer, Günter Allmaier, Luis F. Veiros, Karl Kirchner, "Formation of Mono Oxo Molybdenum(IV) PNP Pincer Complexes: Interplay between Water and Molecular Oxygen", (**Manuscript prepared**)
2. Afrooz Zirakzadeh, Sara R. M. M. de Aguiar, Berthold Stöger, Michael Widhalm, Karl Kirchner, "Enantioselective Transfer Hydrogenation of Ketones Catalyzed by a Manganese Complex Containing an Unsymmetrical Chiral PNP' Tridentate Ligand", *ChemCatChem*, 2017, 9, 1744-1748
3. Sara R. M. M. de Aguiar, Berthold Stöger, Ernst Pittenauer, Günter Allmaier, Luis F. Veiros and Karl Kirchner, "Arene C-H Bond Coordination versus C-H Bond Cleavage in Low Valent Group 6 Carbonyl Pincer Complexes", *Organometallics*, 2016, 35, 3032-3039.
4. Sara R. M. M. de Aguiar, Berthold Stöger, Ernst Pittenauer, Günter Allmaier, Luis F. Veiros and Karl Kirchner, "*Structural Diversity of Halocarbonyl Molybdenum and Tungsten PNP Pincer Complexes through Ligand Modifications*", *Dalton Trans.*, 2016, 45, 13834-13845.
5. Afrooz Zirakzadeh, Sara R. M. M. de Aguiar, Michael Widhalm, Kurt Mereiter, Karl Kirchner, "*Iron(II) complexes featuring chiral PNNP diferrocene: Synthesis and characterization of potential hydrogenation catalysts*", *Journal of Organometallic Chemistry*, 2016, 819, 260-265
6. Sara R. M. M. de Aguiar, Berthold Stöger, Matthias Weil, Karl Kirchner; "*Crystal structure of tetrakis([mu]3-oxido)([mu]2-diphenylphosphinato-[kappa]O,O')-oxidomolybdenum(V)*", *IUCrData*, 2016

Chapter 9 – Curriculum Vitae

7. Matthias Mastalir, Sara R. M. M. de Aguiar, Mathias Glatz, Berthold Stöger, Karl Kirchner; “*A Convenient Solvothermal Synthesis of Group Six PNP Pincer Tricarbonyl Complexes*”, *Organometallics*, 2016, 35, 229-232
8. S. R. M. M. de Aguiar, M. Nicolai, M. Almeida and A. Gomes; “*Electrochemical behaviour of a cobalt–chromium–molybdenum dental alloy in artificial salivas*” *Bio-Medical Materials and Engineering*, 2015, 5, 3–66
9. Sara R. M. M. de Aguiar, Özgür Öztopcu, Berthold Stöger, Kurt Mereiter, Luis F. Veiros, Ernst Pittenauer, Günter Allmaier and Karl Kirchner, “*Synthesis and reactivity of coordinatively unsaturated halocarbonyl molybdenum PNP pincer complexes*”, *Dalton Trans.*, 2014, 43, 14669–14679
10. Sara Raquel M. M. de Aguiar, Berthold Stöger, Ernst Pittenauer, Michael Puchberger, Günter Allmaier, Luis F. Veiros and Karl Kirchner, “*A complete series of halocarbonyl molybdenum PNP pincer complexes - Unexpected differences between NH and NMe spacers*”, *Journal of Organometallic Chemistry*, 2014, 760, 74-83.
11. Sónia Barroso, Sara R.M.M. de Aguiar, Rui F. Munhá and Ana M. Martins, “*New zirconium complexes supported by N-heterocyclic carbene (NHC) ligands: Synthesis and assessment of hydroamination catalytic properties*”, *Journal of Organometallic Chemistry*, 2014, 760, 60-66.
12. Maria Vasconcellos-Dias, Sara Raquel M. M. de Aguiar, Carla D. Nunes, Pedro D. Vaz, Teresa G. Nunes, Maria José Calhorda “*Pyridine Carboxylate Complexes of Mo(II) as Active Catalysts in Homogeneous and Heterogeneous Olefin Epoxidation*”, *Current Inorganic Chemistry*, 2011, 1, 146-155.

Chapter 9 – Curriculum Vitae

13. Neusa L. Figueiredo, Sara Raquel M. M. de Aguiar, Pedro Luis Falé, Lia Ascensão, Maria Luisa M. Serralheiro, Ana Rosa L. Lino “ *The inhibitory effect of *Plectranthus barbatus* and *Plectranthus ecklonii* leaves on the viability, glucosyltransferase activity and biofilm formation of *Streptococcus sobrinus* and *Streptococcus mutans**” Food Chemistry, 2010, 119, 664-668.

Communications

1. Poster in “XXXIV GEQO Congress Organometallic Chemistry Group”, September, 2016, “New development on the chemistry of Group Six PCP Pincer Complexes”, Sara R. M. M de Aguiar, Berthold Stöger and Karl Kichner.
2. Poster in "XXVI International Conference on Organometallic Chemistry", July, 2014, "Synthesis and reactivity of Molybdenum PNP pincer complexes", Sara Raquel M. M. de Aguiar and Karl Kirchner.
3. Poster in "XXV International Conference on Organometallic Chemistry", September, 2012, "Syntheses and reactivity of New Zirconium diphenolate-NHC complexes", Sara Raquel M. M. de Aguiar, Sonia Barroso, and Ana M. Martins.
4. Poster in "XXV International Conference on Organometallic Chemistry", September, 2012, "Reactivity of Molybdenum and Tungsten Complexes supported by Chiral N-Heterocyclic Carbene (NHC) Ligands", Sonia Barroso, Sara Raquel M. M. de Aguiar, Cristina G. Azevedo, Maria José Calhorda and Ana M. Martins.
5. Poster in “8ª Conferência de Química Inorgânica”, Curia, September, 2009, “Synthesis of new molybdenum(II) complexes and their immobilization in clays”, Sara Raquel M.M. de Aguiar, Maria José Calhorda.